



HAL
open science

Noyau de corrélation amélioré pour la réponse linéaire de la théorie de la fonctionnelle de la densité dépendante du temps

Miquel Huix I Rotllant

► **To cite this version:**

Miquel Huix I Rotllant. Noyau de corrélation amélioré pour la réponse linéaire de la théorie de la fonctionnelle de la densité dépendante du temps. Autre [q-bio.OT]. Université de Grenoble, 2011. Français. NNT : 2011GRENV073 . tel-00680039

HAL Id: tel-00680039

<https://theses.hal.science/tel-00680039>

Submitted on 17 Mar 2012

HAL is a multi-disciplinary open access archive for the deposit and dissemination of scientific research documents, whether they are published or not. The documents may come from teaching and research institutions in France or abroad, or from public or private research centers.

L'archive ouverte pluridisciplinaire **HAL**, est destinée au dépôt et à la diffusion de documents scientifiques de niveau recherche, publiés ou non, émanant des établissements d'enseignement et de recherche français ou étrangers, des laboratoires publics ou privés.

THÈSE

Pour obtenir le grade de

DOCTEUR DE L'UNIVERSITÉ DE GRENOBLE

Spécialité : **Chimie Physique Moléculaire et Structurale**

Arrêté ministériel : 7 août 2006

Présentée par

Miquel HUIX I ROTLLANT

Thèse dirigée par **Mark E. CASIDA**

préparée au sein du **Laboratoire de Chimie Théorique**
dans l'**École Doctorale Chimie et Sciences du Vivant**

Improved correlation kernels for linear-response time-dependent density-functional theory

Thèse soutenue publiquement le **19 décembre 2011**,
devant le jury composé de :

Pascale MALDIVI

Professeur, Service de Chimie Inorganique et Biologique, CEA, Grenoble, France. Présidente.

Ángel RUBIO SECADES

Professeur, Nano-Bio Spectroscopy group, UPV, San Sebastián, Espagne et Theoretical Spectroscopy, Fritz-Haber Institut, Berlin, Allemagne. Rapporteur.

Tomasz A. WESOLOWSKI

Professeur, Département de Chimie Physique, Université de Genève, Suisse. Rapporteur.

Ursula RÖTHLISBERGER

Professeur, Institut des Sciences et Ingénierie Chimiques, École Polytechnique Fédérale de Lausanne, Lausanne, Suisse. Rapporteur

Thierry DEUTSCH

Directeur, Institut de Nanoscience et Cryogénie SP2ML_Sim CEA, Grenoble, France. Membre.

Mark E. CASIDA

Professeur, Laboratoire de Chimie Théorique, DCM, UJF, Grenoble, France. Membre.



*Als meus pares i germana.
A les meves àvies, in memoriam.*

Abstract

Time-dependent density-functional theory (TDDFT) is a density-functional method for calculating excited states. TDDFT is formally exact, though in practice one has to approximate the exchange-correlation functional, which contains all the many-body effects. The adiabatic functionals are the most commonly used. Although they are very successful for spectroscopy, the adiabatic functionals are too inaccurate for a general application to photochemistry. In this thesis, we show that the main problem is due to the approximations in the correlation functional. The main result of the thesis is a correlation kernel for linear-response TDDFT, derived using many-body perturbation theory techniques, which generally includes double excitations, thus introducing the leading correlation effects in the excited states. The comparison of this kernel with the adiabatic functionals allowed us to identify which correlation effects are missing in this approximation. We tested the possibility of improving the description of correlation by adding the missing terms from many-body theory to the adiabatic functionals. This mixed kernel is more efficient than the full many-body kernel, and can potentially be applied to systems of medium to large size.

Résumé

La théorie de la fonctionnelle de la densité dépendante du temps (TDDFT) est une méthode basée sur la densité pour calculer les états excités. Bien que la TDDFT soit une théorie exacte, on doit en pratique partir d'une approximation de la fonctionnelle d'échange-corrélation, qui reste inconnue. L'approximation adiabatique est l'approximation de la fonctionnelle la plus courante. Cette approximation donne de très bons résultats pour les propriétés spectroscopiques, mais elle est inexacte pour les simulations en photochimie. Dans cette thèse, on montre que l'origine du problème réside dans l'approximation de la fonctionnelle de corrélation. Le résultat principal de la thèse consiste en un noyau de corrélation, qui peut être utilisé dans la formulation de la réponse linéaire, noyau dérivée à partir de la théorie des perturbations à plusieurs corps. Le noyau inclut de façon générale les excitations doubles qui donnent l'effet principal à la corrélation dans les états excités. La comparaison de ce noyau avec la fonctionnelle adiabatique nous a permis d'identifier les termes manquants à ce dernier. Nous avons testé la possibilité d'ajouter ces termes comme une correction à l'approximation adiabatique. Le noyau pourrait potentiellement être appliqué à des systèmes de grosse taille.

Acknowledgements

Ja està. Quan acabi aquestes línies ja hauré finalitzat la tesi. Un projecte en el que hi he investit més de tres anys amb gran intensitat. Ha estat dur, costós, ha requerit una gran dosi de paciència i perseverància, però la recompensa que n'he obtingut ha estat molt més gran. He crescut en tots els aspectes: científic i personal. Aquest és l'únic espai on puc deixar constància dels sentiments que m'embriaguen ara. I us ho dedico a vosaltres, perquè sense el vostre suport, ara no escriuria aquestes ratlles.

First and foremost, I thank my thesis director Mark Casida, for entrusting me with the project, for the numerous discussions, and for all the good science I learned from him. I have the feeling that these three years with him will set the pace for my future scientific career.

Secondly, I would like to thank Ángel Rubio for hosting me in his group in San Sebastián, where I felt like at home, for the fruitful and encouraging scientific discussions we had, and all his support in numerous ways through these years of thesis.

My special thanks to all jury members for accepting to be part of the defence, and Ursula Röthlisberger, Tomasz Wesolowski and Ángel Rubio, for additionally accepting to referee this thesis.

Je veux remercier aussi le group de Chimie Théorique, pour m'avoir accueilli chaleureusement au sien du Laboratoire de Chimie Théorique. En particulière, je remercie à Anne Millet et Carlos Pérez del Valle pour l'enorme aide dans tous les sens et pour leur relecture attentive de la thèse et leurs suggestions, and Muhavini Wawire for the numerous scientific discussions, and for his help in many senses; he has become a close friend. Aussi, je veux remercier Bhaarathi Natarajan pour des très bons moments ensemble, et Hélène Jamet, Nicolas Sieffert, Marie-Louise, Loïc, Mircea, Marius, Maylis et Mokhtar. Aussi, je remercie à autre gens qui ont passés par le Département de Chimie Moléculaire pendant ma thèse: la Isabel i la Neus, dues amigues de debò, Fabien, Marcello et Marc, pour les soirées gastronomiques à les Archées.

Aussi, je veux rémercier les gens de l'Institut Néel, du CEA et du CNRS, qui sont involués dans les projets de la Fondation Nanoscience et de l'ETSF, en particuliere Claudio, Valerio et Thierry.

No puc oblidar-me de la gent de Grenoble que m'ha recordat que hi ha vida més enllà del laboratori. Haig d'agrair de manera molt especial i particular a la Laia i a l'Esteve, han estat dues de les coses més boniques que m'enduré de Grenoble i que, encara que els nostres camins se separin, estic convençut que la nostra amistat perdurará. Avec eux, j'ai connu aussi toute de gens incroyables qui sont devenus très très importantes pour moi: Agnès, Salvo, Claudio, Elena et juste à la fin Jorge. Je vous rémercier infiniment tous les précieux moments ensemble.

In diese lange Reise habe ich viele Leute gesammelt, der ich danken sollte. Ich kann aber nicht vergessen diese Leute die, trotz die Entfernung, haben immer an mich gedacht und Kraft gegeben. Besonders, Joanna, die viel bedeutet in meinem Leben und Aleks, mit wem ich immer dankbar sein werde. Auch eine Erinnerung für Fabrizio (mit wem ich viel getauscht habe), Selin, Harkan, Ricky, Adolfo, Walid, Salva, Anna Lluís, Mikel, Alex, und auch meinen ehemaligen Kollegen an der TUM: Manuela, Sergey, Siham, und Egor.

Agradezco mucho al grupo de Ángel Rubio por integrarme como uno más de la familia. En especial agradezco a Joseba, a Pablo, a Fulvio y a Alison por las comidas y charlas juntos. Asimismo, un recuerdo no menos especial para Joana, Amilcare, Fefe, Pier-Luigi, Lorenzo,

Nicole, Marius, Jessica, Matteo, Yann, Annapaola, Umberto, Robert, y Cristina. También un recuerdo para la gente de Donosti que conocí, especialmente por los buenos momentos con Cristian, pero también con Aritz, Eneritz y Paula, mis compañeros de piso.

Els camins són llargs, però hi ha moments a la vida que marquen un punt d'inflexió. Això em va passar durant els cursos de doctorat de Santander, on vaig conèixer persones molt especials (en el sentit més positiu de la paraula). Vull agrair molt especialment l'Anna i la Mieria, dues persones en majúscules i que han estat sempre al meu costat. Ceila, Pablo, Ramón y Laia, con quién he compartido algunos de mis mejores momentos de mi vida. También un especial recuerdo para mi otro compañero de habitación Juanjo Ceibe, y para Abel, Yannick, Sílvia, Alberto, etc.

Vull agrair als meus companys de la Universitat de Girona, pel suport passat i present, amb qui vaig començar a apreciar la química teòrica. En gran part ho dec a en Josep Maria Luis, de qui vaig aprendre les primeres nocions de quàntica. També vull agrair en Miquel Solà i en Miquel Duran, en Lluís, l'Emili, en Pedro, la Sílvia, en Marcel, en Sergey, i els meus primers companys, l'Anna, l'Ángel Jacinto, l'Armangué, la Dachs, en Ferran, etc.

Finalment, vull agrair a la meva família, i en especial als meus pares i a la meva germana, a qui dedico aquesta tesi. Si he arribat on he arribat és en gran part gràcies al seu suport.

Contents

Contents	i
List of Acronyms and Notation	v
Introduction	1
I Basic Concepts	7
1 Theoretical Photochemistry	9
1.1 Introduction	9
1.2 Born-Oppenheimer Separation and Potential Energy Surfaces	10
1.3 Correlation in Excited States	11
1.4 Example of a Photochemical Reaction: Stilbene Photoisomerization	14
1.5 Photoabsorption	16
1.6 Conical Intersections	17
2 Wave-Function Based Electronic Structure	19
2.1 Introduction	19
2.2 Variational Principle	21
2.3 Hartree-Fock	22
2.4 Configuration Interaction	24
2.4.1 Full Configuration Interaction	24
2.4.2 Configuration Interaction Singles	25
2.4.3 Singles and Doubles Configuration Interaction	26
2.4.4 Multireference Self-Consistent Field	27
2.5 Linear Response	27
2.5.1 General Linear Response Theory	28
2.5.2 Equation of Motion of the Polarization Propagator	30
2.5.3 Time-Dependent Hartree-Fock	32
2.5.4 Second-Order Polarization Propagator	33
2.5.5 Polarization Propagator vs. Configuration Interaction	34
3 Density-Functional Based Electronic Structure	35
3.1 Introduction	35
3.2 Density-Functional Theory	37
3.2.1 Formal Foundations	37
3.2.1.1 Existence Theorem	37
3.2.1.2 Variational Principle	38
3.2.1.3 v -Representability and N -Representability	39
3.2.2 Kohn-Sham Equations	40

3.2.3	Exchange-Correlation Functionals	41
3.3	Time-Dependent Density-Functional Theory	45
3.3.1	Formal Foundations	45
3.3.1.1	Existence theorem	46
3.3.1.2	Action principle	47
3.3.1.3	Time-dependent v -representability	50
3.3.2	Time-Dependent Kohn-Sham Equation	50
3.3.2.1	Linear Response	51
3.3.2.2	Real-Time	57
3.3.3	Time-Dependent Exchange-Correlation Functional	58
3.3.3.1	Exact Properties	59
3.3.3.2	Adiabatic Approximation	60
3.3.3.3	Memory	61

II Original Research 67

4	Spin-Flip Time-Dependent Density-Functional Theory	69
4.1	Introduction	69
4.2	Photochemical Ring-Opening of Oxirane (Article)	70
4.2.1	Introduction	71
4.2.2	Spin-Flip TDDFT	78
4.2.3	Computational Details	82
4.2.4	Results	83
4.2.4.1	C_{2v} Ring Opening	84
4.2.4.2	Photochemical Pathway and Conical Intersection	89
4.2.5	Conclusion	93
4.2.6	Acknowledgments	96
4.3	Conclusions and Perspective	96
5	<i>Ab initio</i> Exact Exchange-Correlation Kernel	99
5.1	Introduction	99
5.2	Formal foundations of dressed TDDFT (Article)	100
5.2.1	Introduction	100
5.2.2	Space, Time, and the Exact Kernel	106
5.2.3	Localization	112
5.2.4	Perturbative Approximations to the Polarization Propagator	115
5.2.4.1	Superoperator Polarization Propagator Approach	116
5.2.4.2	First-Order Exchange-Correlation Kernel	120
5.2.4.3	Second-Order Exchange-Correlation Kernel	123
5.2.4.4	Tamm-Dancoff Approximation	127
5.2.5	Dressed TDDFT	128
5.2.6	Conclusion	134
5.2.7	Acknowledgements	135
5.2.8	Appendix A: Collapse, Expansion, and Localization Operators	135

5.2.9	Appendix B: Finite-Basis Representation of the Localization Operator . . .	138
5.2.10	Appendix C: Diagrammatic Rules	140
5.3	Supporting Material	144
5.3.1	Second-Order Diagrams	146
5.4	Conclusions and Perspective	155
6	Dressed Time-Dependent Density-Functional Theory	157
6.1	Introduction	157
6.2	Assessment of Dressed TDDFT (Article)	158
6.2.1	Introduction	159
6.2.2	Formal Equations	161
6.2.3	Implementation	163
6.2.4	Computational Details	165
6.2.5	Results	166
6.2.6	Conclusion	176
6.2.7	Acknowledgments	177
6.2.8	Appendix A: Kohn-Sham-based Second-Order Propagator	178
6.3	Conclusions and Perspective	179
III	Future Prospects and Conclusions	181
7	Coupling between the Reference and the Excitations	183
7.1	Introduction	183
7.2	S ₁ /S ₂ Conical Intersection of Ethylene (in preparation)	183
7.2.1	Introduction	184
7.2.2	Theoretical Method	185
7.2.2.1	Spin-flip TDDFT	185
7.2.2.2	Dressed TDDFT	187
7.2.3	Computational Details	188
7.2.4	Results and Discussion	189
7.2.5	Conclusion and Perspectives	192
7.2.6	Acknowledgments	192
7.3	Conclusions and Perspective	192
8	Real-time Dressed TDDFT	195
9	Final Conclusions	199
	Bibliography	203
	List of Figures	221
	List of Tables	225
	Introduction et Conclusions (en français)	227

List of Acronyms and Notation¹

ALDA	Adiabatic local density approximation.
CI	Configuration interaction.
CIS	Configuration interaction singles.
CISD	Singles and doubles configuration interaction.
DFT	Density-functional theory.
GGA	Generalized gradient approximation.
HF	Hartree-Fock.
HK	Hohenberg and Kohn.
KS	Kohn and Sham.
LDA	Local density approximation.
LR	Linear response.
OEP	Optimized effective potential.
PES	Potential energy surface.
RG	Runge and Gross.
RPA	Random phase approximation.
SF	Spin-flip.
TDA	Tamm-Dancoff approximation.
TDDFT	Time-dependent density-functional theory.
TDHF	Time-dependent Hartree-Fock.
TDKS	Time-dependent Kohn-Sham.
TDSE	Time-dependent Schrödinger equation.
TF	Thomas and Fermi.
xc	Exchange-correlation.
\mathbf{r}_i	Space coordinate of particle i .
σ_i	Spin coordinate of particle i .
$\mathbf{x}_i = (\mathbf{r}_i, \sigma_i)$	Space-spin coordinate of particle i .
$\mathbf{i} = (\mathbf{x}_i, t_i)$	Space-spin-time coordinate of particle i .
A ; a	Boldface letter for matrix or vector notation.
\hat{A}	Hilbert space operator.
\check{A}	Liouville space operator.
$ \Psi\rangle ; \Psi(t)\rangle$	Time-independent/dependent many-body wave function.
$ \Phi\rangle ; \Phi(t)\rangle$	Time-independent/dependent independent single determinant.
$\phi_i(x_j) ; \phi_i^{\sigma_j}(\mathbf{r}_j)$	One particle spin-orbital.
$a - h$	Index for unoccupied orbitals.
$i - o$	Index for occupied orbitals.
$p - z$	Index for unspecified orbitals.
$(i \hat{A} i)$	Integral notation $\int d^3r_1 \phi_i^*(\mathbf{r}_1) \hat{A} \phi_i(\mathbf{r}_1)$.
$(pq rs)$	Integral notation $\int d^3r_1 \int d^3r_2 \phi_p^*(\mathbf{r}_1) \phi_q(\mathbf{r}_1) [1/ \mathbf{r}_1 - \mathbf{r}_2] \phi_r^*(\mathbf{r}_2) \phi_s(\mathbf{r}_2)$.
$(pq rs)$	Direct minus exchange integrals: $(pq rs) = (pq rs) - (ps rq)$.

1. The notation and acronyms of this section define the global notation in this thesis. Beware that in the sections in which the content comes from publications, the notation of the article will be kept, which might repeat or slightly differ from the global notation defined here.

Introduction²

Photochemistry is the study of chemical reactivity happening in electronic excited states. In most molecules, excited states fall in an energy range between the far infrared (700-1200 nm) and the near ultraviolet (200-400 nm.) This energy is transferred to the system by chemical reaction, intermolecular energy transfer or absorption of radiation. Then, the excited system relaxes until it reaches the lowest stationary state, releasing the excess of energy by a combination of several radiative and non radiative mechanisms. Photochemistry has been traditionally used as an alternative synthetic route to thermal reactions. Cycloadditions are a well known example of photochemistry. Photochemical synthesis is regaining much importance in the field of green chemistry, which attempts to develop alternative synthetic routes which involve non-hazardous environmentally friendly reactants [1].

In the last decade, the development of ultrashort laser pulses has provided a new dimension to photochemistry. These lasers permit the development of quantum control, in which ultrashort pulses are used to produce interferences in coherent quantum states in order to direct the dynamics of wave packets [2]. In this way, reactivity in the excited state can be controlled, thus opening the way for new applications of photochemistry.

An important example that illustrates the potential of controlling photochemistry is the photosynthesis in green plants. Photosynthesis captures, transfers, and harvests sunlight energy through a series of chain reactions across several proteins. The exact electron dynamics of the efficient energy transfer reactions is yet unknown. Recent experiments on the Fenna-Matthews-Olson complex of the green sulfur bacteria (a simpler protein with a role alike to photosystems I-II in green plants) indicate that the efficient energy transfer could be due to a long-lived coherent state between the absorbing antennas and the harvesting site [3]. This state is modulated by the environment, permitting to select, upon each photon absorption, the antenna molecules that will perform more efficiently the chain of energy transfer reactions [4].

Understanding electron dynamics in biological systems will have a great impact in improving the efficiency of photovoltaic cells, although much research is still needed to understand the mechanisms. A simpler strategy for improving the efficiency of solar cells would be to use materials that generate multiple electron-hole pairs (excitons) out of a single sunlight photon [5, 6]. If these excitons could then be efficiently split and diffused to the junction, the number of charge carriers would enormously increase and so would the efficiency [7]. The possibilities of finding a cheap material with such characteristics are remote, but interesting materials are being discovered in this field [8].

The full possibilities of photochemistry are just starting to be understood and exploited, thanks in part to the use of ultrashort pulsed lasers in chemistry – the so-called femtochemistry – pioneered by the Nobel laureate A. Zewail [9]. Prior to ultrashort laser pulses, excited-state mechanisms were unaccessible experimentally, since photoproducts that last for a few femtoseconds could not be resolved with traditional spectroscopy. The theoretical predictions were matched indirectly against experiments, comparing radiative lifetimes and product distributions at the

2. Pour l'introduction en français voir le chapitre intitulé Introduction et Conclusions (en français) à la fin de la thèse

end of the photoreaction. Now, femtosecond lasers allow a direct observation of ultrashort excited state events, as well as to record properties of short-lived intermediates. A major breakthrough is the recent publication of the first direct experimental observation of a funnel in the cis to trans isomerization of 11-trans retinal molecule, which is found in the active center of the rhodopsin protein responsible of vision [10]. Funnels (avoided crossings and conical intersections) are a common non radiative mechanism in photochemistry, which allows an ultrafast hopping of the wave packet between excited states. Funnels were already predicted in the 1950s, but they were never experimentally observed before 2010.

The new time-resolved experimental techniques bring new requirements for theoretical models. Femtosecond spectroscopies are compared to simulations of real-time molecular dynamics in the excited-states. The dynamics are computationally demanding, as they can include the degrees of freedom of nuclei and the bath as well as the electron coordinates. There is an urgent need for methods that can efficiently describe electron-nuclear dynamics. A good candidate for such a method is time-dependent density-functional theory (TDDFT) [11,12]. However, present approximations in TDDFT limit its applicability to photochemistry. TDDFT is a relatively new theory, made formally exact by the Runge-Gross theorem in 1984 [13], that extends the applicability of density-functional theory (DFT) [14, 15] to non-stationary Hamiltonians. In practice, one has to approximate the unknown exchange-correlation functional. The adiabatic approximation of the functional is commonly used, and consists in taking the adiabatic limit of the exact TDDFT functional for all times. This approximation describes correlation inaccurately and, therefore, is unsuitable for photochemistry. In particular, funnels are in general not well described due to certain types of correlation effects missing in any adiabatic functional. The global objective of this thesis is to improve TDDFT functionals for describing correlation accurately enough to be generally applied to photochemistry.

Correlation is a purely quantum mechanical effect, which encompasses the cooperative movement of interacting electrons, usually decreasing the classical electron repulsion energy. For convenience, correlation will be described in the formalism of second-quantization [16]. In second-quantization, correlation contributions are depicted in Feynman diagrams that show precisely the physical electron interactions. This allows a clear classification of correlation effects. For the purposes of this thesis, it will be enough to restrict the discussion of correlation to lowest order, and hence to diagrams with interactions of double excitations at most. A generalization to higher orders is straightforward. Throughout this thesis, both the terms “correlation” and “double excitations” will be used to mean the effects beyond exchange.

The specific objectives for this thesis have been to (i) assess existing methods that include a reduced number of double excitations, (ii) provide a new method that can include double excitations in general, (iii) identify which correlation diagrams are missing in adiabatic TDDFT functionals, and (iv) add the contributions from these diagrams to adiabatic TDDFT functionals and test the potential of these many-body perturbation theory corrections to describe double excitations of systems of medium to large size.

In my work towards solving the double excitation problem, I will mainly take the perspective of quantum chemistry. TDDFT entered the quantum chemists’ toolbox thanks in part to Casida’s formulation of linear-response TDDFT (LR-TDDFT) [17]. Casida formulated LR-TDDFT in a matrix form similar to time-dependent Hartree-Fock (TDHF) [18]. In that way, LR-TDDFT could be easily implemented on top of previous implementations of TDHF. Soon after Casida’s work, LR-TDDFT was available in the main quantum chemistry packages for an enormous

community of potential users. LR-TDDFT became especially popular due to its efficiency in calculating excited states and oscillator strengths, thus opening a route to applications which were computationally forbidden to wave function methods. Optical properties of systems such as fullerenes [19–21], proteins [22, 23] and explicit solvent effects on optical properties [24] are now routinely published in scientific journals. However, LR-TDDFT with conventional functionals showed some deficiencies in the hands of the scientific community, such as the underestimation of the continuum threshold, and Rydberg [25] and charge-transfer excitations [26]. These deficiencies are partially remediated by using better exchange functionals [27, 28].

The usefulness of LR-TDDFT is now widely accepted. Notwithstanding, theoretical chemists distrust (not without reason) the ability of TDDFT to represent excited state potential energy surfaces at key points of the reaction mechanism. In this field, TDDFT must compete with multireference wave function methods at the limit of present day computers. In 2006, Martínez and coworkers stated the two main problems of TDDFT for photochemical applications: conical intersections and double excitations [29]. In 2007, Casida and coworkers clarified the ideas of Martínez *et al.* from a more correct TDDFT perspective, by performing an extensive study on the photochemical ring-opening of oxirane and the dynamics through the conical intersection [30, 31]. From these works, we can restate the two problems of TDDFT as a need for better correlation functionals, and the problem of non-interacting v -representability. In this thesis, I will focus on the correlation problem, and the v -representability problem is only briefly mentioned.

The properties of the exchange functional in TDDFT have been extensively studied in the literature [27, 32–34]. The correlation functional has attracted less attention, probably due to the complicated properties of the functional, which depends non-locally on past densities. These dependencies make the correlation functional strongly non-local in both space and time variables [35–37]. Adiabatic functionals, which are completely local in time, are frequently a crude approximation to the correlation functional. At the time in which this thesis was developed, there existed two methods that partially improved correlation beyond the adiabatic functionals: spin-flip TDDFT [38–42] developed by Krylov, Ziegler and Wang and dressed TDDFT [43, 44] developed by Maitra, Burke and coworkers. In this thesis, I provide a more general solution to the problem, by deriving a LR-TDDFT kernel with correlation using *ab initio* techniques [45]. I will show that the correlation TDDFT functional in the adiabatic approximation completely misses some second-order diagrams, which are responsible for coupling single and double excitations. These diagrams can be added to existing functionals to improve the description of correlation. A similar approach was used by Sangalli and coworkers in the context of the Bethe-Salpeter equation for extended systems using screened potentials [46–48]. They come to conclusions similar to ours.

This thesis is organized in three parts: Part I provides the background material of concepts and methodology. In chapter 1, I describe the theoretical description of photochemistry. In chapter 2, I describe *ab initio* wave function theory, focusing on the description of correlation in the excited states. In chapter 3, I describe density-functional electronic structure theory. Part II contains original research, either published and/or made available on the arXiv e-print server. In chapter 4, I describe the assessment of spin-flip TDDFT in the photochemical ring opening of oxirane. In chapter 5, I describe the derivation of a correlation functional derived from *ab initio* techniques. This kernel includes all double excitations. In chapter 6, several approximations of the *ab initio* kernel are provided and tested, that generalize the idea of dressed TDDFT and can be applied to medium and large systems. Finally, Part III contains unpublished results, future

prospects and conclusions. Throughout this thesis, I will use atomic units ($\hbar = m_e = e = 1$) unless otherwise stated.

Part I
Basic Concepts

Chapter 1

Theoretical Photochemistry

1.1 Introduction

Theoretical photochemistry provides information about the relaxation mechanisms that bring the system from the excited states back to the ground state. In this chapter, I give a phenomenological description of photochemistry, especially focusing on the role, description and physical interpretation of correlation. This will set forth the effects that we would like to describe with TDDFT.

The first step in any photochemical mechanism describes the population of a specific excited state. Excited states are populated by two main mechanisms: radiation absorption and energy transfer. In radiation absorption, the molecule absorbs a photon of a characteristic wavelength. Energy transfer occurs when a molecule in a high energy state transfers its energy to another molecule in a low energy state. The energy can be transferred either radiatively (exchange of a photon) or by electron exchange. In this chapter, I will restrict the discussion to electromagnetic radiation absorption.

Photon absorption is the easiest mechanism to selectively populate an excited state. Low-lying valence excited states are the most accessible, falling in the range of far infra-red to near ultra-violet in typical molecules. This energy is provided by radiation sources of monochromatic light, such as mercury vapor lamps. The absorption and excited state population is regulated by the dipole moment selection rules. The excited molecule relaxes back to the ground state by undergoing a series of structural changes that propitiate the release of energy.

Theoretical photochemistry explores the potential energy surfaces (PES) in search of the structures that bring the system back to a lowest-energy stationary state. The PES describes the electronic energy at a fixed nuclear position, and is a consequence of the Born-Oppenheimer approximation. The decay can be radiative (luminescence) when the molecule emits a photon, or non-radiatively when it goes through an interstate crossing (funnel.) The study of the PES gives a static picture of the possible reaction mechanisms. Often, several competing mechanisms can occur, which determine the selectivity of the reaction. This information can be obtained by performing dynamic simulations. The dynamics are beyond the scope of this thesis and will not be described. For the interested reader, see a review of dynamics and TDDFT in Ref. [49].

The chapter is organized as follows: Sec. 1.2 explains the Born-Oppenheimer separation, Sec. 1.3 clarifies the role of correlation in different regions of the PES, Sec. 1.4 describes a typical photochemical mechanism by taking the example of stilbene Z to E photoisomerization, Sec. 1.5 gives some details on the initiation of photochemical reactions by absorption of electromagnetic radiation and Sec. 1.6 describes conical intersections.

1.2 Born-Oppenheimer Separation and Potential Energy Surfaces

In a typical chemical reaction, molecules undergo a series of formation and breaking of bonds. This is intrinsically a dynamical process. The full dynamics of electrons and nuclei is described by the time-dependent Schrödinger equation,

$$i \frac{\partial}{\partial t} \Psi_I(\mathbf{x}, t, \mathbf{R}) = \hat{H} \Psi_I(\mathbf{x}, t, \mathbf{R}), \quad (1.1)$$

where $\mathbf{x}(\mathbf{R})$ is a vector of all electron(nuclei) coordinates, \hat{H} is the full Hamiltonian of the system and $\Psi_I(\mathbf{x}, \mathbf{R}, t)$ is the wave function of state I . In this section, we consider only time-independent Hamiltonians. The direct solution of Eq. (1.1) is a formidable problem. Instead, Born and Oppenheimer proposed a two-step solution by separating the electron and nuclear motions [50]. The full Hamiltonian can be separated in the nuclear kinetic operator \hat{T}_N , the nuclear repulsion \hat{V}_{NN} , and the electronic Hamiltonian (Born-Oppenheimer separation),

$$\hat{H}(\mathbf{r}, \mathbf{R}) = \hat{T}_N(\mathbf{R}) + \hat{H}^e(\mathbf{r}; \mathbf{R}) + V_{NN}(\mathbf{R}), \quad (1.2)$$

where the electron operator depends only parametrically on the nuclear geometry. The solutions of the electronic Hamiltonian describe the electronic motion at a fixed nuclear geometry,

$$\hat{H}^e(\mathbf{r}; \mathbf{R}) \Psi_I^e(\mathbf{x}; \mathbf{R}) = E_I^e(\mathbf{R}) \Psi_I^e(\mathbf{x}; \mathbf{R}). \quad (1.3)$$

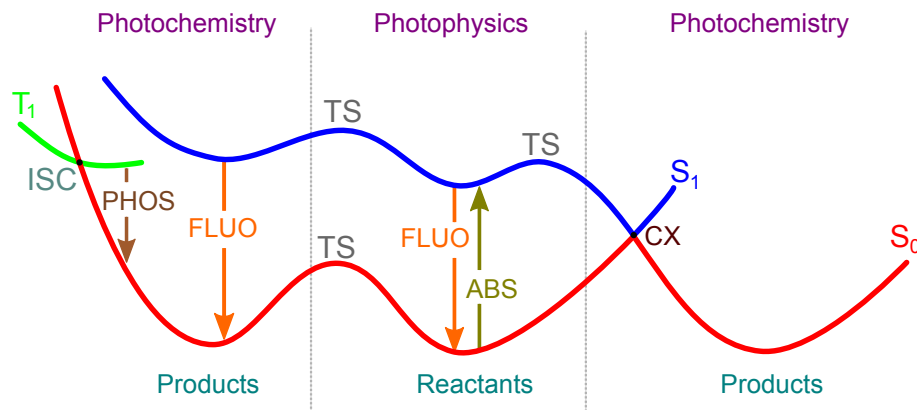
The energy $E_I^e(\mathbf{R}) + V_{NN}(\mathbf{R})$ is the so-called adiabatic energy, and its plot versus different nuclear internal coordinates is the so-called potential energy surface (PES.) This energy is a physically valid description whenever the nuclei move more slowly than the electrons. Equations (1.2) and (1.3) define the Born-Oppenheimer approximation.

The solutions of Eq. (1.3) are usually a valid approximation for describing ground-state reactivity. Photochemistry, instead, frequently reaches regions in the PES of the excited states in which the approximation breaks down. To illustrate that, a generic photochemical mechanism is shown in Fig. 1.1, in which the critical points of a photoreaction are shown. Reactants start initially in the minimum basin of the lowest PES. After energy is absorbed, the system reaches the excited state and starts to propagate on the first singlet PES. A mechanism to decay back to the ground state happens when the system reaches the conical intersection region. Around this point, in which the ground and the excited PES are degenerate, the nuclei move as fast as the electrons, and the Born-Oppenheimer separation is not valid. In this case, the coupling between the electrons and nuclear dynamics (vibronic coupling) has to be taken into account. This coupling can be included in a post-Born-Oppenheimer calculation via the Born-Huang approach [51],

$$\left[\hat{T}_N(\mathbf{R}) + E_I^e(\mathbf{R}, t) \right] \chi_I(\mathbf{R}, t) - \sum_J V_{IJ}(\mathbf{R}) \chi_J(\mathbf{R}, t) = i \frac{\partial \chi_I(\mathbf{R}, t)}{\partial t}, \quad (1.4)$$

where $V_{IJ}(\mathbf{R})$ are the vibronic coupling terms that couple different adiabatic states and $\chi_I(\mathbf{R}, t)$ is the nuclear wave function of adiabatic state I . For the purposes of this thesis, it is not necessary

Figure 1.1 Schematic plot of three electronic state potential energy surfaces $E^e(\mathbf{R}) + V_{NN}(\mathbf{R})$ corresponding to the ground-state singlet S_0 and the first triplet T_1 and singlet S_1 excited states. The ordinate component corresponds to some nuclear geometry and the abscissa gives the total electronic energy. In the graph, TS stands for transition state, ISC stands for intersystem crossing, PHOS stands for phosphorescence, FLUO stands for fluorescence, ABS stands for absorption and CX stands for conical intersection.



to go further into details regarding the actual form of the vibronic couplings. For the interested reader, excellent literature exist on this topic [52–54].

The funnel region is more easily described in terms of the diabatic PES than in coupled adiabatic PESs. The diabatic surfaces are defined as the unitary transformation of adiabatic states in which the coupling terms are zero, $V_{IJ}(\mathbf{R}) = 0$. Whenever possible, this representation allows a clearer interpretation of funnels in terms of the wave functions of Eq. (1.3). Note that, strictly speaking this is only rigorously possible in the case of two electronic states, though an approximate diabaticization may be possible for several electronic states at a time.

1.3 Correlation in Excited States

An accurate account of correlation is required for a reasonable physical description of electronic states in general and excited states in particular. For many molecules, the existence of funnels between electronic states is possible thanks to electron correlation. In this section, I clarify the physical effects introduced by correlation.

Correlation is a concept frequently discussed in quantum chemistry, which encompasses many effects due to electronic interaction. Unfortunately, the definition of correlation depends upon the choice of a zero-order uncorrelated system of electrons. A common choice is due to Löwdin, who defined correlation as the difference between the exact energy and the Hartree-Fock energy

$$E_c = E_{exact} - E_{HF}, \quad (1.5)$$

where E_{exact} is the exact lowest eigenvalue of Eq. (1.3). This definition can be misleading, as it is geometry dependent, due to the fact that it relies on the Born-Oppenheimer approximation. In fact, correlation can include completely different physical effects in different regions of the potential energy surface. Furthermore, Löwdin's definition cannot be easily applied to excited states, as they are usually described by more than one determinant.

Correlation can be roughly classified as static or dynamic, depending respectively whether near degeneracies or an accurate description of the electron-electron wave function cusp is judged to be more critical. Each electronic state requires a specific treatment of both correlation effects. In fact, the choice of basis sets and correlation methods has to be carefully studied for each system [55,56]. In order to guide the choice of method, states are commonly classified as valence or Rydberg according to the diffuseness of the density, and ionic or covalent according to the valence-bond interpretation of the wave function. States are valence if they are characterized by compact densities, and they are Rydberg if densities span a large space. Rydberg states are usually more difficult to describe as they require the use of large diffuse basis sets. Even if one aims to describe valence states only, nearby Rydberg states must still be converged. This means that diffuse bases are still needed to avoid unrealistic valence-Rydberg state mixing. Further, a state is ionic if the valence-bond analysis of the wave function give localized electron pairs in atoms, or covalent if electrons are shared between neighbor atomic sites. Ionic states usually have larger contributions due to dynamic correlation, since the localization of electrons induces larger polarizations of the density. Covalent states have a larger contribution of static correlation in order to eliminate the ionic contributions of the wave function.

In general, it is difficult to determine *a priori* whether an electronic state will be ionic or covalent, valence, or Rydberg. However, the basis set and the correlation method has to be carefully chosen according to the nature of the state, since otherwise the wrong qualitative picture is obtained. For example, there are still long-standing controversies concerning the energetic position of valence $\pi \rightarrow \pi^*$ states in many conjugated organic molecules. These molecules have two characteristic singlet states, one ionic (L_a) and one covalent (L_b). The L_a state normally requires a treatment of dynamic correlation whereas static correlation is more important in L_b . Difficulties arise when the two states are nearly degenerate, like in the butadiene molecule, for which no consensus has been reached on the ordering of the 1^1B_u (L_a) and the 2^1A_g (L_b) states. I will describe this example in more detail in the up-coming chapters, as the 2^1A_g is a prototypical state with a large double-excitation contribution.

To illustrate the role of correlation in ionic and covalent states, I will discuss the dissociation of molecular hydrogen [57]. The H_2 molecule is particularly suitable for the discussion of correlation, since the role of exchange is only to correct the self-interaction error. In a minimal basis set of one atomic orbital per hydrogen atom, the H_2 molecule has two orbitals, the σ -bonding orbital

$$\sigma(\mathbf{r}) = \frac{1}{\sqrt{2(1+S)}} [1s_A(\mathbf{r}) + 1s_B(\mathbf{r})], \quad (1.6)$$

and the σ -antibonding orbital

$$\sigma^*(\mathbf{r}) = \frac{1}{\sqrt{2(1-S)}} [1s_A(\mathbf{r}) - 1s_B(\mathbf{r})], \quad (1.7)$$

where the functions $1s_{A(B)}$ are the atomic orbitals centered one on each hydrogen center and S is the overlap between the two, $S = \langle 1s_A | 1s_B \rangle$. At the equilibrium geometry, the ground state is well represented by the single Slater determinant $|\sigma^\alpha \sigma^\beta\rangle$. The singlet and triplet excited states are combinations of the determinant formed by substituting one of the ground-state σ orbitals by a σ^* orbital. Pure spin states require minus and plus combinations of the two determinants, $|\sigma^\alpha \sigma^{*\beta}\rangle \pm |\sigma^\beta \sigma^{*\alpha}\rangle$. In a second-quantization description, these states can be seen as a promotion of one electron from one occupied orbital to a virtual, and therefore they are referred to as single excitation states. Finally, one can form a third excited state by substituting two σ orbitals by two σ^* orbitals. This is a double excitation $|\sigma^{*\alpha} \sigma^{*\beta}\rangle$ with respect to the ground state determinant.

The ionic or covalent character of the ground-state wave function depends on the distance between the two hydrogen atoms. At the equilibrium geometry, the ground-state wave function is well represented by the single determinant $|\sigma^\alpha \sigma^\beta\rangle$. The corresponding valence-bond wave function of this state is given by

$$|\sigma^\alpha \sigma^\beta\rangle = \frac{1}{2(1+S)} \left[|1s_A^\alpha 1s_A^\beta\rangle + |1s_B^\alpha 1s_B^\beta\rangle + |1s_A^\alpha 1s_B^\beta\rangle + |1s_B^\alpha 1s_A^\beta\rangle \right]. \quad (1.8)$$

The first two contributions are clearly ionic, representing the configurations $H_A^- H_B^+$ and $H_A^+ H_B^-$ (two electrons localized in one center,) whereas the two last contributions are covalent, representing the configurations $H_A^\uparrow H_B^\downarrow$ and $H_A^\downarrow H_B^\uparrow$ (one electron in each center.) Then, the ground-state has equal contributions of ionic and covalent components. For this state, correlation is only dynamic, describing the slight polarization of the orbitals with respect to a pure covalent picture. The excited states are represented by different linear combinations of the same ionic and covalent contributions. For example, the double excitation is represented by

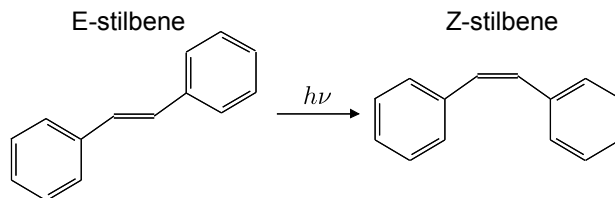
$$|\sigma^{*\alpha} \sigma^{*\beta}\rangle = \frac{1}{2(1-S)} \left[|1s_A^\alpha 1s_A^\beta\rangle + |1s_B^\alpha 1s_B^\beta\rangle - |1s_A^\alpha 1s_B^\beta\rangle - |1s_B^\alpha 1s_A^\beta\rangle \right]. \quad (1.9)$$

At the dissociation limit, the ground-state wave function becomes purely covalent. This is the classical assumption taken by Heitler and London to describe dissociation of homopolar diatomic molecules [58], so that two equivalent atoms are obtained at infinite interatomic distance, described by the single determinant $|1s_A^\alpha 1s_B^\beta\rangle$. In a molecular orbital picture, this is represented by

$$|1s_A^\alpha 1s_B^\beta\rangle = \frac{1+S}{\sqrt{2}} |\sigma^\alpha \sigma^\beta\rangle + \frac{1-S}{\sqrt{2}} |\sigma^{*\alpha} \sigma^{*\beta}\rangle - \frac{1}{\sqrt{2}} \left[|1s_A^\alpha 1s_B^\beta\rangle + |1s_B^\alpha 1s_A^\beta\rangle \right]. \quad (1.10)$$

The molecular orbital picture gives a mixture of the ground-state and the double excitation determinants. Here, the role of double excitations is to eliminate the ionic contributions of the ground-state wave function. A single Slater determinant of molecular orbitals will overestimate the ionic contributions, and therefore is unsuccessful in describing dissociation. This is a typical example in which a treatment of static correlation is needed.

Figure 1.2 Photoisomerization reaction of E-stilbene to Z-stilbene. The reaction takes place after absorption of a photon of 500 nm or shorter wavelength.



1.4 Example of a Photochemical Reaction: Stilbene Photoisomerization

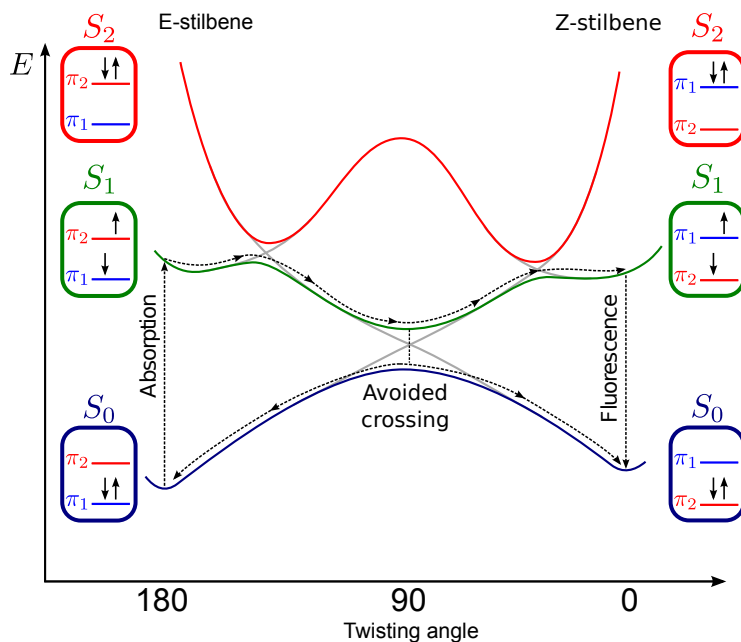
Previous sections have described in some detail potential energy surfaces, the Born-Oppenheimer approximation, and role of correlation energy. These are the disjoint parts needed for understanding photochemical mechanisms. In this section, we shall focus on the theoretical description of photochemical mechanisms as a whole.

In Fig. 1.1, we already saw a schematic representation of the general decay mechanisms that can occur for excited states. Initially, the reactants start at the minimum of some ground-state surface. After absorption of a photon, the system reaches the excited state surface. This transition is considered to be essentially a vertical excitation (Franck-Condon transition), in which the nuclear geometry undergoes little change. The region of the excited-state surface around the ground-state reactant minimum is called the Franck-Condon region, where the decay to the ground state brings the system back to the initial geometry in the lowest energy state (photophysics.) Photochemistry happens away from the Franck-Condon region, when geometrical relaxation brings the system in a new minimum corresponding to the products. The decay might be radiative (luminescence) or through a conical intersection. We distinguish two types of luminescence: fluorescence, when the transition happens between two singlet surfaces, and phosphorescence, when the transition happens between a singlet and a triplet surface.

It is interesting to see how electronic structure theory describes the mechanism in terms of electronic configurations. For that purpose, we take a realistic example: the E to Z photoisomerization [59]. This reaction involves a 180° twisting of the phenyl groups around the central double bond (see Fig. 1.2.) Stilbene and stilbenoid derivatives are an important group of molecules with many applications. Resveratrol is a hydroxylated stilbene derivative found in wine, which is thought to have numerous health benefits (anti-oxidizing, anti-carcinogenic, anti-aging, etc.) The 1,2-bis(2-pyridyl)ethylene, a bidentate ligand with similar structure and photochemical properties to stilbene, is used in organometallic complexes in order to transfer the absorbed energy to the central metal.

The singlet photochemical mechanism of stilbene isomerization is shown in Fig. 1.3, in which the PESs of the first three singlet states are represented against the twisting angle of the central double bond. The blue surface represents the ground-state S_0 , the green surface S_1 is the first

Figure 1.3 Schematic singlet mechanism of stilbene photoisomerization. The E-stilbene absorbs a photon that brings the molecule to the S_1 excited state of single-excitation nature. The decay to the ground-state can happen by two competing mechanisms, either a conical intersection or fluorescence. In the graph, the conical intersection is not completely seen, but just the avoided crossing. This is due to the fact that we are plotting against one dimension only.



excited state and the red surface S_2 is the second excited state. The reaction starts at the left minimum of the S_0 surface with the two phenyl groups separated by 180° (E-stilbene). After absorption of one photon, the molecule is excited to the S_1 surface. The excited molecule can undergo several decay trajectories, shown with a dashed arrowed line. One of the mechanisms brings the molecule in the minimum at the right side of S_1 , decaying to the Z-stilbene minimum of S_0 by fluorescence. Another possibility is to decay non-radiatively through a conical intersection. The figure only shows a piece of the intersection, commonly called an avoided crossing, which indicates that the intersection point falls in a nearby geometry. Traversing a conical intersection is an intrinsically dynamical process, in so far as the direction in which the wave-packet propagates through it depends on the previous propagation and on the form of the intersection region. The decay can therefore take the molecule either way on S_0 , either forming the photoproduct Z-stilbene or going back to the initial E-stilbene reactant.

The whole mechanism can be easily explained by simple electronic structure arguments by using a two-level model of π orbitals. The S_0 , S_1 , and S_2 surfaces of both E-stilbene and Z-stilbene

at the respective equilibrium geometries are well represented by a single Slater determinant. Similar to the case of H_2 dissociation, the S_1 is a single excitation with respect to S_0 , and S_2 is a double excitation. It is interesting to notice that there is a swap ping of electronic configurations between the E and Z forms, i.e., the S_0 configuration of E-stilbene is the same as the S_2 of Z-stilbene and the S_2 configuration of E-stilbene becomes the S_0 of Z-stilbene. This swap of configurations occurs at the avoided crossings, which happen whenever two surfaces with the same symmetry cross. At each avoided crossing, two grey lines are depicted, representing the diabatic surfaces. Following the diabatic lines helps to visualize the change of configuration that is taking place. For example, $|\pi_1^\alpha \pi_1^\beta\rangle$ is the dominant configuration of the S_0 surface of equilibrium E-stilbene. When the central double bond is twisted, an avoided crossing occurs at around 90° , indicating a mixture with the double excitation $|\pi_2^\alpha \pi_2^\beta\rangle$ that is coming down. The diabatic line follows the configuration in the case of no interaction. After 90° , the configuration that corresponded previously to S_0 is now S_1 . At around 50° , another crossing occurs between $|\pi_1^\alpha \pi_1^\beta\rangle$ and the single excitation $|\pi_1^\alpha \pi_2^\beta\rangle$. As a result, the S_0 of E-stilbene has become the S_2 of Z-stilbene. The avoided crossings explain the PESs shape of minima and maxima.

1.5 Photoabsorption

The most basic mechanism of accessing the excited state is the absorption of an electromagnetic wave of an appropriate wavelength. The absorption of radiation occurs due to the coupling between the oscillating electric field and the electron density, which induces a transition dipole moment. The transition dipole moment is directly proportional to the oscillator strength, allowing a direct calculation of the absorption spectrum. From Fermi's golden rule, we can establish this relation

$$f_{FI} = \frac{2}{3} \omega_{FI} |\langle \Psi_I^e | \hat{\mu} | \Psi_F^e \rangle|^2, \quad (1.11)$$

where f_{FI} is the oscillator strength, F(I) is the final(initial) state index, $\omega_{FI} = E_F - E_I$ is the excitation energy and $\langle \Psi_I | \hat{\mu} | \Psi_F \rangle$ is the transition dipole moment. Equation (1.11) is derived assuming the dipole approximation, which is valid whenever the wave length of the electromagnetic radiation is much larger than typical bond distances.

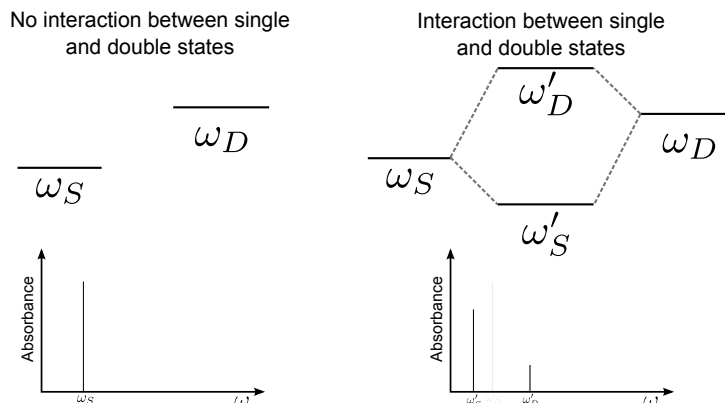
There are electronic states that, due to symmetry reasons, are not coupled by the dipole moment. The states that have a nonzero transition dipole moment and are called bright. States with zero transition dipole moment are called dark. From the spin symmetry, only the singlet states are bright. From the spatial symmetry, a state can only be bright if the decomposition of the direct products of the irreducible representation of the initial state and dipole operator contains the irreducible representation of the final state.

The dipole moment operator is a one electron operator of the form

$$\hat{\mu} = -i\mathbf{r}. \quad (1.12)$$

This operator is only able to couple singly-excited states, and double excitations are in general dark. Still, double excitation states can be populated during the course of a photoreaction. For example, stilbene absorbs one photon and the molecule is brought to the S_1 surface, which is

Figure 1.4 Appearance of dark states in the absorption spectrum due to the coupling with a bright peak. On the left side, when no interaction is present, the dark peak does not appear in the spectrum and the bright peak has full strength. On the right side, the bright and dark states interact through configuration mixing, and the “dark state” appears by borrowing intensity from the bright.



represented by a single-excitation. During the dynamics of the wavepacket in the S_1 surface, the double-excitation state is populated when the funnel region around 90° is reached. In special cases, double-excited states can be coupled by the dipole moment. This happens when a dark peak interacts through correlation with a bright peak, borrowing some of the intensity of the latter. This is schematically represented in Fig. 1.4. In the case of no interaction between a singly-excited state (ω_S) and a doubly-excited state (ω_D), only one peak appears in the spectrum at the excitation energy ω_S . When interaction between the two states occurs, the effect on the spectrum is two fold: on the one hand, a red-shift of the single excitation is seen due to the stabilization of the non-interacting single excitation. On the other hand, the spectrum is split in two peaks. The ω'_S peak is less intense than the original ω_S peak, but a new peak appears at ω'_D . The sum-rule of intensities show that $f'_S + f'_D = f_D$.

1.6 Conical Intersections

Funnels are a ubiquitous mechanism in photochemical reactivity, offering a fast non-radiative route back to the ground-state. The appearance of a funnel indicates an interchange of two electronic configuration of the same symmetry. In the funnel region, the vibronic couplings become important and the Born-Oppenheimer approximation has to be complemented by non-adiabatic terms that couple various adiabatic surfaces. In this section, I briefly describe some further details on the shape and description of conical intersection regions.

There are some conditions for a conical intersection to occur. I take the example of a conical intersection between two electronic states. (It is straightforward to generalize these ideas to three or more electronic states.) Two electronic states form a conical intersection if they become degenerate on one nuclear geometry point at least. Two conditions must be satisfied for that degeneracy to happen. The first condition is obviously that the two electronic states are degenerate,

$$E_1^e(\mathbf{R}_{CI}) = E_2^e(\mathbf{R}_{CI}), \quad (1.13)$$

where \mathbf{R}_{CI} is the nuclear geometry of the conical intersection, at which this condition is satisfied. The second condition is that the interaction between the two states is zero,

$$H_{12}(\mathbf{R}_{CI}) = 0, \quad (1.14)$$

where $H_{12}(\mathbf{R}_{CI})$ is the coupling between the two states with the Hamiltonian at the intersection geometry. These conditions can be satisfied in various ways according to symmetry arguments. We distinguish three main groups: (i) symmetry-required conical intersections, also called Jahn-Teller intersections, happen between states in which symmetry forces the satisfaction of both conditions. This type of intersection has dimension N_{int} , where N_{int} is the number of internal coordinates. An example is the doubly-degenerate E_1 states in H_3 in D_{3h} symmetry. (ii) symmetry allowed conical intersections happen between states of different symmetry. Then, the second condition is trivially satisfied. Such conical intersections have dimension $N_{int} - 1$ and appear as a seam, i.e. a hyperline of degeneracy. (iii) ‘‘accidental’’ same-symmetry conical intersections. These intersections touch in one point and have a dimension of $N_{int} - 2$. They are described by two coordinates, commonly referred as the g-h coordinates or the branching plane, that lift the degeneracy linearly.

Chapter 2

Wave-Function Based Electronic Structure

2.1 Introduction

Wave-function electronic-structure theory is presently the only successful theory to describe accurately enough general photochemical problems. Frequently, density functionals try to mimic the properties of wave function theory in order to improve their description. In this chapter, I will briefly describe the most important wave function methods that can calculate excited states. This will lay the ground for understanding the missing correlation effects of TDDFT functionals. Henceforth, I will assume the Born-Oppenheimer approximation unless otherwise stated (see Chap. 1, Sec. 1.2.)

The principal goal of wave-function-based theory is to obtain the energies and wave functions of the system, that are used to solve the Schrödinger equation. There are two common approaches used to solve the excited states. The first approach considers that excited states are stationary states, in which case we solve a static Schrödinger equation,

$$\hat{H}^e \Psi_I^e(\mathbf{x}; \mathbf{R}) = E_I^e \Psi_I^e(\mathbf{x}; \mathbf{R}). \quad (2.1)$$

This equation has an infinite number of (discrete) solutions, which can be ordered as $E_0 \leq E_1 \leq \dots$, where E_0 is the ground-state energy and $E_I (> E_0)$ are the excited states. The second approach extracts excited state information from the dynamics of some ground-state density in a time-dependent electric field. The dynamics are described by solving the time-dependent Schrödinger equation (TDSE),

$$i \frac{\partial \Psi_I^e(\mathbf{x}, t; \mathbf{R})}{\partial t} = \hat{H}^e(t) \Psi_I^e(\mathbf{x}, t; \mathbf{R}), \quad (2.2)$$

where $\hat{H}^e(t)$ is equal to the static electronic Hamiltonian plus a time-dependent applied field. The static and dynamic descriptions are in fact equivalent when the Hamiltonian is time-independent. In the case of stationary states the wave functions differ by a phase-factor

$$\Psi_I^e(\mathbf{x}, t; \mathbf{R}) = e^{-iE_I t} \Psi_I^e(\mathbf{x}; \mathbf{R}), \quad (2.3)$$

which is irrelevant for the calculation of most physical properties, as it cancels out when we calculate the density matrix (i.e, physical properties of stationary states are stationary in time.)

The variational principle is commonly used to extract solutions of the static Schrödinger equation, by starting with an initial *ansatz* for the wave function $\Psi_I^e(\mathbf{x}; \mathbf{R})$ which is then systematically improved. The *ansatz* is formed as a combination of Hilbert space basis set functions that depend on all the electronic coordinates. The basis functions are normally constructed in the form of determinants of single-particle functions, the so-called Slater determinants. The choice of single-particle functions is not unique. The discussion in this thesis is restricted to molecular orbitals

delocalized over the whole molecule. The molecular orbitals are optimized for each system, by expanding them in a basis of single-particle atom-centered orbitals (atomic orbitals.) This is a common choice in quantum chemistry.

The simplest lowest energy variational solution of the static Schrödinger equation is given by the Hartree-Fock approach. Hartree-Fock (HF) uses a single Slater determinant as *ansatz* for the wave function. The molecular orbitals are optimized so that the HF wave function gives the lowest possible total energy. A single Slater determinant is usually enough to describe the ground-state of closed-shell molecules at their equilibrium geometry. Open-shells and excited states require a more sophisticated *ansatz* with more than one determinant. The extra determinants are systematically constructed using a configuration interaction (CI) expansion, in which excitation operators are applied to a reference determinant. For convenience, the reference is taken as the HF determinant.

Variational solutions give a good first approximation to the wave function, but the correlation energy is inaccurate. In fact, correlation is an effect requiring a large set of basis functions with small contributions to the energy. The variational principle is not efficient enough to include these effects, and correlation is commonly improved in a second step. The easiest correlated post-variational method is perturbation theory, under the assumption that the correlation contributes a small effect to the total energy. In cases in which perturbation theory does not converge, the CI expansion can be used, although it has low convergence and the computational cost is large.

Excited states are difficult to obtain altogether, since a treatment of correlation *a posteriori* is usually unsuccessful if the orbitals of the variational principle are not specifically optimized for the excited states. A variational optimization of orbitals for the excited states is difficult to apply, since the variational principle converges to the lowest energy state by construction. At most, constraints in the variational optimization can be imposed to converge to the lowest energy state of each irreducible representation in symmetric molecules. Higher-energy excited states can be obtained by performing a double variational optimization of the CI expansion coefficients and the orbitals of the determinants, to which the usual post-variational methods (perturbation theory or CI) are applied in a second step to improve correlation. These methods are computationally very expensive, but presently these methods are the state-of-the-art in photochemistry.

The solution of the TDSE does not require the application of the variational principle to the excited states, thus offering an efficient alternative route to obtain excited state solutions. The TDSE is a first-order differential equation in time, and so the whole electron dynamics requires only the exact solution at an initial time. Frequently, the initial condition is taken as an approximate ground-state variational solution of the static Schrödinger equation, which is then propagated over time. There are several ways to propagate this initial state. A simple strategy is to propagate the wave function in real-time by applying classical numerical methods to solve first-order differential equations. In this way, the wave function is known at all times and so any time-dependent property can be calculated. Another method is the linear response solution. This method relies on a perturbative solution of the Fourier-transformed TDSE, from which excitation energies to the stationary excited states are directly obtained.

This chapter is organized as follow. The first part explains in some detail the methods to solve the static Schrödinger equation. In Sec. 2.2, I describe the variational principle of quantum mechanics, in Sec. 2.2, I briefly explain the HF approach, and in Sec. 2.4, I describe the configuration interaction method. The linear response solution of the TDSE is explained in Sec. 2.5. All

these methods are well established in the quantum chemistry community, and good introductions are available in standard textbooks, for example Refs. [57], [60] and [16].

2.2 Variational Principle

The eigenvectors of a bound Hermitian operator form a complete basis set in the Hilbert space [60]. This property of Hermitian operators is used to demonstrate that any trial wave function gives an upper bound to the exact lowest energy eigenvalue. This is in essence the variational principle of quantum mechanics, giving an important criterion to improve approximate wave function.

The demonstration of the variational principle is straightforward. The energy can be written as a functional of the wave function,

$$E_0[\Psi_0] = \frac{\langle \Psi_0 | \hat{H} | \Psi_0 \rangle}{\langle \Psi_0 | \Psi_0 \rangle}, \quad (2.4)$$

Any trial wave function $|\tilde{\Psi}_0\rangle$ (satisfying the same boundary conditions as the true wave function) will have an expansion in the exact wave functions

$$|\tilde{\Psi}_0\rangle = \sum_{I=0}^{\infty} \langle \Psi_I | \tilde{\Psi}_0 \rangle |\Psi_I\rangle, \quad (2.5)$$

which can be inserted in Eq. (2.4) to obtain

$$E_0[\tilde{\Psi}_0] = \sum_{I=0}^{\infty} |\langle \Psi_I | \tilde{\Psi}_0 \rangle|^2 \langle \Psi_I | \hat{H} | \Psi_I \rangle = \sum_{I=0}^{\infty} |\langle \Psi_I | \tilde{\Psi}_0 \rangle|^2 E_I, \quad (2.6)$$

in which we considered that the trial wave function is normalized. Considering that the energies are ordered in increasing order, i.e., $E_0 \leq E_1 \leq E_2 \leq \dots$, and due to the fact that the basis is complete,

$$\sum_{I=0}^{\infty} |\langle \Psi_I | \tilde{\Psi}_0 \rangle|^2 = 1, \quad (2.7)$$

we can straightforwardly conclude that any trial wave function will give an upper bound to the exact ground-state energy

$$E_0[\tilde{\Psi}_0] > E_0[\Psi_0]. \quad (2.8)$$

In the next section, we apply the variational principle to the simplest wave function, a single Slater determinant.

2.3 Hartree-Fock

The HF approximation considers that the exact wave function is well described by a single Slater determinant

$$|\Psi\rangle \approx |\Phi\rangle = \frac{1}{\sqrt{N!}} \sum_i^{N!} (-1)^{i+1} \mathcal{P}_i \{ \phi_1(\mathbf{x}_1) \dots \phi_N(\mathbf{x}_N) \}, \quad (2.9)$$

where \mathcal{P}_i is the i -th permutation of the electron coordinates. The functions $\phi_1(\mathbf{x}_1)$ are molecular spin-orbitals that contain one electron. These orbitals are solution of a one-electron Schrödinger equation

$$\hat{f}\phi_i(\mathbf{x}) = \epsilon_i \phi_i(\mathbf{x}), \quad (2.10)$$

where \hat{f} is a Fock operator, and ϵ_i is the orbital energy. The HF orbitals are the solution of a one particle equation of that type, with the constraint that they minimize the total energy. The total energy of a general single Slater determinant is

$$E[\Phi](\mathbf{R}) = T_s[\Phi] + V_{ext}[\Phi](\mathbf{R}) + E_H[\Phi] + E_x[\Phi] + V_{NN}(\mathbf{R}), \quad (2.11)$$

where T_s is the electronic kinetic energy contribution

$$T_s[\Phi] = -\frac{1}{2} \sum_i^{occ} \int d^3r \phi_i^*(\mathbf{r}) \nabla^2 \phi_i(\mathbf{r}), \quad (2.12)$$

$V_{ext}[\Phi](\mathbf{R})$ contains the electron-nuclear attraction

$$V_{ext}[\Phi] = - \sum_{I(i \in occ)} Z_I \int d^3r \phi_i^*(\mathbf{r}) \frac{1}{|\mathbf{R}_I - \mathbf{r}|} \phi_i(\mathbf{r}), \quad (2.13)$$

$E_H[\Phi]$ is the Hartree energy

$$E_H[\Phi] = \frac{1}{2} \sum_{ij}^{N_e} \int d^3r_1 \int d^3r_2 \frac{\phi_i^*(\mathbf{r}_1) \phi_i(\mathbf{r}_1) \phi_j^*(\mathbf{r}_2) \phi_j(\mathbf{r}_2)}{|\mathbf{r}_1 - \mathbf{r}_2|} = \frac{1}{2} \int d^3r_1 \int d^3r_2 \frac{\rho(\mathbf{r}_1) \rho(\mathbf{r}_2)}{|\mathbf{r}_1 - \mathbf{r}_2|}, \quad (2.14)$$

and $E_x[\Phi]$ is the exchange energy

$$E_x[\Phi] = -\frac{1}{2} \sum_{ij}^{N_e} \int d^3x_1 \int d^3x_2 \frac{\phi_i(\mathbf{x}_1) \phi_j^*(\mathbf{x}_1) \phi_i^*(\mathbf{x}_2) \phi_j(\mathbf{x}_2)}{|\mathbf{r}_1 - \mathbf{r}_2|} = -\frac{1}{2} \int d^3x_1 \int d^3x_2 \frac{\gamma(\mathbf{x}_1, \mathbf{x}_2) \gamma(\mathbf{x}_2, \mathbf{x}_1)}{|\mathbf{r}_1 - \mathbf{r}_2|}. \quad (2.15)$$

The nuclear-nuclear attraction is a constant number that does not depend on the Slater determinant

$$V_{NN}(\mathbf{R}) = \frac{1}{2} \sum_{I,J}^{N_N} \frac{Z_I Z_J}{|\mathbf{R}_I - \mathbf{R}_J|}. \quad (2.16)$$

The optimal orbitals (the HF orbitals) that minimize the energy are obtained by constructing

$$L[\Phi] = E[\Phi] - \sum_{ij} \lambda_{ij} (1 - \langle \phi_i | \phi_j \rangle), \quad (2.17)$$

and minimizing with respect to variations of the orbitals. The result is an equation of the form of Eq. (2.10), where the Fock operator \hat{f}^{HF} is given by

$$\hat{f}^{HF}(\mathbf{x}; \mathbf{R}) = \hat{t}(\mathbf{r}) + v^{HF}[\phi_k](\mathbf{x}; \mathbf{R}), \quad (2.18)$$

where

$$\hat{t}(\mathbf{r})\phi_k(\mathbf{x}) = \frac{\delta T_s[\Phi]}{\delta \phi_k^*(\mathbf{x})} = -\frac{1}{2}\nabla^2\phi_k(\mathbf{x}) \quad (2.19)$$

and $v^{HF}[\phi_k](\mathbf{x})$ is the mean field potential that an electron feels due to its interaction with other electrons,

$$\begin{aligned} \hat{v}^{HF}[\phi_k](\mathbf{x}; \mathbf{R})\phi_k(\mathbf{r}) &= \left(\frac{\delta V_{ext}[\Phi](\mathbf{R})}{\delta \phi_k^*(\mathbf{x})} + \frac{\delta E_H[\Phi]}{\delta \phi_k^*(\mathbf{x})} + \frac{\delta E_x[\Phi]}{\delta \phi_k^*(\mathbf{x})} \right) \phi_k(\mathbf{x}) \\ &= \left(v_{ext}(\mathbf{r}; \mathbf{R}) + v_H(\mathbf{r}) + \hat{\Sigma}_x^{HF}[\gamma] \right) \phi_k(\mathbf{x}), \end{aligned} \quad (2.20)$$

where the external potential is defined as

$$v_{ext}(\mathbf{r}; \mathbf{R}) = - \sum_I^{N_N} \frac{Z_I}{|\mathbf{R}_I - \mathbf{r}|}, \quad (2.21)$$

the Hartree potential is defined as

$$v_H(\mathbf{r}) = \int d^3r_1 \frac{\rho(\mathbf{r}_1)}{|\mathbf{r} - \mathbf{r}_1|} \quad (2.22)$$

and the exchange self-energy operator is defined as

$$\hat{\Sigma}_x^{HF}[\gamma]\phi_k(\mathbf{x}) = - \sum_i^{N_e} \phi_i^*(\mathbf{x}) \int d^3x_1 \frac{\phi_k^*(\mathbf{x}_1)\phi_i(\mathbf{x}_1)}{|\mathbf{r} - \mathbf{r}_1|}. \quad (2.23)$$

The exchange self-energy is a functional of the density matrix γ , and hence the HF potential is itself a functional of the HF orbitals. This requires an iterative solution of Eq. (2.10) until the potential is converged. The potential that outcomes from this procedure is the so-called self-consistent field.

As such, HF is essentially a ground-state theory, although its eigenvalues can be used to calculate some excited-state properties. The occupied orbitals see a field of $N_e - 1$ electrons and the unoccupied orbitals see a the field of N_e electrons. These orbitals satisfy the so-called Koopman's theorem [61], which states that the occupied and virtual orbital eigenvalues can be interpreted as ionization potentials and electron affinities respectively, to first order in the

electron repulsion [61]. The HF orbital energies are not well suited for calculation of neutral excitations, where both occupied and virtual orbitals should see the same field.

2.4 Configuration Interaction

The variational principle gives an upper bound to the lowest energy state of the static Schrödinger equation. Excited states can be extracted by applying a constrained version of the variational principle. The constraint requires that the wave function of state I is orthogonal to all the wave functions of the same irreducible representation with a lower eigenvalue. For example, the constraint variational principle for the first excited state is

$$E_1 = \min_{\Psi_1 \perp \Psi_0} E[\Psi_1], \quad (2.24)$$

where we imposed the condition that $\langle \Psi_1 | \Psi_0 \rangle = 0$. This is however difficult to apply, since it would require the knowledge of the exact wave functions, which are normally not available. Fortunately, Hylleras, Undheim, and MacDonald formulated a theorem that proves that upper bounds to the exact eigenvalues are obtained by projecting the Hamiltonian in any arbitrary set of orthonormal trial wave functions that satisfy the same boundary conditions as the true wave functions [62, 63].

Configuration interaction exploits the Hylleras-Undheim-MacDonald theorem by expanding the Hamiltonian in a basis set of orthogonal Slater determinants. The basis determinants are systematically constructed by applying second-quantization excitation operators to a reference determinant (like the HF determinant.) This is possible since the excitation operators form a complete basis set in the Hilbert space [64]. The full CI approach corresponds to the diagonalization of the Hamiltonian in the complete basis. In the limit of an infinite basis set, the full CI approach would give all the exact solution of the Schrödinger equation. In practice, full CI is prohibitive even in small basis sets due to the large number of configurations that are generated. Instead, truncated CI expansions are commonly used, hoping that the leading effects are considered. The most important truncations are singles CI (CIS), which truncates the excitation operators to single excitations, and the singles doubles CI (CISD), which truncates the excitation operators to single and double excitations. In the next subsections, the complete and truncated CI expansions are explained in some detail. For a more detailed discussion, the user is referred to the literature (for example, Ref. [60].)

2.4.1 Full Configuration Interaction

The full CI applies the variational procedure to a wave function *ansatz* including all Slater determinants that can be formed in a given basis set. These determinants, commonly known as configuration state functions, are conveniently expressed as excitations from a reference determinant $|\Phi\rangle$. The full CI wave function *ansatz* is written as

$$|\Psi^{FCI}\rangle = \left(1 + \sum_{I=1}^N \tau_I^\dagger \mathbf{C}_I \right) |\Phi\rangle, \quad (2.25)$$

where \mathbf{C}_I and τ_I^\dagger are respectively a column vector of coefficients and a row vector of neutral excitation operators,

$$\tau_1^\dagger = \{\hat{a}_a^\dagger \hat{a}_i\} \quad (2.26)$$

$$\tau_2^\dagger = \{\hat{a}_a^\dagger \hat{a}_i \hat{a}_b^\dagger \hat{a}_j\} \quad (2.27)$$

$$\dots \quad (2.28)$$

Unless otherwise specified, the indexes a, b, \dots indicate virtual spin-orbitals, i, j, \dots indicate occupied spin-orbitals and p, q, \dots are unspecified. The full CI wave function tends to the exact solution in the limit of an infinite number of orbitals in the reference $|\Phi\rangle$. In general, truncation of the orbital space and also the level of excitation are necessary for making a computationally viable method.

The coefficients of the full CI wave functions are determined variationally by solving an eigenvalue problem of the form

$$\begin{bmatrix} E[\Phi] & \mathbf{H}_{01} & \mathbf{H}_{02} & \mathbf{H}_{03} & \dots \\ \mathbf{H}_{10} & \mathbf{H}_{11} & \mathbf{H}_{12} & \mathbf{H}_{13} & \dots \\ \mathbf{H}_{20} & \mathbf{H}_{21} & \mathbf{H}_{22} & \mathbf{H}_{23} & \dots \\ \mathbf{H}_{30} & \mathbf{H}_{31} & \mathbf{H}_{32} & \mathbf{H}_{33} & \dots \\ \dots & \dots & \dots & \dots & \dots \end{bmatrix} \begin{bmatrix} C_0 \\ C_1 \\ C_2 \\ C_3 \\ \dots \end{bmatrix} = E \begin{bmatrix} 1 & \mathbf{0}_{01} & \mathbf{0}_{02} & \mathbf{0}_{03} & \dots \\ \mathbf{0}_{10} & \mathbf{1}_{11} & \mathbf{0}_{12} & \mathbf{0}_{13} & \dots \\ \mathbf{0}_{20} & \mathbf{0}_{21} & \mathbf{1}_{22} & \mathbf{0}_{23} & \dots \\ \mathbf{0}_{30} & \mathbf{0}_{31} & \mathbf{0}_{32} & \mathbf{1}_{33} & \dots \\ \dots & \dots & \dots & \dots & \dots \end{bmatrix} \begin{bmatrix} C_0 \\ C_1 \\ C_2 \\ C_3 \\ \dots \end{bmatrix}, \quad (2.29)$$

where the blocks \mathbf{H}_{IJ} are defined as

$$\mathbf{H}_{IJ} = \langle \Phi | \tau_I \hat{H} \tau_J^\dagger | \Phi \rangle, \quad (2.30)$$

and the metric is defined as

$$\delta_{IJ} = \langle \Phi | \tau_I \tau_J^\dagger | \Phi \rangle, \quad (2.31)$$

in which we defined δ_{IJ} is a matrix of Kronecker deltas.

The Hamiltonian matrix of the full CI is pentadiagonal. Since the Hamiltonian has a two-electron interaction at most, the blocks with excitation level $|I - J| \geq 3$ are always zero. Additionally, in the case that the reference $|\Phi\rangle$ is the HF wave function, the coupling block of the reference and single excitations is also zero, $\mathbf{H}_{01} = \mathbf{0}$. This property of the HF wave function is usually called Brillouin's theorem, and is a direct consequence of the fact that the HF wave function is correct to first-order in perturbation theory.

2.4.2 Configuration Interaction Singles

Configuration Interaction Singles truncates the full CI wave function *ansatz* to only contain the reference and the single excitations,

$$|\Psi^{CIS}\rangle = \left(1 + \tau_1^\dagger \mathbf{C}_1\right) |\Phi\rangle. \quad (2.32)$$

The variational solution of such an *ansatz* has a simple matrix form

$$\begin{bmatrix} E[\Phi] & \mathbf{H}_{01} \\ \mathbf{H}_{10} & \mathbf{H}_{11} \end{bmatrix} \begin{bmatrix} C_0 \\ \mathbf{C}_1 \end{bmatrix} = E \begin{bmatrix} 1 & \mathbf{0}_{01} \\ \mathbf{0}_{10} & \mathbf{1}_{11} \end{bmatrix} \begin{bmatrix} C_0 \\ \mathbf{C}_1 \end{bmatrix}. \quad (2.33)$$

In the case of a HF reference, this is even simpler, since by virtue of the Brillouin's theorem $\mathbf{H}_{01} = \mathbf{0}$ and the two equations are completely decoupled. Therefore, the energy of the ground state in CIS is directly given by the HF energy $E_0 = E[\Phi^{HF}]$, and the singly-excited state energies are obtained

$$\mathbf{H}_{11} \mathbf{C}_1 = E_1 \mathbf{C}_1. \quad (2.34)$$

Subtracting the ground-state energy from both sides, we can write an equation for the excitation energies, $\omega_1 = E_1 - E_0$, directly,

$$\mathbf{A}_{11} \mathbf{c}_1 = \omega_1 \mathbf{c}_1, \quad (2.35)$$

where we defined $\mathbf{A}_{11} = \mathbf{H}_{11} - E_{HF} \mathbf{1}_{11}$. Explicitly,

$$[A_{11}]_{ia,jb} = (\epsilon_a - \epsilon_i) \delta_{ij} \delta_{ab} + (ia|bj) - (ij|ba), \quad (2.36)$$

where the orbital basis in the zero-order Slater determinant is considered canonical.

2.4.3 Singles and Doubles Configuration Interaction

Singles and doubles CI is the next rung in the CI hierarchy of methods after CIS. The advantages over CIS is that one obtains a larger number of solutions from the Hamiltonian and that the reference energy is also corrected. Unlike CIS, correlation effects are taken into account (from perturbation theory, doubles are shown to introduce the leading contribution to correlation.) In CISD, the full CI wave function *ansatz* is truncated to contain the reference and both single and double excitations,

$$|\Psi^{CISD}\rangle = \left(1 + \tau_1^\dagger \mathbf{C}_1 + \tau_2^\dagger \mathbf{C}_2\right) |\Phi\rangle. \quad (2.37)$$

The variational solution of such an *ansatz* has the matrix form

$$\begin{bmatrix} E[\Phi] & \mathbf{H}_{01} & \mathbf{H}_{02} \\ \mathbf{H}_{10} & \mathbf{H}_{11} & \mathbf{H}_{12} \\ \mathbf{H}_{20} & \mathbf{H}_{21} & \mathbf{H}_{22} \end{bmatrix} \begin{bmatrix} C_0 \\ \mathbf{C}_1 \\ \mathbf{C}_2 \end{bmatrix} = E \begin{bmatrix} 1 & \mathbf{0}_{01} & \mathbf{0}_{02} \\ \mathbf{0}_{10} & \mathbf{1}_{11} & \mathbf{0}_{12} \\ \mathbf{0}_{20} & \mathbf{0}_{21} & \mathbf{1}_{22} \end{bmatrix} \begin{bmatrix} C_0 \\ \mathbf{C}_1 \\ \mathbf{C}_2 \end{bmatrix}, \quad (2.38)$$

where the number of solutions is one (for the ground state) plus the number of single and double excitations. When the reference is taken as the HF wave function, the reference and the single excitations are decoupled, but the ground and singles still couple with the double excitations, which introduces a correlation correction in the HF energy. The solution for the excitation energies gives

$$\begin{bmatrix} 0 & \mathbf{0}_{01} & \mathbf{A}_{02} \\ \mathbf{0}_{10} & \mathbf{A}_{11} & \mathbf{A}_{12} \\ \mathbf{A}_{20} & \mathbf{A}_{21} & \mathbf{A}_{22} \end{bmatrix} \begin{bmatrix} C_0 \\ \mathbf{C}_1 \\ \mathbf{C}_2 \end{bmatrix} = E \begin{bmatrix} 1 & \mathbf{0}_{01} & \mathbf{0}_{02} \\ \mathbf{0}_{10} & \mathbf{1}_{11} & \mathbf{0}_{12} \\ \mathbf{0}_{20} & \mathbf{0}_{21} & \mathbf{1}_{22} \end{bmatrix} \begin{bmatrix} C_0 \\ \mathbf{C}_1 \\ \mathbf{C}_2 \end{bmatrix}. \quad (2.39)$$

In addition to Eq. (2.36), we obtain,

$$[A_{02}]_{1,aijb} = (jb||ia) + (ia||jb) - (ib||ja) - (ja||ib) \quad (2.40)$$

$$[A_{12}]_{ck,aijb} = -\delta_{ik}(bc||aj) + \delta_{jk}(bc||ai) - \delta_{bc}(ai||kj) + \delta_{ac}(bi||kj) \quad (2.41)$$

$$\begin{aligned} [A_{22}]_{aijb,ckld} &= (\epsilon_a + \epsilon_b - \epsilon_i - \epsilon_j) \delta_{ac} \delta_{ik} \delta_{bl} \delta_{jd} \\ &\quad - \delta_{ac} h(bd) - \delta_{bd} h(ac) + \delta_{ad} h(bc) + \delta_{bc} h(ad) - \delta_{ac} \delta_{bd} (kj||li) - \delta_{jl} \delta_{ki} (ad||bc), \end{aligned} \quad (2.42)$$

with

$$h(pq) = \delta_{ik}(lj||pq) + \delta_{jl}(ki||pq) - \delta_{kj}(li||pq) - \delta_{il}(kj||pq). \quad (2.43)$$

2.4.4 Multireference Self-Consistent Field

The main problem of CI is that the wave functions converge very slowly to the true solutions [65]. This is due to the fact that the molecular orbitals in the reference configuration, optimized for the ground-state, are usually not suitable for describing the excited states. Multi-reference self-consistent field methods try to avoid that by performing a double variational optimization of the orbitals and the configuration coefficients at the same time.

Multireference methods are computationally very demanding, but presently these are the only methods that can describe photochemistry in general. There are several strategies that have been developed to alleviate the computational burden. A common strategy is to select a restricted number of orbitals (active space) for which the CI expansion is applied. A full CI in an active space is known as complete active space self-consistent field, whereas other truncated CI expansions are known as restricted active space self-consistent field. The choice of the active space is critical, and depends on the problem under study.

The multireference excited state wave functions are much improved with less effort than the CI counterparts. However, a post-correlation method is usually required to account for dynamical correlation, an effect which is due to a large number of configurations and is not well represented in a small active space.

2.5 Linear Response

The previous sections described methods that extracted excited states from the static Schrödinger equation. Instead, the linear response method solves the time-dependent version of the Schrödinger equation, albeit in the frequency (energy) representation. The Hamiltonian contains an extra time-dependent external field which, in our case, will couple to the electronic density. First, I will discuss general properties of linear response, and then I will apply it to the

first-order (time-dependent Hartree-Fock) and second-order. The main references followed for this section are Refs. [16, 45, 66].

2.5.1 General Linear Response Theory

There are several ways to formulate the linear response theory. A simple formulation of the linear response starts out with a time-dependent Hamiltonian consisting of a static part and a dynamic applied field,

$$\hat{H}(t) = \hat{H}^e + \int d^3r \delta v_{appl}(\mathbf{r}, t) \rho(\mathbf{r}). \quad (2.44)$$

In our case, the applied field will represent an electromagnetic radiation. This time-dependent field introduces a fluctuation in the density, and the exact ground-state wave function becomes time-dependent, satisfying the TDSE

$$i \frac{\partial |\Psi_0(t)\rangle}{\partial t} = \hat{H}(t) |\Psi_0(t)\rangle. \quad (2.45)$$

This equation can be formally solved,

$$|\Psi_0(t)\rangle = \hat{U}(t, t_0) |\Psi_0(t_0)\rangle = \mathcal{T} \left[e^{-i \int_{t_0}^t dt' \hat{H}(t')} \right] |\Psi_0(t_0)\rangle, \quad (2.46)$$

where \mathcal{T} is a time-ordering operator and $\hat{U}(t, t_0)$ is the time evolution operator. It is convenient to partition the total time-dependent Hamiltonian in a time-independent part and the time-dependent perturbation, i.e., switching to the so-called interaction picture [16]. This facilitates the application of time-dependent perturbation theory. The solution of the zero-field part of the Hamiltonian give the stationary wave functions,

$$|\Psi_0(t)\rangle = \hat{U}_0(t, t_0) |\Psi_0(t_0)\rangle = e^{-i \hat{H}^e (t-t_0)} |\Psi_0(t_0)\rangle. \quad (2.47)$$

The exact evolution operator $\hat{U}(t, t_0)$, can then be partitioned in a zero-field part and a part due to the applied field,

$$\hat{U}(t, t_0) = \hat{U}_0(t, t_0) \hat{U}_{appl}(t, t_0). \quad (2.48)$$

This separation is useful since the operator $\hat{U}_{appl}(t, t_0)$ contains the whole effect of the perturbation. This operator has a particular Schrödinger equation

$$i \frac{\partial \hat{U}_{appl}(t, t_0)}{\partial t} = \int d^3r \delta v_{appl}(\mathbf{r}, t) \hat{\rho}(\mathbf{r}, t - t_0) \hat{U}_{appl}(t, t_0), \quad (2.49)$$

where the time-dependent density operator is defined as

$$\hat{\rho}(\mathbf{r}, t - t_0) = e^{i \hat{H}^e (t-t_0)} \hat{\rho}(\mathbf{r}) e^{-i \hat{H}^e (t-t_0)}. \quad (2.50)$$

Equation (2.49) has the formal solution

$$\hat{U}_{appl}(t, t_0) = \mathcal{T} \left[e^{-i \int d^3 t' \delta v_{appl}(t')} \right] \hat{\rho}(t' - t_0). \quad (2.51)$$

For simplicity, the spatial variables have been omitted. The linear response approximation of this operator is given by

$$\hat{U}_{appl}^{(1)}(t, t_0) = 1 - i \int d^3 t' \delta v_{appl}(t') \hat{\rho}(t' - t_0), \quad (2.52)$$

which introduces a first-order change in the wave function given by

$$|\delta\Psi_0(t)\rangle = -i \sum_{I \neq 0} |\Psi_I(t)\rangle \int_{t_0}^t dt' \delta v_{appl}(t') \langle \Psi_I(t') | \hat{\rho} | \Psi_0(t') \rangle, \quad (2.53)$$

in which we defined the time-dependent wave function as

$$|\Psi_0(t')\rangle = U_0(t', t_0) |\Psi_0(t_0)\rangle \quad (2.54)$$

The first-order response of the wave function allows us to calculate the linear response of any time-dependent property of the system due to the application of the applied field. For the purposes of this thesis, the linear response of the density matrix is especially important,

$$\delta\rho(\mathbf{r}, t) = \langle \delta\Psi_0(t) | \hat{\rho}(\mathbf{r}) | \Psi_0(t) \rangle + \langle \Psi_0(t) | \hat{\rho}(\mathbf{r}) | \delta\Psi_0(t) \rangle. \quad (2.55)$$

Substituting the expression of the first-order wave function, we obtain

$$\begin{aligned} \delta\rho(\mathbf{r}, t) = & -i \int_{t_0}^t dt' \int d^3 r' \left[\sum_{I \neq 0} \langle \Psi_0(t') | \hat{\rho}(\mathbf{r}') | \Psi_I(t') \rangle \langle \Psi_I(t) | \hat{\rho}(\mathbf{r}) | \Psi_0(t) \rangle \right. \\ & \left. + \langle \Psi_0(t) | \hat{\rho}(\mathbf{r}) | \Psi_I(t) \rangle \langle \Psi_I(t') | \hat{\rho}(\mathbf{r}') | \Psi_0(t') \rangle \right] \delta v_{appl}(\mathbf{r}', t'). \end{aligned} \quad (2.56)$$

This equation is important since it relates directly the response of the density to the variations of the applied field.

For extracting excited state energies from the linear-response of the density, it is more convenient to work in the Fourier-transformed space. The Fourier transform of Eq. (2.56) is only possible if the function tends to 0 in the limits $\pm\infty$, but Eq. (2.56) is not zero in neither limits. Fortunately, both limits can be enforced. The $-\infty$ limit is enforced by considering an adiabatically switched applied field,

$$\delta w_{appl}(t, t') = e^{\eta(t-t')} \delta v_{appl}(t'), \quad (2.57)$$

where the limit $\eta \rightarrow 0$ is taken after the Fourier transformation is done. The $+\infty$ limit is regularized by introducing a Heaviside function $\Theta(t - t')$ in the time-dependent integral. Then, Eq. (2.56) becomes

$$\begin{aligned} \delta\rho(\mathbf{r}, t) = & \int_{-\infty}^{\infty} dt' \int d^3r' \left[-i\Theta(t-t') \sum_{I \neq 0} \langle \Psi_0 | \hat{\rho}(\mathbf{r}') | \Psi_I \rangle \langle \Psi_I | \hat{\rho}(\mathbf{r}) | \Psi_0 \rangle e^{-i(E_I - E_0 - i\eta)(t-t')} \right. \\ & \left. + \langle \Psi_0 | \hat{\rho}(\mathbf{r}) | \Psi_I \rangle \langle \Psi_I | \hat{\rho}(\mathbf{r}') | \Psi_0 \rangle e^{-i(E_0 - E_I - i\eta)(t-t')} \right] \delta v_{appl}(\mathbf{r}', t'), \end{aligned} \quad (2.58)$$

where all the exponentials have been collected. This equation has a common short-hand notation

$$\delta\rho(\mathbf{r}, t) = \int_{-\infty}^{\infty} dt' \int d^3r' \chi(\mathbf{r}, \mathbf{r}', t-t') \delta v_{appl}(\mathbf{r}', t'). \quad (2.59)$$

The function $\chi(\mathbf{r}, \mathbf{r}', t-t')$ is normally called the susceptibility or density-density response function, and expresses the “easiness” of the density to be polarized by the applied field.

The Fourier transform of the density-density response function gives

$$\chi(\mathbf{r}, \mathbf{r}', \omega) = \lim_{\eta \rightarrow 0} \sum_{I \neq 0} \left[\frac{\langle \Psi_0 | \hat{\rho}(\mathbf{r}') | \Psi_I \rangle \langle \Psi_I | \hat{\rho}(\mathbf{r}) | \Psi_0 \rangle}{\omega - \omega_I + i\eta} - \frac{\langle \Psi_0 | \hat{\rho}(\mathbf{r}) | \Psi_I \rangle \langle \Psi_I | \hat{\rho}(\mathbf{r}') | \Psi_0 \rangle}{\omega + \omega_I + i\eta} \right], \quad (2.60)$$

where the excitation energies ω_I are defined as $\omega_I = E_I - E_0$. Due to the convergence factor η , the frequency can be viewed as a complex variable and the response function as a function defined in the complex plane, allowing the application of the powerful techniques of complex analysis. The response function is an analytic function in the upper half part of the complex plane, and a meromorphic function in the lower half plane with singularities (simple poles) at $\omega = \omega_I$. This is a mathematical consequence of causality, that is, the fact that the response of any property appears only after the perturbation has been applied and not before. Most importantly, the response function diverges at the excitation energies, which establishes a criterion for extracting excitation energies from the response function. In the next sections, I will explain how this is done in a practical way.

2.5.2 Equation of Motion of the Polarization Propagator

The response function of Eq. (2.60) has singularities at the exact excitation and de-excitation energies of the system. However, its construction requires the knowledge of all wave functions of the static Schrödinger equation, which are not usually available. Instead, many-body perturbation techniques give reasonable approximations to the response function. In this section, I describe the general techniques, and in the next sections I give practical expressions of the first- and second-order approximations. In this section, I will follow the algebraic method of Jørgensen and Oddershede (Ref. [45].)

The response function is equivalent to the diagonal of the retarded part of the polarization propagator [16],

$$\Pi^R(\mathbf{r}_1, \mathbf{r}_1, \mathbf{r}_2, \mathbf{r}_2; t_1 - t_2) = -i\Theta(t_1 - t_2) \langle \Psi_0 | \hat{\rho}(\mathbf{r}_1, t_1) \hat{\rho}(\mathbf{r}_2, t_2) | \Psi_0 \rangle. \quad (2.61)$$

For the sake of simplicity in the notation, we will use the full polarization propagator, since it has a more symmetric form. The full polarization propagator is given by

$$\Pi(\mathbf{r}_1, \mathbf{r}_1, \mathbf{r}_2, \mathbf{r}_2; t_1 - t_2) = -i \langle \Psi_0 | \mathcal{T} [\hat{\rho}(\mathbf{r}_1, t_1) \hat{\rho}(\mathbf{r}_2, t_2)] | \Psi_0 \rangle. \quad (2.62)$$

The use of the full polarization propagator is legitimate, since it has the same singularities as the retarded part, the only difference being the analytic structure. In particular, the denominator of the second term becomes $\omega + \omega_I - i\eta$, that is, the singularities are on the upper half plane for $\omega > 0$ and on the lower half plane for $\omega < 0$. This difference will not affect the conclusions of this section. Expanding the time-ordering operator and collecting the exponentials, one can write

$$\begin{aligned} \Pi(\mathbf{r}_1, \mathbf{r}_1, \mathbf{r}_2, \mathbf{r}_2; t_1 - t_2) &= -i \Theta(t_1 - t_2) \langle \Psi_0 | \left(e^{i\check{H}(t_1 - t_2)} \hat{\rho}(\mathbf{r}_1) \right) \hat{\rho}(\mathbf{r}_2) | \Psi_0 \rangle \\ &\quad + i \Theta(t_2 - t_1) \langle \Psi_0 | \hat{\rho}(\mathbf{r}_2) \left(e^{i\check{H}(t_1 - t_2)} \hat{\rho}(\mathbf{r}_1) \right) | \Psi_0 \rangle. \end{aligned} \quad (2.63)$$

In this equation, I used the notation \check{H} for indicating that the Hamiltonian is in fact a Liouville operator. A Liouville operator or superoperator \check{A} is defined by its action upon a Hilbert space operator \hat{B} as

$$\check{A}\hat{B} = [\hat{A}, \hat{B}] = \hat{A}\hat{B} - \hat{B}\hat{A}. \quad (2.64)$$

The identity superoperator $\check{1}$ is an exception,

$$\check{1}\hat{B} = \hat{B}. \quad (2.65)$$

The superoperator offers a compact notation for Green's functions. The Fourier transform of Eq. (2.63) gives

$$\begin{aligned} \Pi(\mathbf{r}_1, \mathbf{r}_1, \mathbf{r}_2, \mathbf{r}_2; \omega) &= - \langle \Psi_0 | \left[\left(\omega \check{1} + \check{H} \right)^{-1} \hat{\rho}(\mathbf{r}_1) \right] \hat{\rho}(\mathbf{r}_2) | \Psi_0 \rangle \\ &\quad + \langle \Psi_0 | \hat{\rho}(\mathbf{r}_2) \left[\left(\omega \check{1} + \check{H} \right)^{-1} \hat{\rho}(\mathbf{r}_1) \right] | \Psi_0 \rangle. \end{aligned} \quad (2.66)$$

For brevity, we omitted the η , although strictly speaking, it should be carried along and the $\eta \rightarrow 0$ limit should be taken at the end. Defining a superoperator metric as

$$(\hat{A} | \check{H} | \hat{B}) = \langle \Psi | \left[\hat{A}^\dagger, \left[\hat{H}, \hat{B} \right] \right] | \Psi \rangle, \quad (2.67)$$

we can write Eq. (2.66) as

$$\Pi(\mathbf{r}_1, \mathbf{r}_1, \mathbf{r}_2, \mathbf{r}_2; \omega) = (\hat{\rho}^\dagger(\mathbf{r}_1) | \left(\omega \check{1} + \check{H} \right)^{-1} | \hat{\rho}(\mathbf{r}_2)), \quad (2.68)$$

This form is important since the superoperator resolvent $(\omega \check{1} + \check{H})^{-1}$ is made apparent, which allows the application of the resolvent formalism of complex analysis. Now, the polarization propagator is constructed by calculating appropriate matrix elements of the resolvent. This is

clearly seen in second-quantization. The second-quantization form of the equation is given by

$$\Pi(\mathbf{r}_1, \mathbf{r}_1, \mathbf{r}_2, \mathbf{r}_2; \omega) = \sum_{pqrs} [\Pi(\omega)]_{pq,rs} \phi_q^*(\mathbf{r}_1) \phi_p(\mathbf{r}_1) \phi_r^*(\mathbf{r}_2) \phi_s(\mathbf{r}_2), \quad (2.69)$$

where

$$[\Pi]_{pq,rs} = (\hat{a}_p^\dagger \hat{a}_q | (\omega \check{\mathbb{I}} + \check{H})^{-1} | \hat{a}_r^\dagger \hat{a}_s). \quad (2.70)$$

To calculate the matrix elements of the resolvent, a complete basis of operators is needed. The complete set of operators in the superoperator formalism is equivalent to a complete basis set of basis functions for Hilbert operators. Dalggaard showed that neutral excitation and de-excitation operators form a complete basis set for expanding the resolvent [64],

$$\mathbf{T}^\dagger = \{\mathbf{T}_1^\dagger; \mathbf{T}_2^\dagger; \dots\} = \{\hat{a}_a^\dagger \hat{a}_i, \hat{a}_i^\dagger \hat{a}_a; \hat{a}_a^\dagger \hat{a}_i \hat{a}_b^\dagger \hat{a}_j, \hat{a}_i^\dagger \hat{a}_a \hat{a}_j^\dagger \hat{a}_b; \dots\}, \quad (2.71)$$

which forms a resolution of the identity in the metric of the superoperator

$$\check{\mathbb{I}} = |\mathbf{T}^\dagger\rangle \langle \mathbf{T}^\dagger|^{-1} \langle \mathbf{T}^\dagger|. \quad (2.72)$$

Introducing the resolution of the identity in Eq. (2.70), and after some rearrangements we obtain

$$[\Pi]_{pq,rs} = (\hat{a}_p^\dagger \hat{a}_q | \mathbf{T}^\dagger) (\mathbf{T}^\dagger | \omega \check{\mathbb{I}} + \check{H} | \mathbf{T}^\dagger)^{-1} (\mathbf{T}^\dagger | \hat{a}_r^\dagger \hat{a}_s), \quad (2.73)$$

where we considered a normalization of the operator space, $\langle \mathbf{T}^\dagger | \mathbf{T}^\dagger \rangle = 1$. The pole structure is entirely given by the matrix $\langle \mathbf{T}^\dagger | \omega \check{\mathbb{I}} + \check{H} | \mathbf{T}^\dagger \rangle$, from which we can straightforwardly extract with an eigenvalue problem

$$\sum_j (\mathbf{T}_i^\dagger | \check{H} | \mathbf{T}_j^\dagger) \mathbf{X}_j = \omega \sum_k (\mathbf{T}_i^\dagger | \mathbf{T}_k^\dagger) \mathbf{X}_k. \quad (2.74)$$

In the next section, I show how the first-order approximation gives the TDHF equations.

2.5.3 Time-Dependent Hartree-Fock

In this section I will show how to derive the TDHF equations by approximating Eq. (2.74) to first order. I will take the zero order Hamiltonian as

$$H^{(0)}(\mathbf{x}_1) = H^{HF}(\mathbf{x}_1) = t(\mathbf{r}_1) + v^{HF}(\mathbf{x}_1), \quad (2.75)$$

and the first-order potential

$$H^{(1)}(\mathbf{r}_1, \mathbf{r}_2) = v_{fluc}(\mathbf{r}_1, \mathbf{r}_2) = \frac{1}{|\mathbf{r}_1 - \mathbf{r}_2|} - [v^{HF}(\mathbf{x}_1) - v_{ext}(\mathbf{r}_1)]. \quad (2.76)$$

The HF wave function is correct to first-order and no further corrections are needed. Additionally, the space of operators can be truncated to \mathbf{T}_1^\dagger which contains single excitation and de-excitation

operators only. Higher-order excitations include second-order or higher terms. The size of the excitation operator space cannot be determined *a priori*, but it can be shown that to a given order, higher-order excitations do not contribute. The calculation of the TDHF has a simple form

$$\begin{bmatrix} \mathbf{A}_{11}^{(0+1)} & \mathbf{B}_{11}^{(0+1)} \\ \mathbf{B}_{11}^{(0+1)} & \mathbf{A}_{11}^{(0+1)} \end{bmatrix} \begin{bmatrix} \mathbf{X}_1 \\ \mathbf{Y}_1 \end{bmatrix} = \begin{bmatrix} \mathbf{1}_{11} & \mathbf{0}_{11} \\ \mathbf{0}_{11} & -\mathbf{1}_{11} \end{bmatrix} \begin{bmatrix} \mathbf{X}_1 \\ \mathbf{Y}_1 \end{bmatrix}, \quad (2.77)$$

where the blocks $\mathbf{A}_{11}^{(0+1)}$ are the matrix elements of the superoperator resolvent for the excitation-excitation and de-excitation-de-excitation blocks and $\mathbf{B}_{11}^{(0+1)}$ are the matrix elements of the superoperator resolvent for the excitation-de-excitation and de-excitation-excitation blocks. The superindex $0 + 1$ indicates that the zero- and first-order contributions are included in the calculation of the block. Their calculation gives

$$\begin{aligned} [A_{11}^{(0+1)}]_{ai,bj} &= (\hat{a}_i^\dagger \hat{a}_a | \check{H} | \hat{a}_b^\dagger \hat{a}_j)^{(0+1)} = \langle \Psi^{HF} | [\hat{a}_a^\dagger \hat{a}_i, [\hat{H}, \hat{a}_b^\dagger \hat{a}_j]] | \Psi^{HF} \rangle^{(0+1)} = (\epsilon_a - \epsilon_i) + (ai|jb) - (ab|ij) \\ [B_{11}^{(0+1)}]_{ai,bj} &= (\hat{a}_i^\dagger \hat{a}_a | \check{H} | \hat{a}_j^\dagger \hat{a}_b)^{(0+1)} = \langle \Psi^{HF} | [\hat{a}_a^\dagger \hat{a}_i, [\hat{H}, \hat{a}_j^\dagger \hat{a}_b]] | \Psi^{HF} \rangle^{(0+1)} = (ai|bj) - (aj|bi). \end{aligned} \quad (2.78)$$

Note that the expression for the \mathbf{A}_{11} block is equivalent to the CIS matrix [see Eq. (2.36).]

2.5.4 Second-Order Polarization Propagator

The second-order calculation is more involved. The HF wave function has the second-order Møller-Plesset correction

$$|\Psi^{HF,(2)}\rangle = -\frac{1}{2} \sum_{ijab} \frac{|(ai|jb)|^2}{\epsilon_a + \epsilon_b - \epsilon_i - \epsilon_j}, \quad (2.79)$$

which has to be considered in the approximation of the resolvent. The second-order approximation of the resolvent requires an operator space containing \mathbf{T}_1^\dagger and \mathbf{T}_2^\dagger . The eigenvalue problem is then formed by

$$\begin{bmatrix} \mathbf{A}_{11}^{(0+1+2)} & \mathbf{A}_{12}^{(1)} & \mathbf{B}_{11}^{(0+1+2)} & \mathbf{0}_{12} \\ \mathbf{A}_{21}^{(1)} & \mathbf{A}_{22}^{(0)} & \mathbf{0}_{21} & \mathbf{0}_{22} \\ \mathbf{B}_{11}^{(0+1+2)} & \mathbf{0}_{12} & \mathbf{A}_{11}^{(0+1+2)} & \mathbf{A}_{12}^{(1)} \\ \mathbf{0}_{21} & \mathbf{0}_{22} & \mathbf{A}_{21}^{(1)} & \mathbf{A}_{22}^{(0)} \end{bmatrix} \begin{bmatrix} \mathbf{X}_1 \\ \mathbf{X}_2 \\ \mathbf{Y}_1 \\ \mathbf{Y}_2 \end{bmatrix} = \begin{bmatrix} \mathbf{1}_{11} & \mathbf{0}_{12} & \mathbf{0}_{11} & \mathbf{0}_{12} \\ \mathbf{0}_{21} & \mathbf{1}_{22} & \mathbf{0}_{21} & \mathbf{0}_{22} \\ \mathbf{0}_{11} & \mathbf{0}_{12} & -\mathbf{1}_{11} & \mathbf{0}_{12} \\ \mathbf{0}_{21} & \mathbf{0}_{22} & \mathbf{0}_{21} & -\mathbf{1}_{22} \end{bmatrix} \begin{bmatrix} \mathbf{X}_1 \\ \mathbf{X}_2 \\ \mathbf{Y}_1 \\ \mathbf{Y}_2 \end{bmatrix}, \quad (2.80)$$

where the blocks to the different orders are

$$[A_{11}^{(0+1+2)}]_{ia,jb} = [A^{(0+1)}]_{ia,jb} + \frac{\delta_{ac}}{2} \sum_{ide} \frac{(le||kd)(dl||ei)}{\epsilon_d + \epsilon_e - \epsilon_i - \epsilon_m} - \frac{\delta_{ik}}{2} \sum_{lmd} \frac{(ld||mc)(dl||ma)}{\epsilon_a + \epsilon_d - \epsilon_m - \epsilon_l} \quad (2.81)$$

$$\begin{aligned} [B_{11}^{(0+1+2)}]_{ia,jb} &= [B^{(0+1)}]_{ia,jb} - \sum_{md} \frac{(ce||ad)(di||em)}{\epsilon_d + \epsilon_e - \epsilon_i - \epsilon_m} - \sum_{me} \frac{(ce||mi)(ak||me)}{\epsilon_a + \epsilon_e - \epsilon_k - \epsilon_m} \\ &\quad - \frac{1}{2} \sum_{de} \frac{(ce||ad)(dk||ei)}{\epsilon_d + \epsilon_e - \epsilon_i - \epsilon_k} - \frac{1}{2} \sum_{ml} \frac{(ik||ml)(ac||ml)}{\epsilon_a + \epsilon_c - \epsilon_l - \epsilon_m} \end{aligned} \quad (2.82)$$

$$[A_{12}^{(1)}]_{kc,iajb} = -\delta_{ik}(bc||aj) + \delta_{jk}(bc||ai) - \delta_{bc}(ai||kj) + \delta_{ac}(bi||kj) \quad (2.83)$$

$$[A_{22}^{(0)}]_{iajb,ckld} = (\epsilon_a + \epsilon_b - \epsilon_i - \epsilon_j) \delta_{ik} \delta_{ac} \delta_{bd} \delta_{jl} . \quad (2.84)$$

2.5.5 Polarization Propagator vs. Configuration Interaction

In this thesis, we will take advantage of the structural similarities of the polarization propagator and TDDFT, to introduce some desired physical effects from the former to the latter. We will also include some effects from CIS to TDDFT. This is possible since these theories, though formulated differently, describe the same physical effects. In this section, we compare the CI and the polarization propagator equations.

The similarities between the polarization propagator and the CI equations are made apparent in the Tamm-Dancoff approximation (TDA) of the former, i.e., setting to zero the off-diagonal block \mathbf{B} that couples excitations and de-excitations. In this approximation, the first-order polarization propagator (or TDHF) and the CIS equations are completely equivalent. The first difference comes in second-order. The TDA approximation of the second-order polarization propagator resembles partially the CISD equations. There are three main differences. First, the single-single block of the polarization propagator is corrected to second-order in perturbation theory, whereas the single-single block in CIS is only correct to first order. Second, the double-double block is correct to zero order in the polarization propagator and to first-order in CISD. Third, the CISD has a coupling block between the reference and the excited states, whereas the second-order polarization propagator includes these terms in the \mathbf{A}_{11} and \mathbf{B}_{11} blocks.

Both full CI and infinite-order polarization propagator should give the same state energies, and therefore, both theories should contain the same physical information. The truncated orders, however, redistribute differently this information in each of the blocks (see for instance Figs. 16 and 17 of Ref. [45].) In principle, the polarization propagator converges faster the excitation energies than truncated CI, and has a more direct relation to TDDFT, but both theories can help in guiding the construction of better kernels in linear-response TDDFT.

Chapter 3

Density-Functional Based Electronic Structure

3.1 Introduction

Density-functional-based methods have revolutionized the way in which we calculate electronic structure theory. The density contains enough information about the wave function, so that it can be used as the main variable to formulate quantum mechanics, with the obvious advantage that it is easier to deal with a global physical observable that depends only on 3 spatial coordinates and spin. This chapter describes density-functional methods both for ground- and excited-state simulations, putting special emphasis on the information that is lost in the transition from the exact formal theory to the practical approximate models.

The greatest challenge in density-functional theory has been to successfully reformulate quantum mechanics in terms of the density, the main complication being that a practical form of the exact energy as a functional of the density is unknown. The first density-functional method dates back to the discovery of the Schrödinger equation [67]. In 1927, Thomas and Fermi (TF) independently developed a semiclassical model which attempted to extract the total energy from the density [68, 69]. Even though better density functionals were introduced later by Dirac and Weizsäcker, the model was not very popular, especially when it was shown that it could not predict bonding [70]. A more successful reformulation in terms of the density is the DFT developed by Hohenberg, Kohn and Sham. In 1964, Hohenberg and Kohn (HK) formulated two theorems proving that the density could be used as the basic variable for electronic structure calculations [14]. In 1965, Kohn and Sham (KS) developed a density-functional method which expands the density in a set of orthonormal orbitals which are variationally optimized [15]. The main achievement of the KS method is an accurate calculation of the kinetic energy (which was the main problem of the TF model.) The price to pay is that one has to approximate the exchange-correlation (xc) functional, which contains all the unknown terms of the energy functional. The simplest approximation is the local density approximation (LDA), which parameterizes the functional in order to reproduce the exchange and correlation energies of the homogeneous electron gas. Numerous approximated functionals have appeared afterwards, which improve upon the LDA functional. Functional development has converted DFT in a method with a good balance between precision and efficiency.

The formulation of quantum mechanics in terms of the densities showed some difficulties that were not apparent in the wave function formulation. Specially important is the v -representability problem, which puts in doubt the application of the second HK theorem, since the original formulation requires that the densities correspond to physical external potentials, which is not always the case. Fortunately, a reformulation of the original DFT functionals allows us to apply the variational principle without having to worry about the v -representability [71]. In KS theory, non-interacting v -representability has to be considered too, which assumes that any density can be represented by a non-interacting potential. This assumption is known to fail in some cases, for example, when degeneracies occur in the non-interacting system. In these cases, DFT can be

extended to use an ensemble of densities. There is no general proof of ensemble non-interacting v -representability but, to date, no counter example has been found.

The KS equations have some structural similarities to the HF equations, but there are substantial differences between the two. The HF equations are approximate and do not include correlation, whereas the KS equations are formally exact, including correlation at the self-consistent level. Additionally, in KS both the occupied and virtual orbitals see the same field, making them especially suitable for describing neutral excitations. But the HK theorems are only proven for the ground-state density and excited states are not accessible in general. Several methods exist to calculate some excited state properties, such as the Δ SCF method [72], the multiplet sum method [73] and constrained density-functional theory [74], which can calculate some excited states from DFT.

A complete theory for excited states came with the development of TDDFT. Similar to DFT, TDDFT attempts to reformulate the time-dependent Schrödinger equation in terms of the time-dependent density. The formal foundations for TDDFT were established in 1984, with the seminal paper of Runge and Gross (RG) [13]. The basic theorems of existence and the action principle are analogous to the two HK theorems. The main result of the RG theorems are the time-dependent Kohn-Sham (TDKS) equations, which are solved similarly to the TDSE of Chap. 2. The initial condition is normally taken as the KS ground-state density. The linear-response TDDFT method was developed by Casida [17] and the real-time TDDFT has been recently implemented by Marques *et al.* [75].

The RG theorems are not as general as the HK equivalents. Two constraints are imposed in the RG proof of existence, namely, that the external potentials have to be t -analytic and that the density has to vanish at infinity. These conditions are not always satisfied, though still the RG theorems encompass most physical cases and are considered to lay the foundations of modern TDDFT. A more severe problem of the initial RG theorems was the original definition of the action, which lead to unphysical non-casual xc functionals [76]. This was later traced as a wrong application of the Frenkel-Dirac action principle defined in terms of the density [77]. The proper application of the action changes the definition of the xc potential, though the same TDKS equations are obtained.

The problem of time-dependent v -representability is less problematic in TDDFT than in DFT, since the initial condition required for solving the TDKS equations takes care of it. Interestingly, a proof for non-interacting v -representability exists in TDDFT. The proof relies on the t -analyticity of both densities and potentials [78]. The t -analyticity of densities is a restrictive condition, and extensions of the proof that avoids this requirement are being explored [79, 80].

Like DFT, TDDFT adds up all the unknown terms in an xc action. Approximations to the action are more involved, since the xc effects at time t depend on all the previous densities, and on the initial state of the interacting and non-interacting systems. These dependencies are commonly called memory effects. The exact role of memory is yet unknown, but exotic properties are seen in the TDDFT equations, which were not apparent in the DFT formulation. The xc functionals in TDDFT are highly non-local both in space and time, i.e., the TDDFT functionals have a long remembrance of the past. Even so, in most calculations it is enough to forget the effect of past densities altogether. This is the essence of the adiabatic approximation in TDDFT, which only takes into account the effects of the instantaneous density to approximate the xc effects. This is normally a good approximation for excited states dominated by single excitations, which are not too diffuse and do not involve long-range charge transfer.

For states dominated by double excitations, charge transfer excitations, Rydberg states, states along the dissociation coordinate, funnels, etc. the adiabatic approximation normally fails. For these applications, more sophisticated memory functionals are required. Memory functionals are still in their infancy, though much progress has been done in recent years. Especially important are the studies of the exact exchange TDDFT functional. Less attention has been put in the description of correlation, which is directly associated with relevant problems in photochemistry such as the description of double excitations and conical intersections.

This chapter is organized as follow. In Sec. 3.1, I briefly describe DFT. The formal foundations established by HK theorems and the problems of using the density as the main variable are described in 3.2.1, the KS equations are described in 3.2.2 and the xc functionals in 3.2.3. TDDFT is discussed in Sec. 3.3. The formal foundations established by RG theorems and the problems of using the density as the main variable are described in 3.3.1, the TDKS equations are described in 3.3.2, and the xc TDDFT functionals in 3.3.3.

3.2 Density-Functional Theory

3.2.1 Formal Foundations

In 1964, Hohenberg and Kohn published an article entitled “Inhomogeneous electron gas” [14], which put on firm grounds the semiclassical reformulation of Schrödinger’s equation in terms of the density by Thomas [68] and Fermi [69]. The two main results of Hohenberg and Kohn are two theorems. The first theorem is called the existence theorem and proves that the density determines unequivocally the Hamiltonian (see Sec. 3.2.1.1.) The second theorem establishes a variational principle in terms of the densities (see Sec. 3.2.1.1.) These two theorems constitute the advent of modern density-functional theory. A reformulation of wave function theory in terms of the density alone needs to address some questions like the v -representability, which puts some restrictions in the application of the variational principle. This is explained in Sec. 3.2.1.3.

3.2.1.1 Existence Theorem

The usage of the density as a main variable for electronic structure theory needs to be proven. The first theorem of HK proves the

Existence theorem: For a nondegenerate system, there is a one-to-one correspondence between the external potential and the ground-state density up to an arbitrary additive constant.

In other words, two external potentials differing by more than a constant cannot give rise to the same density. The proof is relatively simple. Imagine that we have two external potentials $v_{ext}^1(\mathbf{r})$ and $v_{ext}^2(\mathbf{r})$ associated with two different non-degenerate wave functions $|\Psi_1\rangle$ and $|\Psi_2\rangle$ that give the same density. The variational principle states that

$$\begin{aligned}
E_0^1[\rho] &= \langle \Psi_1[\rho] | \hat{H}_1 | \Psi_1[\rho] \rangle < \langle \Psi_2[\rho] | \hat{H}_1 | \Psi_2[\rho] \rangle = \langle \Psi_2[\rho] | \hat{H}_2 | \Psi_2[\rho] \rangle + \langle \Psi_2[\rho] | \hat{H}_1 - \hat{H}_2 | \Psi_2[\rho] \rangle \\
&= E_0^2[\rho] + \int d^3r [v_{ext}^1(\mathbf{r}) - v_{ext}^2(\mathbf{r})] \rho(\mathbf{r}),
\end{aligned} \tag{3.1}$$

where the exact energy density functional was written as

$$E[\rho] = \langle \Psi[\rho] | \hat{H} | \Psi[\rho] \rangle = F^{HK}[\rho] + \int d^3r v_{ext}(\mathbf{r}) \rho(\mathbf{r}), \tag{3.2}$$

in which we defined the universal functional $F^{HK}[\rho]$ as

$$F^{HK}[\rho] = \langle \Psi[\rho] | \hat{T} + \hat{W} | \Psi[\rho] \rangle. \tag{3.3}$$

The operators \hat{T} and \hat{W} are the kinetic and the electron-repulsion operators respectively. Equivalent to E_0^1 , for E_0^2 we get the condition

$$E_0^2[\rho] < E_0^1[\rho] - \int d^3r (v_{ext}^1(\mathbf{r}) - v_{ext}^2(\mathbf{r})) \rho(\mathbf{r}). \tag{3.4}$$

Adding up Eqs. 3.1 and (3.4), we arrive to the absurd conclusion

$$E_0^1 + E_0^2 < E_0^1 + E_0^2. \tag{3.5}$$

This proves that our initial assumption was wrong, hence that two different external potentials must give rise to different electronic densities. The proof also shows that the correspondence between the density and the wave function is one-to-one. Since the wave function is uniquely associated with a Hamiltonian (up to a phase factor), the density itself determines the Hamiltonian uniquely (up to an arbitrary additive constant.)

3.2.1.2 Variational Principle

The existence proof is of no practical use if a variational principle cannot be defined in terms of the density. The second HK theorem is the

Variational theorem: The exact non-degenerate ground state's density gives the minimum energy of the exact energy density-functional.

In fact, this is a corollary of the first Hohenberg and Kohn theorem. Recalling the variational principle in terms of the wave functions,

$$E_0[\Psi] < E_0[\tilde{\Psi}], \tag{3.6}$$

one can write it in terms of the density by using Eq. (3.2),

$$F^{HK}[\rho] + \int d^3r v_{ext}(\mathbf{r}) \rho(\mathbf{r}) < F^{HK}[\tilde{\rho}] + \int d^3r v_{ext}(\mathbf{r}) \tilde{\rho}(\mathbf{r}), \tag{3.7}$$

in which we used the fact (existence theorem) that two different wave functions give two different densities. It is now straightforward to conclude that,

$$E_0[\rho] < E_0[\tilde{\rho}]. \quad (3.8)$$

The exact energy functional is unknown, and in practice the variational theorem is only applied with approximations to it.

3.2.1.3 v -Representability and N -Representability

The existence and variational principles are enough to set up a density-functional-based electronic structure theory. But some restrictions have to be imposed on the densities, as the HK theorems are only valid for reasonable densities that are associated with a physical external potential. A reasonable density has the following properties:

$$\int d^3r \rho(\mathbf{r}) = N_e \quad (3.9)$$

$$\rho(\mathbf{r}) \geq 0 \quad \forall \mathbf{r} \quad (3.10)$$

$$\int d^3r |\nabla(\rho(\mathbf{r})^{1/2})|^2 < \infty, \quad (3.11)$$

which are easily satisfied in general (see Ref. [81] and references therein.) The second HK requirement that the density corresponds to a physical external potential is less obvious. This condition is usually referred as the v -representability in DFT.

The v -representability is yet an unresolved question. Some partial proofs exist for certain classes of densities [82], but the exact conditions for a density to be v -representable are unknown. In fact, it has been shown that some reasonable densities do not correspond to a physical potentials [83, 84]. A simple example is given by a Hamiltonian that has k degenerate ground-state wave functions $\{\Psi_1, \Psi_2, \dots, \Psi_k\}$: its density $\rho(\mathbf{r}) = \sum_{i=1}^k C_i \rho_i(\mathbf{r}) = \sum_{i=1}^k C_i \langle \Psi_i | \hat{\rho}(\mathbf{r}) | \Psi_i \rangle$ does not correspond to any external potential $v_{ext}(\mathbf{r})$ [85].

Fortunately, a reformulation of the original HK theorems allows the usage of N -representability densities in the variational principle, which is much easier to satisfy than the v -representability. A density is N -representable if it comes from an antisymmetric wave function, which is satisfied by any reasonable density [86]. Levy [71] and Lieb [84] proposed to change the original universal functional [Eq. (3.3),] which only admits v -representable densities, to a constrained-search universal functional of the form,

$$F^{LL}[\tilde{\rho}] = \inf_{\tilde{\Psi} \rightarrow \tilde{\rho}} \langle \tilde{\Psi} | \hat{T} + \hat{W} | \tilde{\Psi} \rangle. \quad (3.12)$$

When $\tilde{\rho}$ equals the real density, the Hohenberg-Kohn and the Levy functionals are equal. The variational principle is now a two-step minimization,

$$E[\rho] = \inf_{\tilde{\rho} \rightarrow \rho} \left\{ F^{LL}[\tilde{\rho}] + \int d^3r \tilde{\rho}(\mathbf{r}) v_{ext}(\mathbf{r}) \right\} = \inf_{\tilde{\rho} \rightarrow \rho} \left\{ \inf_{\tilde{\Psi} \rightarrow \tilde{\rho}} \left\{ \langle \tilde{\Psi} | \hat{T} + \hat{W} + \sum_i^{N_e} v_{ext}(\mathbf{r}_i) | \tilde{\Psi} \rangle \right\} \right\}. \quad (3.13)$$

In the minimization, we restrict the densities to be searched in the space of wave functions and from those, we pick the one that gives the lowest energy. In this way, we do not need to invoke the mapping between densities and potentials, and the only requirement is for the densities to be N -representable.

3.2.2 Kohn-Sham Equations

The real practical route to DFT is given by the KS method. The main virtue of KS is that the kinetic energy is calculated very accurately. In this section, I derive the KS equations.

The energy expression in terms of the density is given by

$$E[\rho] = F^{LL}[\rho] + \int d^3r \rho(\mathbf{r}) v_{ext}(\mathbf{r}), \quad (3.14)$$

In the KS method, the density is expanded in an auxiliary set of orthonormal orbitals,

$$\rho(\mathbf{r}) = \sum_i^{N_e} |\phi_i^{KS}(\mathbf{r})|^2. \quad (3.15)$$

This is the KS assumption, i.e., assuming that the density can be represented by a set of orbitals solution of a non-interacting auxiliary Hamiltonian. In this way, the non-interacting kinetic energy functional is given by

$$T_s[\rho] = -\frac{1}{2} \inf_{\Psi_s \rightarrow \rho} \left\{ \sum_i^{N_e} (\phi_i^{KS} | \nabla^2 | \phi_i^{KS}) \right\}. \quad (3.16)$$

The energy is then calculated as

$$E[\rho] = T_s[\rho] + \int d^3r \rho(\mathbf{r}) v_{ext}(\mathbf{r}) + E_H[\rho] + E_{xc}[\rho], \quad (3.17)$$

where the xc functional contains all the unknown terms of the exact energy functional,

$$E_{xc}[\rho] = F^{LL}[\rho] - T_s[\rho] - E_H[\rho]. \quad (3.18)$$

The energy expression can then be minimized by setting up

$$L[\{\phi_i^{KS}\}] = E[\rho] - \sum_{ij}^{N_e} \epsilon_{ij} [1 - \langle \phi_i^{KS} | \phi_j^{KS} \rangle], \quad (3.19)$$

and enforcing that the variations of the functional with respect to variations in the orbitals are zero. The minimization gives the KS equations

$$\hat{f}^{KS} \phi_i^{KS}(\mathbf{r}) = \epsilon_i^{KS} \phi_i^{KS}(\mathbf{r}), \quad (3.20)$$

where the KS Fock operator is given by

$$\hat{f}^{KS} = \hat{t}_s(\mathbf{r}) + \hat{v}_{ext}(\mathbf{r}) + \hat{v}_H[\rho](\mathbf{r}) + \hat{v}_{xc}[\rho](\mathbf{r}). \quad (3.21)$$

The operators are defined as in the HF approach with the difference that the non-local exchange operator is substituted by the local xc potential,

$$v_{xc}[\rho](\mathbf{r}) = \frac{\delta E_{xc}[\rho]}{\delta \rho(\mathbf{r})}, \quad (3.22)$$

which includes all the exchange and correlation effects.

3.2.3 Exchange-Correlation Functionals

In KS theory, all the approximations are concentrated in the exchange-correlation functional,

$$E_{xc}[\rho] = (W[\rho] - E_H[\rho]) + (T[\rho] - T_s[\rho]), \quad (3.23)$$

where the electron repulsion is defined as

$$W[\rho] = \langle \Psi | \hat{W} | \Psi \rangle, \quad (3.24)$$

and the kinetic energy operator as

$$T[\rho] = \langle \Psi | \hat{T} | \Psi \rangle. \quad (3.25)$$

For the rest of this section, I will consider that the difference between the interacting and non-interacting kinetic energies is negligible. The exchange functional is defined as

$$E_x[\rho] = \langle \Phi^{KS}[\rho] | \hat{W} | \Phi^{KS}[\rho] \rangle - E_H[\rho], \quad (3.26)$$

where $\Phi^{KS}[\rho]$ is the KS wave function, and the correlation functional is defined as

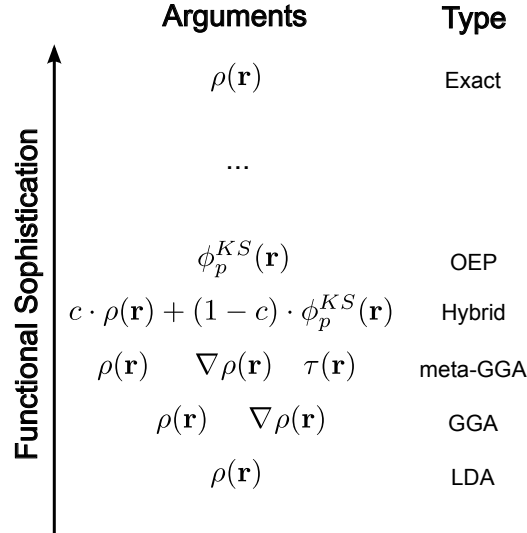
$$E_c[\rho] = W[\rho] - (E_H[\rho] + E_x[\rho]). \quad (3.27)$$

However, it seems more practical to approximate the two contributions directly, and rarely the exchange and correlation contributions are calculated separately.

Classification of functionals: Jacob's Ladder

Most of the work that helped to popularize DFT among chemists is the development of successful approximations to the exact xc functional. Nowadays, the number of available functionals

Figure 3.1 Jacob’s ladder of static density functionals. LDA stands for local density approximation, GGA stands for generalized gradient approximation, and OEP stands for optimized effective potential.



is enormous and ever growing. The methods of construction are varied. Some try to mimic as many of the sum rules of the exact functional as possible, others take a more pragmatic approach by parameterizing functionals and fitting the functional to reproduce benchmark sets of properties.

The number of available functionals makes it difficult to determine the level of approximation. Perdew and Schmidt proposed a classification of functionals according to the functional dependencies, commonly called the Jacob’s ladder [87]. This ladder is depicted in Fig. 3.1. On climbing the ladder, functionals depend on an increasing number of variables (larger computational cost) in the hope that more information can be build in. Although using a higher rung is not a guarantee of better accuracy, it is generally believed that the more sophisticated the functional is, the more accurate xc energy can be obtained. The choice of a functional rung is a compromise between accuracy, and computational cost.

The lowest rung of the ladder is the LDA, which is the simplest possible functional. The next rung is consists of the generalized gradient approximation (GGA), which additionally incorporates gradients of the density. The meta-GGAs incorporate the kinetic density $\tau(\mathbf{r})$. Up to this point, the functionals are called pure DFT functionals, since they only include density information. The fourth rung, hybrid functionals, include a portion of orbital-dependent functionals, and the optimized effective potential (OEP) makes full use of orbital-dependent functionals. These functionals are implicit density functionals, since the KS orbitals are density functionals too.

Exact functional

There are numerous exact conditions that the exact xc functional satisfies (see Ref. [37] and references therein.) For example, from the variational principle we have,

$$E_{xc}[\rho] \leq 0 \quad , \quad E_c[\rho] \leq 0 \quad , \quad \text{and} \quad E_x[\rho] \leq 0. \quad (3.28)$$

From the Galilean-invariance condition, i.e., that the xc energy remains constant for a rigid shift of the density, we obtain the zero-force and the zero torque theorems,

$$\int d^3r \rho(\mathbf{r}) \nabla v_{xc}(\mathbf{r}) = 0, \quad (3.29)$$

$$\int d^3r \rho(\mathbf{r}) \mathbf{r} \times \nabla v_{xc}(\mathbf{r}) = 0. \quad (3.30)$$

For any one-electron system, we have the self-interaction condition

$$E_x[\rho] = -E_H[\rho] \quad , \quad E_c[\rho] = 0. \quad (3.31)$$

The asymptotic behavior of the xc-potential is given by

$$v_{xc}(\mathbf{r}) \rightarrow -\frac{1}{\mathbf{r}} \quad (\mathbf{r} \rightarrow \infty), \quad (3.32)$$

and the highest occupied KS eigenvalue equals the minus ionization potential

$$\epsilon_{HOMO} = -I. \quad (3.33)$$

Rung 1: Local Density Approximation

The LDA functional $E^{LDA}[\rho]$ is the simplest and oldest xc functional, approximating it for the homogeneous electron gas. The exchange functional for the homogeneous gas is known analytically,

$$E_x[\rho] = -\frac{3}{4} \left(\frac{3}{\pi} \right)^{1/3} \int d^3r \rho^{4/3}(\mathbf{r}). \quad (3.34)$$

It is commonly known as Dirac exchange, as P.A.M. Dirac derived it to improve on the TF model. No analytical expression exists for the correlation functional, but accurate parameterizations exist. The most accurate correlation energy is given by the 5-parameter functional of Vosko, Wilk, Nusair, who fitted it with accurate quantum Monte Carlo calculations of the correlation for the homogeneous gas [88, 89].

The LDA functional was initially supposed to work well for systems with homogeneous densities, but it works well far beyond this limit. There is still no convincing explanation of the reason, but it is generally believed that this is because the LDA satisfies most of the sum rules of the exact functional. The main problems with LDA is the large underestimation of the deriva-

tive discontinuity, the self-interaction error and the wrong long-range behavior of exchange and correlation potentials.

Rung 2: Generalized Gradient Approximation

The LDA functional depend exclusively on the density $\rho(\mathbf{r})$, in which the density is supposed to be uniform. The GGA functionals $E^{GGA}[\rho, \nabla\rho, \dots]$ try to incorporate local deformities in the density by including gradients. Therefore, they are normally called semilocal functionals. A general gradient expansion is valid in the case of slowly varying densities

$$E_{xc}^{GGE}[\rho, |\nabla\rho(\mathbf{r})|^2, \dots] = \int d^3r (a(\mathbf{r})\rho(\mathbf{r}) + b(\mathbf{r})|\nabla\rho(\mathbf{r})|^2 + \dots). \quad (3.35)$$

However, it was seen that at some distances, this expansion leads to unphysical overestimation and fluctuations of the energy contributions. The GGA applies different strategies to avoid these problems.

The GGA functionals give better total energies in general, which are normally underestimated by LDA. However, important problems associated with LDA (derivative discontinuity, self-interaction error and incorrect long-range) are still present.

A popular functional of this type is the PBE [90,91].

Rung 3: meta-Generalized Gradient Approximation

The meta-GGA functionals $E^{mGGA}[\rho, \nabla\rho, \dots, \tau]$ are similar to the GGA but including extra information from the kinetic density operator,

$$\tau(\mathbf{r}) = \sum_i^{N_e} |\nabla\phi_i^{KS}(\mathbf{r})|^2. \quad (3.36)$$

Meta-GGA functionals are constructed in the same way as GGAs. However, they are computationally more demanding and difficult to implement, due to the terms that arise when deriving the functionals with respect to the density,

$$\frac{\delta\tau(\mathbf{r})}{\delta\rho(\mathbf{r})}. \quad (3.37)$$

The meta-GGAs give similar results as the GGAs in terms of the total energy. However, they account better for the derivative discontinuity.

Popular functionals of these type are the Minnesota functionals [92].

Rung 4: Hybrid functionals

Semi-local functionals improve the total energy of LDA, but not, for example, derivative discontinuity and self-interaction errors. This might be partially remediated by introducing a portion of HF exchange,

$$E^{Hyb}[\rho] = (1 - c_x) \cdot E_x^{DFT} + c_x \cdot E_x^{HF} + E_c^{DFT}, \quad (3.38)$$

where E^{DFT} is a local or semi-local density functional. Interestingly, most parameterizations agree that the best portion of HF exchange is around 20-25%. Note that these are practical functionals but, strictly speaking, they are not legitimate as they break important sum rules of the exact functional.

These functionals give good total energies, the derivative discontinuity problem is largely remediated and the self-interaction error is improved. The long-range of exchange is still wrong, but can be enforced *a posteriori*.

Popular functionals of this type include B3LYP (20% HF exchange) [93], the long-range corrected CAM-B3LYP [94] and the PBE0 (PBE with 25% HF exchange) [95].

Recently, double hybrid functionals have arisen, which include also a portion of second-order Møller-Plesset correlation energy [96],

$$E^{dHyb}[\rho] = (1 - c_x) \cdot E_x^{DFT} + c_x \cdot E_x^{HF} + (1 - c_c) \cdot E_c^{DFT} + c_c \cdot E_c^{MP2}. \quad (3.39)$$

Rung 5: Optimized Effective Potentials

The OEP functionals are the most sophisticated functionals presently. They map rigorous orbital-dependent functionals of *ab initio* wave function theory into DFT [97]. The best known example is the exact exchange, which maps the exact HF exchange into DFT [98,99]. The exact-exchange DFT functional gives the correct asymptotic decay of exchange and exact self-energy correction. The derivative discontinuity is largely overestimated, but this is remediated by using OEP correlation functionals mapped, for example, from the RPA correlation formulas.

The main difficulty, which makes them computationally very demanding, is to obtain derivatives with respect to the density. There exist several schemes that attempt to construct OEP potentials, such as the integro-differential OEP equations or the Sham-Schlüter equations [100].

A similar functional to the OEP is the correlation functional from the adiabatic connection fluctuation-dissipation theorem, which calculates the correlation energy by integrating the response functions in the Coulson contour [101].

3.3 Time-Dependent Density-Functional Theory

3.3.1 Formal Foundations

TDDFT extends the applicability of density-functional theory to non-stationary problems. TDDFT is a stand alone theory which relies on two theorems similar to the HK theorems of DFT. These theorems enable us to formulate the TDSE in terms of the density. The first theorem, the existence theorem, proves that the time-dependent density can determine the time-dependent Hamiltonian and the wave function up to a time-dependent phase factor. That means

that both the wave function and the density contains the same information, since the phase factor cancels out when calculating the expectation value of any operator (that does not contain any time derivatives.) The second theorem provides us with a variational principle, the so-called least action principle, that enables us to calculate the time-dependent density. Although several versions of these theorems existed in the literature prior to RG paper [102–105], the RG proof is widely considered the seminal work that establishes the modern foundations of TDDFT [13]. In this section, I will discuss the Runge-Gross theorems in some detail, as well as the time-dependent v -representability problem.

3.3.1.1 Existence theorem

Imagine that we start from an unperturbed wave function $|\Psi(t_0)\rangle$ to which we apply a perturbation. We can propagate the wave function to time $|\Psi(t)\rangle$ by applying the time-dependent Hamiltonian $\hat{H}(t)$. This provides a mapping F between the time-dependent external potential and the wave function, $F : v_{ext}(t) \rightarrow |\Psi(t)\rangle$. From the wave function at time t we can calculate the density, providing us with a second mapping, $G : |\Psi(t)\rangle \rightarrow \rho(t)$. What is there to prove is that the mapping G is invertible, so that there is a one-to-one correspondence between the time-dependent density and the external potential. In other words, we have to prove the

Existence theorem: There is a one-to-one correspondence between the time-dependent external potential and the time-dependent density up to an additive function of time.

The proof of Runge and Gross goes as follow. Suppose that two different external potentials $v_{ext}^1(\mathbf{r}, t)$ and $v_{ext}^2(\mathbf{r}, t)$ give two densities $\rho^1(\mathbf{r}, t)$ and $\rho^2(\mathbf{r}, t)$. Requiring the external potentials to be t -analytic around t_0 , so that we can write the Taylor expansion

$$v_{ext}(\mathbf{r}, t) = \sum_{k=0}^{\infty} \frac{1}{k!} \left. \frac{\partial^k v_{ext}(\mathbf{r}, t)}{\partial t^k} \right|_{t=t_0} (t - t_0)^k, \quad (3.40)$$

we can write the condition that the two external potentials are different as the existence of a smallest k for which

$$\left. \frac{\partial^k [v_{ext}^2(\mathbf{r}, t) - v_{ext}^1(\mathbf{r}, t)]}{\partial t^k} \right|_{t=t_0} \neq 0, \quad (3.41)$$

The fact that the external potential has to be t -analytic is the only supposition of the Runge and Gross proof. This condition limits its applicability. Considering the equation-of-motion for the longitudinal (also called paramagnetic) time-dependent current

$$\frac{\partial \mathbf{j}(\mathbf{r}, t)}{\partial t} = -i \langle \Psi(t) | [\hat{\mathbf{j}}(\mathbf{r}), \hat{H}(t)] | \Psi(t) \rangle. \quad (3.42)$$

Supposing that both external potentials $v_{ext}^1(\mathbf{r}, t)$ and $v_{ext}^2(\mathbf{r}, t)$ start from the same initial state $|\Psi(t_0)\rangle$, at time t_0 we have

$$\left. \frac{\partial^{k+1} [\mathbf{j}^2(\mathbf{r}, t) - \mathbf{j}^1(\mathbf{r}, t)]}{\partial t^{k+1}} \right|_{t=t_0} = i\rho(\mathbf{r}, t_0) \nabla \cdot \left. \frac{\partial^k [v_{ext}^1(\mathbf{r}, t) - v_{ext}^2(\mathbf{r}, t)]}{\partial t^k} \right|_{t=t_0}, \quad (3.43)$$

where the current operator is defined as

$$\hat{\mathbf{j}}(\mathbf{r}) = \frac{1}{2i} \sum_{\sigma} \left([\nabla \cdot \hat{\psi}^{\dagger}(\mathbf{x}, t)] \hat{\psi}(\mathbf{x}, t) - \hat{\psi}^{\dagger}(\mathbf{x}, t) \nabla \cdot \hat{\psi}(\mathbf{x}, t) \right). \quad (3.44)$$

Since we suppose the condition Eq. (3.41), it is just demonstrated that the currents $\mathbf{j}^1(\mathbf{r}, t) \neq \mathbf{j}^2(\mathbf{r}, t)$ at a time immediately after t_0 . Now, introducing Eq. (3.43) in the continuity equation

$$\frac{\partial [\rho^1(\mathbf{r}, t) - \rho^2(\mathbf{r}, t)]}{\partial t} = -\nabla \cdot [\mathbf{j}^1(\mathbf{r}, t) - \mathbf{j}^2(\mathbf{r}, t)], \quad (3.45)$$

we obtain a direct relation of the external potential and the time-dependent density,

$$\left. \frac{\partial^{k+2} [\rho^1(\mathbf{r}, t) - \rho^2(\mathbf{r}, t)]}{\partial t^{k+2}} \right|_{t=t_0} = -\nabla \cdot \left[\rho(\mathbf{r}, t) \cdot \nabla \left. \frac{\partial^k [v_{ext}^1(\mathbf{r}, t) - v_{ext}^2(\mathbf{r}, t)]}{\partial t^k} \right|_{t=t_0} \right]. \quad (3.46)$$

It remains to prove that this relation is one-to-one, that is, that the condition established by Eq. (3.41) implies that the right-hand side of Eq. (3.46) is non-zero, implying that $\rho^2(\mathbf{r}, t) - \rho^1(\mathbf{r}, t) \neq 0$ infinitesimally after t_0 . The proof consists in applying Green's theorem to the right-hand side of Eq. (3.46)

$$\int d^3r u(\mathbf{r}, t) \nabla \cdot [\rho(\mathbf{r}, t) \cdot \nabla u(\mathbf{r}, t)] = \frac{1}{2} \oint dS \rho(\mathbf{r}, t) [\nabla u^2(\mathbf{r})], \quad (3.47)$$

where $u(\mathbf{r}, t)$ is a short-hand notation for the k th derivative of the difference of external potentials. If we consider that the density vanishes fast enough at infinity, the surface integral vanishes, and so the right hand side of Eq. (3.47). But there is no way in which $u(\mathbf{r}, t)$ can be zero if we suppose that the potentials are different, therefore arriving to a contradiction.

3.3.1.2 Action principle

The existence theorem does not provide a practical way for extracting the time-dependent density. For that, we need to provide a variational principle, which in the case of time-dependent phenomena is called the least action principle. The second Runge and Gross theorem is the

Action theorem: The time-dependent density can be found by applying the least action principle to the Frenkel-Dirac action defined as follows:

$$A^{RG}[\rho; \Psi_0] = \int_{-\infty}^{\infty} dt \langle \Psi[\rho; \Psi_0](t) | i \frac{\partial}{\partial t} - \hat{H}(t) | \Psi[\rho; \Psi_0](t) \rangle. \quad (3.48)$$

The RG action is equivalent to the Frenkel-Dirac action, which is used to derive the TDSE. The TDSE is obtained by applying the least action principle, that is, by requiring that the variations of the action when we vary the wave function gives zero,

$$0 = \delta A^{RG}[\rho; \Psi_0] = \int_{t_0}^{t_f} dt \langle \delta \Psi[\rho; \Psi_0](t) | i \frac{\partial}{\partial t} - \hat{H}(t) | \Psi[\rho; \Psi_0](t) \rangle + \int_{t_0}^{t_f} dt \langle \Psi[\rho; \Psi_0](t) | i \frac{\partial}{\partial t} - \hat{H}(t) | \delta \Psi[\rho; \Psi_0](t) \rangle. \quad (3.49)$$

If we now integrate the second term by parts, we obtain

$$0 = \delta A^{RG}[\rho; \Psi_0] = \int_{t_0}^{t_f} dt \langle \delta \Psi[\rho](t) | i \frac{\partial}{\partial t} - \hat{H}(t) | \Psi[\rho](t) \rangle + \int_{t_0}^{t_f} dt \langle \left(i \hbar \frac{\partial}{\partial t} - \hat{H}(t) \right) \Psi[\rho](t) | \delta \Psi[\rho](t) \rangle - i \hbar \langle \Psi[\rho] | \delta \Psi[\rho] \rangle \Big|_{t_0}^{t_f}. \quad (3.50)$$

In the derivation of the TDSE, we apply the boundary conditions that $\delta \Psi(t_0) = \delta \Psi(t_f) = 0$, so that the last term of Eq. (3.50) cancels out and we obtain the TDSE,

$$i \hbar \frac{\partial |\Psi(t)\rangle}{\partial t} = \hat{H}(t) |\Psi(t)\rangle. \quad (3.51)$$

The same boundary conditions were initially imposed by Runge and Gross, i.e., $\delta \Psi[\rho](t_0) = \delta \Psi[\rho](t_f) = 0$. Vignale [77] pointed out that the final condition is not controllable, since we have no control of the density at the final point. That means that $\delta \Psi[\rho](t_f) \neq 0$. Vignale defined an action with this extra term

$$A^V[\rho; \Psi_0] = A^{RG}[\rho; \Psi_0] - i \hbar \langle \Psi(t_f) | \delta \Psi(t_f) \rangle, \quad (3.52)$$

which is essential for the correct physical definition of the time-dependent xc potential and kernel.

In order to derive the TDKS equations [106], we separate the Vignale action between the external and the universal functional as

$$A^V[\rho; \Psi_0] = B^V[\rho; \Psi_0] - \int_{t_0}^{t_f} dt \int d^3 r v_{ext}(\mathbf{r}, t) \rho(\mathbf{r}, t), \quad (3.53)$$

where we defined the universal time-dependent action

$$B^V[\rho; \Psi_0] = \int_{t_0}^{t_f} dt \langle \Psi[\rho] | i \frac{\partial}{\partial t} - i \hbar \langle \Psi(t_f) | \delta \Psi(t_f) \rangle - \hat{T} - \hat{W} | \Psi[\rho] \rangle dt. \quad (3.54)$$

We now introduce the same partitioning as the fictitious KS system

$$B^V[\rho; \Psi_0; \Phi_0] = B_s[\rho; \Psi_0] - \frac{1}{2} \int d^3 r \int d^3 r' \frac{\rho(\mathbf{r}, t) \rho(\mathbf{r}', t)}{|\mathbf{r} - \mathbf{r}'|} - A_{xc}^V[\rho; \Psi_0; \Phi_0], \quad (3.55)$$

where the non-interacting universal functional is defined

$$B_s[\rho; \Psi_0] = \int_{t_0}^{t_f} \langle \Phi[\rho; \Psi_0](t) | i\hbar \frac{\partial}{\partial t} - \hat{H}(t) | \Phi[\rho; \Psi_0](t) \rangle dt, \quad (3.56)$$

and the exchange-correlation Vignale action is defined

$$A_{xc}^V[\rho; \Psi_0; \Phi_0] = B^V[\rho; \Phi_0] - B_s[\rho; \Psi_0] + \frac{1}{2} \int d^3r \int d^3r' \frac{\rho(\mathbf{r}, t)\rho(\mathbf{r}', t)}{|\mathbf{r} - \mathbf{r}'|} - i\hbar \langle \Phi(t_f) | \delta\Phi(t_f) \rangle. \quad (3.57)$$

In the above equations, $|\Phi[\rho](t)\rangle$ is a single determinant. Equation (3.55) provides with a definition of time-dependent exchange-correlation action. This introduces an extra dependence on the action, that of the initial state of the non-interacting system.

The density that gives the least action is obtained by the condition

$$\frac{\delta A^V[\rho; \Psi_0; \Phi_0]}{\delta \rho(\mathbf{r}, t)} = 0, \quad (3.58)$$

supposing that we search in the space of v -representable time-dependent densities. Using Eq. (3.53) with the definitions of Eq. (3.55) and Eq. (3.56), we obtain the TDKS equation

$$i\hbar \frac{\partial \phi_i^{KS}(\mathbf{r}, t)}{\partial t} = \left(-\frac{\hbar^2}{2m_e} \nabla^2 + \hat{v}_{ext}(\mathbf{r}, t) + \hat{v}_H(\mathbf{r}, t) + \hat{v}_{xc}[\rho; \Psi_0; \Phi_0](\mathbf{r}, t) \right) \phi_i^{KS}(\mathbf{r}, t), \quad (3.59)$$

where $\phi_i^{KS}(\mathbf{r}, t)$ are the KS orbitals (i runs over the occupied orbitals) that gives the time-dependent density

$$\rho(\mathbf{r}, t) = \sum_i |\phi_i^{KS}(\mathbf{r}, t)|^2, \quad (3.60)$$

the Hartree potential is defined as

$$v_H[\rho^t](\mathbf{r}, t) = \int d^3r' \frac{\rho(\mathbf{r}', t)}{|\mathbf{r} - \mathbf{r}'|}, \quad (3.61)$$

which is a functional of the instantaneous density, and the exchange correlation potential is defined as

$$v_{xc}[\rho; \Phi_0; \Psi_0](\mathbf{r}, t) = \frac{\delta A_{xc}^V[\rho; \Phi_0; \Psi_0]}{\delta \rho(\mathbf{r}, t)}, \quad (3.62)$$

which depends on the density from t_0 to time t , and the initial states of the non-interacting and the interacting systems. Another important quantity is the exchange-correlation kernel,

$$f_{xc}(\mathbf{r}, \mathbf{r}'; t - t') = \frac{\delta v_{xc}[\rho; \Phi_0; \Psi_0](\mathbf{r}, t)}{\delta \rho(\mathbf{r}', t')} = \frac{\delta^2 A_{xc}^V}{\delta \rho(\mathbf{r}, t) \delta \rho(\mathbf{r}', t')}. \quad (3.63)$$

The necessity of using the Vignale action instead of the Runge-Gross action is subtle. If we calculate the second-derivative exchange-correlation action, we obtain the so-called exchange-correlation kernel,

$$f_{xc}(\mathbf{r}, \mathbf{r}'; t - t') = \frac{\delta^2 A_{xc}^{RG}}{\delta \rho(\mathbf{r}, t) \delta \rho(\mathbf{r}', t')} = \frac{\delta^2 A_{xc}^{RG}}{\delta \rho(\mathbf{r}', t') \delta \rho(\mathbf{r}, t)}, \quad (3.64)$$

where the second equality is obtained by virtue of the Schwarz equality of second derivatives. This is, however, an unfortunate property of the Runge-Gross action, since this property breaks causality [76]. The causality property states that the effect of a perturbation at time t can only be seen at $t' > t$. This is not satisfied by Eq. (3.64), which would imply that density variations at space-time \mathbf{r}, t seen at space-time \mathbf{r}', t' with $t' > t$ are equal to the reverse, which is obviously in contradiction with the causality principle.

3.3.1.3 Time-dependent v -representability

The RG theorems bear a close analogy to the HK theorems. This begs the equivalent question of whether the time-dependent density corresponds to some physical external potential, i.e., the time-dependent version of the v -representability problem. In TDDFT, this difficulty is lessened by the fact that the TDKS equation depends on the initial wave function, which takes care of the v -representability problem. A less obvious question is whether the non-interacting density is v -representable. There exist several proofs for the non-interacting v -representability. Mearns and Kohn showed the conditions under which the linear-response density is v -representable [107]. They proved that the non-interacting v -representability of the linear-response density is guaranteed below the first resonance frequency (supposing that the initial density is also non-interacting v -representable.) Beyond this limit, the linear response may not be non-interacting v -representable if the response function has vanishing eigenvalues (which is normally the case.) A more general proof was provided by van Leeuwen [78]. The proof imposes constraints on the initial state. The obvious one is the KS condition that the KS wave function and the real wave function gives the same density,

$$\langle \Phi^{KS} | \hat{\rho}(\mathbf{r}) | \Phi^{KS} \rangle = \langle \Psi | \hat{\rho}(\mathbf{r}) | \Psi \rangle. \quad (3.65)$$

The second condition is a consequence of the continuity equation,

$$\langle \Phi^{KS} | \nabla \hat{\mathbf{j}}(\mathbf{r}) | \Phi^{KS} \rangle = \langle \Psi | \nabla \hat{\mathbf{j}}(\mathbf{r}) | \Psi \rangle, \quad (3.66)$$

which is less obvious, but not difficult to satisfy. The latter condition implies that the initial momenta of the interacting and non-interacting systems are the same. Then, it can be proven that there is a unique mapping between time-dependent densities and one-particle time-dependent potentials. The proof of van Leeuwen relies on the t -analyticity of both the densities and potentials. Unfortunately, t -analytic external potentials do not guarantee analytic densities. In fact, it has been shown not to be applicable to many densities of physical interest [79]. Recently, the v -representable of densities is equivalently reformulated as a proof of existence of a certain class of non-linear Schrödinger equation [79, 80]. The non-interacting v -representability question is still open in TDDFT.

3.3.2 Time-Dependent Kohn-Sham Equation

The RG existence theorem proves that there exists a one-to-one correspondence between time-dependent densities and t -analytic time-dependent external potentials. However, it is the second theorem which provides us with a practical way to calculate the time-dependent density. The main result of the second theorem is the TDKS equation, Eq. (3.59), which requires an initial condition and an approximation to the xc-functional.

In this section, I give some details regarding the two main ways to solve the TDKS equation: linear-response and real-time propagation. Linear response offers a perturbative solution of the TDKS equation in frequency space. Linear response is the preferred method when the system is of small to medium size and the perturbative field we are using is small enough. When fields are stronger, one is obliged to solve the full TDKS equation. The real-time solution has a better scaling with the number of electrons since, unlike linear response, it does not require knowledge of virtual orbitals, which are numerically difficult to obtain.

3.3.2.1 Linear Response

Linear-response equations were first introduced in quantum chemistry with the polarization propagator approach [45], from which the TDHF equations and higher-order approximations were derived. In TDDFT, linear-response equations were first derived by Casida [17], and a year later Petersilka, Grossman and Gross gave an alternative derivation [108]. In this section, I will provide a derivation based on ideas of these two references.

Formalism

The linear-response is a perturbative approach. This requires an initial Hamiltonian, the TDKS Hamiltonian

$$\hat{H}_0^{KS} = \hat{t}_s + \hat{v}_{Hxc}[\rho_0] + \hat{v}_{ext}^0, \quad (3.67)$$

where \hat{t}_s is the non-interacting kinetic-energy operator, $\hat{v}_{Hxc}[\rho_0]$ is the Hartree-exchange-correlation potential evaluated at the ground-state density, and \hat{v}_{ext}^0 is the external potential, which in our case will be restricted to fixed positive point charges. The application of a time-dependent field,

$$\hat{v}_{appl}(t) = \hat{v}_{ext}(t) + \hat{v}_{ext}^0 = \int_{t_0}^t dt \mathcal{E}(t) \hat{\rho}(t) + \hat{v}_{ext}^0, \quad (3.68)$$

introduces a time-dependence in the KS Hamiltonian

$$\begin{aligned} \hat{H}^{KS}(t) &= \hat{t}_s + \hat{v}_H[\rho_t](t) + \hat{v}_{xc}[\rho](t) + \hat{v}_{ext} + \hat{v}_{ext}(t) \\ &= \hat{H}_0^{KS} + \delta\hat{v}_{Hxc}[\rho](t) + \delta\hat{v}_{ext}(t) = \hat{H}_0^{KS} + \delta\hat{v}_s(t), \end{aligned} \quad (3.69)$$

where we defined $\delta\hat{v}(t) = \hat{v}(t) - \hat{v}(t_0)$. The change in the time-dependent self-consistent field potential $\delta\hat{v}_s$ introduces changes in the time-dependent density. The linear changes of the density are related to the potential through the density-density response function,

$$\delta\hat{\rho}(t) = \int_{t_0}^t dt' \hat{\chi}_s(t-t')\delta\hat{v}_s(t') \quad (3.70)$$

where $\hat{\chi}_s(t-t')$ is the non-interacting response function, also called susceptibility. By the KS assumption, the density response of Eq. (3.70) is equal to the density response of the interacting system. In the interacting system, the interacting response function relates the density changes to the applied field

$$\delta\hat{\rho}(t) = \int_{t_0}^t dt' \hat{\chi}(t-t')\delta\hat{v}_{ext}(t'). \quad (3.71)$$

The fact that both Eqs. (3.70) and (3.71) give the same density has an interesting consequence that allows us to relate the response functions of the non-interacting and the interacting system. Considering the definition of the variations on the KS potential

$$\delta\hat{v}_s(t) = \delta\hat{v}_{Hxc}[\rho](t) + \delta\hat{v}_{appl}(t), \quad (3.72)$$

we can divide by the density response to obtain

$$\frac{\delta\hat{v}_s(t)}{\delta\hat{\rho}(t')} = \frac{\delta\hat{v}_{Hxc}[\rho](t)}{\delta\hat{\rho}(t')} + \frac{\delta\hat{v}_{ext}(t)}{\delta\rho(t')}, \quad (3.73)$$

which using the definitions of the response functions [Eq. (2.59)] and the Hartree-exchange-correlation kernel [Eq. (3.63)] leads to a Dyson-type equation for the response functions,

$$\hat{\chi}_s^{-1}(t-t') = \hat{f}_{Hxc}(t-t') + \hat{\chi}^{-1}(t-t'). \quad (3.74)$$

The importance of the response functions is in its Fourier transform. If we convolute with the time-dependent density response and we Fourier transform the Dyson-type equation we obtain

$$\hat{\chi}_s^{-1}(\omega)\delta\hat{\rho}(\omega) = \hat{f}_{Hxc}(\omega)\delta\rho(\omega) + \hat{\chi}^{-1}(\omega)\delta\rho(\omega). \quad (3.75)$$

Using back Eq. (3.71) and rearranging terms, we finally arrive at the linear-response equation

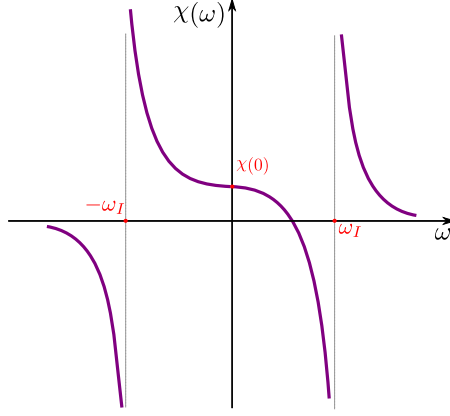
$$\left[\hat{\chi}_s^{-1}(\omega) - \hat{f}_{Hxc}(\omega) \right] \delta\hat{\rho}(\omega) = \delta\hat{v}_{ext}(\omega). \quad (3.76)$$

The importance of Eq. (3.76) is that we related changes in the exact density directly to the time-dependent applied potential, just by knowing the response function of the interacting system and the exchange-correlation kernel.

A key feature of linear-response is that the response of the density is independent of the form of the applied field (as long as it is weak enough to apply perturbation theory.) This is easily seen, but it requires a careful look at the response functions. The Fourier-transform of the interacting response function [defined in Eq. (3.71)] has the following form

$$\hat{\chi}(\omega) = \lim_{\eta \rightarrow 0} \sum_{I \neq 0} \left[\frac{\langle \Psi_0 | \hat{\rho} | \Psi_I \rangle \langle \Psi_I | \hat{\rho} | \Psi_0 \rangle}{\omega - \omega_I + i\eta} - \frac{\langle \Psi_0 | \hat{\rho} | \Psi_I \rangle \langle \Psi_I | \hat{\rho} | \Psi_0 \rangle}{\omega + \omega_I + i\eta} \right]. \quad (3.77)$$

Figure 3.2 Schematic plot of the response function $\chi(\omega)$ versus ω . At the frequencies $-\omega_I$ and ω_I , corresponding to a de-excitation and excitation energy, the response function goes to \pm infinity. At $\omega = 0$, the static response function $\chi(0)$ is obtained.



In this equation, $\hat{\rho}$ is the density operator, $|\Psi_0\rangle$ and $|\Psi_I\rangle$ are respectively the ground-state and excited state wave functions of the exact system, and $\omega_I = (E_I - E_0)$ is the excitation frequency containing the energy difference of the excited state I and the ground state. Similarly, the non-interacting response function $\chi_s(\omega)$ is defined as

$$\hat{\chi}_s(\omega) = \lim_{\eta \rightarrow 0} \sum_I \left[\frac{\langle \Phi_0 | \hat{\rho} | \Phi_I \rangle \langle \Phi_I | \hat{\rho} | \Phi_0 \rangle}{\omega - \omega_I + i\eta} - \frac{\langle \Phi_0 | \hat{\rho} | \Phi_I \rangle \langle \Phi_I | \hat{\rho} | \Phi_0 \rangle}{\omega + \omega_I + i\eta} \right]. \quad (3.78)$$

A schematic picture of the structure of the response function is depicted in Fig. 3.2. It is a monotonically decreasing odd function. At $\omega = 0$, the static response function is obtained, which is an important feature for defining an adiabatic approximation in dressed TDDFT as we will see in Chapter 5. For the present discussion, an important feature of the response function is that it has discontinuities at the (de-)excitation frequencies $\pm\omega_I$. The converse is also true: we are at a resonance frequency whenever the response function is infinite. This structural property of the response function will allow us to easily extract the excitation energies. In Eq. (3.71), we established the relation between variations of the applied potential to the variations of the density. If we are at a resonance frequency, the response function has an infinite value. This would cause an unphysical density response unless the variations in the applied field are exactly 0, in which case the product is undefined and the density variations can be finite. In this way, we have a simple condition to extract the excitation poles from Eq. (3.76),

$$\left[\hat{\chi}_s^{-1}(\omega_I) - \hat{f}_{Hxc}(\omega_I) \right] \delta\hat{\rho}(\omega) = 0. \quad (3.79)$$

The Eq. (3.79) is ready to be solved, but a practical implementation requires the transformation of the equations into matrix form,

$$\sum_{rs} \left[[\chi_s(\omega)]_{pq,rs} - (pq|f_{Hxc}|rs) \right] [\delta\rho(\omega)]_{rs} = [0]_{pq}, \quad (3.80)$$

with the definitions

$$(pq|f_{Hxc}|rs) = \int d^3r \int d^3r' \phi_p^*(\mathbf{r}) \phi_q(\mathbf{r}) \left[\frac{1}{|\mathbf{r} - \mathbf{r}'| + f_{xc}(\mathbf{r}, \mathbf{r}'; \omega)} \right] \phi_r^*(\mathbf{r}') \phi_s(\mathbf{r}'). \quad (3.81)$$

We can easily calculate the matrix elements of $\chi_s(\omega)$

$$[\chi_s]_{pq,rs} = \sum_{pq} \frac{(f_q - f_p)}{\omega - (\epsilon_p - \epsilon_q)} \delta_{pr} \delta_{qs}, \quad (3.82)$$

where f_p is the occupation number of spin orbital p and ϵ_p is its eigenvalue. Substituting it in Eq. (3.80) and rearranging terms, we arrive to the eigenvalue problem

$$\sum_{rs} \left(\frac{\epsilon_p - \epsilon_q}{f_q - f_p} \delta_{pr} \delta_{qs} + (pq|f_{Hxc}(\omega)|rs) \right) [\delta\rho(\omega)]_{rs} = \frac{\omega}{f_q - f_p} [\delta\rho(\omega)]_{pq}. \quad (3.83)$$

The indexes p, q indicate general orbitals, but only two (coupled) equations give a finite solution, when p is occupied and q is unoccupied (excitation) and vice-versa (de-excitation),

$$\begin{aligned} \sum_{jb} \left(\frac{\epsilon_i - \epsilon_a}{f_a - f_i} \delta_{ij} \delta_{ab} + (ia|f_{Hxc}(\omega)|bj) \right) [\delta\rho(\omega)]_{jb} + (ia|f_{Hxc}(\omega)|jb) [\delta\rho(\omega)]_{bj} &= \frac{\omega}{f_i - f_a} [\delta\rho(\omega)]_{ia} \\ \sum_{jb} \left(\frac{\epsilon_a - \epsilon_i}{f_i - f_a} \delta_{ij} \delta_{ab} + (jb|f_{Hxc}(\omega)|ai) \right) [\delta\rho(\omega)]_{jb} + (jb|f_{Hxc}(\omega)|ia) [\delta\rho(\omega)]_{bj} &= \frac{\omega}{f_a - f_i} [\delta\rho(\omega)]_{ai} \end{aligned} \quad (3.84)$$

which can be cast in the typical RPA matrix form as

$$\begin{bmatrix} \mathbf{A}(\omega) & \mathbf{B}(\omega) \\ \mathbf{B}^*(\omega) & \mathbf{A}^*(\omega) \end{bmatrix} \begin{bmatrix} \mathbf{X}(\omega) \\ \mathbf{Y}(\omega) \end{bmatrix} = \omega \begin{bmatrix} \boldsymbol{\lambda} & \mathbf{0} \\ \mathbf{0} & -\boldsymbol{\lambda} \end{bmatrix} \begin{bmatrix} \mathbf{X}(\omega) \\ \mathbf{Y}(\omega) \end{bmatrix} \quad (3.85)$$

in which we defined the following matrices

$$\begin{aligned} [A(\omega)]_{ia,jb} &= \frac{\epsilon_a - \epsilon_i}{f_a - f_i} \delta_{ij} \delta_{ab} + (ia|f_{Hxc}(\omega)|bj) \\ [B(\omega)]_{ia,jb} &= (ia|f_{Hxc}(\omega)|jb), \end{aligned} \quad (3.86)$$

the matrix elements of the density response are written as

$$[X]_{ia} = [\delta\rho(\omega)]_{ia} \quad (3.87)$$

$$[Y]_{ia} = [\delta\rho(\omega)]_{ai}, \quad (3.88)$$

and the metric as

$$[\lambda]_{ia,jb} = \frac{1}{f_a - f_i} \delta_{ij} \delta_{ab}. \quad (3.89)$$

The names of these matrices are inherited from random phase approximation (RPA) theory. However, even though the mathematical form of Eq. (3.85) is similar to the RPA equation, they are quite different equations. Actually, Eq. (3.85) is non-linear due to the dependency of the Hartree-exchange-correlation kernel on the excitation frequency. This non-linearity is very important, since it gives extra solutions not present in the usual RPA as we will see in the next sections. Also, the solution of the linear response equation provides an exact solution when the exact exchange-correlation kernel is known.

The Tamm-Dancoff approximation, common in RPA theory, is also applicable in TDDFT. It accounts for setting $\mathbf{B} = \mathbf{0}$, in which case the excitations and de-excitations are decoupled and the TDDFT equations are simply

$$\mathbf{A}(\omega)\mathbf{X} = \omega\mathbf{X}. \quad (3.90)$$

Although the sum rules are not exactly satisfied in this approximation, it normally give more accurate excitation energies [109].

Numerical Implementation in DEMON2K

The linear-response equations in the form of Eq. (3.85) are a typical eigenvalue problem. The spin orbitals, spin orbital energies and an approximation to the exchange-correlation kernel are the sole ingredients necessary to construct Eq. (3.86), which is then diagonalized to obtain the excitation energies and the response functions of the exact interacting system. However, Eq. (3.85) is cast in a form of a non-Hermitian eigenvalue problem, and the most efficient eigenvalue solvers are optimized for Hermitian eigenvalue problems. Luckily, Eq. (3.85) can be simply cast in a Hermitian form. In this derivation, we will consider that the spin orbitals are real and therefore, all complex conjugate symbols will be left out. If we add up and subtract the two equations of Eq. (3.85), we obtain

$$\begin{aligned} [\mathbf{A}(\omega) + \mathbf{B}(\omega)] [\mathbf{X}(\omega) + \mathbf{Y}(\omega)] &= \omega\lambda[\mathbf{X}(\omega) - \mathbf{Y}(\omega)] \\ [\mathbf{A}(\omega) - \mathbf{B}(\omega)] [\mathbf{X}(\omega) - \mathbf{Y}(\omega)] &= \omega\lambda[\mathbf{X}(\omega) + \mathbf{Y}(\omega)]. \end{aligned} \quad (3.91)$$

We now have both equations in Hermitian form, but we have lost the eigenvalue equation form of Eq. (3.85). To obtain an eigenvalue form, we introduce the second equation into the first

$$\lambda^{-1} [\mathbf{A}(\omega) + \mathbf{B}(\omega)] \lambda^{-1} [\mathbf{A}(\omega) - \mathbf{B}(\omega)] [\mathbf{X}(\omega) - \mathbf{Y}(\omega)] = \omega^2 [\mathbf{X}(\omega) - \mathbf{Y}(\omega)]. \quad (3.92)$$

This equation does not have the desired symmetric form, but symmetrizing can be easily done by multiplying $[\mathbf{A}(\omega) - \mathbf{B}(\omega)]^{-\frac{1}{2}}$ in both sides, so that

$$[\mathbf{A}(\omega) + \mathbf{B}(\omega)]' [\mathbf{X}(\omega) - \mathbf{Y}(\omega)]' = \omega^2 [\mathbf{X}(\omega) - \mathbf{Y}(\omega)]' , \quad (3.93)$$

where we defined

$$[\mathbf{A}(\omega) + \mathbf{B}(\omega)]' = [\mathbf{A}(\omega) - \mathbf{B}(\omega)]^{\frac{1}{2}} \boldsymbol{\lambda}^{-1} [\mathbf{A}(\omega) + \mathbf{B}(\omega)] [\mathbf{A}(\omega) - \mathbf{B}(\omega)]^{\frac{1}{2}} \boldsymbol{\lambda}^{-1} , \quad (3.94)$$

and

$$[\mathbf{X}(\omega) - \mathbf{Y}(\omega)]' = [\mathbf{A}(\omega) - \mathbf{B}(\omega)]^{\frac{1}{2}} [\mathbf{X}(\omega) - \mathbf{Y}(\omega)] . \quad (3.95)$$

Most implementations of linear response solve Eq. (3.93). The price is that we cannot have access to $\mathbf{X}(\omega)$ and $\mathbf{Y}(\omega)$ separately, but still the difference of these two vectors is enough to calculate all relevant properties.

A final remark has to be made that helps to understand the reason why linear response equations in density-functional theory are more efficient than the equivalent TDHF equations. The HF exchange kernel does not have the symmetry property of the exact exchange-correlation kernel of density-functional theory,

$$f_{xc}(\mathbf{r}, \mathbf{r}'; \omega) = f_{xc}(\mathbf{r}', \mathbf{r}; \omega) . \quad (3.96)$$

This property makes the $\mathbf{A}(\omega) - \mathbf{B}(\omega)$ matrix a simple diagonal matrix, whereas in TDHF, this matrix has to be specifically constructed. In TDDFT, the matrix $[\mathbf{A}(\omega) + \mathbf{B}(\omega)]'$ have a the simple form

$$\begin{aligned} [A(\omega) + B(\omega)]_{ia,jb} &= (\epsilon_a - \epsilon_i)^2 (f_i - f_a) \delta_{ij} \delta_{ab} \\ &+ 2 \cdot \sqrt{(f_a - f_i)(\epsilon_a - \epsilon_i)} (ia|f_{Hxc}(\omega)|bj) \sqrt{(f_b - f_j)(\epsilon_b - \epsilon_j)} . \end{aligned} \quad (3.97)$$

The implementation of these equations in DEMON2K was mainly done by Andrei Ipatov *et al.* [110], based on a previous version of Jamorski and Casida called DEMON-DYNARHO [25, 111]. The implementation is remarkable for exploiting the resolution of the identity to convert four-center integrals into three-center integrals,

$$(pq|f_{Hxc}(\omega)|rs) = \sum_{IJKL} (pq|g_I) S_{IJ}^{-1} (g_J|f_{Hxc}(\omega)|g_K) S_{KL}^{-1} (g_L|rs) , \quad (3.98)$$

where g_I is an auxiliary function, and $S_{IJ} = (g_I|g_J)$ is the overlap matrix of auxiliary functions using the electron repulsion as a metric. Also, a Davidson diagonalizer is used. This is a Krylov space method that extracts a reduced number of eigenvalues from a matrix without having to save the whole matrix [110].

The version of linear-response in DEMON2K needed some clean up, which I did by exploiting the techniques of code optimization from a very good introductory book on the subject by S. Goedecker and A. Hoisie [112]. There have been no real tests of performance of the optimized code, but the calculations take 10-20% less time on average. Additional features have been implemented, which give the user the freedom to perform more effective calculations. Especially, for big systems it might be interesting to apply the frozen core approximation without losing much accuracy.

Physical properties from linear response

From the solution of Eq. (3.85), one obtains the excitation energies (poles of the response function) and the eigenvalues, which gives the response of the density,

$$\delta\rho(\mathbf{r},\omega) = \sum_{ia} X_{ia}(\omega)\phi_a^{*,KS}(\mathbf{r})\phi_i^{KS}(\mathbf{r}) + Y_{ia}(\omega)\phi_i^{*,KS}(\mathbf{r})\phi_a^{KS}(\mathbf{r}). \quad (3.99)$$

This is enough for calculating many properties of the system. The transition dipole moment is given by

$$\langle\Phi_0|\mathbf{r}|\Phi_I\rangle = \sum_{ia} X_{ia}(\omega)\langle\phi_i^{KS}|\mathbf{r}|\phi_a^{KS}\rangle + Y_{ia}(\omega)\langle\phi_a^{KS}|\mathbf{r}|\phi_i^{KS}\rangle \quad (3.100)$$

which allows us to calculate the oscillator strength by applying the Fermi golden rule

$$f_I = \frac{2}{3}|\langle\Phi_0|\mathbf{r}|\Phi_I\rangle|^2\omega_I. \quad (3.101)$$

From the oscillator strength, a number of energy weighted sum rules can be derived. Most importantly are the Thomas-Reiche-Kuhn sum rule,

$$N_e = \sum_I f_I, \quad (3.102)$$

and the static polarizability, which is given by

$$\alpha = \sum_I \frac{f_I}{\omega_I^2}. \quad (3.103)$$

Similarly, the frequency-dependent polarizability is given by

$$\alpha(\omega) = \sum_I \frac{f_I}{\omega_I^2 - \omega^2}. \quad (3.104)$$

These sum rules are not exactly satisfied in the Tamm-Dancoff approximation.

3.3.2.2 Real-Time*Formalism*

In the previous section, I derived the linear response equation, which is the most relevant equation for the purposes of this thesis. We have seen that the linear response applies perturbation theory to extract directly excitation energies and properties. However, when the field is intense, for example a molecule in a laser field, linear response is not appropriate. In this cases, one attempts to solve directly the TDKS equation by propagating the KS wave function in real time. Starting from Eq. (3.59), and considering that at the initial time t_0 the wave function

$|\Phi_s(t_0)\rangle$ is the KS wave function of the ground-state, we can formally solve it obtaining,

$$|\Phi_s(t)\rangle = \hat{U}_s(t, t_0)|\Phi_s(t_0)\rangle = \mathcal{T} \left[e^{-i\hbar \int_{t_0}^t \hat{H}_s(t) dt} \right] |\Phi_s(t_0)\rangle, \quad (3.105)$$

where $\hat{U}_s(t, t_0)$ is the KS time evolution operator from t_0 to t and the Hamiltonian $\hat{H}_s(t)$ is the same as that of Eq. (3.69). The density matrix operator at time t is then obtained simply by

$$\hat{\rho}(t) = |\Phi_s(t)\rangle\langle\Phi_s(t)|, \quad (3.106)$$

which can be used to calculate any property. For small fields and to a first order approximation, this density is exactly the same as the one obtained from linear response. A subtle difference is that in real-time, we only propagate the occupied orbitals, and no information about unoccupied orbitals is needed. Also, the form of the applied field is relevant. For normal applications, a general kick-potential is applied at time t_0 , which drives the system out of equilibrium. However, it is also possible to use other kinds of applied fields. Especially important is the optimal control, which designs a field that drives the system in a desired direction [2]. This can be used, for example, to dissociate specific bonds in a molecule by applying a tuned laser field [113].

Numerical implementation in OCTOPUS

The numerical implementation of real-time TDDFT focuses on the efficient application of the time propagator on the wave function. For convenience, the time is chopped in sufficiently small steps so that the integral of Eq. (3.105) can be more easily approximated. For example, a classical approximation is the exponential mid-point propagator,

$$|\Phi_s(t + \Delta t)\rangle \approx e^{-i\hbar \hat{H}_s(t + \Delta t/2) \Delta t} |\Phi_s(t)\rangle, \quad (3.107)$$

where Δt is the time step. The fact that we need to compute the Hamiltonian at future times, requires some sort of interpolation of the density in order to calculate it.

The bottleneck of real-time calculations is in the application of the exponential on the wave functions. Several strategies have been implemented in OCTOPUS, which are lengthly explained in Ref. [75]. A classical way to apply the exponentials is by using a Taylor expansion,

$$e^{-i\hat{H}\Delta t} \approx \sum_{k=0}^{\infty} \frac{(-i\Delta t)^k}{k!} \hat{H}^k. \quad (3.108)$$

3.3.3 Time-Dependent Exchange-Correlation Functional

The exchange-correlation functional of TDDFT has little in common with the DFT functional. The exact TDDFT functional has exotic properties like the ultra-non-locality, the causality or the memory effects, which arise from the nature of the TDSE. In practice, TDDFT inherits the DFT functionals (adiabatic approximation.) This is however not always a good approximation to the action, especially when the effects of past densities become important. Consistent param-

eterization of memory functionals is not straightforward, due to the non-local dependencies in space and time. Memory functionals are still in their infancy, and they are the main challenge of future developments of TDDFT. In Ref. [114], it was proposed to establish a Jacob's ladder of TDDFT differently from DFT, in which the memory effects are central in building in more information. The lowest rung is occupied by the local in time adiabatic functionals. The higher rungs are then equivalent theories, in which quantum dynamics are easily expressed, such as time-dependent current-density theory or time-dependent deformation theory.

3.3.3.1 Exact Properties

In this section, we explore the exact conditions of the time-dependent xc functional. For the interest of this thesis, most of the properties will be formulated for the xc kernel. The conditions for the xc potential are discussed in detail in the TDDFT monographs of Refs. [37, 115].

A simple exact condition of TDDFT is the adiabatic limit,

$$f_{xc}(\mathbf{r}, \mathbf{r}'; \omega) = \frac{\delta E_{xc}[\rho]}{\delta \rho(\mathbf{r})\rho(\mathbf{r}')} \quad \omega \rightarrow 0^+, \quad (3.109)$$

and the zero-force and zero-torque conditions for the xc kernel,

$$\int d^3r \rho(\mathbf{r}) \nabla_{\mathbf{r}} f_{xc}(\mathbf{r}, \mathbf{r}'; \omega) = -\nabla_{\mathbf{r}'} \quad (3.110)$$

$$\int d^3r \rho(\mathbf{r}) \mathbf{r} \times \nabla_{\mathbf{r}} f_{xc}(\mathbf{r}, \mathbf{r}'; \omega) = -\mathbf{r}' \times \nabla_{\mathbf{r}'}. \quad (3.111)$$

The attentive reader will note the strange fact that an integral over space on the left-hand side of the two conditions gives a frequency-independent quantity on the RHS. This is only possible if the xc kernel has an infinite long-range, which is always present irrespective of the interaction strength [35, 36]. The different non-local behaviour has been termed ultra-non-locality.

The self-interaction condition for one-electron systems has to be satisfied at all times

$$f_x(\mathbf{r}, \mathbf{r}'; \omega) = -\frac{1}{|\mathbf{r} - \mathbf{r}'|} \quad f_c(\mathbf{r}, \mathbf{r}'; \omega) = 0. \quad (3.112)$$

Due to the relation of the xc kernel and the retarded response functions [Eq. (3.74)], the xc kernel satisfies extra mathematical conditions. One of them is the symmetry property used in Eq. (3.96), which stems from the symmetry of the response functions. Also, the kernel is an analytic function of ω in the upper half plane of the complex plane, and approaches a real function when $\omega \rightarrow \infty$. Therefore, it satisfies the Kramers-Kronig relations

$$\Re[f_{xc}(\mathbf{r}, \mathbf{r}'; \omega) - f_{xc}(\mathbf{r}, \mathbf{r}'; \infty)] = P \int \frac{d\omega'}{\pi} \frac{\Im f_{xc}(\mathbf{r}, \mathbf{r}'; \omega')}{\omega' - \omega}, \quad (3.113)$$

and

$$\Im f_{xc}(\mathbf{r}, \mathbf{r}'; \omega') = P \int \frac{d\omega}{\pi} \frac{\Re[f_{xc}(\mathbf{r}, \mathbf{r}'; \omega) - f_{xc}(\mathbf{r}, \mathbf{r}'; \infty)]}{\omega' - \omega}. \quad (3.114)$$

where P is the Cauchy principal value. The exact xc kernel is real-valued in space and time domain, which leads to the condition in the frequency domain

$$f_{xc}(\mathbf{r}, \mathbf{r}'; \omega) = f_{xc}^*(\mathbf{r}, \mathbf{r}'; -\omega). \quad (3.115)$$

3.3.3.2 Adiabatic Approximation

The most commonly used approximated TDDFT functional is the adiabatic approximation. This functional is defined in terms of the xc potential as

$$v_{xc}^{AA}(\mathbf{r}, t) = \left. \frac{\delta E_{xc}[\rho_t]}{\delta \rho_t(\mathbf{r})} \right|_{\rho=\rho_0}, \quad (3.116)$$

where ρ_t is the density at time t , and the E_{xc} is the DFT functional. Similarly, the adiabatic approximation of the xc kernel is given by

$$f_{xc}^{AA}(\mathbf{r}, \mathbf{r}'; t - t') = \delta(t - t') \left. \frac{\delta^2 E_{xc}[\rho_t]}{\delta \rho_t(\mathbf{r}') \delta \rho_t(\mathbf{r})} \right|_{\rho=\rho_0}. \quad (3.117)$$

In fact, this approximation takes the adiabatic limit of the exact TDDFT functional and uses it at all times. In other words, the density reacts instantaneously and without memory. The adiabatic approximation trivially satisfies most of the sum rules of the exact functional, simply because it does not have any time dependence. In practice, the adiabatic functionals turn out to be a good approximation in many cases, especially for excited states of main single excitation character, which are not too delocalized and do not involve too much charge transfer. The exact implications of the adiabatic approximation are not known. In this section, we try to analyze some of the problems of the adiabatic approximation.

Problems associated with the approximate ground-state functional

The adiabatic approximation uses approximate DFT functionals and therefore inherits all the problems associated with them. Especially important are the problems associated with approximate exchange. The lack of derivative discontinuity predicts too small a HOMO-LUMO gap. The wrong asymptotic behavior of exchange places the continuum of states too low (as much as 5 eV), and predicts unrealistic mixing between bound and unbound states. The problems of the Rydberg states can be similarly associated with the wrong asymptotic behavior of exchange.

This problem can be easily alleviated by using a more sophisticated DFT functional. The time-dependent exact exchange cures all these problems, although it is computationally expensive and largely overestimates the gap. A good compromise between accuracy and reliability is given by the asymptotically-corrected hybrid functionals.

Lack of double excitations

Doubly and higher excited states are not present in adiabatic TDDFT. The easiest way to see this is in the linear response equations [Eq. (3.85)]. The Fourier transformed adiabatic kernel is frequency independent

$$f_{xc}^{AA}(\mathbf{r}, \mathbf{r}') = \frac{\delta^2 E_{xc}[\rho_t]}{\delta\rho_t(\mathbf{r}')\delta\rho_t(\mathbf{r})} \Big|_{\rho=\rho_0}, \quad (3.118)$$

which converts Casida equations to,

$$\begin{bmatrix} \mathbf{A} & \mathbf{B} \\ \mathbf{B}^* & \mathbf{A}^* \end{bmatrix} \begin{bmatrix} \mathbf{X} \\ \mathbf{Y} \end{bmatrix} = \omega \begin{bmatrix} \lambda & \mathbf{0} \\ \mathbf{0} & -\lambda \end{bmatrix} \begin{bmatrix} \mathbf{X} \\ \mathbf{Y} \end{bmatrix}, \quad (3.119)$$

in which we used the f_{xc}^{AA} in the block definitions of \mathbf{A} and \mathbf{B} [see Eq. (3.86).] Now, the linear response equations are no longer non-linear, and the number of solutions is exactly the same as the dimension of the matrices, that is, the number of single excitations.

To regain back the double excitations, memory functionals are required. Then, time-dependent functionals are obtained, which are frequency dependent upon Fourier transformation. The exact exchange functional has a trivial frequency dependence which is not enough for obtaining double excitations. For this, better correlation functionals are needed, as demonstrated in subsequent chapters.

Bond dissociation and Funnels

The adiabatic approximation fails to represent excited states along the bond dissociation coordinate and conical intersections. The origin of these problems have an origin both in DFT and TDDFT. From the DFT side, the non-interacting v -representability problem is the main difficulty. From the TDDFT site, the adiabatic approximation does not include double excitations, which are necessary for describing these effects, especially for funnels. Another problem of TDDFT, which has never been addressed, is the interaction between the excited states and the reference.

3.3.3.3 Memory¹

The exact TDDFT potential [Eq. (3.62)] is a functional of the whole history of past densities and the initial conditions. These dependencies, known as memory, are completely neglected in common TDDFT applications using the adiabatic approximation. The adiabatic potential [Eq. (3.116)] approximates xc-effects by using only the density at the present time. Adiabatic functionals work fairly well when the non-interacting system is a reasonable physical first approximation to the interacting system, but it can fail dramatically in cases like 2p2h² excited states [44], conical intersections [29,30], charge transfer and Rydberg excitations [26,27], excited states along the bond dissociation coordinate [116], one-dimensional extended systems [117,118], band-gaps in solids [119] and spectra of semiconductors [119–121]. In such cases, the contribution of past densities to the xc energy becomes essential, requiring memory functionals specifically

1. This section has been submitted as part of a review article (Ref. [114]). The references to equations of other parts of the review are substituted by the equivalents on this document.

2. 2-particle/2-hole

designed for TDDFT. In this section, we will review the most successful memory functionals available at the present time. Due to the difficulties associated with the action, few attempts have been made to approximate directly the xc-action [122]. Instead, most memory functionals approximate the derivatives. Therefore, our discussion will focus on the construction of memory xc-potentials and especially memory xc-kernels.

Memory and Nonlocality

Memory introduces strong requirements for TDDFT functionals [37], which forbids the intuitively simple functional approximations of ground-state DFT. For example, a simple parameterization of a spatially-local memory LDA xc-kernel for the homogeneous electron gas (HEG) [123] violates, by construction, the zero-force theorem [35, 36], introducing unphysical damping effects during the time propagation of the density and a corresponding loss of total energy. Several schemes have appeared that enforce the sum rules *a posteriori* [124, 125]. Most importantly, these studies showed that memory functionals must be non-local in space. This property forbids the application of the popular gradient expansion to memory functionals [126], ultimately a consequence of the ultra-nonlocality property of the exact xc-functional.

The ultra-nonlocality property of the exact functional indicates that the density is perhaps not the best reduced variable to express time-dependent xc-effects. This redirected attention to other time-dependent theories where memory effects are described by local functionals, such as in TDCDFT³ [122, 126–129], and in Lagrangian TDDFT (L-TDDFT) [130–132].

Current Density-Functional Theory

TDCDFT is very much related to TDDFT, though its range of applications is broader. In fact, the one-to-one correspondence between currents and external potentials is the first step in the Runge-Gross existence proof for TDDFT [13]. However, the TDCDFT proof does not resort to any surface integral, which makes its application to solids more straightforward than TDDFT. The first memory functional for TDCDFT is due to Vignale and Kohn, which consists of a parameterization of a memory LDA xc-kernel tensor for the HEG [126]. This kernel is local in space and, unlike the corresponding in TDDFT, it satisfies the zero-force theorem. However, the kernel introduces too strong damping effects that induce a decoherence mechanism, which allows the density to decay back to a ground-state with higher entropy, different from the real ground-state, in which the total energy is conserved [133]. The Vignale-Kohn kernel has been used successfully to calculate the static polarizabilities of one-dimensional conjugated chains, which were largely overestimated by common adiabatic LDA [117]. However, it fails for one-dimensional hydrogen chains, which require more sophisticated kernels [118]. The Vignale-Kohn kernel also shows the characteristic double-peak spectrum of bulk silicon [134], a feature that is not present in the adiabatic LDA spectrum. Memory kernels of TDCDFT can then be mapped into TDDFT kernels maintaining part of the features of the Vignale-Kohn kernel [135].

Lagrangian Density-Functional Theory

3. Time-dependent current-density-functional theory

L-TDDFT has less applications to realistic systems, but it has provided deeper insight as to the role of memory. L-TDDFT is a reformulation of TDDFT, in which the electronic density is re-expressed in a reference frame (Lagrangian frame) that moves along with the fluid [130, 131]. This allows memory to be expressed locally in terms of the position of fluid elements and the deformation tensor. The deformation tensor accounts for the Coulomb coupling of a differential volume of fluid at position \mathbf{r} and time t with was at a different position \mathbf{r}' at an earlier time $t' < t$. Both TDCDFT and L-TDDFT are equivalent in the linear regime [132].

Optimized Effective Potential Approaches

All the aforementioned memory functionals lack a systematic route to improve upon the present approximations. A more systematic way to construct memory functionals is to use the time-dependent optimized effective potential (TDOEP), in which many-body perturbation theory quantities (MBPT) are mapped into TDDFT [32, 100, 136–140]. An easy way to establish this mapping is to make use of the Kohn-Sham assumption, i.e., requiring that the interacting time-dependent density equals the non-interacting one [100]. This is the basis of the time-dependent Sham-Schlüter equation that allows us to relate the self-energy to the xc-potential and the kernel of the Bethe-Salpeter equation to the xc-kernel. In this way, consistent approximations are possible, that guarantee the satisfaction of exact conditions [138, 141]. Still, there are many ways to derive the time-dependent Sham-Schlüter equation, but similar functionals are obtained if the same MBPT approximation is used. For deriving xc-kernels, a simple way is to require that the diagonal of the MBPT response functions leads to the same spectrum as the TDDFT response function [Eq. (3.77)], which leads to

$$f_{xc}(\mathbf{r}, \mathbf{r}'; \omega) = \int d^3r_1 \int d^3r_2 \int d^3r_3 \int d^3r_4 \Lambda(\mathbf{r}; \mathbf{r}_1, \mathbf{r}_2; \omega) K(\mathbf{r}_1, \mathbf{r}_2; \mathbf{r}_3, \mathbf{r}_4; \omega) \Lambda_s^\dagger(\mathbf{r}_3, \mathbf{r}_4; \mathbf{r}'; \omega), \quad (3.120)$$

relating the exact TDDFT xc-kernel to the kernel K defined from MBPT quantities. The mapping is possible thanks to the localization function Λ , which is expressed in terms of the response functions [Eq. (3.77)],

$$\Lambda(\mathbf{r}_1; \mathbf{r}_2, \mathbf{r}_3; \omega) = \chi^{-1}(\mathbf{r}_1, \mathbf{r}_2; \omega) \chi(\mathbf{r}_2, \mathbf{r}_3; \omega). \quad (3.121)$$

The localizer Λ_s , appearing in Eq. (3.120), has an equivalent definition with the non-interacting response functions instead of the interacting ones. The localizer introduces an extra frequency-dependence in the kernel, which brings in the MBPT quantity the ultra-nonlocality property of the exact TDDFT functional [139, 140, 142, 143]. To date, little is known about the exact role of the localization step, though it is known to have interesting properties. For example, Gonze and Scheffler showed that the single-pole approximation when one applies the linear Sham-Schlüter equation in Eq. (3.121) gives [142]

$$\omega_{ia} = \Delta\epsilon_{ia} + (ia|f_{xc}(\Delta\epsilon_{ia})|ai) = \Delta\epsilon_{ia} + (ii|K(\Delta\epsilon_{ia})|aa), \quad (3.122)$$

where $\Delta\epsilon_{ia} = \epsilon_a - \epsilon_i$. In fact, a cancellation of the localizer is observed, and the exact xc-kernel is equal to a different matrix element of the kernel derived from MBPT quantities. A general treatment of localization is plagued with numerical problems, due to the difficulties in inverting

the singular density response functions that are involved [34,107]. In the linear-response regime, an interesting work around can be used to fully account for the localization effects without the need of explicitly inverting any response function. This is achieved by re-expressing LR-TDDFT as the response of the non-interacting potential [144].

Using a first-order approximation of K , one obtains the time-dependent exact-exchange (TDEXX) kernel [32, 137, 138, 140]. This kernel provides correct description of charge transfer [27] and correct position of the continuum states [145] due to the correct asymptotic decay of exchange. Although the exchange kernel in MBPT is frequency independent, the full TDEXX is a frequency-dependent functional [32,34] due to the localizer Λ . Therefore some (minor) memory effects are taken into account [146]. In general, the frequency dependence of the localizer in the TDEXX is not enough to include 2p2h- and higher-ph excited poles [147,148], and frequency-dependent MBPT kernels are required [46,48,140,149].

2p2h- and Higher-ph Excitations

The lack of 2p2h excitations is an endemic problem of the adiabatic approximation [145]. These poles should be present, since TDDFT is formally exact. However, they are not present when an adiabatic xc-kernel is used in the LR-TDDFT equations. Clearly, the number of solutions of Eq. (3.119) is given by the dimension of the matrices, that is, the number of 1p1h states. Recovering of 2p2h states require frequency-dependent xc-kernels [43,44], which make the LR-TDDFT equations non-linear and extra solutions appear. Frequency dependence can be included via the solution of a Sham-Schlüter equation. The MBPT kernel of the Bethe-Salpeter equation has to be constructed carefully, since otherwise the resulting xc-kernel might introduce spurious transitions [46,48]. The first successful ω -dependent xc-kernel is the kernel of dressed TDDFT (D-TDDFT), first proposed by Burke, Maitra and coworkers [43,44] to include one 2p2h at a time, and later generalized to any number of 2p2h states by using full-featured MBPT techniques [140,149]. The kernel of D-TDDFT can be viewed as a hybrid kernel between the adiabatic xc-kernel and the frequency-dependent part of the MBPT kernel,

$$f_{xc}(\mathbf{r}, \mathbf{r}'; \omega) = f_{xc}^{AA}(\mathbf{r}, \mathbf{r}') + K^\omega(\mathbf{r}, \mathbf{r}; \mathbf{r}', \mathbf{r}'; \omega), \quad (3.123)$$

where $K^\omega(\mathbf{r}, \mathbf{r}; \mathbf{r}', \mathbf{r}'; \omega)$ corresponds to the frequency-dependent part of the kernel derived from a second-order polarization propagator approach (for the mathematical expression see [140] and [145].) The mixture of two different theories, MBPT and TDDFT, can be defined in several ways. In Ref. [145], comparison of the performance of D-TDDFT against benchmark *ab initio* results for 28 organic chromophores, established the proper mixture of adiabatic xc-kernel and frequency-dependent MBPT terms. Strictly speaking, a localization step would be required in the MBPT part of Eq. (3.123), but the treatment of localization can easily lead to numerical instabilities and is deliberately dropped out. The Gonze-Scheffler relation of Eq. (3.122) encourages the use of Eq. (3.123) directly without localizing, and applications give further support [44,145,150,151]. In Ref. [44], calculations for the 2^1A_g state of butadiene and hexatriene, which is largely overestimated when using adiabatic kernels, showed a very good agreement with *ab initio* multi-reference calculations. Further calculations on similar systems confirmed the excellent agreement [150].

Time-Dependent Reduced Density Matrix Functional Theory

Important recent work has been done by Giesbertz and coworkers extending RDMFT⁴ to the time-dependent case [116, 152–157]. To our minds, the most important result of this work is to show the failure of TD-RDMFT⁵ to obtain the correct $\omega \rightarrow 0$ limit of the adiabatic approximation even for two-electron systems [156]. However including not only the orbitals and occupation numbers in the time-dependent response equations but also their *phases* allows exact solutions to be obtained for two-electron systems [155]. Note that this phase information is not included in the 1-RDM⁶, so that a new functional dependence is needed which goes beyond the density-matrix alone. It may perhaps be assimilated with a memory effect.

4. Reduced density-matrix-functional theory

5. time-dependent RDMFT

6. one-electron reduced density matrix

Part II
Original Research

Chapter 4

Spin-Flip Time-Dependent Density-Functional Theory

4.1 Introduction

Spin-flip TDDFT (SF-TDDFT) is presently the only density-based method that can be generally applied to realistic photochemical problems. The main reason is that SF-TDDFT can easily calculate funnels. Regular TDDFT has problems in the funnel region, because the DFT assumption of non-interacting v -representability fails. SF-TDDFT can work-around this problem by starting from a triplet reference (which is normally non-interacting v -representable) and accessing the ground-state through excitation. This allows the calculation of multi-reference ground states within a single reference method, thus offering a simple solution to describe bond dissociation and funnels. In addition, SF-TDDFT includes a restricted number of double excitations, which are necessary for describing the global shape of PES. This chapter accomplish one of the objectives of this thesis, that is, the assessment of existing methods that include a reduced number of double excitations.

SF-TDDFT was applied to the study case of oxirane’s photoreaction. First, we studied the photochemical pathway. Oxirane undergoes an asymmetric ring opening in the excited state (i.e., cleavage of one of the C–O bonds,) reaching the ground-state via a conical intersection. We assessed the ability of SF-TDDFT to represent the region around the intersection point. Second, we studied the symmetric ring opening. This is a fictitious reaction coordinate, but it offers an excellent example for assessing SF-TDDFT description of an avoided crossing between a doubly-excited state and the ground-state.

The work presented in this chapter lead to a publication [158]. My specific contributions were in various parts. My first contribution was to fix a bug in the initial implementation in DEMON2K, which gave a wrong excitation energy for the reference triplet state. As for the applications, I did major contributions in the calculations, assignment, and interpretation of the results in the symmetric and asymmetric ring opening. I also contributed to the assignment and interpretation of the conical intersection. Finally, I wrote a first draft of the article sections regarding the symmetric and asymmetric ring opening.

From the time of our publication, many advances have been made in SF-TDDFT. One of the major drawbacks of the Ziegler and Wang formulation of SF-TDDFT is that it can only use local functionals, which usually underestimate excited states. Rinkevicius and coworkers proposed a hybrid spin-flip kernel, by mixing Krylov’s spin-flip method with Ziegler and Wang method [159, 160]. The results of such a kernel to polyenes and biradicals show a much better agreement with respect to *ab initio* benchmarks. However, the amount of HF exchange is about 50%, which seems in contradiction with the 20-25% used in most successful functionals in DFT and TDDFT. This might indicate some internal inconsistency, as in the adiabatic limit, both DFT and TDDFT functionals should converge to the same quantity. Minezawa and Gordon have applied the hybrid SF-TDDFT method to study the photoreaction of stilbene. In conjunction

with an optimization algorithm for the excited states, they were able to find the relevant minima and conical intersection that explains the photochemical cis-trans isomerisation mechanism [161].

Another important drawback of SF-TDDFT is the fact that most excited states are spin contaminated. There are two sources of contamination. The reference used in SF-TDDFT is normally an open shell, and therefore it requires an unrestricted KS wave function, with the consequence that most excited states are contaminated. The second (and main) source of spin contamination is due to the fact that $\alpha \rightarrow \beta$ and $\beta \rightarrow \alpha$ are uncoupled in SF-TDDFT. In fact, SF-TDDFT in the present form only yields four spin-pure states. A solution to this problem was proposed by Vahtras and Rinkevicius, who developed a spin-adapted SF-TDDFT method using generalized orbital energy excitations [162] and taking the restricted open-shell KS reference [163]. The resulting equations are quite involved, and no application has appeared to date. More recently, Liu *et al.* proposed a similar approach to that of Vahtras and Rinkevicius [164,165]. The main difference lies in the use of a tensor reference which contains all the open shell configurations needed to produce pure spin states. In this way, they show that the number of generalized excitations is significantly reduced, therefore greatly simplifying the structure of the equations. This method has been applied to the cations of naphthalene and molecular nitrogen, showing a major decrease in errors with respect to unrestricted SF-TDDFT.

This chapter is organized as follow. In Sec. 4.2, a preprint of the published article is included, and in Sec. 4.3, more specific conclusions for the objective of this thesis are stated.

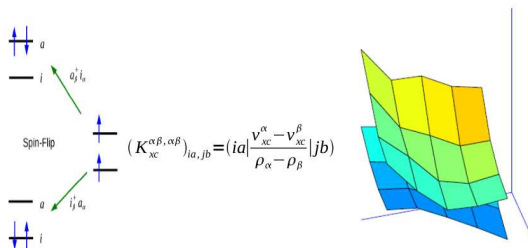
4.2 Photochemical Ring-Opening of Oxirane (Article)¹

Assessment of Noncollinear Spin-Flip Tamm-Dancoff Approximation Time-Dependent Density-Functional Theory for the Photochemical Ring-Opening of Oxirane

Miquel Huix-Rotllant, Bhaarathi Natarajan, Andrei Ipatov, C. Muhavini Wawire, Mark E. Casida[†]
*Laboratoire de Chimie Théorique,
 Département de Chimie Moléculaire (DCM, UMR CNRS/UJF 5250),
 Institut de Chimie Moléculaire de Grenoble (ICMG, FR2607),
 Université Joseph Fourier (Grenoble I),
 301 rue de la Chimie, BP 53,
 F-38041 Grenoble Cedex 9, France*

Thierry Deutsch
CEA, INAC, SP2M, L-Sim, 38054 Grenoble Cedex 9, France

1. This section is a preprint of Ref. [158]. Note: The original format has been adapted to the standards of this thesis.



Under the usual assumption of noninteracting v -representability, density-functional theory (DFT) together with time-dependent DFT (TDDFT) provide a formally exact single-reference method suitable for the theoretical description of the electronic excited-states of large molecules, and hence for the description of excited-state potential energy surfaces important for photochemistry. The quality of this single-reference description is limited in practice by the need to use approximate exchange-correlation functionals. In particular it is far from clear how well approximations used in contemporary practical TDDFT calculations can describe funnel regions such as avoided crossings and conical intersections. These regions typically involve biradical-like structures associated with bond breaking and conventional wisdom would seem to suggest the need to introduce explicit double excitation character to describe these structures. Although this is lacking in ordinary spin-preserving (SP) TDDFT, it is present to some extent in spin-flip (SF) TDDFT. We report our tests of Wang-Ziegler noncollinear SF-TDDFT within the Tamm-Dancoff approximation for describing the avoided crossing in the C_{2v} CC ring-opening reaction of oxirane and for describing the conical intersection relevant for the more physical asymmetric CO ring-opening reaction of oxirane. Comparisons are made with complete active space self-consistent field and quantum Monte Carlo benchmark results from two previous papers on the subject [J. Chem. Phys. **127**, 164111 (2007); *ibid* **129**, 124108 (2008)]. While the avoided crossing in the C_{2v} pathway is found to be reasonably well described, the method was found to be only partially successful for the conical intersection (CX) associated with the physically more important asymmetric pathway. The origin of the difficulties preventing the noncollinear SF-TDDFT method from giving a completely satisfactory description of the CX was traced back to near degeneracy of more than two orbitals near this CX. This article is also the first report of our implementation of SF-TDDFT within the DEMON2K program.

† Corresponding author: Mark.Casida@UJF-Grenoble.Fr

4.2.1 Introduction

Due to its rigorous formal foundations and computational efficiency, time-dependent density-functional theory (TDDFT) is currently a method of choice for treating electronic excited states. It is thus one of several tools to be found in today's photochemical modeling kit (see e.g., Refs. [166–169]). Nevertheless applications of TDDFT are limited by a number of problems due to the inevitable use of approximate functionals in practical applications. Overcoming these limitations is important for extending the domain of applicability of TDDFT. Here we investigate the ability of spin-flip TDDFT (SF-TDDFT) to overcome problems encountered by ordinary TDDFT near funnel regions, namely avoided crossings and conical intersections (CXs). This is especially important in light of the recent development of Tully-type [170, 171] mixed TDDFT/classical trajectory surface-hopping dynamics [11, 31, 172–176]. In the present study, we have chosen the photochemical ring opening of oxirane as a test case for evaluating the ability of noncollinear SF-TDDFT in describing funnel regions because of the availability of high-quality comparison

results [30,31]. Very recent work by Minezawa and Gordon focused on characterizing the CXs of a different molecule (ethylene) using SF-TDDFT based upon a different functional (namely the BHHLYP functional which is 50% Hartree-Fock plus 50% Becke exchange [177] plus Lee-Yang-Parr correlation [178]).

Hohenberg, Kohn, and Sham showed that the static ground state properties of a real system of interacting electrons could in principle be treated exactly by replacing it with a fictitious system of noninteracting electrons [14,15]. In the absence of degeneracies, the wave function of the noninteracting system is single determinantal in nature. The orbitals obey the well-known Kohn-Sham equation,

$$\left(\hat{h}_C^\sigma + v_H + v_{xc}^\sigma\right)\psi_p^\sigma = \epsilon_{p\sigma}\psi_p^\sigma, \quad (4.1)$$

where \hat{h}_C^σ is the usual core (i.e., kinetic energy plus external potential, v_{ext}^σ), v_H is the Hartree (i.e., Coulomb) potential, and (assuming a pure spin-density functional) the exchange-correlation (xc) potential,

$$v_{xc}^\sigma[\rho_\alpha, \rho_\beta](\mathbf{r}) = \frac{\delta E_{xc}[\rho_\alpha, \rho_\beta]}{\delta \rho_\sigma(\mathbf{r})}, \quad (4.2)$$

is the functional derivative of the xc-energy, E_{xc} . (Hartree atomic units are used throughout this paper: $\hbar = m_e = e = 1$.) While the Hohenberg-Kohn-Sham density-functional theory (DFT) is formally exact in principle, it is limited in practice by the use of approximate xc-functionals. The result is that DFT “inherits” some of the problems of Hartree-Fock (HF) theory, notably molecular orbital symmetry breaking when describing the rupture of covalent bonds. Indeed simple arguments show that no symmetry breaking should occur for a closed-shell molecule when the xc-functional is exact [30]. In practice, the broken symmetry solution becomes lower in energy than the unbroken symmetry solution beyond some critical bond distance (Coulson-Fischer point) because of the use of approximate functionals. The above arguments rest on the supposition of noninteracting v -representability (NVR), which means that the energy is minimized with the *Aufbau* filling of the Kohn-Sham orbitals. Interestingly there is some indication that NVR fails for biradicals [31], indicating the need for an ensemble formalism which, however, is beyond the scope of the present paper.

TDDFT extends DFT to handle time-dependent properties. Linear response (LR) theory may then be used to extract information about excited states. Modern TDDFT is based upon the formalism of Runge and Gross who presented Hohenberg-Kohn-like theorems for the time-dependent case and a time-dependent Kohn-Sham equation, [13]

$$\left(\hat{h}_C^\sigma + v_H + v_{xc}^\sigma\right)\psi_p^\sigma = i\frac{\partial}{\partial t}\psi_p^\sigma, \quad (4.3)$$

in which the xc-potential is, in principle, a functional of the time-dependent density, $\rho_\sigma(\mathbf{r}, t)$, and the wave functions of the interacting and noninteracting systems at some initial time. However the first Hohenberg-Kohn theorem tells us that these wave functions are also functionals of the initial density, meaning that the xc-potential depends only on the density for the case of a system initially in its ground stationary state perturbed by a time-dependent applied potential [14]. Applying LR theory to this case leads, in Casida’s formulation [17], to the LR-TDDFT equation,

$$\begin{bmatrix} \mathbf{A}(\omega) & \mathbf{B}(\omega) \\ \mathbf{B}^*(\omega) & \mathbf{A}^*(\omega) \end{bmatrix} \begin{pmatrix} \mathbf{X} \\ \mathbf{Y} \end{pmatrix} = \omega \begin{bmatrix} \mathbf{1} & \mathbf{0} \\ \mathbf{0} & -\mathbf{1} \end{bmatrix} \begin{pmatrix} \mathbf{X} \\ \mathbf{Y} \end{pmatrix}, \quad (4.4)$$

which has paired excitation and de-excitation solutions,

$$\begin{pmatrix} \mathbf{X}_I \\ \mathbf{Y}_I \end{pmatrix} \leftrightarrow \omega_I = E_I - E_0 = -\omega_I \leftrightarrow \begin{pmatrix} \mathbf{Y}_I \\ \mathbf{X}_I \end{pmatrix} \quad (4.5)$$

Here

$$\begin{aligned} A_{ia,jb}^{\sigma,\tau} &= \delta_{a,b}\delta_{i,j}\delta_{\sigma,\tau}(\epsilon_{a\sigma} - \epsilon_{i\sigma}) + K_{ia,jb}^{\sigma,\tau}(\omega) \\ B_{ia,jb}^{\sigma,\tau} &= K_{ia,bj}^{\sigma,\tau}(\omega), \end{aligned} \quad (4.6)$$

and the coupling matrix,

$$K_{ia,bj}^{\sigma,\tau}(\omega) = (ia|\delta_{\sigma,\tau}f_H + f_{xc}^{\sigma,\tau}(\omega)|bj), \quad (4.7)$$

where,

$$f_H(\mathbf{r}_1, \mathbf{r}_2) = \frac{1}{r_{12}}, \quad (4.8)$$

is the Hartree kernel and,

$$f_{xc}^{\sigma,\tau}(\mathbf{r}_1, \mathbf{r}_2; \omega) = \int_{-\infty}^{+\infty} e^{i\omega(t_1-t_2)} \frac{\delta v_{xc}^{\sigma}(\mathbf{r}_1, t_1)}{\delta \rho_{\tau}(\mathbf{r}_2, t_2)} d(t_1 - t_2), \quad (4.9)$$

is the xc-kernel. Integrals are written in Mulliken charge-cloud notation,

$$(pq|f|rs) = \int \int \psi_p^*(\mathbf{r}_1)\psi_q(\mathbf{r}_1)f(\mathbf{r}_1, \mathbf{r}_2)\psi_r^*(\mathbf{r}_2)\psi_s(\mathbf{r}_2) d\mathbf{r}_1 d\mathbf{r}_2. \quad (4.10)$$

The oscillator strength of the I th transition,

$$f_I = \frac{2}{3}\omega_I|\langle 0|\mathbf{r}|I\rangle|^2, \quad (4.11)$$

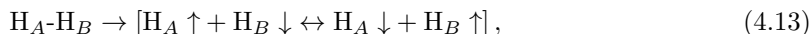
may be calculated from \mathbf{X}_I , \mathbf{Y}_I , and ω_I [17]. Since LR-TDDFT is the primary application of TDDFT and the only one treated in the present article, we will normally just refer to LR-TDDFT as TDDFT. Like conventional DFT, the underlying formalism of TDDFT has been the subject of much healthy criticism (e.g., Refs. [179–181]) and, also like the static ground state formalism, formal TDDFT appears to be “of reasonably sound mind and body.”

Problems arise in practice because of the use of approximate functionals. These have been extensively reviewed in the literature (e.g., Refs. [182] and [183]). Suffice it to say that the normal domain of validity of TDDFT with existant approximate xc-functionals is low-lying 1-electron excitations which are not too delocalized in space and do not involve too much charge transfer. The most basic approximation which is almost universally used in practice, is the adiabatic approximation (AA) which assumes that the xc-potential reacts instantaneously and without memory to any temporal change of the charge density. Mathematically, the AA means that the

xc-potential,

$$v_{xc}^{\sigma}(\mathbf{r}, t) = \frac{\delta E_{xc}[\rho_{\alpha}^t, \rho_{\beta}^t]}{\delta \rho_{\sigma}(\mathbf{r})}, \quad (4.12)$$

may be evaluated in terms of the xc-functional of static ground state DFT. Here $\rho_{\sigma}^t(\mathbf{r})$ means $\rho_{\sigma}(\mathbf{r}, t)$ regarded as a function of the spatial coordinate \mathbf{r} at fixed time t . It is easily seen that the AA limits TDDFT to 1-electron excitations (albeit “dressed” to include some electron correlation effects). In particular, the AA implies that the coupling matrix is frequency-independent and hence that the number of excitation solutions obtained from the LR-TDDFT equation is exactly equal to the number of 1-electron excitations. This is a problem for some applications, such as excitations in polyenes and open-shell molecules, and an active area of research is aimed at going beyond the AA by explicit inclusion of 2- and higher-electron excitations through the frequency-dependence of the xc-kernel [43, 44, 46, 149, 150, 184]. The limitation to 1-electron excitations is *a priori* also a problem for photochemical reactions passing through biradicals since the conventional description of biradical formation involves the mixing of the ground state configuration with a doubly-excited state. Thus for the breaking of the σ bond in H_2 ,



the final state corresponds to the wave function,

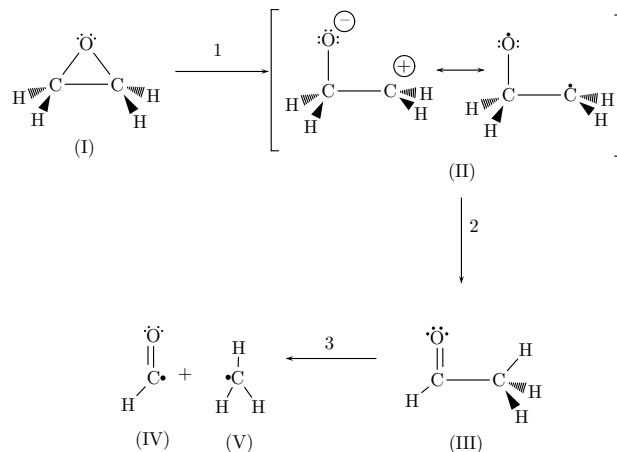
$$\frac{1}{2} (|s_A, \bar{s}_B| + |s_B, \bar{s}_A|) = \frac{1}{2} (|\sigma, \bar{\sigma}| - |\sigma^*, \bar{\sigma}^*|). \quad (4.14)$$

Inclusion of the 2-electron excited state, $|\sigma^*, \bar{\sigma}^*|$, is one of the problems which can be expected to be addressed by SF-TDDFT. A subtler, but important point, is that mixing of the ground and excited configurations is forbidden by the AA but is rigorously necessary to have a CX [29–31]. At first thought such an absence of CX might seem fatal for photodynamics applications. Though the situation is not actually as dark as might at first seem [31], it would be nice to find a way to recover a true CX. Levine *et al.* suggest that SF-TDDFT might also be good for this purpose [29].

Since TDDFT is based upon the response of the ground state, it is also limited by the quality of the DFT description of the ground state. Thus it is seen that symmetry breaking in the ground state occurs if and only if an imaginary triplet excitation energy is found in TDDFT [30, 182, 185, 186]. This is referred to as a triplet instability and is also reflected in underestimations of corresponding singlet excitation energies. However the problem of triplet instabilities may be at least partially overcome by using the Tamm-Dancoff approximation (TDA) [187], which consists of neglecting the \mathbf{B} matrix to obtain just,

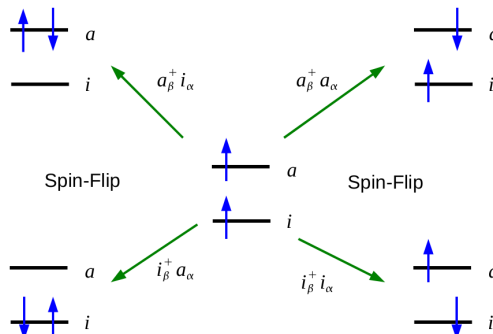
$$\mathbf{A}\mathbf{X} = \omega\mathbf{X}. \quad (4.15)$$

When the TDA is applied to LR time-dependent HF, then the fully variational configuration interaction singles (CIS) is obtained, indicating that the excited-state problem has been decoupled from the ground-state problem in a way that avoids the problem of variational collapse. The situation in TDDFT is similar and TDDFT TDA calculations give much improved excited-state potential energy surfaces (PESs) compared to full TDDFT calculations [30, 185, 186]. The reader interested in further information about TDDFT is referred to a recent book [188] and two special journal issues [189, 190] devoted to TDDFT.

Figure 4.1 Gomer-Noyes mechanism for the ring-opening of oxirane (I). [191]

Oxiranes are an important class of compounds in photochemistry. (See Ref. [192] and the brief review in Appendix B of Ref. [30].) Aryl substitution of oxirane [(I) in Fig. 4.1] favors symmetric ring opening via CC bond cleavage. Cordova *et al.* investigated the ability of TDDFT to describe C_{2v} as well as conrotatory and disrotatory ring opening of oxirane, by comparing TDDFT results against results from high-quality quantum Monte Carlo (QMC) calculations. The high symmetry C_{2v} ring-opening pathway allowed a particularly detailed analysis. Investigation of conrotatory and disrotatory ring opening was inspired by the Woodward-Hoffmann theory of electrocyclic ring-opening reactions. The three principal UV absorption peaks were assigned to Rydberg excitations from the oxygen nonbonding orbital, which are difficult to describe quantitatively because of the well-known problem of underestimation of the ionization threshold [25], but which can nevertheless be described qualitatively correctly even with the simple local density approximation (LDA). The C_{2v} ring-opening pathway showed a cusp in the ground state potential energy surface when the occupied $6a_1(\sigma)$ and unoccupied $4b_2(\sigma^*)$ orbitals became quasidegenerate. Also in this region, the energy of the lowest unoccupied molecular orbital (LUMO) fell below that of the highest occupied molecular orbital (HOMO). We shall refer to this as an “effective failure of NVR,” though we expect to the failure to be significantly less severe or even nonexistent had we the exact xc-functional. A consequence of this effective failure are severe self-consistent field (SCF) convergence problems when using a program which tries to enforce the *Aufbau* principle. Triplet instabilities were found to be omnipresent for all the symmetric ring-opening pathways investigated. It was pointed out that the TDA is a practical necessity for avoiding triplet instabilities and singlet near instabilities. With the TDA, the excited-state potential energy surfaces were found to be energetically reasonable even during bond breaking.

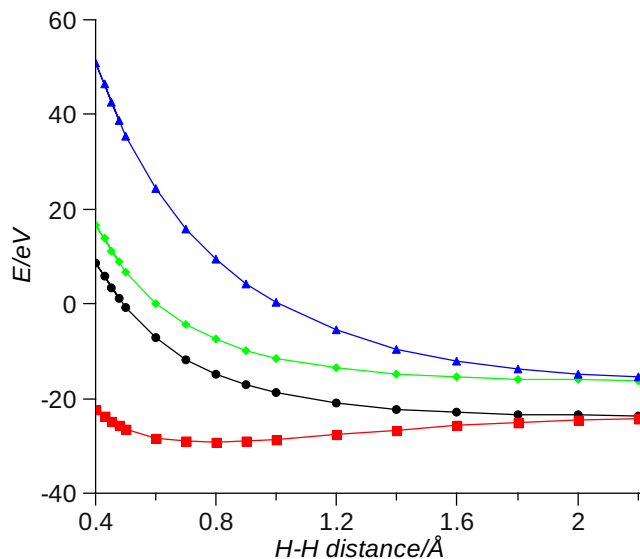
Alkyl substitution of oxirane and indeed oxirane itself does not undergo symmetric ring opening. Rather photochemical ring-opening of oxirane is believed to proceed via the three step Gomer-Noyes mechanism shown in Fig. [191]. In Ref. [31], Tapavicza *et al.* carried out Tully-

Figure 4.2 Two-orbital model of TDDFT excitations with a triplet reference configuration.

type TDDFT/classical trajectory surface-hopping photodynamics calculations using the TDA. This study confirmed and detailed the Gomer-Noyes mechanism. It was shown that the $^1(n, 3p_z)$ Rydberg state is directly linked to a $^1(n, \sigma^*)$ valence CO antibonding state. Initial excitation leads within 100 femtoseconds or so population of the $^1(n, 3p_z)$ state and thereby to spontaneous ring-opening (step 1 in Fig. 4.1). Structure (II) is a CX with mixed zwitterionic and biradical character permitting electronic de-excitation directly to a vibrationally hot (4000 K) electronic ground state. At this point there is enough energy for several things to happen, one of which is hydrogen abstraction (III) followed by CC bond breaking. High-quality QMC calculations were carried out along a typical trajectory and used for comparison purposes. Once again an effective failure of NVR was encountered, but difficulties with SCF convergence problems are minimized in dynamics calculations by restarting the SCF for each new geometry from the converged result of the previous geometry, so that orbital-following rather than *Aufbau* filling is enforced. This work confirmed the absence of a true CX in the TDDFT calculation. Instead, an approximate CX was found in the form of two interpenetrating rather than touching cones, in the same vicinity of the corresponding complete active space SCF (CASSCF) CX. This proved adequate for a qualitative investigation of the reaction mechanism, but it would be nice to have a DFT-based method which would give a true CX. In this article we follow up on the suggestion by Levine *et al.* that SF-TDDFT would be just such a method [29].

In principle, SF-TDDFT offers a clever solution to some of the above-mentioned problems. The main idea of SF-TDDFT is shown in Fig. 4.2. We must first make the common pragmatic assumption that DFT applies not only to the ground state but also to the lowest energy state of a given spin-symmetry. This assumption is especially plausible if the a single-determinant provides a reasonable first approximation to the state in question. Excited states normally excluded from TDDFT are included in SF-TDDFT by beginning from the lowest triplet state and flipping spins while exciting electrons from one orbital to another. In this manner we arrive at exactly the ground configuration and the doubly-excited configuration needed to describe bond breaking. Ideally then H_2 will dissociate correctly without recourse to symmetry breaking [193] (Fig. 4.3). Moreover the problem of an effective failure of NVR is very much reduced leading

Figure 4.3 Dissociation of H_2 obtained with the present implementation of SF-TDDFT. The black $1^3\Sigma_u$ curve is the triplet SCF reference state from which excitations are taken. It is nearly degenerate with the $M_S = 0$ triplet state (not shown) generated by SF-TDDFT. The red $1^1\Sigma_g$ ground state is a mixture of $|\sigma, \bar{\sigma}|$ and $|\sigma^*, \bar{\sigma}^*|$ configurations, with the $|\sigma, \bar{\sigma}|$ dominating at the equilibrium geometry. The $1^1\Sigma_g$ and $1^3\Sigma_u$ states dissociate to the same neutral “diradical” limit, namely $[H\uparrow + H\downarrow \leftrightarrow H\downarrow + H\uparrow]$. The blue $2^1\Sigma_g$ state is also a mixture of $|\sigma, \bar{\sigma}|$ and $|\sigma^*, \bar{\sigma}^*|$ configurations, but the “doubly-excited” $|\sigma^*, \bar{\sigma}^*|$ configuration dominates at the ground state equilibrium geometry. The green curve is the $1^1\Sigma_u(\sigma \rightarrow \sigma^*)$ singly-excited state. The $2^1\Sigma_g$ and $1^1\Sigma_u(\sigma \rightarrow \sigma^*)$ states dissociate to the same ionic limit, namely $[H^+ + H^- \leftrightarrow H^- + H^+]$.



to much improved convergence. Historically designing an appropriate functional for SF-TDDFT has proven to be not entirely straightforward. This problem is reviewed in some detail the next section.

Computational details and a brief description of our own implementation of SF-TDDFT are given in Sec. 4.2.3. In Sec. 4.2.4, we report results pertinent to oxirane photochemistry. Section 4.2.5 summarizes our main conclusions about the effectiveness of SF-TDDFT for describing photochemical funnels.

4.2.2 Spin-Flip TDDFT

No new solution to the SF-TDDFT problem is proposed in the present paper, but this section reviews existant solutions to the problem of developing appropriate functionals for SF-TDDFT. We do this partly to keep this paper self-contained, but also to point out that some aspects of present SF solutions might also be improved if the goal is complete compatabiity between SF-TDDFT and conventional TDDFT.

The most basic requirement of the SF method is the generalization of the one-component collinear approach in which each orbital is associated with either spin α or spin β aligned along an arbitrary z -axis, to a two-component noncollinear approach in which each orbital is a linear combination of spin α and spin β components. Lifting of the collinear requirement is needed to allow spins to rotate in response to an external spin-dependent perturbation and hence to be able to flip. Orbitals become two-component spinors,

$$\psi_p(\mathbf{r}) = \begin{pmatrix} \psi_p^\alpha(\mathbf{r}) \\ \psi_p^\beta(\mathbf{r}) \end{pmatrix}, \quad (4.16)$$

which are obtained by solving the 2×2 matrix equation in spin,

$$\begin{bmatrix} \hat{h}_C^{\alpha,\alpha} + v_H + v_{xc}^{\alpha,\alpha} & \hat{h}_C^{\alpha,\beta} + v_{xc}^{\alpha,\beta} \\ \hat{h}_C^{\beta,\alpha} + v_{xc}^{\beta,\alpha} & \hat{h}_C^{\beta,\beta} + v_{xc}^{\beta,\beta} \end{bmatrix} \begin{pmatrix} \psi_p^\alpha(\mathbf{r}) \\ \psi_p^\beta(\mathbf{r}) \end{pmatrix} = \epsilon_p \begin{pmatrix} \psi_p^\alpha(\mathbf{r}) \\ \psi_p^\beta(\mathbf{r}) \end{pmatrix}. \quad (4.17)$$

Note that the core hamiltonian may now have a spin-dependence due to a spin-dependent external potential. The density is also a 2×2 matrix in spin,

$$\rho(\mathbf{r}) = \begin{bmatrix} \rho_{\alpha,\alpha}(\mathbf{r}) & \rho_{\alpha,\beta}(\mathbf{r}) \\ \rho_{\beta,\alpha}(\mathbf{r}) & \rho_{\beta,\beta}(\mathbf{r}) \end{bmatrix}. \quad (4.18)$$

Consequently the xc-kernel has four spin indices,

$$f_{xc}^{\sigma,\sigma';\tau,\tau'}(\mathbf{r}_1, \mathbf{r}_2; \omega) = \int_{-\infty}^{\infty} e^{i\omega(t-t')} \frac{\delta v^{\sigma,\sigma'}(\mathbf{r}, t_1)}{\delta \rho_{\tau,\tau'}(\mathbf{r}_2, t_2)} d(t_1 - t_2), \quad (4.19)$$

or, in the AA,

$$f_{xc}^{\sigma,\sigma';\tau,\tau'}(\mathbf{r}_1, \mathbf{r}_2) = \frac{\delta^2 E_{xc}[\rho]}{\delta \rho_{\sigma,\sigma'}(\mathbf{r}_1) \delta \rho_{\tau,\tau'}(\mathbf{r}_2)}. \quad (4.20)$$

Naturally the TDDFT coupling matrix also has four spin indices.

Normal practice is to apply SF-TDDFT using orbitals and orbital energies obtained from an ordinary one-component collinear calculation, rather than as a post two-component noncollinear calculation. Thus the assumption is that the one-component noncollinear calculation is an adequate approximation at the SCF level to a full two-component noncollinear SCF calculation. In the end, the noncollinear model only serves in deriving the SF-TDDFT formalism, not in actually carrying it out.

Applying the SF-TDDFT formalism to the usual collinear pure xc-functionals because,

$$f_{xc}^{\sigma,\sigma';\tau,\tau'} = \delta_{\sigma,\sigma'} \delta_{\tau,\tau'} f_{xc}^{\sigma,\tau}, \quad (4.21)$$

leads to nothing new. This however is not true in HF because the kernel of the exchange operator, $\hat{\Sigma}_x^{\sigma,\tau}$, is given by,

$$\Sigma_x^{\sigma,\tau}(\mathbf{r}_1, \mathbf{r}_2) = -\frac{\gamma_{\sigma,\tau}(\mathbf{r}, \mathbf{r}')}{r_{12}}, \quad (4.22)$$

where $\gamma_{\sigma,\sigma'}(\mathbf{r}, \mathbf{r}')$ is the one-electron reduced density matrix. Consequently,

$$f_x^{\sigma,\tau;\sigma',\tau'}(\mathbf{r}_1, \mathbf{r}_2; \mathbf{r}'_1, \mathbf{r}'_2) = \frac{\delta \Sigma_x^{\sigma,\tau}(\mathbf{r}_1, \mathbf{r}_2)}{\delta \gamma_{\sigma',\tau'}(\mathbf{r}'_1, \mathbf{r}'_2)} = -\delta_{\sigma,\sigma'} \delta_{\tau,\tau'} \frac{\delta(\mathbf{r}_1 - \mathbf{r}'_1) \delta(\mathbf{r}_2 - \mathbf{r}'_2)}{r_{12}}, \quad (4.23)$$

and the exchange-part of the HF coupling matrix is,

$$K_{pq,rs}^{\sigma,\tau;\sigma',\tau'} = -\delta_{\sigma,\sigma'} \delta_{\tau,\tau'} (ps|f_H|rq). \quad (4.24)$$

This means that hybrid functionals allow SF because they include a portion of HF exchange. This in fact was the first form of SF-TDDFT. It was proposed by Anna Krylov and coworkers who used their approach to study the ground and excited states of diradicals [38,39]. In order to get good agreement with experiment, they found it necessary to use a significantly higher amount of HF exchange (50%) than is typically used for ground state properties ($\sim 25\%$). Even higher percentages of HF exchange ($> 50\%$) have been reported to be necessary for calculating second hyperpolarizabilities of diradical systems by this spin-flip method [194]. Although the use of a different functional for ground and excited states is disturbing, the basic idea is admirable and this method continues to be used [194–196]. In particular, this is the SF-TDDFT approach recently used by Minezawa and Gordon who found the method to give a relatively good description of CXs in ethylene [197].

The next and most recent major advance in SF-TDDFT came with an article by Wang and Ziegler [193]. (See also Ref. [42].) It is intimately related to work by Wenjian Liu and coworkers on relativistic four-component TDDFT [198]. Basing their approach on ideas from relativistic two-component DFT [199,200], Wang and Ziegler proposed that any pure spin-density xc-functional, $E_{xc}[\rho_\alpha, \rho_\beta]$, could be used to make a noncollinear xc-functional, $E_{xc}^{SF}[\boldsymbol{\rho}]$, suitable for SF calculations by making the substitution,

$$\begin{aligned} \rho_\alpha &\rightarrow \rho_+ = \frac{1}{2}(\rho + s) \\ \rho_\beta &\rightarrow \rho_- = \frac{1}{2}(\rho - s), \end{aligned} \quad (4.25)$$

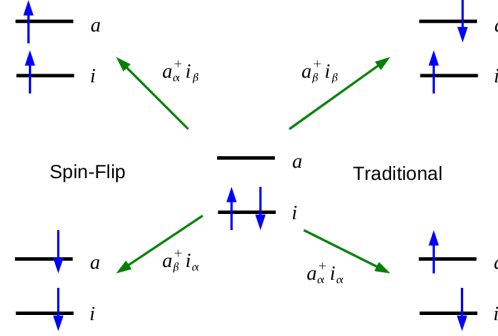
involving two quantities which are invariant under a unitary transformation of the spin coordinates. These are the total charge density,

$$\rho = \rho_{\alpha,\alpha} + \rho_{\beta,\beta}, \quad (4.26)$$

and the magnetization, s , whose square is given by,

$$s^2 = (\rho_{\alpha,\alpha} + \rho_{\beta,\beta})^2 + 2(\rho_{\alpha,\beta}^2 + \rho_{\beta,\alpha}^2). \quad (4.27)$$

Figure 4.4 Two-orbital model of TDDFT excitations with a closed-shell singlet reference configuration.



The collinear limit of s is just the spin-polarization,

$$s \rightarrow \rho_\alpha - \rho_\beta, \quad (4.28)$$

after an appropriate choice of phase. The factor of $1/2$ has been introduced by us so that,

$$\begin{aligned} \rho_+ &\rightarrow \rho_\alpha \\ \rho_- &\rightarrow \rho_\beta, \end{aligned} \quad (4.29)$$

in the same limit. After taking derivatives and the noncollinear limit, the xc-kernel becomes,

$$\begin{bmatrix} f_{xc}^{\alpha,\alpha;\alpha,\alpha} & f_{xc}^{\alpha,\alpha;\beta\beta} & f_{xc}^{\alpha,\alpha;\alpha,\beta} & f_{xc}^{\alpha,\alpha;\beta,\alpha} \\ f_{xc}^{\beta,\beta;\alpha,\alpha} & f_{xc}^{\beta,\beta;\beta,\beta} & f_{xc}^{\beta,\beta;\alpha,\beta} & f_{xc}^{\beta,\beta;\beta,\alpha} \\ f_{xc}^{\alpha,\beta;\alpha,\alpha} & f_{xc}^{\alpha,\beta;\beta,\beta} & f_{xc}^{\alpha,\beta;\alpha,\beta} & f_{xc}^{\alpha,\beta;\beta,\alpha} \\ f_{xc}^{\beta,\alpha;\alpha,\alpha} & f_{xc}^{\beta,\alpha;\beta\beta} & f_{xc}^{\beta,\alpha;\alpha,\beta} & f_{xc}^{\beta,\alpha;\beta,\alpha} \end{bmatrix} = \begin{bmatrix} f_{xc}^{\alpha,\alpha} & f_{xc}^{\alpha,\beta} & 0 & 0 \\ f_{xc}^{\beta,\alpha} & f_{xc}^{\beta,\beta} & 0 & 0 \\ 0 & 0 & \frac{v_{xc}^\alpha - v_{xc}^\beta}{\rho_\alpha - \rho_\beta} & 0 \\ 0 & 0 & 0 & \frac{v_{xc}^\alpha - v_{xc}^\beta}{\rho_\alpha - \rho_\beta} \end{bmatrix}. \quad (4.30)$$

This approach to SF-TDDFT has been applied to the dissociation of H_2 [193] and to calculate the spectra of open-shell molecules [41, 201, 202]. Very recent work has used the Wang-Ziegler approach to treat the reaction path for the *cis-trans* photochemical isomerization of 4-styrylpyridine [203]. The Wang-Ziegler approach has also been proposed as the basis of a more general spin-coupled TDDFT [162].

At first glance, Eq. (4.30) is very pretty because it contains ordinary TDDFT for spin-preserving (SP) transitions. However we can be more demanding. For example, we can require that the three triplets which are generated from the singlet referenced two-orbital model shown in Fig. 4.4 be strictly degenerate. In the TDA, ordinary TDDFT gives the $M_S = 0$ triplet excitation energy,

$$\omega_T = \epsilon_a - \epsilon_i + (ia|f_{xc}^{\alpha,\alpha} - f_{xc}^{\alpha,\beta}|ia). \quad (4.31)$$

Also in the TDA, SF-TDDFT gives the $M_S = \pm 1$ triplet excitation energies,

$$\omega_T = \epsilon_a - \epsilon_i + (ia|\frac{v_{xc}^\alpha - v_{xc}^\beta}{\rho_\alpha - \rho_\beta}|ia). \quad (4.32)$$

Since $\rho_\alpha = \rho_\beta$, the right-hand-side of Eq. (4.32) can only be interpreted as a derivative. That is, we set $\rho_\alpha = \rho_\beta + \delta$ and take the limit that the function $\delta \rightarrow 0$. Then,

$$\begin{aligned} \frac{v_{xc}^\alpha(\mathbf{r}) - v_{xc}^\beta(\mathbf{r})}{\rho_\alpha(\mathbf{r}) - \rho_\beta(\mathbf{r})} &= \lim_{\delta \rightarrow 0} \frac{v_{xc}^\alpha[\rho_\beta + \delta, \rho_\beta](\mathbf{r}) - v_{xc}^\beta[\rho_\beta + \delta, \rho_\beta](\mathbf{r})}{\delta(\mathbf{r})} \\ &= \lim_{\delta \rightarrow 0} \frac{\int f_{xc}^{\alpha,\alpha}(\mathbf{r}, \mathbf{r}')\delta(\mathbf{r}') d\mathbf{r}' - \int f_{xc}^{\beta,\alpha}(\mathbf{r}, \mathbf{r}')\delta(\mathbf{r}') d\mathbf{r}'}{\delta(\mathbf{r})}, \end{aligned} \quad (4.33)$$

which is rigorously only equal to $f_{xc}^{\alpha,\alpha} - f_{xc}^{\alpha,\beta}$ for the LDA, in which case Eqs. (4.31) and (4.32) reduce to the same thing. That, of course, is quite good (probably even adequate for most applications), but it would have been nice to have a theory which was completely general.

As emphasized in the introduction, the case that most interests us in practice is when we begin with a triplet reference configuration as in the two-orbital model of Fig. 4.2 and look at $\Delta M_S = -1$ transitions. This leads to a triplet-triplet SF-TDDFT TDA excitation energy which is equal to zero when orbital relaxation is neglected. The demonstration involves making use of the identity,

$$F_{p,q}^\alpha - F_{p,q}^\beta = (pq|\frac{v_{xc}^\alpha - v_{xc}^\beta}{\rho_\alpha - \rho_\beta}|aa) - (pq|\frac{v_{xc}^\alpha - v_{xc}^\beta}{\rho_\alpha - \rho_\beta}|ii). \quad (4.34)$$

However the usual SP-TDDFT excited singlet-triplet energy difference formula,

$$\omega_S - \omega_T = 2(ia|f_H + f_{xc}^{\alpha,\beta}|ia), \quad (4.35)$$

cannot be recovered in the SF-TDDFT formalism where instead is found,

$$\omega_S - \omega_T = 2(ii|\frac{v_{xc}^\alpha - v_{xc}^\beta}{\rho_\alpha - \rho_\beta}|aa). \quad (4.36)$$

The ground to triplet excitation energy formulae obtained from the two formalisms are equally different. Furthermore there is no analogue of Brillouin's theorem in the sense that the coupling between the ground configuration and the singly excited configurations is nonzero in this formalism. While these suggest that there are grave problems in harmonizing the formulae of the two different TDDFT formalisms, they do not suggest any fatal problems since different looking formulae can lead to nearly similar numerical results. It will, however, turn out that the SF-TDDFT triplet energy is lower than the corresponding SP-TDDFT triplet energy because orbital relaxation in the triplet is more easily described when beginning from a triplet reference than from a singlet reference. Thus the two formalisms are at least shifted with respect to one another.

Despite these potentially irritating problems, *we have chosen to use the Wang-Ziegler functional in the present paper for our noncollinear SF-TDDFT calculations.* This is because we

believe pure density-functionals, rather than Hartree-Fock exchange, to be at the heart of DFT. It thus seems more attractive to us to use the local density approximation (LDA) or a generalized gradient approximation (GGA) in conjunction with the Wang-Ziegler noncollinear spin-flip approach than not to use potentially different amounts of Hartree-Fock exchange in hybrid functionals for ground and excited states while completely ignoring the pure DFT part of the hybrid functional as implied by the pioneering SF-TDDFT approach of Krylov and coworkers. At the same time, we acknowledge the impressive recent results of Minezawa and Gordon for CXs in ethylene [204] with the Krylov approach, albeit with what we consider to be a mostly *ad hoc* functional.

4.2.3 Computational Details

The benchmark geometries and electronic structure calculations used in the present work are taken from the literature. For the C_{2v} CC ring-opening pathway, we used the geometries and quantum Monte Carlo (QMC) potential energy curves given in Appendix C of Ref. [30]. The idea behind QMC is to use statistical techniques to go beyond typical high-quality *ab initio* calculations, such as complete active space self-consistent field (CASSCF) and configuration interaction (CI), through the use of more general types of wave functions. The QMC calculations of Ref. [30] began with a conventional CASSCF calculation. This was then reoptimized by variational Monte Carlo in the presence of a Jastrow factor to include dynamical correlation. Finally diffusion Monte Carlo was used to further improve on the result of the variational Monte Carlo calculation. Suffice it to say that the result is an electronic structure calculation of very high quality (certainly better than the CASSCF starting point or multireference CI.) Geometry optimizations are not presently possible with QMC, so the benchmark geometries are those obtained by C_{2v} structure optimization at fixed ring-opening angle using DFT with the B3LYP functional [93]. For asymmetric CO ring-opening, we used the geometries and QMC potential energy curves from Appendix C of Ref. [31]. The QMC calculations in this reference are similar to those of Ref. [30], but are carried out along a typical pathway for CO ring-opening obtained by mixed TDDFT/classical surface hopping photodynamics calculations. They pass close to a CX which was characterized at the CASSCF level in Ref. [31]. While exact CXs with the ground state are impossible in conventional TDDFT, [29] it was shown in Ref. [31] that the CX is described to a reasonably good approximation by TDDFT in the form of an interpenetrating double cone.

Calculations for the present work were performed with the Grenoble development version of DEMON2K (density of Montreal 2000) [205]. Where needed additional calculations were carried out with GAUSSIAN 03 [206] in order to fix orbital symmetry assignments since the particular version of DEMON2K used here did not yet have automatic symmetry assignments. The DEMON2K program makes use of two Gaussian-type basis sets. In addition to the usual orbital basis set, there is a second auxiliary charge-density fitting basis set. Its use permits the elimination of all four-center integrals. As with other DFT programs, DEMON2K uses a grid to evaluate xc-integrals. A description of the implementation of standard (spin-preserving) TDDFT in DEMON2K has been published elsewhere [207]. The present work is the first reported use of our implementation of Wang-Ziegler SF-TDDFT in DEMON2K. Results were compared against

those obtained from the ADF (Amsterdam density-functional) [208] package and were found to be acceptably close.

The DEMON2K calculations in the present work were carried out using the Vosko-Wilk-Nusair parameterization of the LDA [89]. Density-fitting was carried out *without* imposing the charge conservation constraint [207] using the GEN-A3* density-fitting basis. The orbital basis was the extensive 6-311++G**(2d,2p) basis set [209,210]. The SCF convergence was set at 10^{-7} and the FIXED FINE option was always used for the grid. Our SF-TDDFT calculations used the TDA and the reference state was always the lowest energy triplet.

4.2.4 Results

We are interested in the ability of TDDFT to describe funnel regions. These are regions where potential energy surfaces (PESs) come close enough together that surface hopping becomes possible. Typical funnels are avoided crossings (AXs) and conical intersections (CXs). Rather than being distinct phenomena, AXs and CXs are actually very closely related.

Let us understand why. The PESs of a molecule with f (15 in the case of oxirane) nuclear internal degrees of freedom, \mathbf{R} , is an f -dimensional hypersurface in an $(f + 1)$ -dimensional hyperspace. The condition that the I th and J th PESs cross,

$$E_I(\mathbf{R}) = E_J(\mathbf{R}), \quad (4.37)$$

reduces the dimensionality of the intersection to an $(f - 1)$ -dimensional hyperline. If this were all that there were to it, then we could talk about “surfaces that cross without seeing each other.” However quantum mechanics typically also requires zeroing out a CI-like coupling matrix element,

$$A_{I,J}(\mathbf{R}) = 0, \quad (4.38)$$

denoted \mathbf{A} here to indicate that it could be the linear response matrix in the TDA. (However we could equally well have called it \mathbf{H} for the CI matrix in a CASSCF calculation.) This second condition reduces the dimensionality of the intersection to an $(f - 2)$ -dimensional hyperpoint. CXs are impossible for diatomics because $f = 1$ and $f - 2 = -1$ is impossible. So only AXs are seen for diatomics. However, in general, there will be two coordinates in hyperspace along which the two intersecting PESs will separate. These two branching coordinates are normally defined by the derivative nonadiabatic coupling vector (DC),

$$h_q^{(I,J)} = \mathbf{X}_I^\dagger \frac{\partial \mathbf{H}}{\partial q} \mathbf{X}_J, \quad (4.39)$$

and the unscaled gradient difference (UGD) vector,

$$g_q^{(I,J)} = \mathbf{X}_I^\dagger \frac{\partial \mathbf{H}}{\partial q} \mathbf{X}_I - \mathbf{X}_J^\dagger \frac{\partial \mathbf{H}}{\partial q} \mathbf{X}_J, \quad (4.40)$$

and there is quite a literature on finding and characterizing them (see e.g., Ref. [53]). Within the 3-dimensional space defined by the two branching coordinates plus the energy coordinate, a CX takes on the form of a double cone. Choosing a one-dimensional slice within the space of branching coordinates means that we will typically pass near but not through the CX and so see an AX.

In this section we report the results of our calculations to see to what extent SF-TDDFT calculations give a better than ordinary SP-TDDFT description of funnel regions in oxirane photochemistry in comparison with the results of previously reported-high benchmark calculations. [30] Results are divided into two parts. In the first part we look at C_{2v} ring opening which involves breaking the CC single bond. This is a one-dimensional slice and so any funnel region will appear as an AX. However it has two advantages: firstly that it represents our “normal” picture of how bonds break and secondly that we can analyze it in great detail. In the second part we look at the CX region for asymmetric CO ring opening along the typical photochemical pathway. Here we are restricted to using CASSCF branching coordinates because we are not yet able to find CXs within TDDFT. This means that our conclusions cannot be conclusive as those of the recent study of Minezawa and Gordon [197], but are nevertheless indicative of some of the strengths and weaknesses of Ziegler-Wang SF-TDDFT for this type of application.

4.2.4.1 C_{2v} Ring Opening

Although not particularly physical, C_{2v} ring-opening has the great advantage that symmetry facilitates the analysis. Thus this is a good place to start in our study of SF-TDDFT in funnel regions.

The reference in our SF-TDDFT calculations is the lowest triplet. While the configuration of oxirane at the initial equilibrium geometry [30],

$$\dots [6a_1(\sigma)]^2 [2b_1(n)]^2 [7a_1(3s)]^0 [4b_2(\sigma^*)]^0 \dots \quad (4.41)$$

suggests that the reference is the $1^3B_1[2b_1(n) \rightarrow 7a_1(3s)]$ state, this is at most true below a ring-opening angle of about 75° . Beyond this angle the reference triplet is the $1^3B_2[6a_1(\sigma) \rightarrow 4b_2(\sigma^*)]$ state. This is true not only in the range 75 - 120° when the configuration is,

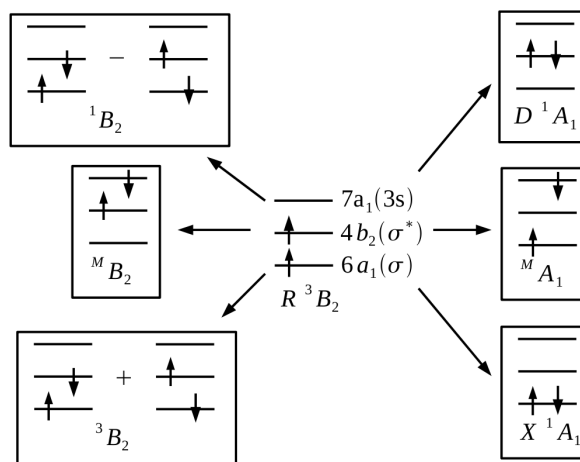
$$\dots [2b_1(n)]^2 [6a_1(\sigma)]^2 [4b_2(\sigma^*)]^0 [7a_1(3s)]^0 \dots, \quad (4.42)$$

but also beyond 120° when the σ and σ^* orbitals change order,

$$\dots [2b_1(n)]^2 [4b_2(\sigma^*)]^2 [6a_1(\sigma)]^0 [7a_1(3s)]^0 \dots, \quad (4.43)$$

Figure 4.5 shows the frontier molecular orbitals in our SF-TDDFT calculations (which however make use of all, not just the of the frontier, molecular orbitals). Both the ground X^1A_1 and doubly excited D^1A_1 configurations are accessible by spin-flip from the R^3B_2 reference state. Taking the symmetric and antisymmetric combinations of the $6a_1(\sigma)$ and $4b_2(\sigma^*)$ SF configurations leads to B_2 states, the triplet of which is expected to be degenerate with the R^3B_2 reference state. Two states of mixed spin symmetry ($^M B_2$ and $^M A_1$) are also formed. These states are unphysical and yet are necessarily present in any SF-TDDFT calculation (including in

Figure 4.5 Principal frontier molecular orbital spin-flip transitions involved in the C_{2v} ring-opening of oxirane beginning from the $R^3B_2[6a_1(\sigma) \rightarrow 4b_2(\sigma^*)]$ reference state.



the Krylov approach to SF-TDDFT). They are readily identifiable in our calculations and have been excluded from the following discussion.

Figure 4.6 shows the results of the SF-TDDFT calculations. The four states predicted in our qualitative discussion are all present. The R^3B_2 SCF reference curve and the corresponding 2B_2 SF-TDDFT curve are not identical, but they are indistinguishable on the scale of the figure. The figure also shows a very important feature, namely the classic avoided crossing corresponding to the breaking of the CC σ bond. The traditional picture is that of H_2 described in the introduction where mixing of the σ^2 and $(\sigma^*)^2$ configurations is necessary for bond breaking. In order to confirm this two-orbital model, we isolated the part of the SF-TDDFT corresponding to the $4b_2(\sigma^*) \rightarrow 6a_1(\sigma)$ and $6a_1(\sigma) \rightarrow 4b_2(\sigma^*)$ SF transitions. Diagonalizing this 2×2 matrix give the two-orbital model adiabatic curves in Fig. 4.6, which are seen to be in semiquantitative agreement with the results of the full SF-TDDFT calculation. The diagonal elements of the 2×2 matrix give the corresponding diabatic curves. These show how the σ^2 ground state configuration at small angles continues on at large angles to become an excited state and how the $(\sigma^*)^2$ excited state configuration at small angles continues on at large angles to become the ground state at large angles. Thus it would seem that SF-TDDFT can correctly describe avoided crossings associated with bond breaking.

Figure 4.7 compares the present SF-TDDFT calculations with both ordinary SP-TDDFT calculations obtained with the LDA functional and the TDA (Ref. [30]) and with the QMC benchmark calculations. Let us begin first with the comparison with SP-TDDFT calculations. As explained in Ref. [30], the bond-breaking region around 120° is an example of effective failure of NVR where the LUMO falls lower in energy than the HOMO. The result is that “normal” DFT programs which insist on filling the Kohn-Sham orbitals according to the *Aufbau* principle

Figure 4.6 C_{2v} potential energy curves: full calculation (solid lines), two-orbital model (dashed lines).

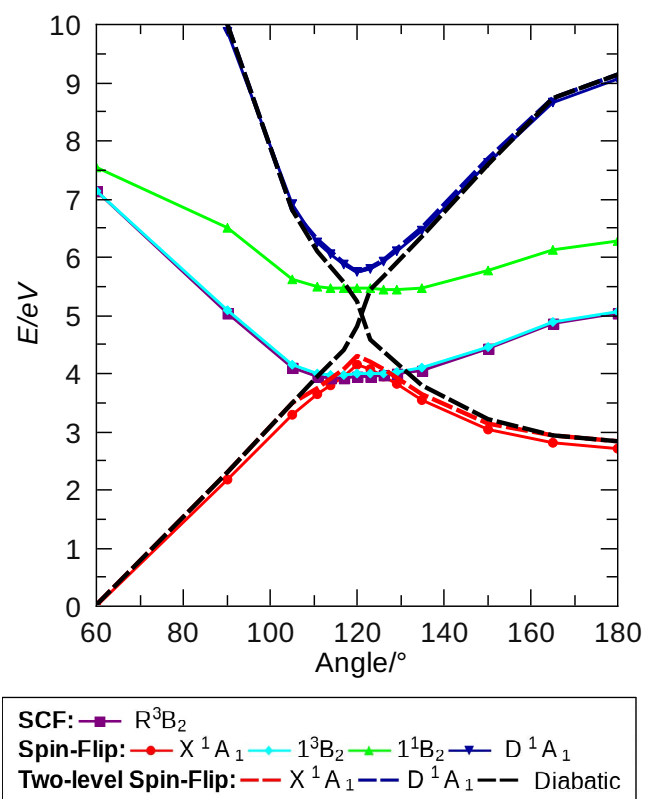


Figure 4.7 Comparison between different methods for the X^1A_1 , 1^3B_2 , and D^1A_1 C_{2v} ring-opening potential energy curves: SF-TDDFT triplet SCF reference state (black dashed line), SF-TDDFT (circles), SP-TDDFT (triangles), and DMC (squares). All curves have been shifted to give the same ground state energy at a ring-opening angle of 75° .

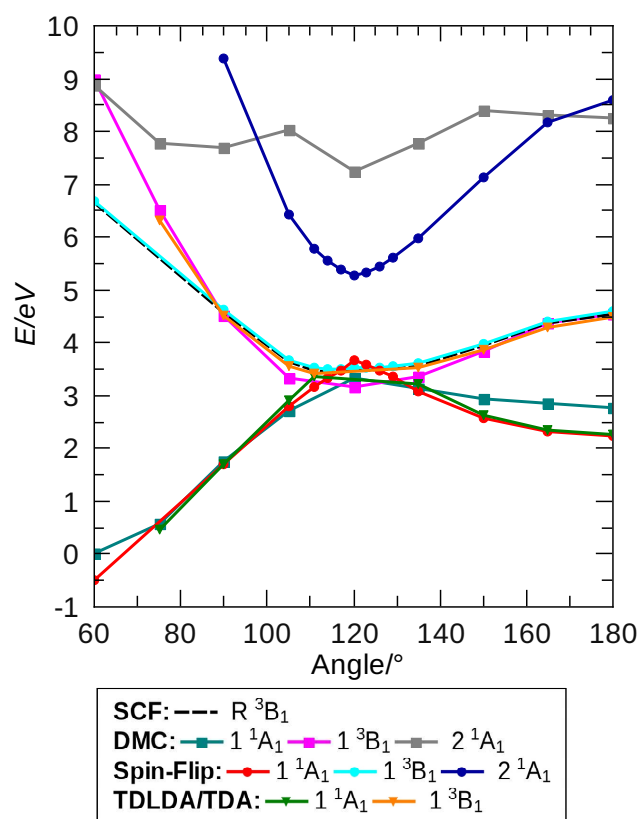
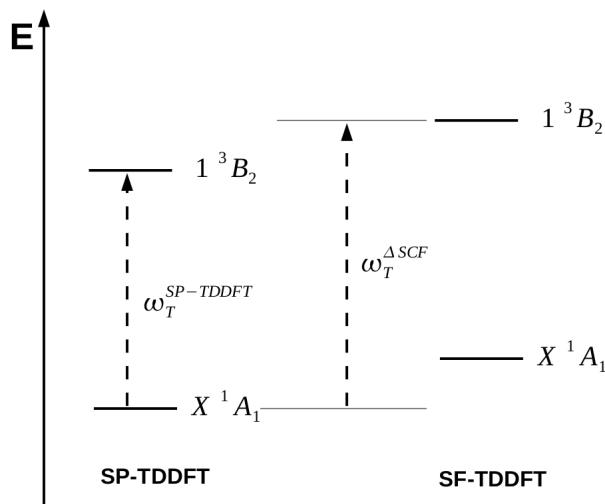


Figure 4.8 Illustration of orbital relaxation effects in SF versus SP TDDFT

will inevitably fail to converge in this region. This is why there are neither SCF ground state nor SP-TDDFT results near 120° in the figure. Very significantly no convergence difficulties are encountered for the triplet reference state. This would seem to be very good news for those who would like to carry out routine photodynamics calculations where SCF convergence failures can be highly inconvenient if not fatal to the calculations.

In the region where the SCF ground state does converge the *shape* of the ground X^1A_1 and excited 1^3B_2 curves are very similar for SF-TDDFT and SP-TDDFT calculations. However the SF-TDDFT curves are actually 0.41 eV in energy higher than the corresponding SP-TDDFT curves. Differences between SCF and TDDFT triplet excitation energies have been previously discussed by Casida *et al.* [185] who gave an analysis within a two-level model. The result is that the SF-TDDFT triplet reference is expected to be higher in energy than the SP-TDDFT triplet by the charge-transfer correction (really a density-transfer correction or relaxation effect),

$$\omega_T^{\Delta SCF} - \omega_T^{SP-TDDFT} \approx \frac{1}{2}(\Delta\rho|f_H + f_{xc}^{\alpha,\alpha}|\Delta\rho) > 0. \quad (4.44)$$

This is illustrated in Fig. 4.8. Simultaneously there is a problem describing the ground state with orbitals optimized for a triplet. The result is that the SF-TDDFT method overestimates the ground state energy. However energy differences do appear to be similar in SF-TDDFT and in SP-TDDFT when the same configurations are concerned, so that a rigid shift of energy levels is reasonable.

Having established the similarity and differences of the DFT approaches, let us now compare against the QMC benchmark calculations. Just as relaxation effects lead to the underestimation of the SP-TDDFT $1^3B_2[6a_1(\sigma) \rightarrow 4b_2(\sigma^*)]$ state with respect to the SF-TDDFT SCF reference

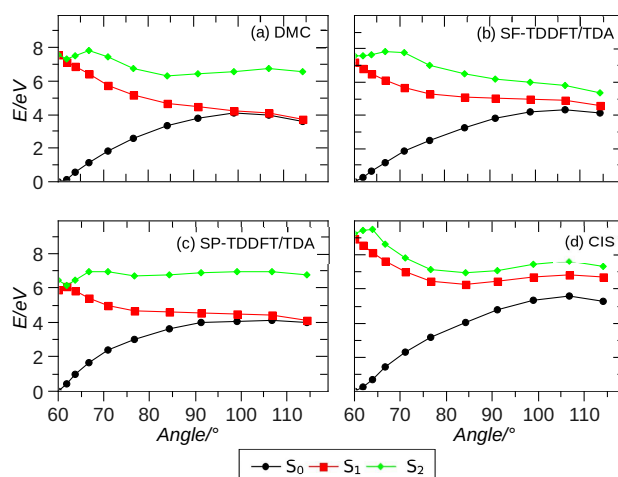
state, so we can expect the SF-TDDFT $D^1A_1\{[6a_1(\sigma)]^2 \rightarrow [4b_2(\sigma^*)]^2\}$ to be underestimated with respect to an SCF calculation with the doubly-excited configuration. This may help to explain why the SF-TDDFT D^1A_1 is significantly below the corresponding QMC curve. Consequently we may also expect important differences between the SF-TDDFT and QMC description of the ground state curve in the region of the avoided crossing. Nevertheless, except for the point at 60° , the shape of the QMC and DFT ground state curves agree reasonably well below about 100° . Significant differences only really appear in Fig. 4.7 between the DFT and QMC ground state curves at higher angles. We must conclude that SF-TDDFT is not able to capture all of the correlation effects present in QMC at these angles. Note that the QMC D^1A_1 also seems to be mixing with one or more singly-excited states (see Table II of Ref. [30]), none of which are accessible to the SF-TDDFT formalism used here. The result is a QMC D^1A_1 curve which is rather flatter than its SF-TDDFT counterpart.

4.2.4.2 Photochemical Pathway and Conical Intersection

The real photoreaction proceeds via an asymmetric pathway. This ring opening has been studied by mixed TDDFT/classical trajectory surface hopping calculations in Ref. [31] where benchmark calculations were given along a typical CO ring-opening trajectory. We want to compare the results of our SF-TDDFT calculations both along this trajectory and for the CASSCF CX branching space given in the same reference.

Before doing so, we first give a brief review of key results which emerged from the earlier study. Only the initial geometry has C_{2v} symmetry, so we fall back on a more chemical nomenclature for key molecular orbitals. The first excited singlet state, S_1 , is initially assigned as $1^1B_1[b_1(n) \rightarrow a_1(3s)]$ and there after as simply $^1(n, 3s)$. This state remains of Rydberg character throughout the photoreaction. However the second excited singlet state, S_2 , does not. Instead, S_2 is initially $2^1B_1[b_1(n) \rightarrow a_1(3p_z)]$, remains of $^1(n, 3p_z)$ Rydberg type for only a short time, soon falling in energy to become the new S_1 as it takes on valence-type CO antibonding character, $^1(n, \sigma_{CO}^*)$. At that point $^1(n, 3s)$ is the new S_2 . In fact, what happens is qualitatively very much in-line with the Woodward-Hoffmann orbital correlation scheme described in Ref. [30] (Fig. 1 of that reference) for the C_{2v} ring-opening reaction but without the symmetry. The trajectory finally passes through (or near) a CX where surface hopping takes place.

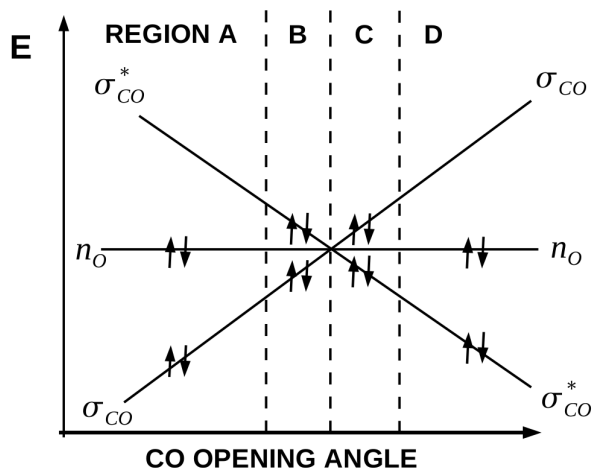
Let us delay our discussion of the CX for a brief moment and focus on how SF-TDDFT does in describing the potential energy curves for S_0 , S_1 , and S_2 along the typical CO ring-opening trajectory used in Ref. [31]. than convergence of SP-TDDFT with the ground state single determinant as reference. The results are shown in Fig. 4.9 along side those from QMC and SP-TDDFT. Configuration interaction singles (CIS) calculations obtained using GAUSSIAN [206] and the same basis set have also been included in the figure. It appears from this figure that the S_1/S_0 CX is perhaps a bit better described by SP-TDDFT than by SF-TDDFT and, as expected, that both are significantly better than the CIS description of the same CX. Most dramatic however is the difference between the behavior of the SP-TDDFT S_2 state, which is in relatively good agreement with the QMC S_2 state and in qualitatively reasonable agreement with the CIS S_2 state, and the SF-TDDFT S_2 state which takes an energetic dive as the ring opens.

Figure 4.9 Potential energy curves for asymmetric ring-opening in oxirane calculated with various methods.

It is tempting to conclude that the SF-TDDFT S_2 state contains double excitation character which cause it to differ from the SP-TDDFT and CIS S_2 states which are of single excitation character. Such an argument is a bit less evident in the case of QMC which can also describe double excitations. However we have already seen in the case of the C_{2v} ring-opening pathway that QMC places the double excitation higher in energy than does the present Wang-Ziegler SF-TDDFT. Unfortunately examination of the orbital transitions involved for the S_0 , S_1 , and S_2 SF-TDDFT curves is complicated by our use of a spin-unrestricted (different-orbitals-for-different-spin) triplet reference. Already at the initial ground state equilibrium geometry, the triplet configuration spin α orbitals have changed order with respect to the ground state order, so that the oxygen lone pair is no longer the highest occupied spin α molecular orbital as it is in the ground state. More dramatically the lowest unoccupied spin beta molecular orbitals have also changed order and have even intermixed to the point that the correspondance between spin α and spin β molecular orbitals has been partially lost. This is different than the case of C_{2v} ring opening where symmetry helped to keep the orbital interpretation clean. For this reason we give no detailed assignment of the S_0 , S_1 , and S_2 SF-TDDFT curves.

Let us now take a closer look at what is happening around the CX. Let us review some of the conclusions of Ref. [31]. Earlier Levine *et al.* had noted that a true CX could not exist between S_0 and S_1 because condition 4.38 is a consequence of the formalism and hence cannot serve as a criterion for fixing the dimensionality of the intersection space. [29] Tapavicza *et al.* verified this point but showed that an approximate CX did exist in adiabatic TDDFT for the asymmetric ring opening of oxirane, provided appropriate care was taken in treating convergence problems. These convergence problems result from an effective failure of NVR near the CX as shown schematically in Fig. 4.10. The representation can only be schematic because the orbitals mix and their

Figure 4.10 Schematic Walsh diagram showing how the orbital fillings during asymmetric ring-opening in a normal TDDFT calculation. Regions B and C show effective violation of NVR.



energetic ordering varies with the mixing. However this representation, while simplified, is as close as possible to what emerged during lengthy discussions between one of us (MEC) and Enrico Tapavicza. [211] Arguments are given in Ref. [31] why NVR should be violated even for the xc-functional energy is exact. On a practical level, convergence is not normally possible under such circumstances when using most DFT codes because they impose integer occupation number and *Aufbau* filling. However Tapavicza *et al.* were able to maintain the lower energy solution with its “hole below the Fermi level” by taking the result of the SCF of the previous geometry as the initial guess for the SCF of the current geometry, as is typical in dynamics calculations, thereby achieving a sort of “orbital following.” The result is an approximate TDDFT CX in the form of interpenetrating double cones as shown in Fig. 4.11. The similarity between the behavior of the TDDFT and CASSCF PESs is perhaps even more clear in Fig. 4.12 where the $S_0 \rightarrow S_1$ excitation energy is shown for the CASSCF branching plane.

Given the results obtained in the case of the symmetric C_{2v} CC ring-opening reaction, we expected that SF-TDDFT would give a rather good description of the asymmetric CO ring-opening reaction by mixing configurations with doubly occupied σ_{CO} and doubly occupied σ_{CO}^* orbitals. Levine *et al.* also suggested that SF-TDDFT might be the solution to the CX problem in TDDFT. [29] Figures 4.11 and 4.12 show that the situation is not so simple. These results do seem to confirm what is expected theoretically, namely that SF-TDDFT is able to produce a CX by coupling ground and excited states. However the SF-TDDFT S_0/S_1 intersection is located at a position between that found in CIS and that found with CASSCF (and approximately by SP-TDDFT).

Figure 4.11 Comparison of the S_0 and S_1 PESs calculated using different methods for the CASSCF branching coordinate space. All but the SF-TDDFT part of the figure have been adapted from Ref. [31]. See also that reference for a detailed description of the branching coordinates.

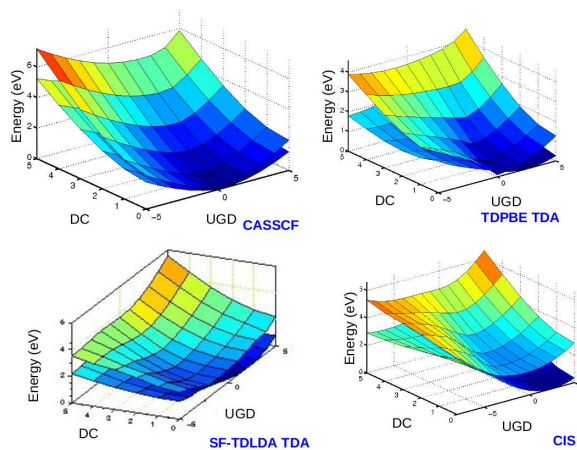


Figure 4.12 Comparison of the $S_0 \rightarrow S_1$ excitation energy surfaces calculated using different methods for the CASSCF branching coordinate space. See Ref. [31] for a detailed description of the branching coordinates.

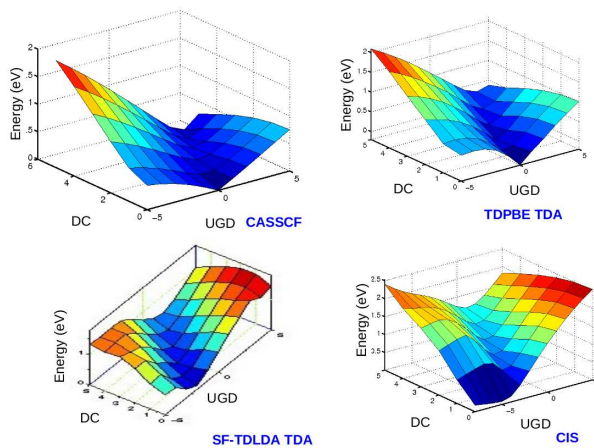
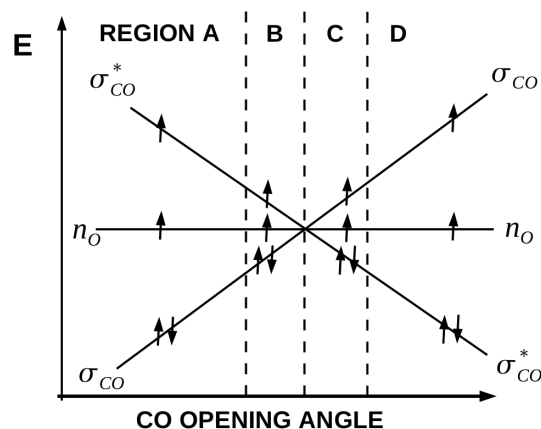


Figure 4.13 Schematic Walsh diagram showing how the orbital fillings vary during asymmetric ring-opening in a SF-TDDFT calculation.



It is worth taking a closer look. Figure 4.11 shows that, while not identical, the SF-TDDFT ground state more closely resembles the CIS ground state than the CASSCF ground state. In particular both the SF-TDDFT and the CIS PESs have a minimum at $(DC, UGD)=(0,2)$ while the CASSCF PES has its minimum at the origin. This indicates that it is highly unlikely that $(\sigma_{CO})^2-(\sigma_{CO}^*)^2$ configuration mixing is actually occurring near $(DC, UGD)=(0,0)$. (As might be expected in the absence of double excitations, straight DFT also gives a result similar to SF-TDDFT for the ground state.) Our explanation lies in Fig. 4.13 which shows how the reference triplet configuration evolves with ring-opening angle. This explanation must be taken as rather rough for several reasons. Not only do the spin α and β orbitals have different energies in our spin-unrestricted calculation, but significant orbital remixing occurs so that spin α and β orbitals can no longer be put in exact correspondance. Nevertheless conclusions based upon Fig. 4.13 explain our results rather well, because there is no geometry where SF-TDDFT can simultaneously lead to both the $(\sigma_{CO})^2$ and $(\sigma_{CO}^*)^2$ configurations.

We have tried to carry out SF-TDDFT by enforcing an initial $\sigma_{CO}/\sigma_{CO}^*$ triplet state, but enforcing this condition turned out to be far from trivial for all the reasons described above. In particular the orbitals lose their “chemical character” due to strong mixing of nearly degenerate orbitals, particularly in the region of effective failure of NVR (Regions B and C of Figs. 4.10 and 4.13, thus making these calculations highly ambiguous. Suffice it to say only that the shape of the ground state surface did seem to improve in the region of the CX but that we were not able to recover a clear SF-TDDFT with our new choice of triplet reference.

4.2.5 Conclusion

The present paper is a contribution to our understanding of how well TDDFT, and SF-TDDFT in particular, is able to describe critical funnels in photochemical reactions. We have chosen the small molecule oxirane for our study because of the availability of previously reported high-quality *ab initio* results [30,31] for comparison and have investigated the avoided crossing (AX) in the C_{2v} ring-opening pathway, the more physical CO ring-opening pathway, and the associated conical intersection (CX).

As pointed out in the introduction, the recent development of mixed TDDFT/classical trajectory SH photodynamics [11, 31, 172–176] is fueling investigations of the ability of TDDFT to describe critical funnel regions [29–31, 212–217]. Such regions often correspond to the formation of diradicals through bond breaking. Traditional wisdom tells us that a correct description of such regions requires mixing of the ground-state configuration with doubly-excited configurations, which are not normally available to ordinary spin-preserving (SP) TDDFT. In particular, Levine *et al.* argued convincingly that CXs cannot exist between the ground and excited states in SP-TDDFT in the usual case where the TDDFT adiabatic approximation is employed. [29] This is counter to the idea that exact TDDFT should be able to describe this coupling [30] and that an approximate CX has been found in practice [31]. Nevertheless it is highly desirable to find a way to include double excitations so as to obtain a more rigorous description of funnel regions. One active area of research which may lead to a better understanding of the problem, if not a solution, is the explicit inclusion of 2- and higher-electron excitations through the frequency-dependence of the xc-kernel [43, 44, 46, 149, 150, 184]. In the meantime, spin-flip (SF) TDDFT [38, 39, 41, 42, 162, 193–196, 201–203] offers an attractive alternative. Indeed this was also recognized by Levine *et al* [31]. The present work reports our implementation of Wang-Ziegler noncollinear SF-TDDFT in the program DEMON2K and constitutes a test of the usefulness of SF-TDDFT for photochemical funnels.

We know of only two previous works on this subject. One is unpublished work by Lawson Daku, Linares, and Boillot who used Wang-Ziegler SF-TDDFT to investigate the *cis/trans* photoisomerization of 4-styrylpyridine [203]. The other is recent work by Minezawa and Gordon who characterized CXs in ethylene using the Krylov variant of SF-TDDFT [197]. While both of those applications appeared to be successful, they are both restricted to *cis/trans* isomerization around a double bond. Here we treat something very different, namely photochemical ring-opening and are only able to report mixed success.

We first applied SF-TDDFT to study the AX along the C_{2v} ring-opening pathway. A few problems show up which are not present in the obligatory test of dissociation of H_2 (Fig. 4.3). One problem is the presence of unphysical states of mixed spin symmetry (Fig. 4.5). Fortunately these were readily identifiable and so could be appropriately ignored. A second problem arises in comparing the results of SP-TDDFT beginning from the ground-state singlet determinant reference and SF-TDDFT beginning from the lowest triplet determinant reference. The different choice of reference immediately implies the possible presence of an orbital relaxation energy correction and indeed the SF-TDDFT potential energy curves are shifted by about 0.4 eV from the corresponding SP-TDDFT curves. Nevertheless SF-TDDFT is to be quite successful in describing the interesting AX.

This is especially true when it is realized that the usual SP-TDDFT calculations run into serious convergence problems in the vicinity of the AX [30]. This is exactly a region of effective violation of noninteracting v -representability [31]. Minimizing the total energy with integer occupation number leads to a violation of the *Aufbau* principle with the LUMO below the HOMO or (to put it in more solid-state physics language) with a hole below the Fermi level. Most quantum chemistry programs seek to enforce the *Aufbau* principle even in this case with the result that convergence is not possible at this geometry. In contrast, no particular convergence problems were encountered using SF-TDDFT and the triplet reference.

The question arises as to what can be done in order to remove the unphysical mixed spin-symmetry states in the SF-TDDFT calculations. Vahtras and Rinkevicius have proposed what appears to be a very elegant formal solution [162]. They propose a reformulation of TDDFT which makes use from the very beginning of explicit spin-coupled excitation and de-excitation operators. This requires using the same orbitals for different spin (i.e., a spin-restricted formalism) which is often viewed as at odds with the variational principle in density-functional theory, but this perhaps is a small price to pay. More importantly putting the Vahtras-Rinkevicius scheme into practice still means finding explicit ways to include matrix elements involving 2-electron and higher excitations. We have already mentioned research aimed at the explicit inclusion of 2- and higher-electron excitations through the frequency-dependence of the xc-kernel [43,44,46,149,150,184]. Another approach which should be mentioned is to handle these states by a transformed reference via an intermediate configuration Kohn-Sham TDDFT procedure proposed by Seth and Ziegler with its very appropriate acronym “TRICKS-TDDFT” [201]. The basic idea is to combine SF-TDDFT with different reference states using ideas from the Ziegler-Rauk-Baerends multiplet sum method to make first-order estimates of the pure spin-states corresponding to the mixed states. [73] Thus, in the case of the $^M(a_1 \rightarrow b_1)$ mixed state on the right hand side of Fig. 4.5 obtained from SF-TDDFT, we could calculate the energy for the corresponding $^3(a_1 \rightarrow b_1)$ triplet state from conventional SP-TDDFT and then use the multiplet sum formula

$$\omega_S^{\text{TRICKS-TDDFT}} = 2\omega_M^{\text{SF-TDDFT}} - \omega_T^{\text{SP-TDDFT}}, \quad (4.45)$$

to estimate the energy of the $^1(a_1 \rightarrow b_1)$ singlet state. Similar ideas have been used to advantage in the recent study of the reaction path for the *cis/trans* photochemical isomerization of 4-styrylpyridine [203]. The main drawback, and the reason that this approach was not considered here, is that finding corresponding spin α and β orbitals is not only not always easy but also not always possible in the spin-unrestricted (i.e., different-orbitals-for-different-spins) approach. It turns out that this is especially true in the funnel regions which interest us most.

Perhaps the most interesting and important result in this paper came when we pursued the CO ring-opening path way and examined the physically-important CX. The situation is very different than the case of *cis/trans* photoisomerization. In that case, the HOMO and LUMO are typically the π and π^* orbitals associated with the double bond around which rotation is occurring. It is also true that the HOMO and LUMO involved in the C_{2v} ring-opening reaction are the σ and σ^* orbitals associated with breaking the CC bond. The oxygen lone pair (n) is tightly enough bound that it stays out of the way. However along the physical CO ring-opening reaction route, elementary chemical arguments indicate that the oxygen lone pair intercedes as HOMO between the relevant CO σ and σ^* orbitals. This means that taking the lowest triplet as reference does not lead to an optimal description of the biradical present at the CO ring-opening CX. Still

S_0/S_1 coupling exists and SF-TDDFT meaning that a CX is theoretically possible. Indeed such a feature is seen in our SF-TDDFT calculations roughly half-way between the location of the CASSCF CX and the CIS seam.

Our attempt to rechoose the triplet reference in a more appropriate manner gave moderately encouraging, but not yet fully satisfactory, results. The reason for this frustrating situation is in our use of different orbitals for different spin and the high degree of orbital mixing observed near the CX. Indeed no clear σ and σ^* orbitals are found near the CASSCF CX geometry.

We conclude that, depending upon the molecule and the CX, the lowest triplet state may or may not be the optimal choice of reference for SF-TDDFT. However the asymmetric ring-opening reaction in oxirane should be taken as a warning that choosing a suitable triplet reference for SF-TDDFT may require a nontrivial use of chemical intuition. This is likely to be especially problematic for larger molecules and is unlikely to be practical for on-the-fly photodynamics calculations. Thus, for the moment, SF-TDDFT remains an *ad hoc* solution for particular problems rather than a universal panacea.

4.2.6 Acknowledgments

We thank Enrico Tapavicza, Ivano Tavernelli, and Claudia Filippi for helpful discussions. Latévi Max Lawson Daku is thanked for supplying comparison data from the ADF program so that we could double check the correctness of our implementation of the noncollinear spin-flip method in DEMON2K. C. M. W. would like to acknowledge a scholarship from the French Embassy in Kenya. M. H. R. would like to acknowledge an *Allocation de Recherche* from the French Ministry of Education. B. N. would like to acknowledge a scholarship from the *Fondation Nanoscience*. A. I. would like to acknowledge postdoctoral funding from the *Laboratoire d'Études Dynamiques et Structurales de la Sélectivité* (LEDSS) which has now become part of the *Département de Chimie Moléculaire* (DCM). Those of us at the *Université Joseph Fourier* would like to thank Pierre Vatton, Denis Charapoff, Régis Gras, Sébastien Morin, and Marie-Louise Dheu-Andries for technical support at the (DCM) and for technical support in the context of the *Centre d'Expérimentation du Calcul Intensif en Chimie* (CECIC) computers used for the calculations reported here. This work has been carried out in the context of the French Rhône-Alpes *Réseau thématique de recherche avancée (RTRA): Nanosciences aux limites de la nanoélectronique* and the Rhône-Alpes Associated Node of the European Theoretical Spectroscopy Facility (ETSF).

4.3 Conclusions and Perspective

We have applied SF-TDDFT to study the photochemical ring opening of oxirane. We have shown that the C_{2v} ring opening represents better the ground-state than adiabatic TDDFT, although a small cusp is still present compared to benchmark diffusion quantum Monte Carlo simulations. The double excitation state given by diffusion quantum Monte Carlo and SF-

TDDFT are of different nature. SF-TDDFT cannot represent the same state as diffusion quantum Monte Carlo due to the spin contamination problems. This is clearly seen in the asymmetric ring opening, in which the SF-TDDFT ground state (S_0) and the first singly-excited state (S_1) compare well with diffusion quantum Monte Carlo, but the double excitation is of different nature. This problem has consequences for the conical intersection, in which the intersection point with SF-TDDFT is displaced to a slightly different geometry with respect to regular TDDFT and complete active space self-consistent field.

In conclusion, SF-TDDFT is a good candidate for being applied to photochemistry, as it avoids the non-interacting v -representability. The main problem lies in the restricted number of double excitation poles, which restricts its application to well-defined problems in which the lowest doubly-excited state gives the main contribution. We have shown that in more complicated cases, such as the oxirane ring opening, SF-TDDFT is insufficient, requiring a general approach that include double excitations in general.

Chapter 5

Ab initio Exact Exchange-Correlation Kernel

5.1 Introduction

This chapter contains a derivation of a TDDFT kernel capable of including all double excitations. The kernel is calculated in two steps: the first step constructs the second-order kernel derived from the many-body polarization propagator, and the second step maps (localizes) the kernel into TDDFT using a similar approach to the Sham-Schlüter equation [218]. The kernel has an explicit frequency dependence that goes beyond any adiabatic functional. The frequency arises from both the polarization propagator and the localizer. Both quantities are thoroughly analyzed and discussed. In this chapter, two main objectives of this thesis are accomplished, namely, we provide a method that can include double excitations in general and we identify which correlation diagrams are missing in adiabatic TDDFT functionals.

These results are described in the next section, which contains a preprint of the article to be submitted in the *Journal of Chemical Physics*. My specific contribution was mainly in the derivation of the polarization propagator kernel. This required the application of time-independent perturbation theory to the polarization propagator, using a general Fock operator (later identified as the Kohn-Sham operator) in the order definition. The diagrammatic expansion facilitates the identification of the terms missing in the adiabatic approximation. I also had a considerable contribution in the writing of the article, especially in the sections about the perturbation approximation of the polarization propagator.

There are at least two reasons for choosing the polarization propagator in the construction of the TDDFT kernel. First, there is an obvious connection between the response functions of TDDFT and the polarization propagator, which allows a direct comparison of the structure and diagrammatic expansion of the kernels in both theories. This allowed us to identify the missing correlation terms in the adiabatic functionals. Second, the truncated perturbative expansion of the polarization propagator treats both direct and exchange diagrams in the same footing. This is necessary to avoid the appearance of spurious excitations [46, 48].

The first-order approximation to the polarization propagator gives an alternative derivation for the time-dependent exact-exchange kernel [32]. The most important result of this section is the derivation of a second-order polarization propagator, which gives an exact TDDFT kernel with correlation. As a result, the TDDFT response functions contains extra poles consisting of the double excitations which are missing in the adiabatic approximation. For the purposes of this thesis, the derivation was truncated to the second-order, which is enough to show the appearance and role of double-excitation poles. Higher orders are trivially derived and would bring in higher-excitation poles.

5.2 Formal foundations of dressed TDDFT (Article)¹

Formal Foundations of Dressed Time-Dependent Density-Functional Theory for Many-Electron Excitations

Miquel Huix-Rotllant and Mark E. Casida[†]

*Laboratoire de Chimie Théorique,
Département de Chimie Moléculaire (DCM, UMR CNRS/UJF 5250),
Institut de Chimie Moléculaire de Grenoble (ICMG, FR2607),
Université Joseph Fourier (Grenoble I),
301 rue de la Chimie, BP 53,
F-38041 Grenoble Cedex 9, France*

In so far as time-dependent density-functional theory (TDDFT) provides an exact formalism for calculating molecular absorption spectra, TDDFT should be able to describe not only 1-electron excited states but also 2-electron, 3-electron, etc. excited states which show up in molecular spectra by borrowing intensity from 1-electron excited states. This requires going beyond conventional adiabatic TDDFT where the exchange-correlation kernel is frequency independent, f_{xc} , to include an appropriate frequency dependence, $f_{xc}(\omega)$. Maitra, Zhang, Cave, and Burke gave a heuristic derivation of a frequency-dependent correction to adiabatic TDDFT (an approach they called “dressed TDDFT”) designed to bring in one double excitation [J. Chem. Phys. **120**, 5932 (2004)] and Casida showed how dressed TDDFT might be generalized in the form of a polarization propagator (PP) correction to adiabatic TDDFT [J. Chem. Phys. **122**, 054111 (2005)]. This paper presents a further exploration of the PP approach to dressed TDDFT using an approach which is significantly more rigorous than previous dressed TDDFT work and previous work on a PP correction to adiabatic TDDFT. A link is also made with work based directly upon the Bethe-Salpeter equation. At first order we recover the exact exchange result of Görling [Int. J. Quant. Chem. **69**, 265 (1998).] A second-order treatment brings in 2-electron excitations. An important result of Gonze and Scheffler [Phys. Rev. Lett. **82**, 4416 (1999)] emerges as a trivial consequence of this formalism. Concrete formulae for the nonadiabatic correction are derived at the level of the second-order polarization propagator (SOPPA) and algebraic diagrammatic construction (ADC) approaches. The example of butadiene is used to make a connection with the pioneering dressed theory of Maitra *et al.*

[†] Corresponding author: Mark.Casida@UJF-Grenoble.Fr

5.2.1 Introduction

The time-dependent extension of density-functional theory (DFT) is currently providing many opportunities and challenges for modeling electronic time-dependent properties and excitation spectra. [188–190] The conventional DFT of Hohenberg, Kohn, and Sham, though a formally exact theory, is limited to static ground state properties. [14, 15] Time-dependent DFT (TDDFT) is a formally exact extension of DFT designed to treat time-dependent phenomena, [13] from which excited states may be extracted using linear response theory. [17] Linear-response TDDFT (LR-TDDFT) calculations have become a method of choice for calculating the spectra of medium and large sized molecules. Limitations on TDDFT arise because the exact exchange-correlation (xc) functional must be approximated in practice. Thus conventional LR-TDDFT works best for

1. This section is a preprint of Ref. [140]. Note: The original format has been adapted to the standards of this thesis.

low-energy 1-electron excited states which do not involve too much charge transfer and are not too delocalized in space. [182,183] This paper is a contribution towards overcoming the restriction to 1-electron excitations. In particular we propose a method for placing the “dressed TDDFT” of Maitra, Zhang, Cave, and Burke [43] within the well-defined context of many-body perturbation theory (MBPT). After some well-defined approximations, we will derive an expression for the frequency-dependent xc-kernel, $f_{xc}(\omega)$, of LR-TDDFT at the level of the second-order polarization propagator (SOPPA) [45,219–221] and algebraic diagrammatic construction (ADC) [66,222] approaches. The result is a powerful formalism which englobes several previous results from the literature but which also allows us to go beyond these results to arrive at a rigorous and quite general polarization propagator formulation of dressed TDDFT.

In the most applications of TDDFT, we first begin with a molecule in its ground state where it is described by the usual Kohn-Sham equation, [15]

$$\left(\hat{h}_H + v_{xc}(\mathbf{1})\right) \psi_r(\mathbf{1}) = \epsilon_r \psi_r(\mathbf{1}), \quad (5.1)$$

and introduce an external time-dependent perturbation, $v_{appl}(\mathbf{1})$. The time-dependent Kohn-Sham equation [13] is then,

$$\left(\hat{h}_H + v_{xc}(\mathbf{1}) + v_{appl}(\mathbf{1})\right) \psi_r(\mathbf{1}) = i \frac{\partial \psi_r(\mathbf{1})}{\partial t}. \quad (5.2)$$

[We use Hartree atomic units, $\hbar = m_e = e = 1$, and space-spin coordinates throughout. Also $i = (\mathbf{r}_i, \sigma_i)$ represents the space and spin coordinates of particle i while $\mathbf{i} = (i, t_i)$ (bold face) is the corresponding space-time coordinate.] Practical applications of TDDFT almost always make use of the adiabatic approximation (AA),

$$v_{xc}^{AA}(\mathbf{1}) = \frac{\delta E_{xc}[\rho_t]}{\delta \rho_t(\mathbf{1})}, \quad (5.3)$$

and $\rho_t(\mathbf{x})$ is the density $\rho(\mathbf{x}, t)$ considered as a function only of \mathbf{x} . This amounts to assuming that the response of the xc-potential, v_{xc} , to any temporal change in the density, is instantaneous and without memory. The usual form of LR-TDDFT [17] involves solving a pseudoeigenvalue problem,

$$\begin{bmatrix} \mathbf{A}(\omega) & \mathbf{B}(\omega) \\ \mathbf{B}^*(\omega) & \mathbf{A}^*(\omega) \end{bmatrix} \begin{pmatrix} \mathbf{X} \\ \mathbf{Y} \end{pmatrix} = \omega \begin{bmatrix} \mathbf{1} & \mathbf{0} \\ \mathbf{0} & -\mathbf{1} \end{bmatrix} \begin{pmatrix} \mathbf{X} \\ \mathbf{Y} \end{pmatrix}, \quad (5.4)$$

where,

$$\begin{aligned} A_{ia,jb}(\omega) &= \delta_{i,j} \delta_{a,b} \epsilon_{a,i} + (ia|f_{Hxc}(\omega)|jb) \\ B_{ia,bj}(\omega) &= (ia|f_{Hxc}(\omega)|bj). \end{aligned} \quad (5.5)$$

Here, $f_{Hxc}(\omega) = f_H + f_{xc}(\omega)$ where $f_H(1,2) = 1/r_{12}$ is the Hartree kernel and $f_{xc}(\omega)$ is the Fourier transform of the xc-kernel,

$$f_{xc}(1,2;t_1 - t_2) = \frac{\delta v_{xc}(\mathbf{1})}{\delta \rho(\mathbf{2})}. \quad (5.6)$$

Also we have introduced the compact notation,

$$\epsilon_{rs\dots,uv\dots} = (\epsilon_r + \epsilon_s + \dots) - (\epsilon_u + \epsilon_v + \dots). \quad (5.7)$$

Equation (5.4) has paired excitation and de-excitation solutions. Its eigenvalues are (de-)excitation energies (or frequencies since $\hbar = 1$),

$$\omega_I = E_I - E_0, \quad (5.8)$$

and the vectors \mathbf{X} and \mathbf{Y} provide information about transition moments. In particular the oscillator strength,

$$f_I = \frac{2}{3} \omega_I |\langle 0 | \mathbf{r} | I \rangle|^2, \quad (5.9)$$

of the transition with excitation energy ω_I may be calculated from \mathbf{X}_I and \mathbf{Y}_I . [17] When the AA is made, the \mathbf{A} and \mathbf{B} matrices become independent of frequency, and it is easy to show that the number of solutions is equal to the number of 1-electron excitations, albeit dressed to include electron correlation effects. Allowing the \mathbf{A} and \mathbf{B} matrices to have a frequency dependence allows the explicit inclusion of 2-electron excited states.

This is easiest to understand within the Tamm-Dancoff approximation (TDA). The usual AA TDA equation,

$$\mathbf{A}\mathbf{X} = \omega\mathbf{X}, \quad (5.10)$$

resembles a configuration interaction (CI) equation, [223]

$$(\mathbf{H} - E_0\mathbf{1})\mathbf{C} = \omega\mathbf{C}. \quad (5.11)$$

However, while Eq. (5.10) is restricted to single excitations, Eq. (5.11) includes not only single but also higher excitations. Nevertheless there is a simple transformation which recasts Eq. (5.11) into the form of Eq. (5.10), but with a frequency-dependent $\mathbf{A}(\omega)$. Thus the matrix $\mathbf{A}^{CI} = \mathbf{H} - E_0\mathbf{1}$ may be partitioned into 1-electron excitations (“singles”, denoted here by the subscript “1”) and other excitations (typically “doubles”, but possibly also higher excited terms, denoted here by “2+”) as,

$$\begin{bmatrix} \mathbf{A}_{1,1}^{CI} & \mathbf{A}_{1,2+}^{CI} \\ \mathbf{A}_{2+,1}^{CI} & \mathbf{A}_{2+,2+}^{CI} \end{bmatrix} \begin{pmatrix} \mathbf{C}_1 \\ \mathbf{C}_{2+} \end{pmatrix} = \omega \begin{pmatrix} \mathbf{C}_1 \\ \mathbf{C}_{2+} \end{pmatrix}, \quad (5.12)$$

provided we can ignore any coupling between the ground state and our singles, doubles, and higher excited states. According to standard Löwdin (Feshbach) partitioning theory (see, for example, Ref. [224]),

$$\left[\mathbf{A}_{1,1}^{CI} + \mathbf{A}_{1,2+}^{CI} (\omega\mathbf{1}_{2+,2+} - \mathbf{A}_{2+,2+}^{CI})^{-1} \mathbf{A}_{2+,1}^{CI} \right] \mathbf{C}_1 = \omega\mathbf{C}_1. \quad (5.13)$$

It is tempting to identify, [223]

$$\mathbf{A}(\omega) \approx \mathbf{A}_{1,1}^{CI} + \mathbf{A}_{1,2+}^{CI} (\omega\mathbf{1}_{2+,2+} - \mathbf{A}_{2+,2+}^{CI})^{-1} \mathbf{A}_{2+,1}^{CI}. \quad (5.14)$$

This is effectively what Maitra, Zhang, Cave, and Burke did in their dressed TDDFT, except that they went further and considered only the case of coupling between a single 1-electron

excitation (S) and a single 2-electron excitation (D). [43] This is the model shown in Fig. 5.1. Let us try to understand the basic physics. A bright singly-excited state with excitation energy ω_S and oscillator strength $f_S = 1$ interacts with a dark doubly-excited state with excitation energy ω_D and oscillator strength $f_D = 0$ via a coupling matrix element x . The CI problem is simply,

$$\begin{bmatrix} \omega_S & x \\ x & \omega_D \end{bmatrix} \begin{pmatrix} C_S \\ C_D \end{pmatrix} = \omega \begin{pmatrix} C_S \\ C_D \end{pmatrix}. \quad (5.15)$$

It has two solutions, namely,

$$\begin{bmatrix} \omega_S & x \\ x & \omega_D \end{bmatrix} \begin{pmatrix} \cos \theta \\ \sin \theta \end{pmatrix} = \omega_a \begin{pmatrix} \cos \theta \\ \sin \theta \end{pmatrix}, \quad (5.16)$$

and

$$\begin{bmatrix} \omega_S & x \\ x & \omega_D \end{bmatrix} \begin{pmatrix} -\sin \theta \\ \cos \theta \end{pmatrix} = \omega_b \begin{pmatrix} -\sin \theta \\ \cos \theta \end{pmatrix}. \quad (5.17)$$

Backsolving we find that,

$$\begin{aligned} \omega_S &= \omega_a \cos^2 \theta + \omega_b \sin^2 \theta \\ \omega_D &= \omega_a \sin^2 \theta + \omega_b \cos^2 \theta, \end{aligned} \quad (5.18)$$

which establishes the unperturbed quantities in terms of the solutions of the perturbed problem. We see the average excitation energy is conserved in the coupled problem,

$$\omega_a + \omega_b = \omega_S + \omega_D. \quad (5.19)$$

Something similar occurs with the oscillator strengths. It is easy to show that,

$$\begin{aligned} f_a &= \frac{2}{3} \omega_a |\langle 0|\mathbf{r}|a\rangle|^2 = \frac{2}{3} \omega_a |\langle 0|\mathbf{r}|S\rangle|^2 \cos^2 \theta \\ f_b &= \frac{2}{3} \omega_b |\langle 0|\mathbf{r}|b\rangle|^2 = \frac{2}{3} \omega_b |\langle 0|\mathbf{r}|S\rangle|^2 \sin^2 \theta. \end{aligned} \quad (5.20)$$

Summing gives,

$$f_a + f_b = \frac{2}{3} (\omega_a \cos^2 \theta + \omega_b \sin^2 \theta) |\langle 0|\mathbf{r}|S\rangle|^2 = \frac{2}{3} \omega_S |\langle 0|\mathbf{r}|S\rangle|^2 = f_S. \quad (5.21)$$

Hence oscillator strength is also conserved. This leads to the common interpretation that the coupling “shatters the singly-excited peak into two satellite peaks.”

Now let us try to obtain the dressed TDDFT form for the nonadiabatic correction to the exchange-correlation kernel. Equation (5.13) reads,

$$\left(\omega_S + \frac{x^2}{\omega - \omega_D} \right) C_S = \omega C_S. \quad (5.22)$$

and ω_a and ω_b are thus solutions of the equation,

$$\omega = \omega_S + \frac{x^2}{\omega - \omega_D}. \quad (5.23)$$

Comparing with the diagonal TDA LR-TDDFT within the two-orbital model,

$$\omega = \epsilon_{a,i} + (ia|f_{Hxc}(\omega)|ia), \quad (5.24)$$

shows that,

$$(ia|f_{Hxc}(\omega)|ia) = (\omega_S - \epsilon_{a,i}) + \frac{x^2}{\omega - \omega_D}. \quad (5.25)$$

Maitra *et al.* interpreted the first term as the adiabatic part,

$$f_{Hxc}^{AA} = \omega_S - \epsilon_{a,i}, \quad (5.26)$$

and second term as the nonadiabatic correction,

$$f_{Hxc}^{NA}(\omega) = \frac{x^2}{\omega - \omega_D}. \quad (5.27)$$

Since

$$x = (\omega_a - \omega_b) \cos \theta \sin \theta, \quad (5.28)$$

it is easy to show that,

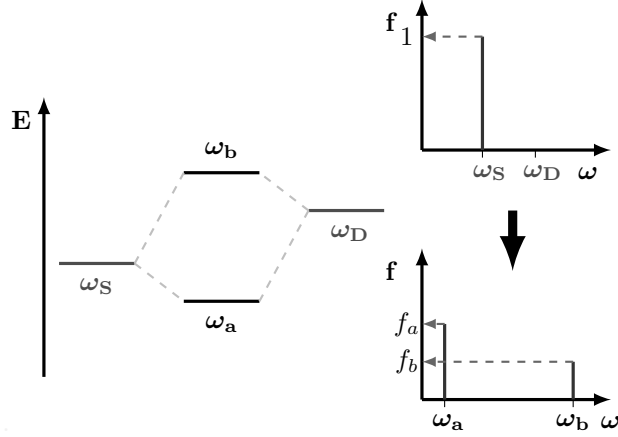
$$x^2 = \omega_S \omega_D - \omega_a \omega_b. \quad (5.29)$$

which is the form of the numerator used by Maitra *et al.* Equation (5.27) then provides a model for including a single double excitation into conventional TDDFT calculations. This basic idea has now been used by several groups. [43, 44, 150, 184]

Maitra *et al.* recognized that dressed TDDFT should ultimately be formulated in terms of linear response theory rather than the wave function CI method, so they gave their justification in terms of generalized susceptibilities. However their formula is the same as the one presented above and apparently involves a double-excitation energy, ω_D , obtained from wave function theory. Casida recognized that a correct formulation of a nonadiabatic correction term to adiabatic LR-TDDFT should come from linear response theory and so used the polarization propagator formalism to devise a polarization propagator correction. [149] This earlier theory had some difficulties which are overcome in the present formulation.

The approach taken here has been termed “*ab initio* DFT” by Bartlett. [225, 226] At the exchange-only level the terms optimized effective potential (OEP) [97, 227] or exact exchange (EXX) [228, 229] are also used, and OEP is sometimes also used to include the correlated case. [230, 231] The objective is to derive expressions for DFT quantities, such as the xc-potential, v_{xc} , and the xc-kernel, $f_{xc}(\omega)$, from many-body perturbation theory (MBPT). (In contrast to the way the term is used in solid-state physics, Bartlett uses the term “*ab initio*” as it is normally used in quantum chemistry to make a distinction between DFT and typically Hartree-Fock-based first-principles theories.) This approach does not give functionals of the density, but can give useful insight into, and computational checks of, the behavior of DFT quantities. We will assume that the xc-potential is known and concentrate on finding MBPT expressions for the frequency-dependent xc-kernel.

Figure 5.1 Two-level model used by Maitra *et al.* in their *ad hoc* derivation of dressed TDDFT. See explanation in text.



Previous work along these lines has been carried out for the static kernel by directly taking the derivative of the OEP energy expression with the constraint that the orbitals come from a local potential. This was first done by Görling in 1998 [32] for the full time-dependent exchange-only problem. In 2002, Hirata *et al.* redid the derivation for the static case. [137] Later, in 2006, a diagrammatic derivation of the static result was given by Bokhan and Bartlett, [226] and the functional derivative of the kernel, g_x , has been treated by Bokhan and Bartlett in the static exchange-only case. [232]

Our approach is more closely related to a second way to derive the same equations which may have the advantage of being more transparent and in any event of having a more direct relation with recent developments in solid-state theory. [119,120,141,233–235] The essential idea starts from the fact that $f_{xc}(\omega)$ satisfies a 2-point Bethe-Salpeter-like equation which must be the result of localizing the corresponding “proper particle-hole self-energy” (also known as the “proper particle-hole scattering kernel” and the “compact vertex part” [66]) that appears in the 4-point Bethe-Salpeter equation in ordinary many-body theory. Tokatly, Stubner, and Pankratov have used this concept to develop a diagrammatic expansion of $f_{xc}(\omega)$. [236,237] This approach has been extended to include 2-electron excitations in recent work by Romaniello *et al.* using a screened interaction approach inherited from solid-state polarization propagators. [46] Their approach is not entirely satisfactory as they show that it gives rise to extra unphysical solutions, a problem which we believe may arise from an imbalanced treatment of antisymmetry due to an asymmetric treatment of direct and exchange diagrams when using a screened interaction. This belief is confirmed by recent work of Sangalli, Romaniello, Colò, Marini, and Onida. [238].

The basic idea of our approach, which does balance contributions from direct and exchange diagrams, is described in the next section. We do not in fact localize the Bethe-Salpeter equation (BSE) though we do the equivalent. The problem is that we wish to work in the frequency repre-

sentation and that the true BSE (before approximations) is an equation in the time representation whose Fourier transform into the frequency representation is fraught with problems. Instead we follow the superoperator polarization propagator approach (SPPA) of Nielsen, Jørgensen, and Oddershede [45, 219–221] and the algebraic diagrammatic construction (ADC) approach of Schirmer [66, 222] and begin with a formally exact form of the polarization propagator (Sec. 5.2.4.) This gives a matrix equation whose elements are then deduced in an order-consistent manner by expanding and matching against Feynman diagrams (Sec. 5.2.4.) (See also earlier work by Paldus and Čížek. [239, 240]) In effect we are resumming these Feynman diagrams in a particular form. The result is a renormalized theory which has proven itself for quantum chemical applications but which so far seems to defy diagrammatic representation. Unfortunately the second-order SPPA and ADC approaches (termed SOPPA and ADC(2) respectively) do not lend themselves to solid-state applications where it is likely that screening must be explicitly taken into account.

Our contribution is to generalize and to adapt these equations for use in *ab initio* DFT. Since we do make some well-defined (though not strictly necessary) approximations to keep future computations tractable, it is important to show that these equations are at least as good as those previously presented in the literature. This we do by indicating how previous literature results emerge in a natural fashion. However our equations are very general and go beyond previous work.

Finally we make the connection with dressed TDDFT (Sec. 5.2.5). The result is what we believe to be a coherent generalization of dressed TDDFT to include an in principle infinite number of 1-electron, 2-electron, and higher-electron excited states and which we are tempted to call “fully-dressed TDDFT” because it includes significantly more states than the original dressed TDDFT. To make the relation between dressed TDDFT and the present theory more clear we present the example of butadiene, previously treated by Maitra *et al.*, thus facilitating comparison with their pioneering work (Sec. 5.2.5). Section 5.2.6 contains our concluding discussion. Appendices have been included where deemed necessary to keep the present work self contained (Appendices 5.2.8 and 5.2.10) or where additional details seem useful (Appendix 5.2.9).

5.2.2 Space, Time, and the Exact Kernel

This section elaborates on the polarization propagator (PP) approach to calculating the xc-kernel, initially suggested by one of us. [17] Not only do we wish to clarify certain approximations implicit in this previous work, but we wish to bring into sharp relief the relation with the Bethe-Salpeter equation (BSE) approach to calculating the xc-kernel popular in the solid-state physics community. [46, 119, 120, 141, 233–235] Thus both approaches involve spatial localization of non-local operators, some of which (*vide infra*) results in new frequency dependencies. However, although the two many-body perturbation theory (MBPT) approaches to *ab initio* DFT are formally equivalent, differences emerge because the BSE approach emphasizes the time representation while the PP approach emphasizes the frequency representation. This can and typically does lead to different approximations. The discussion of dressed TDDFT in the previous section suggests that it will be easier to derive pole structure-conserving approximations needed for treating 2-electron and higher excitations in the frequency representation than in the time

representation. This and prior experience with the PP approach in the quantum chemistry community [45, 66, 219–222] have lead us to favor the PP approach.

The common denominator to all approaches is the fundamental equation of LR-TDDFT which simply says that the response of the density of the interacting system to an applied perturbation must be the same as the response of the density of the Kohn-Sham fictitious system of noninteracting electrons to an effective potential involving the response of the Kohn-Sham single-particle potential, v_s . This response is conveniently described in terms of susceptibilities. The susceptibility

$$\chi(\mathbf{1}, \mathbf{2}) = \frac{\delta\rho(\mathbf{1})}{\delta v_{\text{appl}}(\mathbf{2})}. \quad (5.30)$$

describes the response of the real electrons to the applied perturbation δv_{appl} ,

$$\delta\rho(\mathbf{1}) = \int \chi(\mathbf{1}, \mathbf{2}) \delta v_{\text{appl}}(\mathbf{2}) d\mathbf{2}. \quad (5.31)$$

The response of the density of the Kohn-Sham fictitious system of noninteracting electrons is identical but the potential is now the Kohn-Sham single-particle potential,

$$\delta\rho(\mathbf{1}) = \int \chi_s(\mathbf{1}, \mathbf{2}) \delta v_s(\mathbf{2}) d\mathbf{2}. \quad (5.32)$$

In contrast to the interacting susceptibility of Eq. (5.30), the noninteracting susceptibility,

$$\chi_s(\mathbf{1}, \mathbf{2}) = \frac{\delta\rho(\mathbf{1})}{\delta v_s(\mathbf{2})}, \quad (5.33)$$

is known exactly from MBPT. Of course the effective potential is the sum of the applied potential and the potential due to the response of the self-consistent field, v_{Hxc} ,

$$\delta v_s(\mathbf{1}) = \delta v_{\text{appl}}(\mathbf{1}) + \int f_{Hxc}(\mathbf{1}, \mathbf{2}) \delta\rho(\mathbf{2}) d\mathbf{2}, \quad (5.34)$$

where $f_{Hxc}(\mathbf{1}, \mathbf{2}) = \delta v_{Hxc}(\mathbf{1})/\delta\rho(\mathbf{2})$ is the functional derivative of the Hartree plus exchange-correlation self-consistent field. Manipulating these equations is facilitated by a matrix representation in which the integration is interpreted as a sum over a continuous index. Thus,

$$\delta\rho = \chi \delta v_{\text{appl}} = \chi_s (\delta v_{\text{appl}} + \mathbf{f}_{Hxc} \delta\rho), \quad (5.35)$$

is easily manipulated to give a Bethe-Salpeter-like equation,

$$\chi = \chi_s + \chi_s \mathbf{f}_{Hxc} \chi, \quad (5.36)$$

or, written out more explicitly,

$$\chi(\mathbf{1}, \mathbf{4}) = \chi_s(\mathbf{1}, \mathbf{4}) + \int \chi_s(\mathbf{1}, \mathbf{2}) f_{Hxc}(\mathbf{2}, \mathbf{3}) \chi(\mathbf{3}, \mathbf{4}) d\mathbf{2} d\mathbf{3}. \quad (5.37)$$

We will be making extensive use of MBPT. Perhaps the most common and arguably the most basic quantity in MBPT is the 1-electron Green's function defined by,

$$iG(\mathbf{1}, \mathbf{2}) = \langle 0 | \mathcal{T} \{ \hat{\psi}_H(\mathbf{1}) \hat{\psi}_H^\dagger(\mathbf{2}) \} | 0 \rangle. \quad (5.38)$$

It hardly needs to be defined except to introduce our notation. Here, the subscript H indicates that the field operators are understood to be in the Heisenberg representation. Also \mathcal{T} is the usual time-ordering operator, which includes anticommutation in our case (i.e., for fermions),

$$\mathcal{T} \{ \psi_H(\mathbf{1}) \hat{\psi}_H^\dagger(\mathbf{2}) \} = \theta(t_1 - t_2) \hat{\psi}_H(\mathbf{1}) \hat{\psi}_H^\dagger(\mathbf{2}) - \theta(t_2 - t_1) \hat{\psi}_H^\dagger(\mathbf{2}) \hat{\psi}_H(\mathbf{1}).$$

The usual MBPT approach to evaluating the susceptibility, χ , uses the fact that it is the retarded form,

$$i\chi(\mathbf{1}, \mathbf{2}) = \theta(t_1 - t_2) \langle 0 | [\tilde{\rho}_H(\mathbf{1}), \tilde{\rho}_H(\mathbf{2})] | 0 \rangle, \quad (5.39)$$

of the time-ordered correlation function,

$$i\chi(\mathbf{1}, \mathbf{2}) = \langle 0 | \mathcal{T} \{ \tilde{\rho}_H(\mathbf{1}) \tilde{\rho}_H(\mathbf{2}) \} | 0 \rangle, \quad (5.40)$$

where,

$$\tilde{\rho}_H(\mathbf{1}) = \hat{\psi}_H^\dagger(\mathbf{1}) \hat{\psi}_H(\mathbf{1}) - \langle 0 | \hat{\psi}_H^\dagger(\mathbf{1}) \hat{\psi}_H(\mathbf{1}) | 0 \rangle, \quad (5.41)$$

is the density fluctuation operator. (See for example Ref. [16] pp. 172-175 and p. 151.)

In practice it is much more convenient to work with time-ordered, rather than retarded, quantities. For this reason, *we will generally work with time-ordered Green functions, even when our notation may suggest the corresponding retarded quantity.* The retarded version may be obtained from the time-ordered version of χ by simply changing the sign of the imaginary part in the frequency representation. Since we typically work with finite basis sets and real functions, there is no imaginary part in our calculations and so the problem does not arise except in principle. However it is best to keep in mind the distinction between different types of Green's function time-ordering. (See for example the discussion of Lehmann representations on pp. 72-79 of Ref. [16] for the distinction between retarded, advanced, and time-ordered Green's functions.)

The BSE-like form of the basic equation (5.36) of LR-TDDFT suggests that the most direct link with MBPT should be through the BSE itself. Although the MBPT literature refers to several related equations as BSEs, the original BSE [241] is probably that of the particle-hole (ph) propagator, [66] which we choose to write as,

$$iL(\mathbf{1}, \mathbf{2}; \mathbf{3}, \mathbf{4}) = \langle 0 | \mathcal{T} \{ \tilde{\gamma}(\mathbf{1}, \mathbf{2}) \tilde{\gamma}(\mathbf{4}, \mathbf{3}) \} | 0 \rangle, \quad (5.42)$$

where,

$$\tilde{\gamma}(\mathbf{1}, \mathbf{2}) = \hat{\psi}_H^\dagger(\mathbf{2}) \hat{\psi}_H(\mathbf{1}) - \langle 0 | \mathcal{T} \{ \hat{\psi}_H^\dagger(\mathbf{2}) \hat{\psi}_H(\mathbf{1}) \} | 0 \rangle, \quad (5.43)$$

is a sort of density matrix fluctuation operator (or would be if we constrained $t_1 = t_2$ and $t_3 = t_4$).

[It may be useful to try to place L in the context of other 2-electron propagators: The 2-electron Green's function is (see p. 116 of Ref. [16]),

$$G(\mathbf{1}, \mathbf{2}; \mathbf{3}, \mathbf{4}) = (-i)^2 \langle 0 | \mathcal{T} \{ \hat{\psi}_H(\mathbf{1}) \hat{\psi}_H(\mathbf{2}) \hat{\psi}_H^\dagger(\mathbf{4}) \hat{\psi}_H^\dagger(\mathbf{3}) \} | 0 \rangle. \quad (5.44)$$

The particle-hole response function, [66]

$$R(\mathbf{1}, \mathbf{2}; \mathbf{3}, \mathbf{4}) = G(\mathbf{1}, \mathbf{2}; \mathbf{3}, \mathbf{4}) - G(\mathbf{1}, \mathbf{3})G(\mathbf{2}, \mathbf{4}). \quad (5.45)$$

Then L is related to R by the relation,

$$L(\mathbf{1}, \mathbf{2}; \mathbf{3}, \mathbf{4}) = iR(\mathbf{1}, \mathbf{4}; \mathbf{2}, \mathbf{3}). \quad (5.46)$$

By construction,

$$\chi(\mathbf{1}, \mathbf{2}) = L(\mathbf{1}, \mathbf{1}^+; \mathbf{2}^+, \mathbf{2}), \quad (5.47)$$

where \mathbf{i}^+ is infinitesimally later than \mathbf{i} . In the jargon of MBPT, $\chi(\mathbf{1}, \mathbf{2})$ is a 2-point quantity, while $L(\mathbf{1}, \mathbf{2}; \mathbf{3}, \mathbf{4})$ is a 4-point quantity. The space-time analogue of the Harriman contraction operator (Appendix 5.2.8), Υ_{ST} , allows us to rewrite Eq. (5.47) as a concise matrix equation,

$$\chi = \Upsilon_{ST} \mathbf{L} \Upsilon_{ST}^\dagger. \quad (5.48)$$

Much of the development of the BSE approach to calculating the xc-kernel done in the solid-state physics community [46, 119, 120, 141, 233–235, 238] makes use of Hedin's equations. [242] These cannot be used directly to determine the xc-kernel without at least some manipulation which would take us too far afield. Suffice it so say that an appropriate BSE for

$$L(\mathbf{1}, \mathbf{2}; \mathbf{7}, \mathbf{8}) = L_s(\mathbf{1}, \mathbf{2}; \mathbf{7}, \mathbf{8}) + \int L_s(\mathbf{1}, \mathbf{2}; \mathbf{3}, \mathbf{4}) \Xi_{Hxc}(\mathbf{3}, \mathbf{4}; \mathbf{5}, \mathbf{6}) L(\mathbf{5}, \mathbf{6}; \mathbf{7}, \mathbf{8}) d\mathbf{3}d\mathbf{4}d\mathbf{5}d\mathbf{6}, \quad (5.49)$$

or

$$\mathbf{L} = \mathbf{L}_s + \mathbf{L}_s \Xi_{Hxc} \mathbf{L}, \quad (5.50)$$

in matrix notation. Here

$$iL_s(\mathbf{1}, \mathbf{2}; \mathbf{3}, \mathbf{4}) = G_s(\mathbf{1}, \mathbf{4})G_s(\mathbf{2}, \mathbf{3}), \quad (5.51)$$

is the ph-propagator for the Kohn-Sham fictitious system of noninteracting electrons, and the 4-point quantity, Ξ_{Hxc} , may be deduced from a Feynman diagram expansion as the proper part of the ph-response function “self-energy”.

Combining Eqs. (5.36), (5.48), and (5.50) gives the formally exact equation,

$$\left(\Upsilon_{ST} \mathbf{L}_s \Upsilon_{ST}^\dagger \right) \mathbf{f}_{xc} \left(\Upsilon_{ST} \mathbf{L} \Upsilon_{ST}^\dagger \right) = \Upsilon_{ST} \mathbf{L}_s \Xi_{xc} \mathbf{L} \Upsilon_{ST}^\dagger. \quad (5.52)$$

Note that the Hartree part of Ξ_{Hxc} is just $\Upsilon_{ST}^\dagger \mathbf{f}_H \Upsilon_{ST}$ and so cancels with the Hartree part of $\Upsilon_{ST}^\dagger \mathbf{f}_{Hxc} \Upsilon_{ST}$. Of course, even *ab initio* DFT involves approximations to truncate infinite sums and otherwise keep calculations tractable. A common approximation is to replace the computationally difficult many-body quantity \mathbf{L} with the computationally much simpler single-body quantity \mathbf{L}_s to obtain,

$$\left(\Upsilon_{ST} \mathbf{L}_s \Upsilon_{ST}^\dagger \right) \mathbf{f}_{xc} \left(\Upsilon_{ST} \mathbf{L}_s \Upsilon_{ST}^\dagger \right) = \Upsilon_{ST} \mathbf{L}_s \Xi_{xc} \mathbf{L}_s \Upsilon_{ST}^\dagger. \quad (5.53)$$

This is still very complex because Ξ_{xc} , is a 4-time quantity (or 3-frequency quantity after Fourier transformation [46]). Equation (5.53) is closely related to the ‘‘Nanoquanta approximation’’ (NQA),

$$\left(\Upsilon_{ST}L_s\Upsilon_{ST}^\dagger\right)f_{xc}\left(\Upsilon_{ST}L_s\Upsilon_{ST}^\dagger\right)=\Upsilon_{ST}L_s\left(i\frac{\delta\Sigma_{xc}}{\delta\mathbf{G}}\right)L_s\Upsilon_{ST}^\dagger, \quad (5.54)$$

so named by Lucia Reining because it was simultaneously derived by several different people [119, 120, 141, 233–235] involved with the Nanoquanta group. The NQA simplifies still further in the usual *GW* approximation for the self-energy Σ_{xc} . Although the NQA has proven successful for extended systems, it is not at all clear that it is appropriate for finite systems where vertex effects are likely to be important. However its most severe drawback, and the one which prevents us from using it here, is that it is ill adapted for treating 2-electron and higher excitations.

We have chosen to seek more appropriate approximations within the PP approach. This approach is based upon the 2-time quantity,

$$\Pi(1, 2; 3, 4; t - t') = L(1t, 2t; 3t', 4t'), \quad (5.55)$$

which makes it impossible from the beginning to write down a BSE for the PP (though Bethe-Salpeter-like equations do arise within the PP approach.) Written out explicitly,

$$\begin{aligned} i\Pi(1, 2; 3, 4; t - t') &= \langle 0|\mathcal{T}\{\hat{\psi}_H^\dagger(2t^+)\hat{\psi}_H(1t)\hat{\psi}_H^\dagger(3t'^+)\hat{\psi}_H(4t')\}|0\rangle \\ &\quad - \langle 0|\mathcal{T}\{\hat{\psi}_H^\dagger(2t^+)\hat{\psi}_H(1t)\}|0\rangle\langle 0|\mathcal{T}\{\hat{\psi}_H^\dagger(3t'^+)\hat{\psi}_H(4t')\}|0\rangle. \end{aligned} \quad (5.56)$$

[The second term is often dropped in the definition of the PP. It is there to remove $\omega = 0$ excitations in the Lehmann representation. (See for example pp. 559-560 of Ref. [16].)] The retarded version of the PP is the susceptibility describing the response of the 1-electron density matrix,

$$\gamma(1, 2; t) = \langle 0|\hat{\psi}^\dagger(2t)\hat{\psi}(1t)|0\rangle, \quad (5.57)$$

to a general (not necessarily local) applied perturbation,

$$\Pi(1, 2; 3, 4; t - t') = \frac{\delta\gamma(1, 2; t)}{\delta w_{appl}(3, 4; t')}, \quad (5.58)$$

which is a convolution. After Fourier transform,

$$\delta\gamma(1, 2; \omega) = \int \Pi(1, 2; 3, 4; \omega)\delta w_{appl}(3, 4; \omega) d3d4, \quad (5.59)$$

or,

$$\delta\gamma(\omega) = \mathbf{\Pi}(\omega)\delta\mathbf{w}_{appl}(\omega), \quad (5.60)$$

in matrix form. The connection with with DFT is made by recognizing that the diagonal elements of the density matrix are the density,

$$\begin{aligned}\rho(1; \omega) &= \gamma(1, 1; \omega) \\ \boldsymbol{\rho}(\omega) &= \boldsymbol{\Upsilon} \boldsymbol{\gamma}(\omega),\end{aligned}\tag{5.61}$$

and DFT is typically only concerned with local operators,

$$\begin{aligned}\delta w_{\text{appl}}(1, 1'; \omega) &= \delta(1 - 1') \delta v_{\text{appl}}(1; \omega) \\ \delta \mathbf{w}_{\text{appl}}(\omega) &= \boldsymbol{\Upsilon}^\dagger \delta \mathbf{v}_{\text{appl}}(\omega).\end{aligned}\tag{5.62}$$

Here we have introduced the original form of the very convenient collapse and expansion operators of Harriman (Appendix 5.2.8). Applying this information to Eq. (5.59) gives that,

$$\boldsymbol{\chi}(\omega) = \boldsymbol{\Upsilon} \boldsymbol{\Pi}(\omega) \boldsymbol{\Upsilon}^\dagger.\tag{5.63}$$

The basic LR-TDDFT Eq. (5.36) is a convolution which when Fourier transformed gives,

$$\chi(1, 4; \omega) = \chi_s(1, 4; \omega) + \int \chi_s(1, 2; \omega) f_{Hxc}(2, 3; \omega) \chi(3, 4; \omega) d2d3,$$

or in matrix form,

$$\boldsymbol{\chi}(\omega) = \boldsymbol{\chi}_s(\omega) + \boldsymbol{\chi}_s(\omega) \mathbf{f}_{Hxc}(\omega) \boldsymbol{\chi}(\omega).\tag{5.64}$$

Applying Eqs. (5.61) and (5.62) leads to the exact equation,

$$(\boldsymbol{\Upsilon} \boldsymbol{\Pi}_s(\omega) \boldsymbol{\Upsilon}^\dagger) \mathbf{f}_{Hxc}(\omega) (\boldsymbol{\Upsilon} \boldsymbol{\Pi}(\omega) \boldsymbol{\Upsilon}^\dagger) = \boldsymbol{\Upsilon} (\boldsymbol{\Pi}(\omega) - \boldsymbol{\Pi}_s(\omega)) \boldsymbol{\Upsilon}^\dagger.\tag{5.65}$$

Further approximations are useful in order to minimize the number of times the computationally difficult full PP appears and to facilitate interpretation. However the precise nature of these approximations typically differ depending upon whether the interesting frequencies are far from any higher-order excitations (off-resonant regime) or near a higher-order excitation (resonant regime). In discussing these two cases, it is helpful to rewrite the exact case as,

$$\text{Exact: } \mathbf{f}_{Hxc}(\omega) = \boldsymbol{\Lambda}_s(\omega) (\boldsymbol{\Pi}_s^{-1}(\omega) - \boldsymbol{\Pi}^{-1}(\omega)) \boldsymbol{\Lambda}^\dagger(\omega),\tag{5.66}$$

where the localizer,

$$\boldsymbol{\Lambda}(\omega) = (\boldsymbol{\Upsilon} \boldsymbol{\Pi}(\omega) \boldsymbol{\Upsilon}^\dagger)^{-1} \boldsymbol{\Upsilon} \boldsymbol{\Pi}(\omega).\tag{5.67}$$

Note that this only makes sense if we take care to eliminate the null spaces of $\boldsymbol{\Upsilon} \boldsymbol{\Pi}_s(\omega) \boldsymbol{\Upsilon}^\dagger$ and of $\boldsymbol{\Upsilon} \boldsymbol{\Pi}(\omega) \boldsymbol{\Upsilon}^\dagger$ before taking the inverse (i.e., singular value decomposition.) See Sec. 5.2.3 and Appendices 5.2.8 and 5.2.9 for a detailed discussion of the localizer.

Optimized effective potential theories typically make use of the Born approximation,

$$\boldsymbol{\chi}(\omega) = \boldsymbol{\chi}_s(\omega) + \boldsymbol{\chi}_s(\omega) \mathbf{f}_{Hxc}(\omega) \boldsymbol{\chi}_s(\omega),\tag{5.68}$$

so that,

$$\mathbf{f}_{Hxc}(\omega) = (\boldsymbol{\chi}_s(\omega))^{-1} (\boldsymbol{\chi}(\omega) - \boldsymbol{\chi}_s(\omega)) (\boldsymbol{\chi}_s(\omega))^{-1}.\tag{5.69}$$

This is our first approximation,

1st Approx.:

$$\begin{aligned} \mathbf{f}_{Hxc}(\omega) &= \mathbf{\Lambda}_s(\omega) (\mathbf{\Pi}_s^{-1}(\omega) - \mathbf{\Pi}^{-1}(\omega)) \mathbf{\Lambda}_{1/2}^\dagger(\omega) \\ &= (\mathbf{\Upsilon} \mathbf{\Pi}_s(\omega) \mathbf{\Upsilon}^\dagger)^{-1} (\mathbf{\Pi}(\omega) - \mathbf{\Pi}_s(\omega)) (\mathbf{\Upsilon} \mathbf{\Pi}_s(\omega) \mathbf{\Upsilon}^\dagger)^{-1}. \end{aligned} \quad (5.70)$$

where only one $\mathbf{\Pi}$ has been replaced with $\mathbf{\Pi}_s$ in the localizer,

$$\mathbf{\Lambda}_{1/2}(\omega) = (\mathbf{\Upsilon} \mathbf{\Pi}_s(\omega) \mathbf{\Upsilon}^\dagger)^{-1} \mathbf{\Upsilon} \mathbf{\Pi}(\omega). \quad (5.71)$$

It is expected to work well in the off-resonant regime. As we shall see, this first approximation gives Görling's exact exchange (EXX) kernel for TDDFT. [32] On the other hand, the poles of the kernel in this approximation are *a priori* the poles of the exact and independent particle PPs—that is, the true and single-particle excitation energies—unless well-balanced approximations lead to fortuitous cancellations. The discussion of dressed TDDFT in the introduction shows that this is unlikely to lead to accurate 2-electron and higher excitations.

To correct the poles we make an additional structure-conserving approximation, equivalent to the PP Born approximation,

$$\begin{aligned} \mathbf{\Pi}(\omega) &= \mathbf{\Pi}_s(\omega) + \mathbf{\Pi}_s(\omega) \mathbf{K}_{Hxc}(\omega) \mathbf{\Pi}_s(\omega) \\ \mathbf{K}_{Hxc} &= \mathbf{\Pi}_s^{-1}(\omega) - \mathbf{\Pi}^{-1}(\omega). \end{aligned} \quad (5.72)$$

This is our second approximation,

$$\text{2nd Approx.: } \mathbf{f}_{Hxc}(\omega) = \mathbf{\Lambda}_s(\omega) (\mathbf{\Pi}_s^{-1}(\omega) - \mathbf{\Pi}^{-1}(\omega)) \mathbf{\Lambda}_s^\dagger(\omega). \quad (5.73)$$

Not only does the static localizer enter into the static OEP problem (Appendix 5.2.8), but the dynamic localizer also enters naturally into the time-dependent OEP problem when the initial state is the static ground state. [32] Equation (5.73) simply reads that $\mathbf{f}_{Hxc}(\omega)$ is a spatially localized form of the quantity, $\mathbf{K}_{Hxc}(\omega) = \mathbf{\Pi}_s^{-1}(\omega) - \mathbf{\Pi}^{-1}(\omega)$. This is nothing but the PP analogue of the basic approximation (5.53) used in the BSE approach on the way to the Nanoquanta approximation.

5.2.3 Localization

At the risk of repetition, let us recapitulate what we have done: We have made two Born approximations,

$$\begin{aligned} \mathbf{\Pi}(\omega) &= \mathbf{\Pi}_s(\omega) + \mathbf{\Pi}_s(\omega) \mathbf{K}_{Hxc}(\omega) \mathbf{\Pi}_s(\omega) \\ \mathbf{\chi}(\omega) &= \mathbf{\chi}_s(\omega) + \mathbf{\chi}_s(\omega) \mathbf{f}_{Hxc}(\omega) \mathbf{\chi}_s(\omega), \end{aligned} \quad (5.74)$$

and have thereby arrived at the equation,

$$\mathbf{f}_{Hxc}(\omega) = \mathbf{\Lambda}_s(\omega) \mathbf{K}_{Hxc}(\omega) \mathbf{\Lambda}_s^\dagger(\omega). \quad (5.75)$$

The significance of this equation is that the *ab initio* many-body problem has now been separated into a purely PP part represented by $\mathbf{K}_{Hxc}(\omega)$ and a frequency-dependent localization part represented by $\mathbf{\Lambda}_s(\omega)$ which allows us to recover a TDDFT quantity from *ab initio* theory. This makes manifest earlier ideas suggesting that localizing in space is necessarily associated with “delocalization in time” (i.e., additional frequency dependence. [230, 243] Since $\mathbf{\Pi}(\omega)$ and $\mathbf{\chi}(\omega)$ have the same poles and the same transition densities (but not the same transition density matrices!), spatial localization is *not* necessary if our only goal is to obtain excitation energies and transition densities beyond the TDDFT AA, since it then suffices to carry out an ordinary DFT-based PP calculation. Rather the extra localization step is needed if we wish to remain within TDDFT and hence study intrinsic TDDFT quantities such as the xc-kernel. In such a case, exploration of the behavior of the dynamic localizer is essential. In this section, we give the explicit form of the dynamic localizer from which we easily deduce an important relation first noted by Gonze and Scheffler [142]. This Gonze-Scheffler relation was used in the original justification of dressed TDDFT by Maitra, Zhang, Cave, and Burke. [43] Its importance to the formal foundation of dressed TDDFT is re-examined in Sec. 5.2.5. Eventually it will be desirable to go beyond dressed TDDFT to carry out finite-basis calculations with the dynamic localizer (not done in this paper) and this and a static approximation are discussed in Appendix 5.2.9.

The static localizer is intimately related to the static OEP approach and has been discussed in Appendix 5.2.8. The dynamic localizer,

$$\mathbf{\Lambda}(\omega) = (\mathbf{\Upsilon}\mathbf{\Pi}(\omega)\mathbf{\Upsilon}^\dagger)^{-1} \mathbf{\Upsilon}\mathbf{\Pi}(\omega), \quad (5.76)$$

arises quite naturally in the context of the time-dependent OEP problem. According to Runge-Gross (RG) theory, [13] the exact time-dependent xc-potential, $v_{xc}(t)$, is not only a functional of the density, $\rho(t)$, but also of an initial condition which can be taken as the wave function, $\Psi(t_0)$, at some prior time t_0 . On the other hand, linear response theory begins with the static ground state case where the first Hohenberg-Kohn theorem tells us that the wave function is a functional of the density $\Psi(t_0) = \Psi[\rho_{t_0}]$. Görling has pointed out that this greatly simplifies the problem [32] because we can then show that,

$$\int \Pi_s(1, 1; 2, 2; \omega) v_x(2; \omega) d2 = \int \Pi_s(1, 1; 2, 3; \omega) \Sigma_x(2, 3) d2d3. \quad (5.77)$$

We can write this equation in matrix form using the Harriman’s collapse operator as

$$\mathbf{\Upsilon}\mathbf{\Pi}_s(\omega)\mathbf{\Upsilon}^\dagger \mathbf{v}_x(\omega) = \mathbf{\Upsilon}\mathbf{\Pi}_s(\omega)\mathbf{\Sigma}_x. \quad (5.78)$$

Clearly the dynamic exchange potential is the Hartree-Fock exchange operator localized by the dynamic localization operator,

$$\mathbf{v}_x(\omega) = \mathbf{\Lambda}_s(\omega)\mathbf{\Sigma}_x. \quad (5.79)$$

For the case of the non-interacting susceptibility, we can easily derive an expression for the dynamic localizer. Since

$$\Pi_s(1, 2; 3, 4; \omega) = \sum_i^{occ} \sum_a^{virt} \frac{\psi_i(1)\psi_a^*(2)\psi_i^*(3)\psi_a(4)}{\omega - \epsilon_{a,i}} - \sum_i^{occ} \sum_a^{virt} \frac{\psi_a(1)\psi_i^*(2)\psi_a^*(3)\psi_i(4)}{\omega + \epsilon_{a,i}}, \quad (5.80)$$

we can express the kernel of $\Upsilon\Pi_s(\omega)$ as

$$(\Upsilon\Pi_s)(1; 2, 3; \omega) = \sum_i^{occ} \sum_a^{virt} \frac{\psi_i(1)\psi_a^*(1)\psi_i^*(2)\psi_a(3)}{\omega - \epsilon_{a,i}} - \sum_i^{occ} \sum_a^{virt} \frac{\psi_a(1)\psi_i^*(1)\psi_a^*(2)\psi_i(3)}{\omega + \epsilon_{a,i}}. \quad (5.81)$$

Also, the kernel of $\Upsilon\Pi_s(\omega)\Upsilon^\dagger$ is just,

$$(\Upsilon\Pi_s\Upsilon^\dagger)(1; 2; \omega) = \sum_i^{occ} \sum_a^{virt} \frac{\psi_i(1)\psi_a^*(1)\psi_i^*(2)\psi_a(2)}{\omega - \epsilon_{a,i}} - \sum_i^{occ} \sum_a^{virt} \frac{\psi_a(1)\psi_i^*(1)\psi_a^*(2)\psi_i(2)}{\omega + \epsilon_{a,i}}. \quad (5.82)$$

Like the susceptibility, The two operators have poles at the independent particle excitation energies $\omega = \pm\epsilon_{a,i} = \pm(\epsilon_a - \epsilon_i)$.

(Here and throughout, unless otherwise stated, we use the orbital index convention,

$$\underbrace{a, b, c, \dots, h}_{\text{unoccupied}}, \underbrace{i, j, k, l, m, n}_{\text{occupied}}, \underbrace{o, p, q, \dots, z}_{\text{free}}, \quad (5.83)$$

where free orbitals may be either occupied or unoccupied.)

In order to construct the dynamic localizer, the kernel (5.82) has to be inverted. This is not generally possible to do this analytically, though it can be done in a finite-basis representation (Appendix 5.2.9). However Gonze and Scheffler have noted that exact inversion is possible in the special case of a frequency, $\omega = \epsilon_{b,j}$, of a pole well separated from the other poles. [142] Near this pole, the kernels, $\Upsilon\Pi_s(\omega)$ and $\Upsilon\Pi_s(\omega)\Upsilon^\dagger$, are each dominated by single terms,

$$\begin{aligned} (\Upsilon\Pi_s) &\approx \frac{\psi_j(1)\psi_b^*(1)\psi_j^*(2)\psi_b(3)}{\omega - \epsilon_{b,j}} \\ (\Upsilon\Pi_s\Upsilon^\dagger)(1; 2; \omega) &\approx \frac{\psi_j(1)\psi_b^*(1)\psi_j^*(2)\psi_b(2)}{\omega - \epsilon_{b,j}}. \end{aligned} \quad (5.84)$$

Thus Eq. (5.78) becomes,

$$\frac{\psi_j(1)\psi_b^*(1)}{\omega - \epsilon_{b,j}} \langle \psi_b | v_x(\epsilon_{b,j}) | \psi_j \rangle \approx \frac{\psi_j(1)\psi_b^*(1)}{\omega - \epsilon_{b,j}} \langle \psi_b | \hat{\Sigma}_x | \psi_j \rangle, \quad (5.85)$$

with the approximation becoming increasingly exact as ω approaches $\epsilon_{b,j}$. Hence,

$$\langle \psi_b | v_x(\epsilon_{b,j}) | \psi_j \rangle = \langle \psi_b | \hat{\Sigma}_x | \psi_j \rangle. \quad (5.86)$$

More generally for an arbitrary dynamic kernel, $K(1, 2; \omega)$,

$$(\psi_b \psi_j^* | \Lambda(\epsilon_{b,j}) K(\epsilon_{b,j})) = (\psi_j | K(\epsilon_{b,j}) | \psi_b), \quad (5.87)$$

and we can do the same for $-\epsilon_{b,j}$, obtaining

$$(\psi_j \psi_b^* | \Lambda(-\epsilon_{b,j}) K(-\epsilon_{b,j})) = (\psi_j | K(-\epsilon_{b,j}) | \psi_b) \quad (5.88)$$

We refer to these last two equations as Gonze-Scheffler (GS) relations, since they were first derived by these authors. [142] These relations show that the dynamic localizer, $\Lambda_s(\omega)$, is pole free if the excitation energies, $\epsilon_{a,i}$, are discrete and nondegenerate and suggests that the dynamic localizer maybe a smoother function of ω than might at first be suspected. Equation (5.86) also shows the importance of the dynamic character of the localizer as this is what allows a local operator at certain special frequencies to have exactly the same matrix elements as the original nonlocal operator which was being localized.

We can now return to a particular aspect of Casida's original PP approach [149] which was failure to take proper account of the localizer. The importance of the localizer is made particularly clear by the GS relations in the case of charge transfer excitations. The single-pole approximation to the $i \rightarrow a$ excitation energy is,

$$\omega = \epsilon_{a,i} + (ia|\Lambda(\epsilon_{a,i})K_{xc}(\epsilon_{a,i})\Lambda^\dagger(\epsilon_{a,i})|ai) = \epsilon_{a,i} + (aa|\Pi_s^{-1}(\epsilon_{a,i}) - \Pi^{-1}(\epsilon_{ai})|ii). \quad (5.89)$$

Had the localizer been neglected, then we would have found incorrectly that,

$$\omega = \epsilon_{a,i} + (ia|\Pi_s^{-1}(\epsilon_{ai}) - \Pi^{-1}(\epsilon_{a,i})|ai). \quad (5.90)$$

While the latter reduces to just ϵ_{ai} for charge transfer excitations at a distance (because $\psi_i\psi_a = 0$), the former does not. [27] However, for most excitations the overlap is non-zero. In such cases and around a pole well-separated pole the localizer can be completely neglected.

Away from the poles, the behavior of the localizer becomes much more complicated. It is evident that the range space of the operators $\mathbf{Y}\mathbf{\Pi}_s(\omega)\mathbf{Y}^\dagger$ and $\mathbf{Y}\mathbf{\Pi}_s(\omega)$ and of the localizer $\Lambda_s(\omega)$ is the product basis $\psi_i\psi_a$ made by multiplying together all occupied, ψ_i , and all unoccupied, ψ_a , orbitals. It can be shown that this product basis is complete except for constant functions (because $\int \psi_a(1)\psi_i(1) d1 = 0$) as long as the orbital basis set is complete (Appendix of Ref. [244]). It is, in fact, overcomplete. Even for finite basis sets, the product basis set typically contains linear dependencies. This makes it difficult to solve the localization equation

$$\mathbf{v}(\omega) = \Lambda(\omega)\Sigma(\omega), \quad (5.91)$$

in full generality because we are really solving a least squares problem that seeks to maximize the component of $\mathbf{v}(\omega)$ in the relevant range space. (Note that we have dropped the subscript x and allowed Σ to have a frequency dependence, so that Eq. (5.91) is intended to be general.) This problem is discussed in more detail in Appendix 5.2.9.

5.2.4 Perturbative Approximations to the Polarization Propagator

In this section we review the MBPT techniques needed for the calculation of the key quantities for constructing of xc-kernels within the first and second approximations. In the case of the first approximation, this means deriving an expression for the quantity $\mathbf{\Pi}(\omega) - \mathbf{\Pi}_s(\omega)$. For the second approximation, this means deriving an expression for the quantity $\mathbf{\Pi}_s^{-1}(\omega) - \mathbf{\Pi}^{-1}(\omega)$. Although it is clear that the zero-order approximation should be the Kohn-Sham fictitious system of non-interacting electrons, we have still had to make some choices. In particular, we have

chosen to work with MBPT expansions in terms of the bare electron repulsion [or more exactly the “fluctuation potential” (*vide infra*)], rather than the screened interaction used in solid-state physics. [46, 119] The main advantage of working with the bare interaction is a balanced treatment of direct and exchange diagrams, which we feel is likely to be especially important for treating two- and higher-electron excitations. While we will automatically include what the solid state community refers to as vertex effects, the disadvantage of our approach is that it is likely to break down in solids when screening becomes important. The specific approach taken here is the now well established second-order polarization propagator approximation (SOPPA) of Nielsen, Jørgensen, and Oddershede [45, 219–221]. The usual presentation of the SOPPA approach is based upon the superoperator equation-of-motion (EOM) approach previously used by Casida. [149] However the SOPPA approach is very similar in many ways to the second-order algebraic diagrammatic construction (ADC(2)) approach of Schirmer [66, 222] and we will not hesitate to refer to this approach as needed (particularly with regard to the inclusion of various diagrammatic contributions.) What is new, aside from explicit comparisons with appropriate TDDFT literature, is the change from a Hartree-Fock to a Kohn-Sham zero-order picture and the concomitant inclusion of (many) additional terms. Nevertheless it will be seen that the final working expressions are fairly compact.

5.2.4.1 Superoperator Polarization Propagator Approach

The PP is given in a molecular orbital basis as,

$$\Pi(1, 2, 3, 4; t - t') = \sum_{pqrs} \Pi_{sr,qp}(t - t') \psi_r(1) \psi_s^*(2) \psi_q^*(3) \psi_p(4), \quad (5.92)$$

where

$$\begin{aligned} -\Pi_{sr,qp}(t - t') &= i\theta(t - t') \langle 0 | \hat{r}_H^\dagger(t) \hat{s}_H(t) \hat{q}_H^\dagger(t') \hat{p}_H(t') | 0 \rangle \\ &\quad + i\theta(t' - t) \langle 0 | \hat{q}_H^\dagger(t') \hat{p}_H(t') \hat{r}_H^\dagger(t) \hat{s}_H(t) | 0 \rangle. \end{aligned} \quad (5.93)$$

As explained in Ref. [16] pp. 559-560, this change of convention with respect to that of Eq. (5.56) turns out to be more of a convenience than an inconvenience. Also note that, since the PP depends only upon the time difference, $t - t'$, we can simplify the above expression without loss of generality by shifting the origin of the time-scale so that $t' = 0$. We wish to seek an elegant matrix formulation for Π .

The first step makes use of superoperators. A superoperator \check{X} is defined by its action on an (Hilbert-space) operator \hat{A} as

$$\check{X}\hat{A} = [\hat{X}, \hat{A}] = \hat{X}\hat{A} - \hat{A}\hat{X}. \quad (5.94)$$

When \check{X} is the Hamiltonian operator, \check{H} , one often speaks of the Liouvillian. An exception is the identity superoperator, \check{I} , whose action is simply given by,

$$\check{I}\hat{A} = \hat{A}. \quad (5.95)$$

The Heisenberg form of orbital creation and annihilation operators is easily expressed in terms of the Liouvillian superoperator,

$$\hat{p}_H(t) = e^{i\check{H}t}\hat{p}e^{-i\check{H}t} = e^{i\check{H}t}\hat{p}. \quad (5.96)$$

Then

$$-\Pi_{sr,qp}(t) = i\theta(t)\langle 0| \left[e^{i\check{H}t} (\hat{r}^\dagger \hat{s}) \right] \hat{q}^\dagger \hat{p} |0\rangle + i\theta(-t)\langle 0| \hat{q}^\dagger \hat{p} \left[e^{i\check{H}t} (\hat{r}^\dagger \hat{s}) \right] |0\rangle. \quad (5.97)$$

Taking the Fourier transform (and making use of appropriate convergence factors) gives,

$$-\Pi_{sr,qp}(\omega) = (\hat{p}^\dagger \hat{q} | (\omega \check{\mathbf{I}} + \check{H})^{-1} | \hat{r}^\dagger \hat{s}), \quad (5.98)$$

where we have introduced the superoperator metric,

$$(\hat{A} | \check{X} | \hat{B}) = \langle 0 | [\hat{A}^\dagger, [\hat{X}, \hat{B}]] | 0 \rangle. \quad (5.99)$$

It may be useful to note that,

$$-\Pi_{sr,qp}(\omega) = \Pi_{rs,pq}(\omega), \quad (5.100)$$

follows as an easy consequence of the above definitions. Moreover since we typically use real orbitals and a finite basis set, the PP is a real symmetric matrix. This allows us to simply identify Π and the superoperator resolvent,

$$\Pi_{pq,rs}(\omega) = (\hat{p}^\dagger \hat{q} | (\omega \check{\mathbf{I}} + \check{H})^{-1} | \hat{r}^\dagger \hat{s}). \quad (5.101)$$

Since matrix elements of a resolvent superoperator are harder to manipulate than resolvents of a superoperator matrix, we will transform Eq. (5.98) into the later form by introducing a complete set of excitation operators. The complete set

$$\{\mathbf{T}^\dagger\} = \{\mathbf{T}_1^\dagger; \mathbf{T}_2^\dagger; \dots\} = \{\hat{a}^\dagger \hat{i}, \hat{i}^\dagger \hat{a}; \hat{a}^\dagger \hat{i} \hat{b}^\dagger \hat{j}, \hat{i}^\dagger \hat{a} \hat{j}^\dagger \hat{b}; \dots\}, \quad (5.102)$$

leads to the resolution of the identity (RI),

$$\check{\mathbf{I}} = |\mathbf{T}^\dagger\rangle (\mathbf{T}^\dagger | \mathbf{T}^\dagger)^{-1} \langle \mathbf{T}^\dagger|. \quad (5.103)$$

We have defined the operator space differently from the previous work of one of us [17] to be more consistent with the literature on the field of PP calculations. The difference is actually the commutation of two operators which introduces one sign change.

Insertion into Eq. (5.98) and use of the relation,

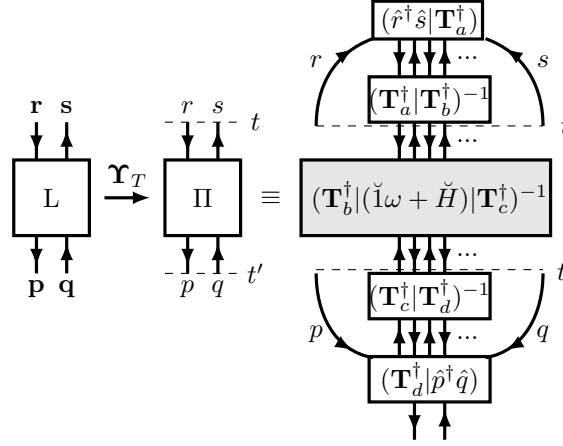
$$(\mathbf{T}^\dagger | (\omega \check{\mathbf{I}} + \check{H})^{-1} | \mathbf{T}^\dagger) = (\mathbf{T}^\dagger | \mathbf{T}^\dagger) (\mathbf{T}^\dagger | \omega \check{\mathbf{I}} + \check{H} | \mathbf{T}^\dagger)^{-1} (\mathbf{T}^\dagger | \mathbf{T}^\dagger) \quad (5.104)$$

then gives,

$$-\Pi_{sr,qp}(\omega) = (\hat{p}^\dagger \hat{q} | \mathbf{T}^\dagger) (\mathbf{T}^\dagger | \omega \check{\mathbf{I}} + \check{H} | \mathbf{T}^\dagger)^{-1} (\mathbf{T}^\dagger | \hat{r}^\dagger \hat{s}). \quad (5.105)$$

The resolvent is now defined as a matrix over an underlying configuration space somewhat analogous to what is done in the configuration interaction (CI) method familiar to quantum

Figure 5.2 Graphical representation of the localization of the 4-time propagator of the Bethe-Salpeter equation into 2-time quantity of the polarization propagator. See text.



chemists [Eq. (5.11)]. However the “CI-expansion” in the EOM method is over an operator space, rather than a wave function.

It is to be emphasized that the PP in Eq. (5.105) is exact and completely general. Its poles are exact many-electron excitation energies and its residues are the corresponding oscillator strengths. As such, it must be equivalent to the BSE which is often expressed diagrammatically in terms of Feynman diagrams. (Diagrams are discussed in Appendix 5.2.10.)

Figure 5.2 shows schematically how the PP diagrams are related to the BSE diagrams. To pass from the BSE diagrams to the PP diagrams, take the time-unordered expansion of the BSE and fix two times so that L becomes Π . This is indicated in Fig. 5.2 by the time-collapse operator Υ_T joining the two left most diagrams. Only two times are fixed in the second diagram, so it is not yet fully time ordered. Taking all possible time orderings joining t and t' , including times both before and after these times, gives the third diagram in Fig. 5.2. The result is that some parts of the diagrams hang down below the earlier time and others are stacked up above the latter time. These “dangling boxes” correspond to the terms $(\hat{p}^\dagger \hat{q} | \mathbf{T}^\dagger)$ and $(\mathbf{T}^\dagger | \hat{r}^\dagger \hat{s})$ and represent the initial and final state correlation effects present in $\langle 0 |$ and $| 0 \rangle$. The multiple time ordering also leads to multiple recrossings of the t and t' lines. This is why the matrix,

$$\mathbf{\Gamma}^{-1}(\omega) = (\mathbf{T}^\dagger | \omega \check{1} + \check{H} | \mathbf{T}^\dagger)^{-1}, \quad (5.106)$$

involves many more than four indices and so corresponds directly to two-, three-, and higher-electron excitations.

We have presented this procedure as if we simply manipulated Feynman diagrams. In reality we expanded the matrices using Wick’s theorem with the help of a home-made FORTRAN program. The result was a series of algebraic expressions which were subsequently analyzed by drawing the corresponding Feynman diagrams. This leads to about 200 diagrams which we

ultimately resum to give a more compact expression. It is the generation of this expression that we now wish to discuss.

Let us analyze this expression for the PP according to the order of excitation operator. Following Casida, [149] we partition the space as,

$$-\Pi_{sr,qp}(\omega) = \left((\hat{p}^\dagger \hat{q} | \mathbf{T}_1^\dagger) \quad (\hat{p}^\dagger \hat{q} | \mathbf{T}_{2+}^\dagger) \right) \mathbf{\Gamma}^{-1}(\omega) \begin{pmatrix} (\mathbf{T}_1^\dagger | \hat{r}^\dagger \hat{s}) \\ (\mathbf{T}_{2+}^\dagger | \hat{r}^\dagger \hat{s}) \end{pmatrix}, \quad (5.107)$$

where \mathbf{T}_{2+}^\dagger corresponds to the operator space of two-electron and higher excitations and

$$\mathbf{\Gamma}^{-1}(\omega) = \begin{bmatrix} \mathbf{\Gamma}_{1,1}(\omega) & \mathbf{\Gamma}_{1,2+} \\ \mathbf{\Gamma}_{2+,1} & \mathbf{\Gamma}_{2+,2+}(\omega) \end{bmatrix}^{-1}, \quad (5.108)$$

has been blocked,

$$\mathbf{\Gamma}_{i,j}(\omega) = (\mathbf{T}_i^\dagger | \omega \check{1} + \check{H} | \mathbf{T}_j^\dagger). \quad (5.109)$$

Using the well-known expression for the inverse of a two-by-two block matrix allows us to transform Eq. (5.107) into,

$$\begin{aligned} -\Pi_{sr,qp}(\omega) &= [(\hat{p}^\dagger \hat{q} | \mathbf{T}_1^\dagger) - (\hat{p}^\dagger \hat{q} | \mathbf{T}_{2+}^\dagger) \mathbf{\Gamma}_{2+,2+}^{-1}(\omega) \mathbf{\Gamma}_{2+,1}] \\ &\quad \mathbf{P}^{-1}(\omega) [(\mathbf{T}_1^\dagger | \hat{r}^\dagger \hat{s}) - \mathbf{\Gamma}_{1,2+} \mathbf{\Gamma}_{2+,2+}^{-1}(\omega) (\mathbf{T}_{2+}^\dagger | \hat{r}^\dagger \hat{s})] \\ &\quad + (\hat{p}^\dagger \hat{q} | \mathbf{T}_{2+}^\dagger) \mathbf{\Gamma}_{2+,2+}^{-1}(\omega) (\mathbf{T}_{2+}^\dagger | \hat{r}^\dagger \hat{s}), \end{aligned} \quad (5.110)$$

where,

$$\mathbf{P}(\omega) = \mathbf{\Gamma}_{1,1}(\omega) - \mathbf{\Gamma}_{1,2+} \mathbf{\Gamma}_{2+,2+}^{-1}(\omega) \mathbf{\Gamma}_{2+,1}. \quad (5.111)$$

Although Eq. (5.110) is somewhat complicated, it turns out that $\mathbf{P}(\omega)$ plays much the same role in the smaller \mathbf{T}_1^\dagger space that $\mathbf{\Gamma}(\omega)$ plays in the full \mathbf{T}^\dagger

To see how this comes about, it is necessary to introduce the concept of order. Our zero-order Hamiltonian is that of the Kohn-Sham fictitious system of non-interacting electrons and the perturbation defining the order is what is left over. Thus,

$$\begin{aligned} \hat{H}^{(0)} &= \hat{h}_{KS} \\ \hat{H}^{(1)} &= \hat{V} + \hat{M}_{xc}, \end{aligned} \quad (5.112)$$

where \hat{V} is the fluctuation operator,

$$\hat{V} = \frac{1}{4} \sum_{pqrs} (pq || rs) \hat{p}^\dagger \hat{r}^\dagger \hat{s} \hat{q} - \sum_{pqr} (pr || rq) \hat{p}^\dagger \hat{q}, \quad (5.113)$$

and,

$$\hat{M}_{xc} = \sum_{pq} (p | \hat{\Sigma}_x^{HF} - \hat{v}_{xc} | q) \hat{p}^\dagger \hat{q}. \quad (5.114)$$

Here $\hat{\Sigma}_x^{HF}$ is the HF exchange operator defined in terms of the occupied Kohn-Sham orbitals and the integral,

$$(pq||rs) = \int \psi_p^*(1)\psi_r^*(2) \frac{1}{r_{12}} (1 - \mathcal{P}_{12})\psi_q(1)\psi_s(2) d1d2, \quad (5.115)$$

is explicitly antisymmetrized. Notice that order parameters have been put as superscripts in parentheses.

We can now perform an order-by-order expansion of Eq. (5.110). Through second order only the \mathbf{T}_2^\dagger part of \mathbf{T}_{2+}^\dagger contributes, so we need not consider higher than double excitation operators. However we shall make some additional approximations. In particular, we will follow the usual practice and drop the last term in Eq. (5.110) because it contributes only at second order (Fig. 10, supporting material [245]) and appears to be small when calculating excitation energies and transitions moments using the Hartree-Fock approximation as zero-order. [66, 246–249] For response functions like dynamic polarizabilities, their inclusion is more critical, improving the agreement with experiments. [219]

We will also have no need to consider the second term in

$$(\hat{p}^\dagger \hat{q} | \mathbf{T}_1^\dagger) - (\hat{p}^\dagger \hat{q} | \mathbf{T}_{2+}^\dagger) \mathbf{\Gamma}_{2+,2+}^{-1}(\omega) \mathbf{\Gamma}_{2+,1}. \quad (5.116)$$

This is because it only enters into the first approximation of the previous section if we go beyond first order and is killed by the second approximation of the previous section.

This means that for the purposes of this paper we can treat the PP in the present work as given by,

$$-\Pi_{sr,qp}(\omega) = (\hat{p}^\dagger \hat{q} | \mathbf{T}_1^\dagger) \mathbf{P}^{-1}(\omega) (\mathbf{T}_1^\dagger | \hat{r}^\dagger \hat{s}). \quad (5.117)$$

Comparing with Eq. (5.105) substantiates our earlier claim that $\mathbf{P}(\omega)$ plays the same role in the \mathbf{T}_1^\dagger space that $\mathbf{\Gamma}(\omega)$ plays over the full \mathbf{T}^\dagger space.

5.2.4.2 First-Order Exchange-Correlation Kernel

We now turn to the first-order exchange-correlation kernel. Our main motivation here is to verify that we obtain the same terms as in exact exchange (EXX) calculations when we evaluate $\mathbf{\Pi} - \mathbf{\Pi}_s$. [32, 250] Since our approach is in some ways more general than previous approaches to the EXX kernel, this subsection may also provide some new insight into the meaning of the EXX equations.

Since we are limited to first order, only zero- and first-order wave function terms need be considered. This implies that all the contributions due to the \mathbf{T}_{2+}^\dagger space (the space of double- and higher-excitations) are zero and substantiates our claim that Eq. (5.117) is exact to first-order. An order-by-order expansion gives,

$$\begin{aligned} -\Pi_{sr,qp}^{(0+1)}(\omega) &= (\hat{p}^\dagger \hat{q} | \mathbf{T}_1^\dagger)^{(1)} \mathbf{P}^{(0),-1}(\omega) (\mathbf{T}_1^\dagger | \hat{r}^\dagger \hat{s})^{(0)} \\ &\quad + (\hat{p}^\dagger \hat{q} | \mathbf{T}_1^\dagger)^{(0)} \mathbf{P}^{(0),-1}(\omega) (\mathbf{T}_1^\dagger | \hat{r}^\dagger \hat{s})^{(1)} \\ &\quad + (\hat{p}^\dagger \hat{q} | \mathbf{T}_1^\dagger)^{(0)} \mathbf{P}^{(1),-1}(\omega) (\mathbf{T}_1^\dagger | \hat{r}^\dagger \hat{s})^{(0)} \\ &\quad - \Pi_{sr,qp}^s(\omega), \end{aligned} \quad (5.118)$$

where,

$$-\Pi_{sr,qp}^s(\omega) = (\hat{p}^\dagger \hat{q} | \mathbf{T}_1^\dagger)^{(0)} (\mathbf{T}_1^\dagger | \omega \check{1} + \check{h}_{KS} | \mathbf{T}_1^\dagger)^{(0),-1} (\mathbf{T}_1^\dagger | \hat{r}^\dagger \hat{s})^{(0)}. \quad (5.119)$$

The evaluation of each of first-order blocks is straightforward using the basic definitions and Wick's theorem.

Let us first consider the \mathbf{P} parts. The zeroth-order contribution is,

$$P_{kc,ia}^{(0)}(\omega) = (\omega - \epsilon_{i,a}) \delta_{ik} \delta_{ac} \quad (5.120)$$

$$P_{ck,ia}^{(0)}(\omega) = 0, \quad (5.121)$$

and the first-order contribution gives

$$P_{kc,ia}^{(1)} = (ai || kc) + M_{ac} \delta_{ik} - M_{ik} \delta_{ac} \quad (5.122)$$

$$P_{ck,ia}^{(1)} = (ci || ak). \quad (5.123)$$

The sum of $\mathbf{P}^{(0)} + \mathbf{P}^{(1)}$ gives the exact pole structure up to first-order in the SOPPA approach.

The zero-order contribution,

$$(\hat{p}^\dagger \hat{q} | \mathbf{T}_1^\dagger)^{(0)} = (\mathbf{T}_1^\dagger | \mathbf{T}_1^\dagger), \quad (5.124)$$

and the first-order contributions are given by,

$$[(\hat{p}^\dagger \hat{q} | \mathbf{T}_1^\dagger)]_{kc,ji}^{(1)} = -\frac{M_{jc}}{\epsilon_{j,c}} \delta_{ik} \quad (5.125)$$

$$[(\hat{p}^\dagger \hat{q} | \mathbf{T}_1^\dagger)]_{ck,ji}^{(1)} = \frac{M_{ic}}{\epsilon_{i,c}} \delta_{kj} \quad (5.126)$$

$$[(\hat{p}^\dagger \hat{q} | \mathbf{T}_1^\dagger)]_{kc,ba}^{(1)} = \frac{M_{ka}}{\epsilon_{k,a}} \delta_{bc} \quad (5.127)$$

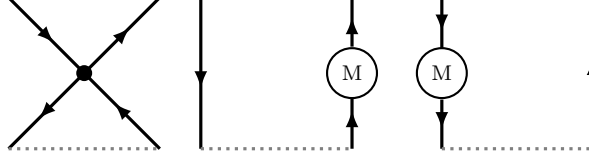
$$[(\hat{p}^\dagger \hat{q} | \mathbf{T}_1^\dagger)]_{ck,ba}^{(1)} = -\frac{M_{kb}}{\epsilon_{k,b}} \delta_{ca}. \quad (5.128)$$

The PP $\mathbf{\Pi}(\omega)$ is now easily constructed by simple matrix multiplication according to Eq. (5.118). Applying the 1st approximation from Sec. 5.2.2 and expanding $\mathbf{\Pi}_s(\omega) - \mathbf{\Pi}(\omega)$ through first order allows us to recover Görling's TD-EXX kernel. [32] The most convenient way to do this is to expand $\mathbf{P}^{(1),-1}$ using,

$$\begin{aligned} (\mathbf{T}_1^\dagger | \omega \check{1} + \check{H} | \mathbf{T}_1^\dagger)^{-1} &\approx (\mathbf{T}_1^\dagger | \omega \check{1} + \check{H}^{(0)} | \mathbf{T}_1^\dagger)^{-1} \\ &+ (\mathbf{T}_1^\dagger | \omega \check{1} + \check{H}^{(0)} | \mathbf{T}_1^\dagger)^{-1} (\mathbf{T}_1^\dagger | \check{H}^{(1)} | \mathbf{T}_1^\dagger) (\mathbf{T}_1^\dagger | \omega \check{1} + \check{H}^{(0)} | \mathbf{T}_1^\dagger)^{-1}. \end{aligned} \quad (5.129)$$

The result is represented diagrammatically in Fig. 5.3. The corresponding expressions agree perfectly with the expanded expressions of the TD-EXX kernel obtained by Hirata *et al.*, [250] which are equivalent to the more condensed form given by Görling. [32] The diagrammatic treatment makes clear the connection with the BSE approach. There are in fact just three time-ordered diagrams shown in Fig. 5.4 whose various time orderings generate the diagrams

Figure 5.4 Topologically different time-unordered diagrams for the First-order contribution to the 4-space 2-time Bethe-Salpeter equation for the case of a general potential. In the case that $\hat{M} = \hat{V}_{HF}$ the diagrams with M circles should be dropped.



in Fig. 5.3. However the “hanging boxes” above and below the central Γ region now have the physical interpretation of initial and final state wave function correlation (Fig. 5.2). Had we applied the 2nd approximation of the previous section, then only diagrams (a-f) of Fig. 5.3 would have survived.

Use of the Gonze-Scheffler relation (see further Sec. 5.2.3) then leads to,

$$\begin{aligned}
 \omega &= \epsilon_{a,i}^{KS} + f_{xc}(\epsilon_{a,i}^{KS}) \\
 &= \epsilon_{a,i}^{KS} + \langle a | \hat{M}_{xc} | a \rangle - \langle i | \hat{M}_{xc} | i \rangle + (ai || ia) \\
 &= \epsilon_{a,i}^{HF} + (ai || ia),
 \end{aligned} \tag{5.130}$$

which is exactly the configuration interaction singles (CIS, i.e., TDHF Tamm-Dancoff approximation) expression evaluated using Kohn-Sham orbitals. This agrees with a previous exact result obtained using Görling-Levy perturbation theory. [142, 251, 252]

5.2.4.3 Second-Order Exchange-Correlation Kernel

Having verified some known results, let us go on to do the MBPT necessary to obtain the pole structure of the xc-kernel through second order in the 2nd approximation. That is, we need to evaluate $\mathbf{\Pi}_s^{-1}(\omega) - \mathbf{\Pi}^{-1}(\omega)$ through second order in such a way that its pole structure is evident. The SOPPA/ADC strategy for this is to make a diagrammatic $\mathbf{\Pi}_s(\omega) - \mathbf{\Pi}(\omega)$ expansion of this quantity and then resum the expansion in an order-consistent way to have the form

$$[\mathbf{\Pi}_s(\omega) - \mathbf{\Pi}(\omega)]_{rs,qp}^{(0+1+\dots+n)} = \sum_{k=0}^n \sum_{i=0}^k \sum_{j=0}^{k-i} (\hat{p}^\dagger \hat{q} | \mathbf{T}_1^\dagger)^{(i)} \mathbf{P}^{(j),-1}(\omega) (\mathbf{T}_1^\dagger | \hat{r}^\dagger \hat{s})^{(k-i-j)},$$

when the Born approximation is applied to the $\mathbf{P}(\omega)$, in the same fashion as in the previous section. The number of diagrams contributing to this expansion is large and, for the sake of simplicity, we will only give the resummed expressions for each block. For a compilation of relevant diagrams the reader is referred to the supplementary material. [245] Evidently, after the

calculation of each block there will be an additional step matrix inversion in order to apply the 2nd approximation to the xc-kernel.

It should be emphasized that although the treatment below may seem simple, application of Wick's theorem is complicated and has been carried out using an in-house FORTRAN program written specifically for the purpose. The result before resummation is roughly 200 diagrams which have been included as supplementary material.

It can be shown that the operator space may be truncated without loss of generality in a second-order treatment to only 1- and 2-electron excitation operators. [66] The wavefunction may also be truncated at second-order. This truncation breaks the orthonormality of the \mathbf{T}_1^\dagger space:

$$(\mathbf{T}_1^\dagger|\mathbf{T}_1^\dagger) \approx (\mathbf{T}_1^\dagger|\mathbf{T}_1^\dagger)^{(0)} + (\mathbf{T}_1^\dagger|\mathbf{T}_1^\dagger)^{(2)} \neq \begin{pmatrix} 1 & 0 \\ 0 & -1 \end{pmatrix}. \quad (5.131)$$

This complication is dealt with by orthonormalizing our operator space. The new operator set expressed in terms of the original set contains only second-order corrections,

$$\begin{aligned} [\hat{a}^\dagger \hat{i}]^{(2)} &= \sum_b \left(\frac{1}{4} \sum_{kl d} \frac{(kd||lb)(dk||al)}{\epsilon_{kl,bd}\epsilon_{kl,da}} + \sum_k \frac{M_{kb}M_{ka}}{\epsilon_{k,b}\epsilon_{k,a}} \right) \hat{b}^\dagger \hat{i} \\ &+ \sum_j \left(\frac{1}{4} \sum_{mcd} \frac{(md||jc)(ci||dm)}{\epsilon_{mj,cd}\epsilon_{im,cd}} + \sum_d \frac{M_{jd}M_{di}}{\epsilon_{j,d}\epsilon_{i,d}} \right) \hat{a}^\dagger \hat{j}. \end{aligned} \quad (5.132)$$

(Note that we have used the linked-cluster theorem to eliminate contributions from disconnected diagrams. For a proof for the EOM of the one- and two-particle the Green's function see Ref. [253])

We may now proceed to calculate,

$$\begin{aligned} -\Pi_{sr,qp}^{(2)}(\omega) &= (\hat{p}^\dagger \hat{q}|\mathbf{T}_1^\dagger)^{(1)} \mathbf{P}^{(1),-1}(\omega) (\mathbf{T}_1^\dagger|\hat{r}^\dagger \hat{s})^{(0)} \\ &+ (\hat{p}^\dagger \hat{q}|\mathbf{T}_1^\dagger)^{(0)} \mathbf{P}^{(1),-1}(\omega) (\mathbf{T}_1^\dagger|\hat{r}^\dagger \hat{s})^{(1)} \\ &+ (\hat{p}^\dagger \hat{q}|\mathbf{T}_1^\dagger)^{(1)} \mathbf{P}^{(0),-1}(\omega) (\mathbf{T}_1^\dagger|\hat{r}^\dagger \hat{s})^{(1)} \\ &+ (\hat{p}^\dagger \hat{q}|\mathbf{T}_1^\dagger)^{(0)} \mathbf{P}^{(2),-1}(\omega) (\mathbf{T}_1^\dagger|\hat{r}^\dagger \hat{s})^{(0)}. \end{aligned} \quad (5.133)$$

The only new contributions that arise at this level are due to the block $\mathbf{P}^{(2)}$, which is given by

$$\mathbf{P}^{(2)} = \mathbf{\Gamma}_{1,1}^{(2)} - \mathbf{\Gamma}_{1,2}^{(1)} \mathbf{\Gamma}_{2,2}^{(0),-1}(\omega) \mathbf{\Gamma}_{2,1}^{(1)}. \quad (5.134)$$

(We are anticipating the ω -dependence of the various $\mathbf{\Gamma}$ -blocks which will be derived below.) Since the block $\mathbf{\Gamma}_{1,1}^{(2)}$ is affected by the orthonormalization procedure, it may be useful to provide a few more details. Expanding order-by-order,

$$\begin{aligned}
\mathbf{\Gamma}_{1,1}^{(2)} = & \langle 0^{(1)} | [\mathbf{T}_1^\dagger, [\omega\check{1} + \check{H}^{(0)}, \mathbf{T}_1^\dagger]] | 0^{(1)} \rangle \\
& + \langle 0^{(0)} | [\mathbf{T}_1^\dagger, [\omega\check{1} + \check{H}^{(0)}, \mathbf{T}_1^\dagger]] | 0^{(2)} \rangle \\
& + \langle 0^{(2)} | [\mathbf{T}_1^\dagger, [\omega\check{1} + \check{H}^{(0)}, \mathbf{T}_1^\dagger]] | 0^{(0)} \rangle \\
& + \langle 0^{(0)} | [\mathbf{T}_1^{\dagger(2)}, [\omega\check{1} + \check{H}^{(0)}, \mathbf{T}_1^\dagger]] | 0^{(0)} \rangle, \\
& + \langle 0^{(0)} | [\mathbf{T}_1^\dagger, [\omega\check{1} + \check{H}^{(0)}, \mathbf{T}_1^{\dagger(2)}]] | 0^{(0)} \rangle, \\
& + \langle 0^{(1)} | [\mathbf{T}_1^\dagger, [\hat{H}^{(1)}, \mathbf{T}_1^\dagger]] | 0^{(0)} \rangle \\
& + \langle 0^{(0)} | [\mathbf{T}_1^\dagger, [\hat{H}^{(1)}, \mathbf{T}_1^\dagger]] | 0^{(1)} \rangle,
\end{aligned} \tag{5.135}$$

where $\mathbf{T}_1^{\dagger(2)}$ is the vector of second-order operators defined in Eq. (5.132). It is easily shown that the first term cancels with the contributions coming from the second-order operators, and that the contributions from second-order wave function are exactly zero. Hence, that block is simply

$$\begin{aligned}
\mathbf{\Gamma}_{1,1}^{(2)} = & \langle 0^{(1)} | [\mathbf{T}_1^\dagger, [\hat{H}^{(1)}, \mathbf{T}_1^\dagger]] | 0^{(0)} \rangle \\
& + \langle 0^{(0)} | [\mathbf{T}_1^\dagger, [\hat{H}^{(1)}, \mathbf{T}_1^\dagger]] | 0^{(1)} \rangle,
\end{aligned} \tag{5.136}$$

which makes it frequency-independent. Its calculation gives

$$\begin{aligned}
[\Gamma_{1,1}^{(2)}]_{kc,ia} = & \delta_{ac} \sum_d \frac{M_{kd}M_{di}}{\epsilon_{i,d}} + \delta_{ik} \sum_l \frac{M_{la}M_{lc}}{\epsilon_{l,a}} \\
& + \frac{\delta_{ac}}{2} \sum_{lde} \frac{(le||kd)(dl||ei)}{\epsilon_{im,de}} - \frac{\delta_{ik}}{2} \sum_{lmd} \frac{(ld||mc)(dl||ma)}{\epsilon_{lm,ad}} \\
[\Gamma_{1,1}^{(2)}]_{ck,ia} = & \frac{M_{ak}M_{id}}{\epsilon_{i,d}} + \frac{M_{ci}M_{ka}}{\epsilon_{k,a}} + 2 \sum_d \frac{M_{dk}(ad||ci)}{\epsilon_{k,d}} \\
& + 2 \sum_l \frac{M_{lc}(lk||ai)}{\epsilon_{l,c}} - \sum_{md} \frac{(ce||ad)(di||em)}{\epsilon_{im,de}} \\
& - \sum_{me} \frac{(ce||mi)(ak||me)}{\epsilon_{km,ae}} - \frac{1}{2} \sum_{de} \frac{(ce||ad)(dk||ei)}{\epsilon_{ik,de}} - \frac{1}{2} \sum_{ml} \frac{(ik||ml)(ac||ml)}{\epsilon_{lm,ac}}.
\end{aligned} \tag{5.138}$$

The block $\mathbf{\Gamma}_{1,2}$ and its adjoint is of at least first-order, due to the fact that the space is orthonormal. For that reason, it is not affected by the orthonormalization at this level of approximation. Its calculation gives

$$\begin{aligned}
[\Gamma_{2,1}^{(2)}]_{kc,jbia} = & -\delta_{ik}(bc||aj) + \delta_{jk}(bc||ai) - \delta_{bc}(ai||kj) + \delta_{ac}(bi||kj) \\
[\Gamma_{2,1}^{(2)}]_{ck,jbia} = & 0.
\end{aligned} \tag{5.139}$$

Finally, the block $\mathbf{\Gamma}_{2,2}(\omega)$ gives

$$\begin{aligned} [\Gamma_{2,2}^{(2)}(\omega)]_{ldkc,jbia} &= (\omega - \epsilon_{ij,ab})\delta_{jl}\delta_{ik}\delta_{ca}\delta_{db} \\ [\Gamma_{2,2}^{(2)}(\omega)]_{ckdl,jbia} &= 0 \end{aligned} \quad (5.140)$$

Notice that double excitations are treated only to zeroth-order in a second-order approach. To obtain a consistent theory with first-order corrections to double excitations, one should go at least to third order. This however becomes computationally quite heavy.

It is interesting to speculate what would happen if we were to include the first-order doubles correction within the present second-order theory. There are, in fact, indications that this can lead to improved agreement between calculated and experimental double excitations, though the quality of the single excitations is simultaneously decreased due to an imbalanced treatment. [254, 255]

We can now construct the PP necessary to construct the 2nd approximation of the xc-kernel Eq. (5.73) according to Eq. (5.117). Since the the localizers of both left- and right-side are constructed from the non-interacting KS PP, we are only concerned with ph and hp contributions. This means that the blocks involving pp or hh indices, corresponding to density shift operators, can be ignored at this level of approximation. This simplifies the construction of $\mathbf{P}(\omega)$ in Eq. (5.117), which up to second-order gives

$$\mathbf{\Pi}^{(0+1+2),-1}(\omega) = (\mathbf{T}_1^\dagger | \mathbf{T}_1^\dagger)^{-1} \mathbf{P}^{(0+1+2)}(\omega) (\mathbf{T}_1^\dagger | \mathbf{T}_1^\dagger)^{-1}. \quad (5.141)$$

Separating ph and hp contributions, the PP takes the form of a 2×2 block-matrix in the same spirit as the LR-TDDFT formulation of Casida,

$$\begin{aligned} \mathbf{\Pi}^{(0+1+2),-1}(\omega) &= \\ &\begin{pmatrix} \mathbf{1} & \mathbf{0} \\ \mathbf{0} & -\mathbf{1} \end{pmatrix} \begin{pmatrix} \mathbf{P}^{(0+1+2)}(\omega) & \mathbf{P}^{(0+1+2)}(\omega) \\ \mathbf{P}^{(0+1+2)}(\omega) & \mathbf{P}^{(0+1+2)}(\omega) \end{pmatrix} \begin{pmatrix} \mathbf{1} & \mathbf{0} \\ \mathbf{0} & -\mathbf{1} \end{pmatrix} \\ &= \begin{pmatrix} \mathbf{P}^{(0+1+2)}(\omega) & -\mathbf{P}^{(0+1+2)}(\omega) \\ -\mathbf{P}^{(0+1+2)}(\omega) & \mathbf{P}^{(0+1+2)}(\omega) \end{pmatrix}. \end{aligned} \quad (5.142)$$

It follows that,

$$\mathbf{\Pi}_s^{-1}(\omega) - \mathbf{\Pi}^{(0+1+2),-1}(\omega) = \begin{pmatrix} \mathbf{P}^{(1+2)}(\omega) & -\mathbf{\Gamma}_{1,1}^{(1+2)} \\ -\mathbf{\Gamma}_{1,1}^{(1+2)} & \mathbf{P}^{(1+2)}(\omega) \end{pmatrix}. \quad (5.143)$$

Note that the off-diagonal (ph,hp)- and (hp,ph)-blocks are frequency-independent and that the diagonal blocks are given by Eq. (5.134). Ignoring localization for the moment, we may now cast the present Kohn-Sham based second-order polarization propagator approximation (SOPPA/KS) into the familiar form of Eq. (5.4) with,

$$\begin{aligned} A_{ia,jb}(\omega) &= \delta_{i,j}\delta_{a,b}(\epsilon_a - \epsilon_i) + P_{ia,jb}^{(1+2)}(\omega) \\ B_{ia,bj}(\omega) &= -\left(\mathbf{\Gamma}_{1,1}^{(1+2)}\right)_{ia,bj}. \end{aligned} \quad (5.144)$$

Localization [Eq. (5.73)] will complicate these formulae by mixing the $\mathbf{P}^{(1+2)}(\omega)$ and $\mathbf{\Gamma}_{1,1}^{(1+2)}$ terms,

$$\begin{aligned}
A_{ia,jb}(\omega) &= \delta_{i,j} \delta_{a,b} (\epsilon_a - \epsilon_i) \\
&+ \left[(\mathbf{\Lambda}_s)_{hp,hp}(\omega) \mathbf{P}^{(1+2)}(\omega) (\mathbf{\Lambda}_s^\dagger)_{hp,hp}(\omega) \right]_{ia,jb} \\
&+ \left[(\mathbf{\Lambda}_s)_{hp,ph}(\omega) \mathbf{P}^{(1+2)}(\omega) (\mathbf{\Lambda}_s^\dagger)_{ph,hp}(\omega) \right]_{ia,jb} \\
&- \left[(\mathbf{\Lambda}_s)_{hp,ph}(\omega) \mathbf{\Gamma}^{(1+2)} (\mathbf{\Lambda}_s^\dagger)_{hp,hp}(\omega) \right]_{ia,jb} \\
&- \left[(\mathbf{\Lambda}_s)_{hp,hp}(\omega) \mathbf{\Gamma}^{(1+2)} (\mathbf{\Lambda}_s^\dagger)_{ph,hp}(\omega) \right]_{ia,jb} \\
B_{ia,bj}(\omega) &= \left[(\mathbf{\Lambda}_s)_{hp,hp} \mathbf{P}^{(1+2)}(\omega) (\mathbf{\Lambda}_s^\dagger)_{hp,ph} \right]_{ia,bj} \\
&+ \left[(\mathbf{\Lambda}_s)_{hp,ph} \mathbf{P}^{(1+2)}(\omega) (\mathbf{\Lambda}_s^\dagger)_{ph,ph} \right]_{ia,bj} \\
&- \left[(\mathbf{\Lambda}_s)_{hp,ph}(\omega) \mathbf{\Gamma}^{(1+2)} (\mathbf{\Lambda}_s^\dagger)_{hp,ph}(\omega) \right]_{ia,bj} \\
&- \left[(\mathbf{\Lambda}_s)_{hp,hp}(\omega) \mathbf{\Gamma}^{(1+2)} (\mathbf{\Lambda}_s^\dagger)_{ph,ph}(\omega) \right]_{ia,bj} .
\end{aligned} \tag{5.145}$$

Of course this extra complication is unnecessary if all we want to do is to calculate improved excitation energies and transition amplitudes by doing DFT-based many-body perturbation theory. It is only needed when our goal is to study the effect of localization on purely TDDFT quantities such as the xc-kernel and the TDDFT vectors \mathbf{X} and \mathbf{Y} .

5.2.4.4 Tamm-Dancoff Approximation

The present theory, without the localizer, takes a particularly transparent and computationally convenient form when the Tamm-Dancoff approximation (TDA) is made. This SOPPA/KS + TDA consists of considering only the (hp,hp)-block. The excitation energies and transition amplitudes are found by solving the pseudo-eigenvalue equation,

$$\left[\mathbf{A}_{1,1}^{(0+1+2)} + \mathbf{A}_{1,2}^{(1)} \left(\omega \mathbf{1}_{2,2} - \mathbf{A}_{2,2}^{(0)} \right)^{-1} \mathbf{A}_{2,1}^{(1)} \right] \mathbf{C}_1 = \omega \mathbf{C}_1, \tag{5.146}$$

or the equivalent true eigenvalue equation,

$$\begin{bmatrix} \mathbf{A}_{1,1}^{(0+1+2)} & \mathbf{A}_{1,2}^{(1)} \\ \mathbf{A}_{2,1}^{(1)} & \mathbf{A}_{2,2}^{(0)} \end{bmatrix} \begin{pmatrix} \mathbf{C}_1 \\ \mathbf{C}_2 \end{pmatrix} = \omega \begin{pmatrix} \mathbf{C}_1 \\ \mathbf{C}_2 \end{pmatrix}. \tag{5.147}$$

Here

$$\begin{aligned}
\left(\mathbf{A}_{1,1}^{(0+1+2)}\right)_{kc,ia} &= \delta_{i,k}F_{a,c}^{(0+1+2)} - \delta_{a,c}F_{i,k}^{(0+1+2)} + (ai||kc) \\
\left(\mathbf{A}_{2,1}^{(1)}\right)_{kc,jbia} &= -\delta_{i,k}(bc||aj) + \delta_{j,k}(bc||ai) \\
&\quad - \delta_{b,c}(ai||kj) + \delta_{k,j}(bi||kj) \\
\left(\mathbf{A}_{2,2}^{(0)}\right)_{ldkc,jbia} &= \delta_{i,k}\delta_{c,a}\delta_{d,b}\epsilon_{ab,ij},
\end{aligned} \tag{5.148}$$

where $F_{r,s}^{(0+1)} = \delta_{r,s}\epsilon_r + M_{r,s}^{xc}$ is the matrix of the Hartree-Fock operator constructed with Kohn-Sham orbitals and

$$\begin{aligned}
F_{a,c}^{(0+1+2)} &= F_{a,c}^{(0+1)} + \sum_l \frac{M_{l,a}M_{l,c}}{\epsilon_{l,a}} - \frac{1}{2} \sum_{l,m,d} \frac{(ld||mc)(dl||am)}{\epsilon_{lm,ad}} \\
F_{i,k}^{(0+1+2)} &= F_{i,k}^{(0+1)} + \sum_d \frac{M_{k,d}M_{d,i}}{\epsilon_{i,d}} - \frac{1}{2} \sum_{l,d,e} \frac{(le||kd)(dl||ei)}{\epsilon_{im,de}},
\end{aligned} \tag{5.149}$$

include second-order corrections. (Note that extra factors of 1/2 will occur in these expressions when spin is taken explicitly into account.) It is immediately seen that truncating to first order recovers the usual CI singles (CIS) equations in a noncanonical basis set.

5.2.5 Dressed TDDFT

Dressed TDDFT (D-TDDFT) is a way to mix conventional adiabatic TDDFT with a non-adiabatic correction derived from many-body theory. Now that we have all the pieces, let us assemble a first-principles PP version of D-TDDFT.

The first step along the way is to understand how to avoid double counting of correlation effects. That is we must generalize the Maitra, Zhang, Cave, and Burke (MZCB) *ansatz* to more than one doubly-excited state. A perturbative generalization of the formula (5.23) involving a single doubly-excited state to the situation involving a manifold of doubly-excited states is,

$$\omega = \omega_S + \sum_{D'} \frac{x_{D'}^2}{\omega - \omega_{D'}}, \tag{5.150}$$

This separates into the static part,

$$\omega_{AA} = \omega_S - \sum_{D'} \frac{x_{D'}^2}{\omega_{D'}}, \tag{5.151}$$

and a remaining dynamic part,

$$\omega_{NA} = \sum_{D'} \left(\frac{\omega}{\omega_{D'}} \right) \frac{x_{D'}^2}{\omega - \omega_{D'}}. \tag{5.152}$$

Since adiabatic TDDFT must agree with static DFT response theory, we can easily identify ω_{AA} as the part described by conventional adiabatic TDDFT.

In order to treat the remaining part, we restrict ourselves to the situation that the excitation energies are well separated with a particular $\omega_D \approx \omega_S$. In this case, we can write that,

$$\begin{aligned}\omega_{NA} &\approx \left(\frac{\omega}{\omega_D}\right) \frac{x_D^2}{\omega - \omega_D} \\ &\approx \frac{x_D^2}{\omega - \omega_D}.\end{aligned}\tag{5.153}$$

This later formula is the dressing to be obtained from PP theory. Note that it assumes that the true excitation energy, $\omega \approx \omega_D$.

Equation (5.146) is of just the right form to apply this type of *ansatz*. Assuming just one (or at most a few) double excitations, our MZCB-like PP *ansatz* is the pseudo-eigenvalue equation,

$$\left[\mathbf{A}_{1,1} + \mathbf{A}_{1,2} (\omega \mathbf{1}_{2,2} - \mathbf{A}_{2,2})^{-1} \mathbf{A}_{2,1} \right] \mathbf{C}_1 = \omega \mathbf{C}_1,\tag{5.154}$$

with

$$\begin{aligned}(\mathbf{A}_{1,1})_{kc,ia} &= \delta_{i,k} \delta_{a,c} \epsilon_{a,i} + (kc|f_{Hxc}^{AA}|ia) \\ (\mathbf{A}_{2,1}^{(1)})_{kc,jbia} &= -\delta_{i,k} (bc||aj) + \delta_{j,k} (bc||ai) \\ &\quad - \delta_{b,c} (ai||kj) + \delta_{k,j} (bi||kj) \\ (\mathbf{A}_{2,2}^{(2)})_{ldkc,jbia} &= \delta_{i,k} \delta_{c,a} \delta_{d,b} \epsilon_{ab,ij}.\end{aligned}\tag{5.155}$$

Equation (5.154) is equivalent to the computationally more convenient form,

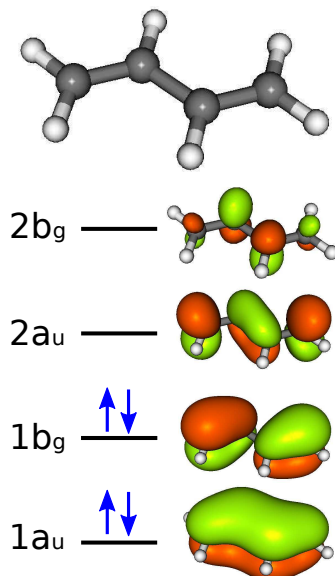
$$\begin{bmatrix} \mathbf{A}_{1,1} & \mathbf{A}_{1,2} \\ \mathbf{A}_{2,1} & \mathbf{A}_{2,2} \end{bmatrix} \begin{pmatrix} \mathbf{C}_1 \\ \mathbf{C}_2 \end{pmatrix} = \omega \begin{pmatrix} \mathbf{C}_1 \\ \mathbf{C}_2 \end{pmatrix},\tag{5.156}$$

which is what we use in practice.

The restriction to one (or at most a few energetically similar) double excitations can be justified on two grounds. First, adiabatic TDDFT already contains electron correlation effects and we wish to avoid double counting. Second, the Gonze-Scheffler relation tells us that the localizer transforms diagonal *ia*-matrix elements of the spatially-local kernel, $f_{Hxc}(1, 2; \omega)$, into matrix elements of the spatially nonlocal operator, $K_{Hxc}(1, 1'; 2, 2'; \omega)$, at frequencies, $\omega = \epsilon_{a,i}$. Were we to consider an increasingly large number of 2h2p-excitations in our theory, there may come a point where it will be necessary to include the localizer when interfacing PP and TDDFT formulae. For the moment we do not do this in any of the calculations presented in this paper. It may be worth emphasizing that the localizer is unnecessary when carrying out PP based upon the Kohn-Sham orbital hamiltonian as zero-order estimate, but is expected to become necessary at some point when interfacing the spatially-local TDDFT and spatially nonlocal PP formalisms.

The formulae (5.155) are highly reminiscent of Casida's earlier work on a PP correction to adiabatic TDDFT. These formulae are just the TDA form of the order-consistent development

Figure 5.5 Frontier molecular orbitals of butadiene calculated using the local density approximation.



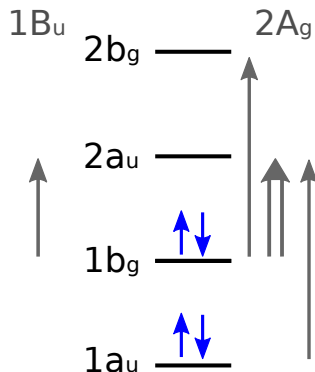
of Eq. (3.9) in Ref. [149]. Comparing with Eqs. (5.148) and (5.149), we see that the block of 1h1p-excitations is given by conventional adiabatic TDDFT while the missing terms involving 2h2p-excitations are taken over from SOPPA/KS+TDA theory. We refer to them here by the acronym D-TDDFT TDA. It is troubling that the zero-order estimate of the double excitation energy is just given by KS orbital energy differences in this order-consistent theory. These may or may not be accurate enough in practice, so we also introduce the notion of extended dressed (ED) TDDFT in which,

$$\begin{aligned} \left(\mathbf{A}_{2,2}^{(1)} \right)_{ldkc,jbia} &= \langle \Psi_{KS} | ck^\dagger dl^\dagger \hat{H} b^\dagger ja^\dagger i | \Psi_{KS} \rangle \\ &\quad - \langle \Psi_{KS} | \hat{H} | \Psi_{KS} \rangle. \end{aligned} \quad (5.157)$$

An explicit expression is straightforward to work out with Wick's theorem but is long and so will not be given here [see Eqs. (49) and (50) of Ref. [45]].

Let us now turn to a specific example, namely that of butadiene ($\text{CH}_2=\text{CH}-\text{CH}=\text{CH}_2$), whose excitation spectra have been extensively studied in the past (see e.g., Ref. [256] and references therein). Let us examine the electronic structure of this molecule in a qualitative manner before embarking on a quantitative study. Figure 5.5 shows the frontier molecular orbitals (MOs) of this molecule, easily obtained by qualitative arguments familiar to most chemists. Several possible excitations may be constructed from these MOs with the dominant ones shown in Fig. 5.6. We

Figure 5.6 Dominant contributions to the low-lying excited states in *trans*-butadiene. **Huix-Rotllant and Casida: dressed TDDFT**



can anticipate a fairly pure one-hole one-particle (1h1p)-excitation of 1^1B_u symmetry. However excitations of 1^1A_g symmetry are more complicated, since it is possible to construct two energetic nearly degenerate 1h1p-excitations from the HOMO \rightarrow LUMO+1 and HOMO-1 \rightarrow LUMO transitions. (HOMO and LUMO are standard acronyms respectively for “highest occupied molecular orbital” and “lowest unoccupied molecular orbital.”) These will interact to form symmetric and antisymmetric combinations, one of which may strongly mix with the HOMO \rightarrow LUMO double (2h2p) excitation. The bright 1^1B_u state is experimentally relatively easy to locate with absorption spectroscopy while the location of the spectroscopically dark 2^1A_g is much harder to locate experimentally. Recent experiments seem to indicate that the 2^1A_g state is slightly lower in energy than the 1^1B_u state, [256] while theory is divided as to whether the 2^1A_g state is slightly higher [257] or slightly lower [256] than the 1^1B_u state (Table 5.1). Probably at this point we should only conclude that the two states are energetically quasidegenerate.

Butadiene has been treated at least twice in the past using D-TDDFT. [44, 150] The earliest treatment was by Cave, Zhang, Maitra, and Burke [44]. They first carried out TDDFT calculations to find the singles-excitation energy, ω_S , and the corresponding single-excitation configurations. They then added an extended dressed term into both the \mathbf{A} and \mathbf{B} matrices and solved the full and TDA dressed TDDFT problem in a noniterative perturbation-like manner using electron repulsion integrals constructed with Hartree-Fock orbitals. Note that their double-excitation energy, ω_D , is calculated not in terms of orbital energy differences but in terms of the difference between the Hartree-Fock ground state and the energy of a doubly-excited Hartree-Fock determinant, similar to our ED-TDDFT theory. Their results are shown in Table 5.1. While the TDPBE0 1^1B_u excitation energy is reasonable, the TDPBE0 2^1A_g excitation energy is much too high compared with the 1^1B_u excitation energy. Their dressed TDDFT gives a 2^1A_g energy similar to the 1^1B_u excitation energy. Mazur and Włocarczyk [150] have recently improved on the work of Cave *et al.* by calculating their electron repulsion integrals from Kohn-Sham, rather than Hartree-Fock, orbitals and by carrying out an iterative solution of an improved form of Eq. (5.23). They obtained results remarkably similar to those of Cave *et al.* Note that none

Table 5.1 Butadiene vertical excitation energies (eV).

	2^1A_g	1^1B_u
Present Work ¹		
TDLDA TDA	6.42	6.38
D-TDLDA TDA	3.91	6.38
ED-TDLDA TDA	6.02	6.38
10-ED-TDLDA TDA	6.253	6.249
Cave <i>et al.</i> ²		
TDB3LYP	7.02	
TDPBE0	7.22	5.98
D-TDPBE0	5.93	
D-TDPBE0 TDA	6.28	
Mazur and Włodarczyk ³		
TDB3LYP TDA	6.56	6.02
TDPBE0 TDA	6.77	6.13
D-TDB3LYP TDA	6.06	6.02
D-TDPBE0 TDA	6.34	6.13
Reference Values		
SOPPA ¹	7.49	6.00
ADC(2)-s ⁴	8.34	7.09
ADC(2)-x ⁴	5.19	6.69
CASPT2 ⁵	6.27	6.23
Best Estimate ⁶	6.55	6.18
Experiment ⁷	5.4-5.8	5.91

¹ Present work: 6-311G(d,p) basis.² Calculations of Cave, Zhang, Maitra, and Burke from Ref. [44]: 6-311G(d,p) basis.³ Calculations of Mazur and Włodarczyk from Ref. [150]: 6-311++G** basis.⁴ Strict (s) and extended (x) ADC(2)/6-31G calculations from Table 2 of Ref. [258].⁵ From Ref. [259].⁶ From Ref. [257].⁷ Values taken from Ref. [256]. See also the discussion of these experimental values in that reference.

of these dressed calculations affects the energy of the 1^1B_u state which belongs to a different irreducible representation of the molecular point group.

We have carried out D-TDDFT calculations with our PP formalism using the Grenoble development version of the DEMON2K program [205]. The implementation of TDDFT in DEMON2K has already been described [207]. The implementation of D-TDDFT and extensive tests of this option will be described elsewhere. [260] Suffice it to say that calculations were carried out at the experimental geometry using the same orbital basis set as in used by Cave, Zhang, Maitra, and Burke [44]. Our calculations are limited to the local density approximation (LDA) rather than the hybrid functionals (PBE0 and B3LYP) used in the previously mentioned work. Our results are collected in Table 5.1 and compared against other D-TDDFT calculations and benchmark values from the literature. We confirm the previous result of Hsu, Hirata, and Head-Gordon [261] that non-hybrid functionals give reasonable agreement with benchmark values for the 2^1A_g excitation energy. As seen in the table, hybrid functionals are even worse in this respect. Including the $1b_g^2 \rightarrow 2a_u^2$ double excitation at the D-TDLDA TDA level of theory lowers the energy of the 2^1A_g state by a very large 2.5 eV. This is because the simple orbital energy difference of the 2h2p excitation energy at 8.01 eV is much too close to the 2^1A_g excitation energy (6.42 eV) obtained without the doubles correction. Using the extended doubles formula (5.157) with a 2h2p excitation energy of 23.84 eV leads to a much more reasonable lowering of the TDLDA TDA energy by 0.4 eV. As explained above, the energy of the 1^1B_u state remains unchanged by the introduction of a double excitation of $1A_g$ symmetry.

It should be emphasized that our implementation of ED-TDDFT is a still more general implementation of the previous implementation of dressed TDDFT by Mazur and Włóarczyk [150] which was already an improvement on the work of Cave *et al.* [44] Not only do we obtain the equivalent of the iterative answer with a noniterative algorithm [compare Eqs. (5.154) and (5.156)] but we are able to include a few additional double excitations. (Moreover we have given the formal framework for further systematic improvements of our theory.) Thus we thought it interesting to go a little further in this preliminary study by including the first 10 doubly-excited states in the ED theory (without including the localizer). This is the calculation denoted 10-ED-TDLDA TDA in Table 5.1. This introduces some double excitations of $1B_u$ symmetry. While some double counting of correlation is inevitable, 10 double excitations is still a very small number compared to the number usually used to describe dynamic correlation. Both the 2^1A_g and 1^1B_u states have shifted to nearly the same value, in better agreement with reference values.

Since our version of D-TDDFT is based upon SOPPA and strict ADC(2) formulae, it may be worth comparing against these values. Table 5.1 shows the results of a SOPPA calculation that we obtained with the DALTON code [262] using the same basis and geometries as our D-TDDFT calculations. The 1^1B_u SOPPA excitation energy is similar to that obtained with the TDLDA TDA and D-TDLDA TDA. However, unlike in our D-TDLDA TDA calculation, the SOPPA 2^1A_g excitation energy remains higher in energy than the 1^1B_u excitation energy. This is consistent with the much larger double excitation orbital energy difference when Hartree-Fock, rather than Kohn-Sham, orbital energies are used. We also give strict [ADC(2)-s] and extended [ADC(2)-x] ADC(2) from Ref. [258]. The ADC(2)-s result should be comparable to our SOPPA result but overestimates our result for the excitation energies of both states because the ADC(2)-s result was calculated with a less extensive basis set. The ADC(2)-x method is to the ADC(2)-s method what our ED-TDLDA TDA method is to our D-TDLDA TDA method. Interestingly, the ED-TDLDA TDA 2^1A_g energy is greater than the D-TDLDA TDA 2^1A_g energy while the

ADC(2)-x 2^1A_g energy is smaller than the ADC(2)-s excitation energy. This is consistent with the correction to the simple orbital energy difference estimate being very different for the ED-TDLDA TDA and ADC(2)-x schemes. In both cases the extended method brings the calculated results closer to experiment.

In finishing this section, it is best to recall that the results given here are only indicative. A much more thorough study will be reported elsewhere. [260] In particular, it should be kept in mind that the 2^1A_g and 1^1B_u states lie above the TDLDA ionization threshold which is artificially low (5.92 eV). [25] Nevertheless the present results give a first indication that our method is up and running and ready for more extensive testing. A particularly interesting question will be to what extent our mixture of TDDFT and PP methods will break symmetry-imposed state degeneracies.

5.2.6 Conclusion

This article has presented a detailed discussion of how the frequency-dependent spatially-local xc-kernel of TDDFT may, in principle, be obtained from the corresponding spatially-nonlocal quantity in PP theory in such a way as to take full account of the interaction between any number of single- and higher-order excitations. This may be termed *ab initio* TDDFT. [226] Because we have made extensive connections with other similar work in the literature, it seems best to conclude by emphasizing what is new in the present work.

The first thing that is new is that we have clarified the relation between the PP work of Casida [149] and similar work within the solid state physics community based upon the Bethe-Salpeter equation (BSE) [46, 119, 120, 141, 233–235]. This is important because different approximations have been developed within the PP approach in chemical physics for molecules than those developed within the BSE approach for solids, yet there is a great deal of interest in these two communities in sharing information with the aim of eventually developing a physical approximations applicable, say, at the nanoscale interface between molecules and solids.

The second thing that is new in the present work is that we have corrected the previous PP work of Casida [149] to include the effect of spatial localization. Within the Born approximation, the resultant expression for the xc-kernel factors into a product of dynamic localizers and the nonlocal PP analogue of the xc-kernel. This localizer arises naturally in OEP and TD-OEP methods. Interestingly the dynamic localizer represents the fact that spatial localization necessarily implies an additional frequency dependence (delocalization in time). Near a pole, when the excitations are well-separated (which is normally what happens for molecules), we obtain a particularly easy demonstration of the Gonze-Scheffler relation [142] which is, among other things, a key ingredient in a correct treatment of charge-transfer excitations in TDDFT. [27] With a future implementation in mind and explicit exploration of the properties of the localizer, we also briefly discussed finite-basis representations of the localizer in an appendix.

The third thing that is new here is that we have developed explicit formulae similar to SOPPA or ADC(2) formulae but based upon a Kohn-Sham zero-order hamiltonian. This involves resumming more than one hundred correction terms but results in compact formulae in the end. We have shown that previous EXX formulae reported in the literature are confirmed exactly by truncating our formulae to lower order.

The fourth thing that is new is that we have discussed and given what we believe to be an improved formulation of dressed TDDFT. A preliminary calculation on butadiene confirms that it is indeed necessary to go beyond a zero-order description of double excitations to at least a first-order description. The results confirm that the method is correctly implemented and are sufficiently encouraging that we are in the process of carrying out a benchmark study of this approach on a much more extensive set of molecules. [260]

Finally we have presented all the pieces in this paper to go from *ab initio* PP theory to extract the corresponding frequency-dependent xc-kernel of TDDFT. The formalism itself offers insight into the analytic structure of this xc-kernel and why dressed TDDFT works and eventually why it might fail and could be further improved. Actual calculations of the *ab initio* xc-kernel can be expected to lead to additional insight, but the necessary code will take some time to put into place.

5.2.7 Acknowledgements

We thank Andrei Ipatov, Valerio Olevano, Giovanni Onida, Lucia Reining, Pina Romaniello, Angel Rubio, Davide Sangalli, Jochen Schirmer, and Eric Shirley for useful discussions. M. H. R. would like to acknowledge an *Allocation de Recherche* from the French Ministry of Education. This work has been carried out in the context of the French Rhône-Alpes *Réseau thématique de recherche avancée (RTRA): Nanosciences aux limites de la nanoélectronique* and the Rhône-Alpes Associated Node of the European Theoretical Spectroscopy Facility (ETSF).

5.2.8 Appendix A: Collapse, Expansion, and Localization Operators

A problem which shares many aspects in common with the present work is that of finding the optimized effective potential (OEP). [97, 263] The OEP is the local potential whose orbitals minimize the Hartree-Fock energy expression, and is, up to a linear response approximation, identical to the exact exchange-only Kohn-Sham potential, v_x , whose functional derivative is the exact exchange-only kernel, f_x . In using Harriman's collapse operator in the present work, we have chosen to follow Hamel, Casida, and Salahub who pointed out that this operator allows a particularly elegant formulation of the OEP problem. [244] The notion of a collapse operator emerges naturally in this context. This appendix introduces the notion of collapse, expansion, and collapse operators in the static case. Some exact and approximate properties are also reviewed.

Harriman considered the relation between the space of kernels of operators and the space of functions. [264, 265] In order to maintain consistency with the rest of this paper, we will generalize Harriman's notion from space-only to space and spin coordinates. Then the collapse operator is defined by,

$$\hat{Y}_{\Sigma_x}(1, 2) = \Sigma_x(1, 1). \quad (5.158)$$

The adjoint of the collapse operator is the so-called expansion operator,

$$\hat{\Upsilon}^\dagger v_x(1) = v_x(1)\delta(1-2). \quad (5.159)$$

The notions are general even if the above two equations suggest that we apply the collapse operator to the kernel of the exchange-only self-energy (i.e., the Hartree-Fock exchange operator) and that the expansion operator be applied to the exchange-only potential, which is our intention.

The exchange-only OEP problem may be written as,

$$\left(\hat{h}_H + v_x\right) \psi_r^{OEP}(\mathbf{x}) = \epsilon_r^{OEP} \psi_r^{OEP}(\mathbf{x}), \quad (5.160)$$

which resembles the Hartree-Fock problem,

$$\left(\hat{h}_H + \hat{\Sigma}_x\right) \psi_r^{HF}(\mathbf{x}) = \epsilon_r^{HF} \psi_r^{HF}(\mathbf{x}). \quad (5.161)$$

It turns out that the answer to the OEP problem is to require that the potential v_x be chosen so that the perturbation transforming the OEP problem into the Hartree-Fock problem makes the linear response of the density zero. [97,263] Since the definition of the exchange-only Kohn-Sham potential is that it produce the Hartree-Fock density, it is easy to see that the OEP v_x is simply a linear response approximation to the exact Kohn-Sham v_x .

We can express this linear response condition very elegantly using the Harriman operators as,

$$\mathbf{0} = \Upsilon \Pi_s (\Sigma_x - \Upsilon^\dagger v_x). \quad (5.162)$$

In order to keep the notation compact by suppressing integrations, we have introduced a matrix notation: The operators Υ and the OEP (Kohn-Sham) independent particle response function (retarded form of the polarization propagator), Π_s , are represented as matrices. The operators Σ_x and v_x are represented as column vectors. Thus Eq. (5.162) becomes,

$$\Upsilon \Pi_s \Upsilon^\dagger v_x = \Upsilon \Pi_s \Sigma_x, \quad (5.163)$$

which may be recognized as a weighted least square fit of $\Upsilon^\dagger v_x$ to Σ_x . It may be solved,

$$v_x = \Lambda_s \Sigma_x, \quad (5.164)$$

where,

$$\Lambda_s = (\Upsilon \Pi_s \Upsilon^\dagger)^{-1} \Upsilon \Pi_s, \quad (5.165)$$

is the localizer. (In particular it is the single-particle localizer because it depends upon the single particle response function Π_s .) Note that this only makes sense if care is taken to eliminate the null space of $\Upsilon \Pi_s \Upsilon^\dagger$ before taking the inverse (i.e., singular value decomposition.)

One of the strong points of this formulation of the OEP problem is that it lends itself to a spectral space representation in terms of orbital and auxiliary basis sets. [244] However solving the OEP equation in this manner is not without its pitfalls. Hamel, Casida, and Salahub emphasized that,

“The v_x which emerges from finite basis OEP calculations is not strictly unique, though its matrix is uniquely defined up to an additive multiple of the matrix of the identity.” [244]

In fact, an improper balance between orbital and auxiliary basis sets can lead to unphysical wiggles in v_x . Staroverov, Scuseria, and Davidson have pointed out that an improper balance between the orbital and auxiliary basis sets can also lead to Hartree-Fock energies which are incorrectly below the true OEP energy. [266] Thus the orbital and auxiliary basis sets should be regarded not as independent but rather are coupled. Methods for avoiding this pitfall have been discussed in the recent literature [267–269] and some are described in the following paragraphs. However, for the purposes of the present work, we need only assume that the pitfall may be avoided using appropriately balanced basis sets.

One way to understand the localizer is to examine its static limit. There are several related approximate solutions to the static OEP equation [Eq. (5.163)]. We focus here on the Krieger-Li-Iafrate (KLI) approximation because of its physical transparency. However a drawback of the KLI approximation is lack of unitary invariance which may be removed by a suitable generalization giving what is variously known as the common energy denominator approximation (CEDA) [270], localized Hartree-Fock (LHF) [271], or effective local potential (ELP) method [267,268], depending upon who derived it.

Krieger, Li, and Iafrate [98,99] followed up on a footnote in Sharp and Horton’s seminal OEP paper. [263] Amazingly the resultant KLI expression works almost as well as the original OEP method. The trick is to recognize that the generalized susceptibility may be rewritten as,

$$\Pi_s(1, 2; 3, 4) = \sum_i \sum_{p \neq i}^{\text{occ}} \frac{\psi_i(1)\psi_p^*(2)\psi_i^*(3)\psi_p(4)}{\epsilon_{i,p}} + \sum_i \sum_{p \neq i}^{\text{occ}} \frac{\psi_p(1)\psi_i^*(2)\psi_p^*(3)\psi_i(4)}{\epsilon_{i,p}}, \quad (5.166)$$

because the terms where p corresponds to an occupied orbital all cancel each other. Now make use Unsöld’s approximation [272] in which we replace the excitation energies with a single average excitation energy,

$$\Pi_s(1, 2; 3, 4) = - \sum_i \sum_{p \neq i}^{\text{occ}} \frac{\psi_i(1)\psi_p^*(2)\psi_i^*(3)\psi_p(4)}{\Delta\epsilon} - \sum_i \sum_{p \neq i}^{\text{occ}} \frac{\psi_p(1)\psi_i^*(2)\psi_p^*(3)\psi_i(4)}{\Delta\epsilon}. \quad (5.167)$$

(Csizmadia and Sylvain gave evidence to suggest that

$$\frac{1}{\Delta\epsilon} = - \frac{1}{N_{\text{occ}}} \sum_i^{\text{occ}} \frac{1}{\epsilon_i}, \quad (5.168)$$

is a good choice when applying Unsöld’s approximation to the calculation of polarizabilities [273].) Using the completeness relation,

$$\sum_p \psi_p(1)\psi_p^*(2) = \delta(1-2), \quad (5.169)$$

then

$$\begin{aligned} \Pi_s(1, 2; 3, 4) = & -\frac{1}{\Delta\epsilon} (\gamma(1, 3)\delta(4-2) + \gamma(4, 2)\delta(1-3) \\ & - 2 \sum_i^{occ} \psi_i(1)\psi_i^*(2)\psi_i^*(3)\psi_i(4) \Big). \end{aligned} \quad (5.170)$$

Inserting into Eq. (5.163) and assuming real orbitals yields after a little algebra,

$$v_x^{KLI}(1) = \frac{\sum_i^{occ} \langle \psi_i | \hat{\Sigma}_x | \psi_i \rangle}{\rho(1)} + \frac{\sum_i^{occ} |\psi_i(1)|^2 \langle \psi_i | v_x^{KLI} - \hat{\Sigma}_x | \psi_i \rangle}{\rho(1)}. \quad (5.171)$$

Notice how $\Delta\epsilon$ has completely canceled out! The first of the two terms is the Slater potential, [274] while the second of the two terms is a “derivative discontinuity correction.”

The presence of the exchange potential on the right hand side of Eq. (5.171) shows the real complexity underlying the apparently simple equation (5.164). Nevertheless we have here an implicit approximate expression for the static localizer. A similar statement also holds for the CEDA (LHF, ELP) approximation.

5.2.9 Appendix B: Finite-Basis Representation of the Localization Operator

We discuss the problem of carrying out dynamic localization,

$$v(1, \omega) = \hat{\Lambda}(\omega)\Sigma(1, 2; \omega), \quad (5.172)$$

[e.g., Eq. (5.79)] in a finite basis representation. Such a computational approach is probably the most rigorous direct way to explore properties of the dynamic localizer.

In a typical finite basis method, v is expanded in a finite auxiliary basis set,

$$v(1; \omega) = \sum_I g_I(1) b_I(\omega). \quad (5.173)$$

It is evident that the g_I must be completely contained within the space of orbital products, otherwise erratic results will be obtained when expanding the orbital space. The implication is that, at a minimum, there is a double convergence problem. For each auxiliary basis set, it is necessary to expand the orbital basis set until convergence is reached. Then the auxiliary basis set can be expanded and convergence attained once again with respect to the orbital basis set. The reverse order (convergence of the auxiliary basis set before the orbital basis set) is not possible. This is at the heart of problems mentioned in Appendix 5.2.8. [266–269]

Nevertheless, with these difficulties in mind, let us make the expansion in the auxiliary basis set [Eq. (5.173)] and rewrite the localization equation as,

$$\sum_I X_{I,J}(\omega) b_J(\omega) = Y_I(\omega), \quad (5.174)$$

with

$$X_{I,J}(\omega) = \sum_i^{occ} \sum_a^{virt} \frac{\langle \psi_a | g_I | \psi_i \rangle \langle \psi_i | g_J | \psi_a \rangle}{\omega - \epsilon_{a,i}} - \sum_i^{occ} \sum_a^{virt} \frac{\langle \psi_i | g_I | \psi_a \rangle \langle \psi_a | g_J | \psi_i \rangle}{\omega + \epsilon_{a,i}}. \quad (5.175)$$

and

$$Y_I(\omega) = \sum_i^{occ} \sum_a^{virt} \frac{\langle \psi_a | g_I | \psi_i \rangle \langle \psi_i | \hat{\Sigma}(\omega) | \psi_a \rangle}{\omega - \epsilon_{a,i}} - \sum_i^{occ} \sum_a^{virt} \frac{\langle \psi_i | g_I | \psi_a \rangle \langle \psi_a | \hat{\Sigma}(\omega) | \psi_i \rangle}{\omega + \epsilon_{a,i}}. \quad (5.176)$$

[Here we are using the compact notation introduced in Eq. (5.7).] For real basis sets,

$$\begin{aligned} X_{I,J}(\omega) &= \sum_i^{occ} \sum_a^{virt} \left(\frac{2\epsilon_{a,i}}{\omega^2 - \epsilon_{a,i}^2} \right) \langle \psi_a | g_I | \psi_i \rangle \langle \psi_i | g_J | \psi_a \rangle \\ Y_I(\omega) &= \sum_i^{occ} \sum_a^{virt} \left(\frac{2\epsilon_{a,i}}{\omega^2 - \epsilon_{a,i}^2} \right) \langle \psi_a | g_I | \psi_i \rangle \langle \psi_i | \hat{\Sigma}(\omega) | \psi_a \rangle. \end{aligned} \quad (5.177)$$

The solution to the localization problem is,

$$\begin{aligned} v(1; \omega) &= \sum_J g_J(1) b_J(\omega) \\ &= \sum_{I,J} g_J(1) X_{J,I}^{-1} Y_I(\omega) \\ &= \sum_J g_J(1) \Lambda_{J,ia}(\omega) \langle \psi_i | \hat{\Sigma}(\omega) | \psi_a \rangle, \end{aligned} \quad (5.178)$$

with the localizer supermatrix given by,

$$\Lambda_{J,ia}(\omega) = \sum_I X_{J,I}^{-1}(\omega) \left(\frac{2\epsilon_{a,i} \langle \psi_a | g_I | \psi_i \rangle}{\omega^2 - \epsilon_{a,i}^2} \right). \quad (5.179)$$

Similar equations can be written down for the KLI and CEDA/LHF approximations but the critical product space is then that of products of occupied orbitals, $\psi_i \psi_j$, which seems to be somewhat easier to handle, to judge by the success of the ELP method [267, 268]. For example, if we make the CEDA/LHF approximation with the energy dependent $\Pi_s(\omega)$, then there will be a factor of $2\Delta\epsilon/[\omega^2 - (\Delta\epsilon)^2]$ which will cancel out and we will arrive back at the CEDA/LHF equations but this time keeping the frequency dependence in $v_x(\omega)$ and in $\Sigma(\omega)$,

$$v(1; \omega) = \frac{\sum_i^{occ} \langle \psi_i | \hat{\Sigma}(\omega) | \psi_i \rangle}{\rho(1)} + \frac{\sum_{i,j}^{occ} \psi_i^*(1) \langle \psi_i | v(\omega) - \hat{\Sigma}(\omega) | \psi_j \rangle \psi_j(1)}{\rho(1)}. \quad (5.180)$$

(This is a more general result than the KLI approximation described in Appendix 5.2.8. The KLI approximation is obtained when $i = j$ in the second sum.) The matrix equations are,

$$\begin{aligned}
\sum_J X_{I,J} b_J(\omega) &= Y_I(\omega) \\
X_{I,J} &= \sum_i^{occ} \langle \psi_i | g_I g_J | \psi_i \rangle - \sum_{i,j}^{occ} \langle \psi_i | g_I | \psi_j \rangle \langle \psi_j | g_J | \psi_i \rangle \\
Y_I(\omega) &= \sum_i^{occ} \langle \psi_i | g_I \hat{\Sigma}(\omega) | \psi_i \rangle - \sum_{i,j}^{occ} \langle \psi_i | g_I | \psi_j \rangle \langle \psi_j | \hat{\Sigma}(\omega) | \psi_i \rangle \\
b_J(\omega) &= \sum_I X_{J,I}^{-1} Y_I(\omega). \tag{5.181}
\end{aligned}$$

It is to be emphasized that the localizer is frequency independent in this approximation. Although this may seem like a great computational simplification, it is at the price that the Gonze-Scheffler relations [Eq. (5.87) and Eq. (5.88)] are no longer exactly satisfied.

A frequency-dependent CEDA has recently been introduced recently by Gritsenko and Baerends. [184]

5.2.10 Appendix C: Diagrammatic Rules

The representation of MBPT expansions in terms of diagrams is very convenient for book-keeping purposes. Indeed certain ideas such as the linked-cluster theorem [253] or the concept of a ladder approximation (see e.g., Ref. [16] p. 136) are most naturally expressed in terms of diagrams. Perhaps most importantly diagrams drawn according to systematic rules allow an easy way to check algebraic expressions. Several types of MBPT diagrams exist in the literature. These divide into four main classes which we call Feynman, Abrikosov, Goldstone, and Hugenholtz. Such diagrams can be distinguished by whether they are time-ordered (Goldstone and Hugenholtz) or not (Feynman and Abrikosov) and by whether they treat the electron repulsion interaction as a wavy or dotted line with an incoming and an outgoing arrow at each end (Feynman and Goldstone) or in a symmetrized way as a point with two incoming and two outgoing arrows (Abrikosov and Hugenholtz). These differences affect how they are to be translated into algebraic expressions as does the nature of the quantity being expanded (wave function, one-electron Green's function, self-energy, polarization propagator, etc.) Given this plethora of types of diagrams and the difficulty of finding a clear explanation of how to read polarization propagator diagrams, we have chosen to present an appendix summarizing how our diagrams should be translated into algebraic expressions. This is perhaps especially necessary because while the usual practice in the solid-state literature is to use time-unordered diagrams with electron repulsions represented as wavy or dotted lines (i.e., Feynman diagrams), while the usual practice in the quantum chemistry literature of using time-ordered diagrams with electron repulsions represented as points (i.e., Hugenholtz diagrams). Since we first derive algebraic expressions and then write the corresponding diagrams, rather than vice versa, we will content ourselves in this

Figure 5.7 Basic time-ordered finite basis set representation PP diagram.

$$\Pi_{sr,qp}(t, t') = \theta(t - t') \begin{array}{c} \text{r} \quad \text{s} \\ \vdots \quad \vdots \\ \downarrow \quad \uparrow \\ \text{p} \quad \text{q} \end{array} + \theta(t' - t) \begin{array}{c} \text{p} \quad \text{q} \\ \vdots \quad \vdots \\ \downarrow \quad \uparrow \\ \text{r} \quad \text{s} \end{array}$$

appendix on how to translate diagrams into algebraic expressions, rather than upon how to generate complete non-redundant sets of diagrams. We will develop the rules gradually, including examples along the way.

The PP expressed in an orbital basis is,

$$\Pi(1, 2, 3, 4; t - t') = \sum_{pqrs} \Pi_{sr,qp}(t - t') \psi_r(1) \psi_s^*(2) \psi_q^*(3) \psi_p(4), \quad (5.182)$$

where,

$$\begin{aligned} \Pi_{sr,qp}(t - t') = & -i\theta(t - t') \langle 0 | \hat{r}_H^\dagger(t) \hat{s}_H(t) \hat{q}_H^\dagger(t') \hat{p}_H(t') | 0 \rangle \\ & - i\theta(t' - t) \langle 0 | \hat{q}_H^\dagger(t') \hat{p}_H(t') \hat{r}_H^\dagger(t) \hat{s}_H(t) | 0 \rangle. \end{aligned} \quad (5.183)$$

This makes it clear that the PP is a two time particle-hole propagator which either propagates forward in time or backward in time. To represent it we introduce the following rules:

- (1) Time increases vertically from bottom to top. This is in contrast to a common convention in the solid-state literature where time increases horizontally from right to left.
- (2) A PP is a two time quantity. Each of these two times is indicated by a horizontal dotted line. This is one type of “event” (representing the creation/destruction of an excitation).
- (3) Time-ordered diagrams use directed lines (arrows). Down-going arrows correspond to holes running backward in time, that is, to occupied orbitals. Up-going arrows correspond to particles running forward in time, that is, unoccupied orbitals.

At this point, the PP diagrams look something like Fig. 5.7. Fourier transforming leads us to the representation shown in Fig. 5.8. An additional rule has been introduced:

- (4) A downward ω arrow on the left indicates forward ph-propagation. An upward ω arrow on the right indicates downward ph-propagation.

Diagrams for the corresponding position space representation are shown in Fig. 5.9. Usually the labels (p , q , r , and s or 1, 2, 3, and 4) are suppressed. If the ω arrows are also suppressed then there is no information about time-ordering and both diagrams may be then written as a single time-unordered diagram as in Fig. 5.10. Typical Feynman diagrams are unordered in time.

Perturbation theory introduces certain denominators in the algebraic expressions corresponding to the diagrams. These may be represented as cuts between events.

Figure 5.8 Basic frequency and finite basis set representation PP diagram.

$$\Pi_{sr,qp}(\omega) = \begin{array}{c} r \quad s \\ \vdots \quad \vdots \\ \downarrow \quad \downarrow \\ \omega \\ \uparrow \quad \uparrow \\ p \quad q \end{array} + \begin{array}{c} p \quad q \\ \vdots \quad \vdots \\ \downarrow \quad \downarrow \\ \omega \\ \uparrow \quad \uparrow \\ r \quad s \end{array}$$

Figure 5.9 Basic frequency and real space representation PP diagram.

$$\Pi(1, 2; 3, 4; \omega) = \begin{array}{c} 1 \quad 2 \\ \vdots \quad \vdots \\ \downarrow \quad \downarrow \\ \omega \\ \uparrow \quad \uparrow \\ 4 \quad 3 \end{array} + \begin{array}{c} 4 \quad 3 \\ \vdots \quad \vdots \\ \downarrow \quad \downarrow \\ \omega \\ \uparrow \quad \uparrow \\ 1 \quad 2 \end{array}$$

Figure 5.10 Time-unordered representation PP diagram.

$$\Pi(\omega) = \begin{array}{c} \vdots \quad \vdots \\ \downarrow \quad \downarrow \\ \omega \\ \uparrow \quad \uparrow \\ \vdots \quad \vdots \end{array}$$

Figure 5.11 Zero-order PP diagrams.

$$\Pi_{sr,qp}(\omega) = i \left[\begin{array}{c} \text{---} \\ \downarrow \\ \text{---} \\ \uparrow \\ \text{---} \end{array} \right] \omega \text{---} a + i \left[\begin{array}{c} \text{---} \\ \uparrow \\ \text{---} \\ \downarrow \\ \text{---} \end{array} \right] \omega \text{---} a$$

- (5) Each horizontal cut between events contributes a factor $(\pm\omega + \sum_p \epsilon_p - \sum_h \epsilon_h)^{-1}$, where \sum_p (\sum_h) stands for the sum over all particle (hole) lines that are cut. The omega line only appears in the sum if it is also cut. It enters with a + sign if it is directed upwards and with a – sign if it is directed downwards.
- (6) There is also an overall sign given by the formula $(-1)^{h+l}$, where h is the number of hole lines and l is the number of closed loops, including the horizontal dotted event lines but ignoring the ω lines.

Diagrams are shown for the independent particle approximation in Fig. 5.11. The first diagram reads,

$$\Pi_{ai,ai}(\omega) = \frac{1}{\omega + \epsilon_i - \epsilon_a}. \quad (5.184)$$

The second diagram reads,

$$\Pi_{ia,ia}(\omega) = \frac{1}{-\omega + \epsilon_i - \epsilon_a} = \frac{-1}{\omega + \epsilon_a - \epsilon_i}. \quad (5.185)$$

These two equations are often condensed in the literature as,

$$\Pi_{pq,rs}(\omega) = \delta_{p,r} \delta_{q,s} \frac{n_q - n_p}{\omega + \epsilon_q - \epsilon_p}. \quad (5.186)$$

Let us now introduce one-electron perturbations in the form of M circles.

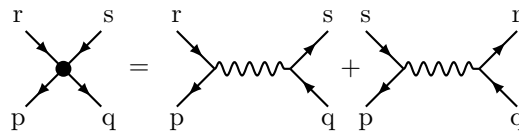
- (7) Each M circle in a diagram contributes a factor of $\langle p | \hat{M}_{xc} | q \rangle$, where p is an incoming arrow and q is an outgoing arrow. For example, the term corresponding to Fig. 5.3 (d) contains a factor of $\langle a | \hat{M}_{xc} | c \rangle$, while the term corresponding to Fig. 5.3 (j) contains a factor of $\langle k | \hat{M}_{xc} | i \rangle$. This is a second type of “event” (representing “collision” with the quantity M_{xc}).

For example, the term corresponding to Fig. 5.3 (b) is,

$$\Pi_{ck,cb}(\omega) = \sum \frac{\langle k | \hat{M}_{xc} | b \rangle}{(\omega - \epsilon_k + \epsilon_c)(\epsilon_k - \epsilon_b)}. \quad (5.187)$$

This brings us to the slightly more difficult treatment of electron repulsions.

- (6) When electron repulsion integrals are represented by dotted lines (Feynman and Goldstone diagrams), each end of the line corresponds to the labels corresponding to the same spatial point. The dotted line representation may be condensed into points (Abrikosov and Hugen-

Figure 5.12 Electron repulsion integral diagrams.

- holtz diagrams) as in Fig. 5.12. A point with two incoming arrows, labeled p and q , and two outgoing arrows, labeled r and s contributes a factor of $(pq||rs) = (pr|f_H|qs) - (ps|f_H|qr)$.
- (7) To determine the number of loops and hence the overall sign of a diagram in which electron repulsion integrals are expanded as dots, then write each dot as a dotted line (it does not matter which one of the two in Fig. 5.12 is chosen) and apply rule (6). The order of indices in each integral $(pq||rs)$ should correspond to the expanded diagrams. (When Goldstone diagrams are interpreted in this way, we call them Brandow diagrams.)
- (8) An additional factor of $1/2$ must be added for each pair of equivalent lines. These are directed lines whose interchange, in the absence of further labeling, leaves the Hugenholtz diagram unchanged.

For example, the term corresponding to Fig. 5.3 (f) is,

$$\begin{aligned} \Pi_{ck,ai}(\omega) &= -\frac{(ka||ic)}{(-\omega + \epsilon_k - \epsilon_c)(-\omega + \epsilon_i - \epsilon_a)} \\ &= \frac{(ak||ic)}{(-\omega + \epsilon_k - \epsilon_c)(-\omega + \epsilon_i - \epsilon_a)}. \end{aligned} \quad (5.188)$$

Additional information about Hugenholtz and other diagrams may be found, for example, in Ref. [275].

5.3 Supporting Material

Supporting Material for the Article, “Formal Foundations of Dressed Time-Dependent Density-Functional Theory for Many-Electron Excitations”

Miquel Huix-Rotllant and Mark E. Casida[†]

*Laboratoire de Chimie Théorique,
Département de Chimie Moléculaire (DCM, UMR CNRS/UJF 5250),
Institut de Chimie Moléculaire de Grenoble (ICMG, FR2607),
Université Joseph Fourier (Grenoble I),
301 rue de la Chimie, BP 53,
F-38041 Grenoble Cedex 9, France*

We seek an order-by-order expansion of the polarization propagator (PP),

$$\begin{aligned}
- \Pi_{sr,qp}(\omega) &= [(\hat{p}^\dagger \hat{q} | \mathbf{T}_1^\dagger) - (\hat{p}^\dagger \hat{q} | \mathbf{T}_{2+}^\dagger) \mathbf{\Gamma}_{2+,2+}^{-1}(\omega) \mathbf{\Gamma}_{2+,1}] \\
&\quad \mathbf{P}^{-1}(\omega) [(\mathbf{T}_1^\dagger | \hat{r}^\dagger \hat{s}) - \mathbf{\Gamma}_{1,2+} \mathbf{\Gamma}_{2+,2+}^{-1}(\omega) (\mathbf{T}_{2+}^\dagger | \hat{r}^\dagger \hat{s})] \\
&\quad + (\hat{p}^\dagger \hat{q} | \mathbf{T}_{2+}^\dagger) \mathbf{\Gamma}_{2+,2+}^{-1}(\omega) (\mathbf{T}_{2+}^\dagger | \hat{r}^\dagger \hat{s}), \tag{5.189}
\end{aligned}$$

where,

$$\mathbf{P}(\omega) = \mathbf{\Gamma}_{1,1}(\omega) - \mathbf{\Gamma}_{1,2+} \mathbf{\Gamma}_{2+,2+}^{-1}(\omega) \mathbf{\Gamma}_{2+,1}. \tag{5.190}$$

That is, we want explicit forms for the lowest orders in the expansion,

$$\begin{aligned}
[\mathbf{\Pi}_s(\omega) - \mathbf{\Pi}(\omega)]_{rs,qp}^{(0+1+\dots+n)} &= \\
&\quad \sum_{k=0}^n \sum_{i=0}^k \sum_{j=0}^{k-i} (\hat{p}^\dagger \hat{q} | \mathbf{T}_1^\dagger)^{(i)} \mathbf{P}^{(j),-1}(\omega) (\mathbf{T}_1^\dagger | \hat{r}^\dagger \hat{s})^{(k-i-j)}, \tag{5.191}
\end{aligned}$$

Following the procedure described in the main article gives the first-order contributions,

$$- \Pi_{sr,qp}^{(1)}(\omega) = (\hat{p}^\dagger \hat{q} | \mathbf{T}_1^\dagger)^{(0)} \mathbf{\Gamma}_{1,1}^{(1),-1}(\omega) (\mathbf{T}_1^\dagger | \hat{r}^\dagger \hat{s})^{(0)} \tag{5.192}$$

$$+ (\hat{p}^\dagger \hat{q} | \mathbf{T}_1^\dagger)^{(1)} \mathbf{\Gamma}_{1,1}^{(0),-1}(\omega) (\mathbf{T}_1^\dagger | \hat{r}^\dagger \hat{s})^{(0)} \tag{5.193}$$

$$+ (\hat{p}^\dagger \hat{q} | \mathbf{T}_1^\dagger)^{(0)} \mathbf{\Gamma}_{1,1}^{(0),-1}(\omega) (\mathbf{T}_1^\dagger | \hat{r}^\dagger \hat{s})^{(1)}. \tag{5.194}$$

The corresponding first-order diagrams are shown in Fig. 3 of the main article [diagrams (a-f) refer to the term (5.193), diagrams (g-j) refer to the term (5.194), and diagrams (k-n) refer to the term (5.193)]. The second-order contributions are

$$- \Pi_{sr,qp}^{(2)}(\omega) = (\hat{p}^\dagger \hat{q} | \mathbf{T}_1^\dagger)^{(0)} \mathbf{\Gamma}_{1,1}^{(2),-1}(\omega) (\mathbf{T}_1^\dagger | \hat{r}^\dagger \hat{s})^{(0)} \tag{5.195}$$

$$+ (\hat{p}^\dagger \hat{q} | \mathbf{T}_1^\dagger)^{(2)} \mathbf{\Gamma}_{1,1}^{(0),-1}(\omega) (\mathbf{T}_1^\dagger | \hat{r}^\dagger \hat{s})^{(0)} \tag{5.196}$$

$$+ (\hat{p}^\dagger \hat{q} | \mathbf{T}_1^\dagger)^{(0)} \mathbf{\Gamma}_{1,1}^{(0),-1}(\omega) (\mathbf{T}_1^\dagger | \hat{r}^\dagger \hat{s})^{(2)} \tag{5.197}$$

$$+ (\hat{p}^\dagger \hat{q} | \mathbf{T}_1^\dagger)^{(1)} \mathbf{\Gamma}_{1,1}^{(0),-1}(\omega) (\mathbf{T}_1^\dagger | \hat{r}^\dagger \hat{s})^{(1)} \tag{5.198}$$

$$+ (\hat{p}^\dagger \hat{q} | \mathbf{T}_1^\dagger)^{(1)} \mathbf{\Gamma}_{1,1}^{(1),-1}(\omega) (\mathbf{T}_1^\dagger | \hat{r}^\dagger \hat{s})^{(0)} \tag{5.199}$$

$$+ (\hat{p}^\dagger \hat{q} | \mathbf{T}_1^\dagger)^{(0)} \mathbf{\Gamma}_{1,1}^{(1),-1}(\omega) (\mathbf{T}_1^\dagger | \hat{r}^\dagger \hat{s})^{(1)} \tag{5.200}$$

$$+ (\hat{p}^\dagger \hat{q} | \mathbf{T}_1^\dagger)^{(0)} \mathbf{\Gamma}_{1,1}^{(0),-1}(\omega) \mathbf{\Gamma}_{1,2}^{(1)} \mathbf{\Gamma}_{2,2}^{(0),-1}(\omega) \mathbf{\Gamma}_{2,1}^{(1)}(\omega) \mathbf{\Gamma}_{1,1}^{(0),-1}(\omega) (\mathbf{T}_1^\dagger | \hat{r}^\dagger \hat{s})^{(0)} \tag{5.201}$$

$$+ (\hat{p}^\dagger \hat{q} | \mathbf{T}_2^\dagger)^{(1)} \mathbf{\Gamma}_{2,2}^{(0),-1} \mathbf{\Gamma}_{2,1}^{(1)} \mathbf{\Gamma}_{1,1}^{(0),-1}(\omega) (\mathbf{T}_1^\dagger | \hat{r}^\dagger \hat{s})^{(0)} \tag{5.202}$$

$$+ (\hat{p}^\dagger \hat{q} | \mathbf{T}_1^\dagger)^{(0)} \mathbf{\Gamma}_{1,1}^{(0),-1}(\omega) \mathbf{\Gamma}_{1,2}^{(1)} \mathbf{\Gamma}_{2,2}^{(0),-1}(\mathbf{T}_1^\dagger | \hat{r}^\dagger \hat{s})^{(1)} \tag{5.203}$$

$$+ (\hat{p}^\dagger \hat{q} | \mathbf{T}_2^\dagger)^{(1)} \mathbf{\Gamma}_{2,2}^{(0),-1}(\omega) (\mathbf{T}_2^\dagger | \hat{r}^\dagger \hat{s})^{(1)}. \tag{5.204}$$

As explained in the main article, we make the usual approximation to drop the last term in Eq. (5.189), which amounts to dropping the term (5.204) and the associated diagrams. These should be included when calculating oscillator strengths.

5.3.1 Second-Order Diagrams

Figure 5.13 Diagrammatic contributions due to Eq.(5.195)

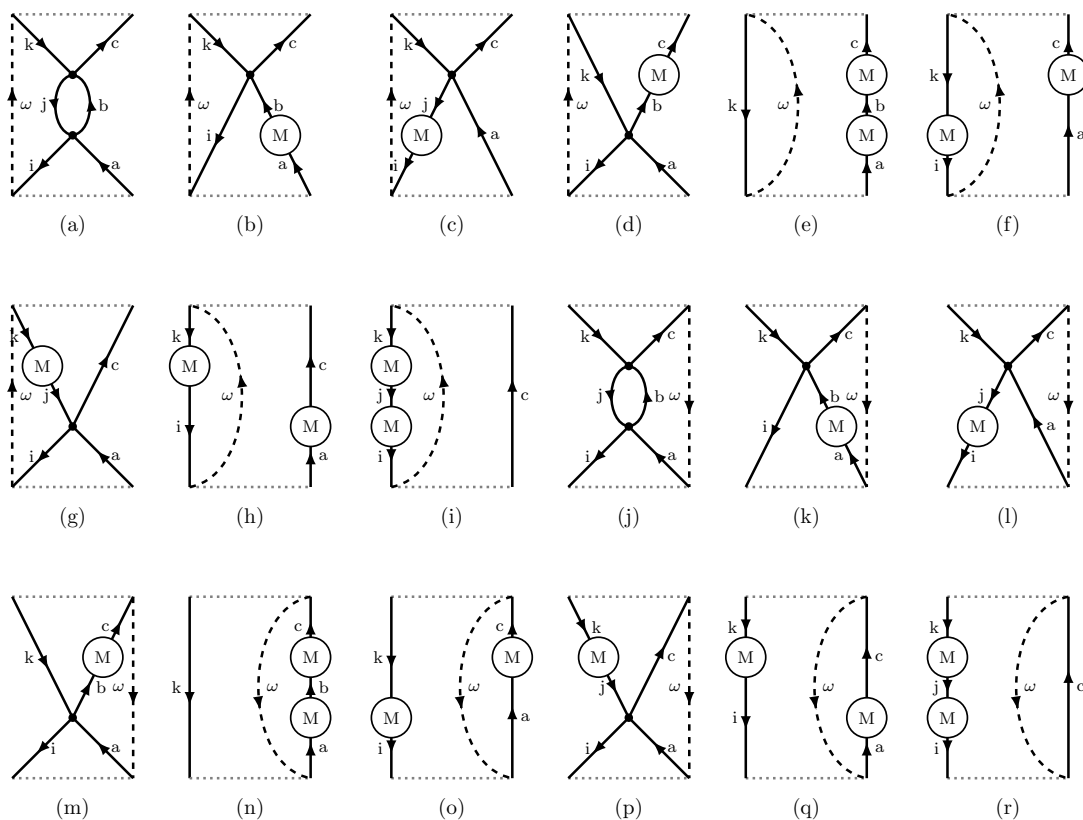


Figure 5.14 Diagrammatic contributions due to Eq.(5.196)

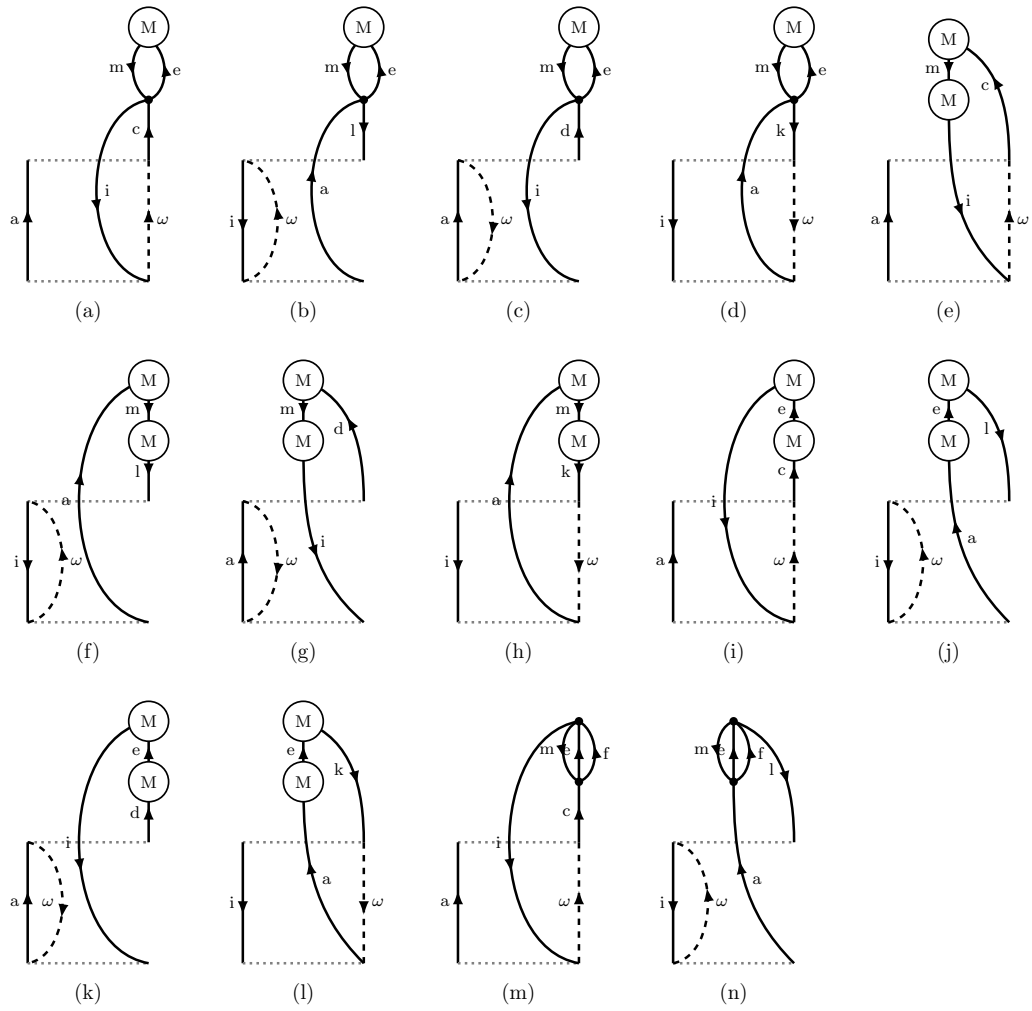


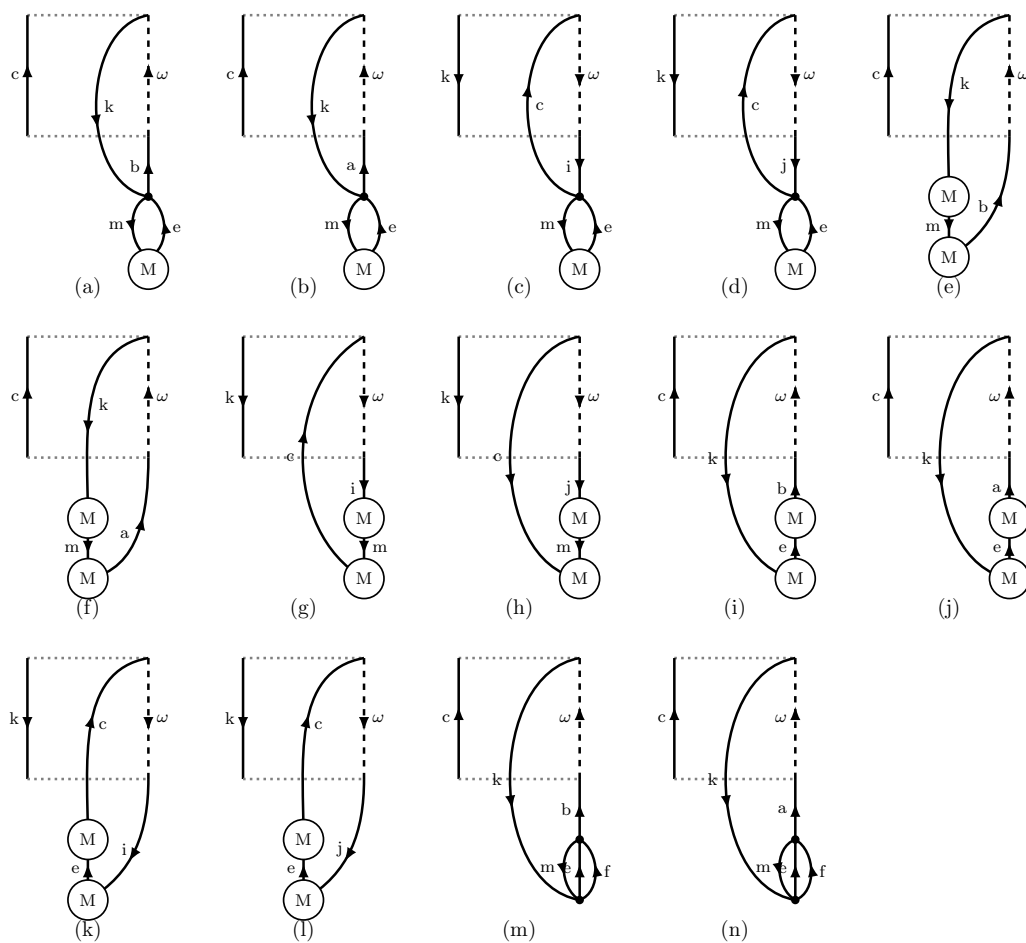
Figure 5.15 Diagrammatic contributions due to Eq.(5.197)

Figure 5.16 Diagrammatic contributions due to Eq.(5.198)

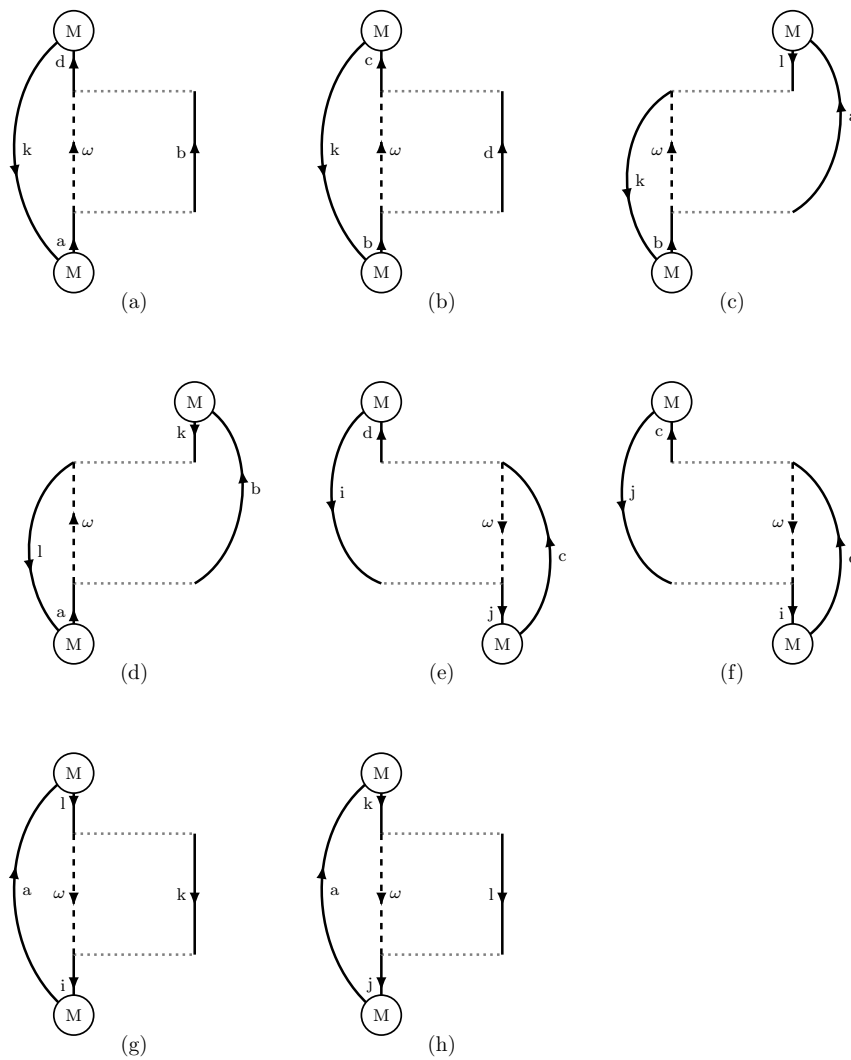


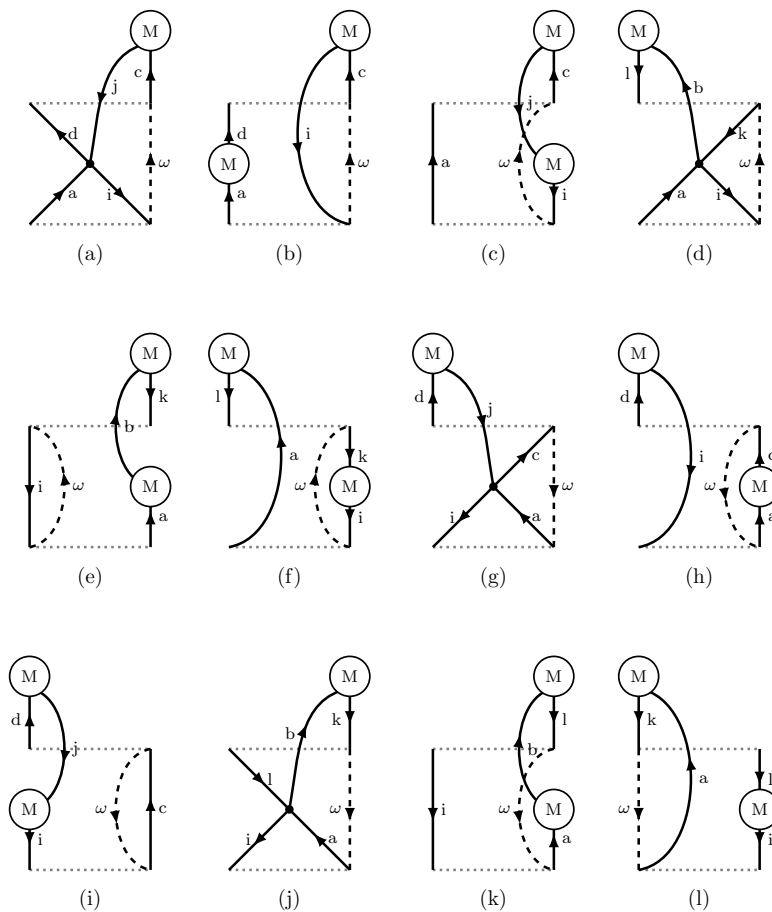
Figure 5.17 Diagrammatic contributions due to Eq.(5.199)

Figure 5.18 Diagrammatic contributions due to Eq.(5.200)

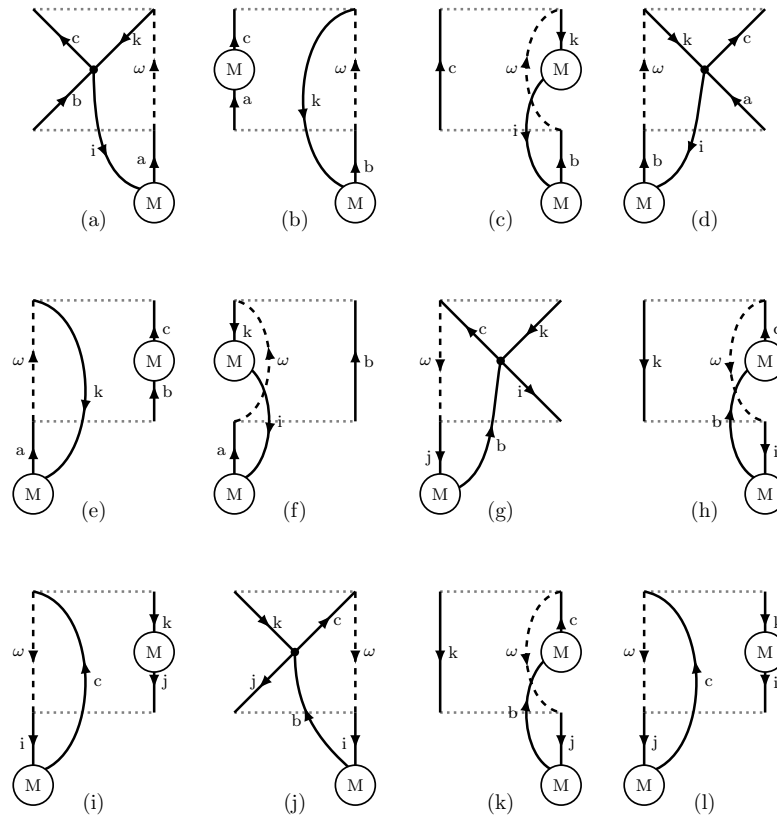


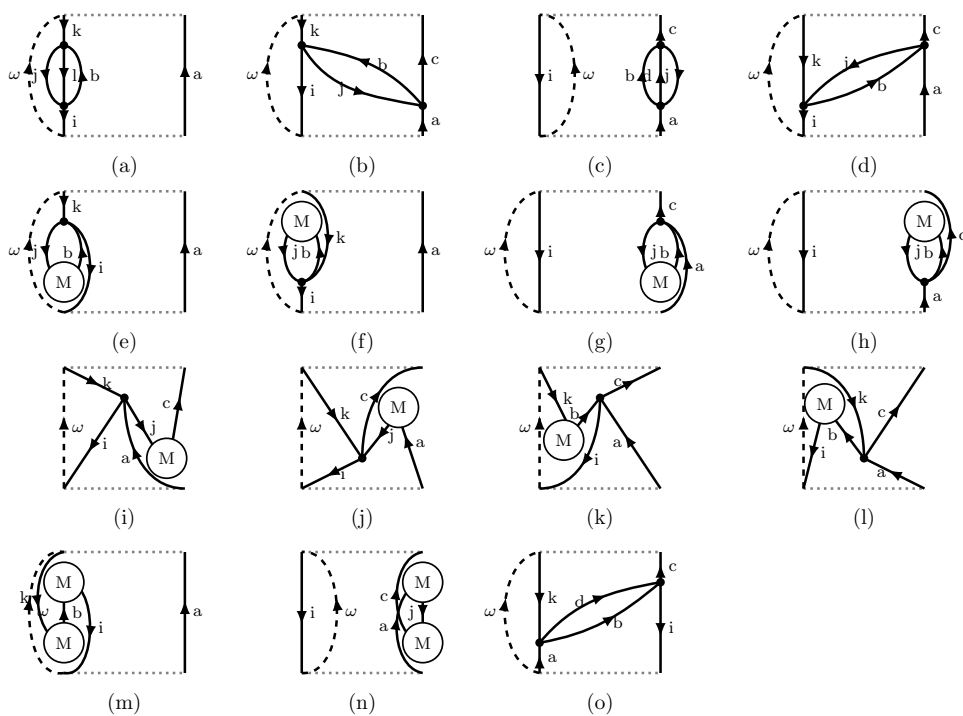
Figure 5.19 Diagrammatic contributions due to Eq.(5.201)

Figure 5.20 Diagrammatic contributions due to Eq.(5.202)

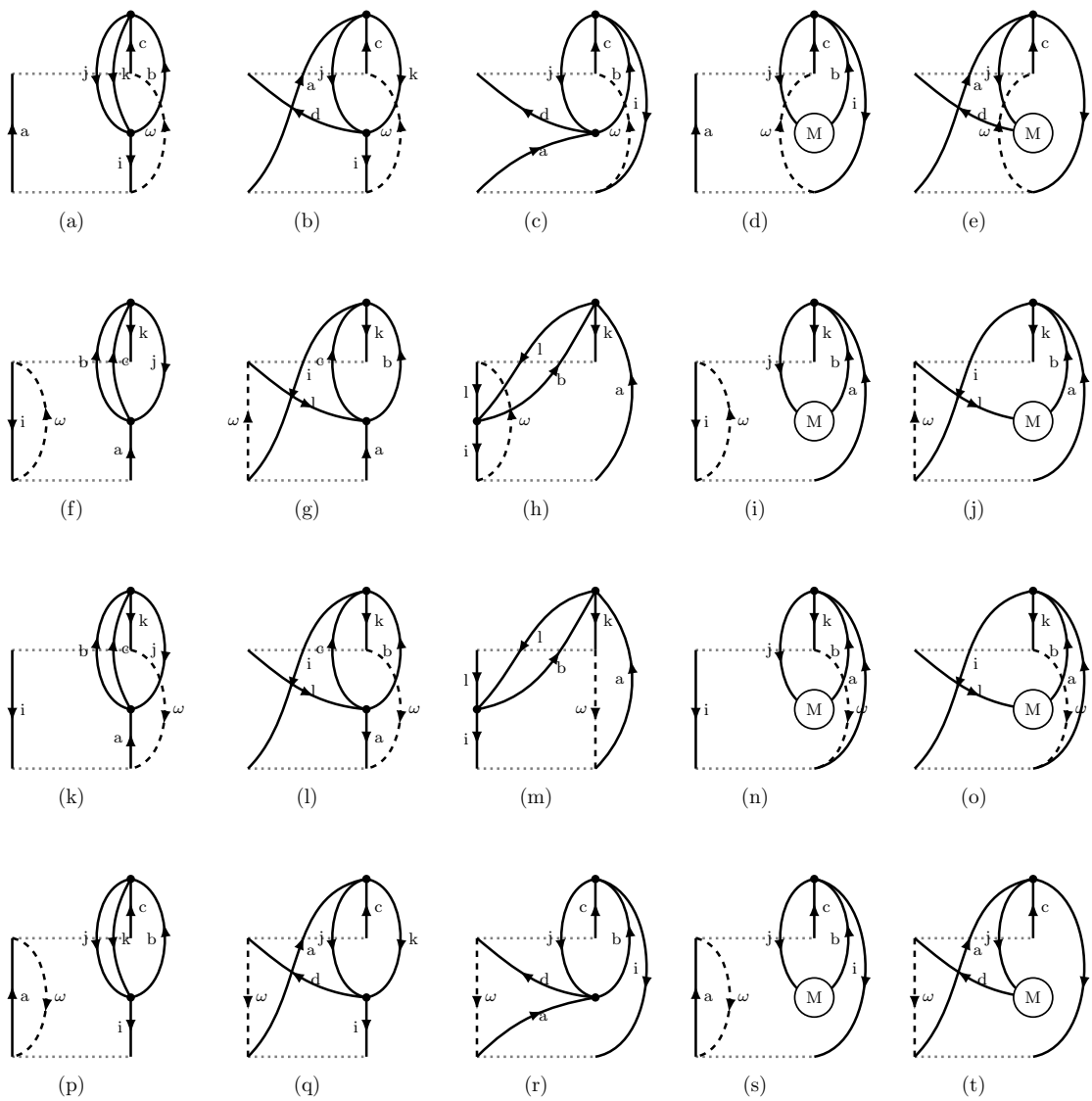


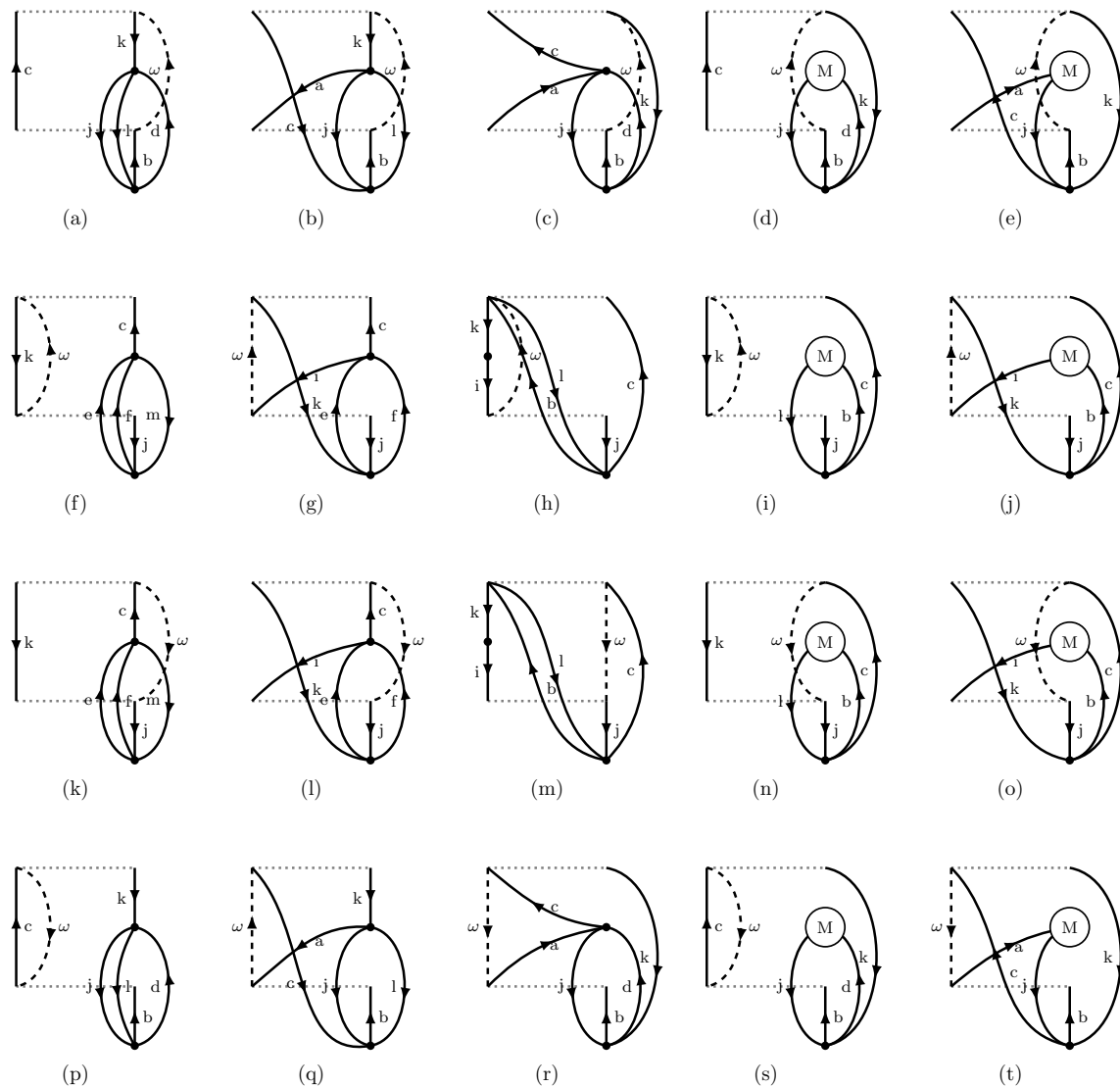
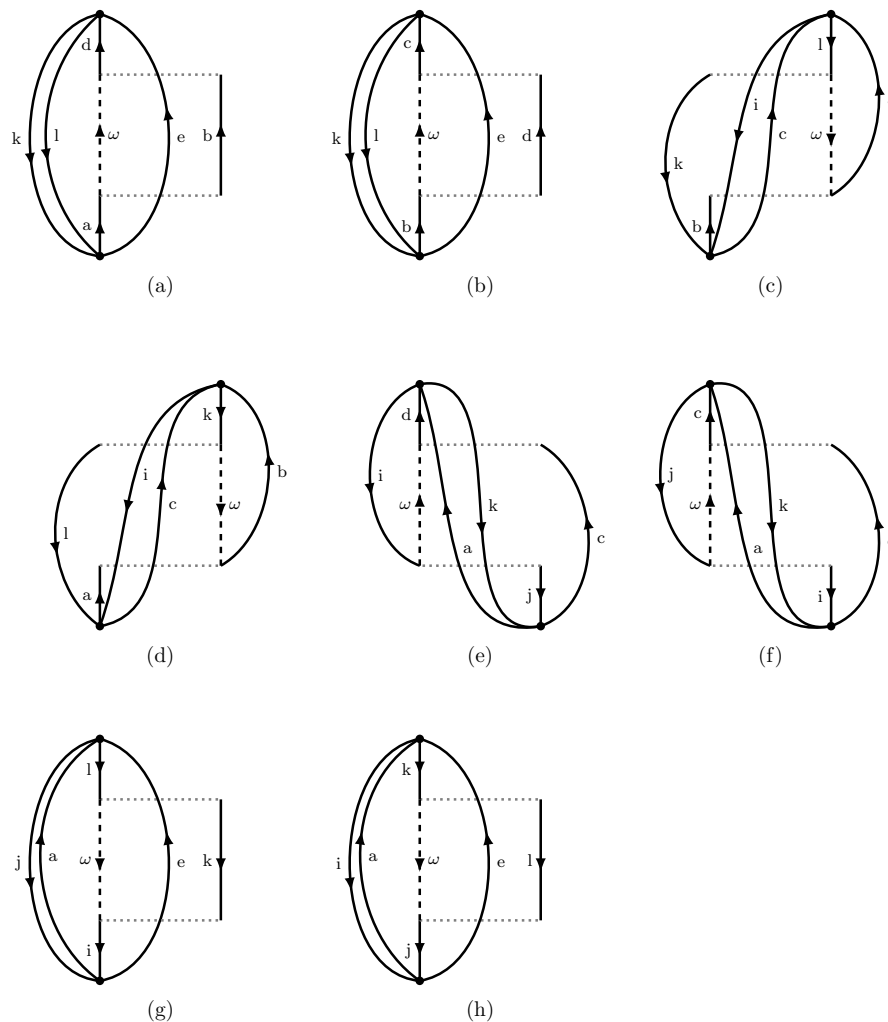
Figure 5.21 Diagrammatic contributions due to Eq.(5.203)

Figure 5.22 Diagrammatic contributions due to Eq.(5.204)

5.4 Conclusions and Perspective

We have derived a general TDDFT kernel that goes beyond the adiabatic approximation. The kernel contains the time-dependent exact exchange kernel plus an exact correlation kernel to second order. The many-body correlation part is frequency dependent, which is necessary for the appearance of double excitation poles in the response function. The overall kernel has an

extra frequency dependence due to the localization function. To our knowledge, this is the first TDDFT kernel that successfully includes all double excitations.

The frequency-dependence of the localizer is responsible of the ultra-non-locality property to the exact TDDFT kernel. The general role of the exact localizer is yet unknown, but it is reasonable to think that the extra frequency dependence that it introduces to the TDDFT kernel cannot give rise to extra poles in the response function. In fact, the exact many-body kernel should carry all the information about the pole structure to the TDDFT kernel. This supposition is supported by the Gonze-Scheffler relations, though it is only proven in the small matrix approximation using the second approximation of the exact kernel [142]. Further support is given by Görling *et al.*, who showed that the localizer cancels out in general in their linear-response formulation in terms of the Kohn-Sham potential instead of the density [144].

The secondary role of the localizer encourages to concentrate the attention in the exact many-body kernel to understand the missing contributions to correlation of the adiabatic approximation. The adiabatic functionals completely miss the terms that arise due to the frequency dependence. The missing terms are depicted in the supporting material (Sec. 5.3.) Specially important are diagrams of Figs. 5.19, 5.20, 5.21 and 5.22. These diagrams depict the correlation effects that arise from double excitations. Figure 5.19 contains the diagrams that introduce the interaction between single and double excitations, whereas the rest of figures contain the diagrams that couples double excitations with the reference. These diagrams are of two types: self-interaction terms and particle-hole terms. In the former, the interaction involves the particle or the hole orbitals separately, whereas in the latter, the interaction is between particle and hole orbitals. The role of the self-interaction terms is to shift the eigenvalues to correlated HF energies, whereas the particle-hole diagrams are responsible of the interaction among single excitations and the single and double excitation interaction.

Chapter 6

Dressed Time-Dependent Density-Functional Theory

6.1 Introduction

The exact kernel of Chapter 5 can include double excitations in general, but the main drawback is that it is computationally expensive to calculate, since we have to construct the many-body kernel in the first step and extract the diagonal in a second step. One of the bottlenecks is in the construction single-single block of the many-body kernel, which contains second-order Møller-Plesset MBPT formulas for each matrix element in the diagonal. Additionally, the localization step is difficult to perform, as it involves the inversion of singular matrices, which is numerically unstable. In this chapter, we propose an alternative TDDFT kernel which avoids this computational burden. To accomplish this, we take the adiabatic functional for describing the single-single block (thus avoiding the numerically intensive part of the *ab initio* kernel) and we add the terms from the polarization propagator that include the single-double coupling. Specifically, we include the diagrams (a), (b), (c) and (o) of Fig. 5.19 (see Sec. 5.3 of Chap. 5) to the adiabatic kernels. This kernel supposes a generalization of the dressed TDDFT model first proposed by Maitra, Burke and coworkers [43,44]. This chapter accomplish the last objective of constructing efficient kernels which include all double excitations and can be applied to systems of medium of large size.

The fact that we are using polarization propagator terms without localization is *ad hoc*. In fact, the dressed kernel can be viewed as a hybrid TDDFT kernel, in a similar way that is done in DFT. The hybrid DFT functionals try to build in more information to the functional by adding HF exchange, which introduces an extra spatial dependence. Equivalently, the dressed kernel tries to include more information by adding polarization propagator terms, which introduce an extra time dependence in the functional.

The dressed kernel needed a validation, since the mixture of adiabatic functionals with polarization propagator terms is done in an *ad hoc* manner. Therefore, we implemented the dressed TDDFT kernel and applied it to 28 organic chromophores. The singlet excitation energies were compared to high quality *ab initio* results, with the aim to determine which combinations of adiabatic functionals and polarization propagator terms would give the best agreement. The results of this study lead to a publication in an special issue on TDDFT in *Chemical Physics*. A preprint of this article is reproduced in the next section. My contribution in this work has been major. I have been responsible of the implementation in DEMON2K, the calculation and analysis of the excited states and the writing and correction of the article.

The main problem of the dressed kernel is the double counting of correlation. Some (unidentified) correlation effects due to second-order self-energy diagrams are already present in the adiabatic approximation functionals, and therefore the same correlation effects are counted twice. A simple strategy to avoid the double counting is to restrict the number of double excitations. The truncation of the double excitation manifold has to be done with care in order to keep states

with a defined spin multiplicity. When done properly, pure spin singlets, triplets and quintuplets are obtained.

6.2 Assessment of Dressed TDDFT (Article)¹

Assessment of Dressed Time-Dependent Density-Functional Theory for the Low-Lying Valence States of 28 Organic Chromophores

Miquel Huix-Rotllant^{1,†}, Andrei Ipatov¹, Angel Rubio², Mark E. Casida^{1,*}

¹ *Laboratoire de Chimie Théorique,
Département de Chimie Moléculaire (DCM, UMR CNRS/UJF 5250),
Institut de Chimie Moléculaire de Grenoble (ICMG, FR2607),
Université Joseph Fourier (Grenoble I),
301 rue de la Chimie, BP 53,
F-38041 Grenoble Cedex 9, France*

² *Nano-Bio Spectroscopy Group and ETSF Scientific Development Centre,
Departamento de Física de Materiales,
Universidad del País Vasco, E-20018 San Sebastián (Spain);
Centro de Física de Materiales
CSIC-UPV/EHU-MPC and DIPC,
E-20018 San Sebastián (Spain);
Fritz-Haber-Institut der Max-Planck-Gesellschaft,
Faradayweg 4-6, D-14195 Berlin-Dahlem, (Germany).*

Almost all time-dependent density-functional theory (TDDFT) calculations of excited states make use of the adiabatic approximation, which implies a frequency-independent exchange-correlation kernel that limits applications to one-hole/one-particle states. To remedy this problem, Maitra *et al.* [J. Chem. Phys. **120**, 5932 (2004)] proposed dressed TDDFT (D-TDDFT), which includes explicit two-hole/two-particle states by adding a frequency-dependent term to adiabatic TDDFT. This paper offers the first extensive test of D-TDDFT, and its ability to represent excitation energies in a general fashion. We present D-TDDFT excited states for 28 chromophores and compare them with the benchmark results of Schreiber *et al.* [J. Chem. Phys. **128**, 134110 (2008).] We find the choice of functional used for the A-TDDFT step to be critical for positioning the 1h1p states with respect to the 2h2p states. We observe that D-TDDFT without HF exchange increases the error in excitations already underestimated by A-TDDFT. This problem is largely remedied by implementation of D-TDDFT including Hartree-Fock exchange.

Keywords: time-dependent density-functional theory, exchange-correlation kernel, adiabatic approximation, frequency dependence, many-body perturbation theory, excited states, organic chromophores

[†] Corresponding author: Miquel.Huix@UJF-Grenoble.Fr

* Corresponding author: Mark.Casida@UJF-Grenoble.Fr

1. This section is a preprint of Ref. [260]. Note: The original format has been adapted to the standards of this thesis.

6.2.1 Introduction

Time-dependent density-functional theory (TDDFT) is a popular approach for modeling the excited states of medium- and large-sized molecules. It is a formally exact theory [13], which involves an exact exchange-correlation (xc) kernel with a role similar to the xc-functional of the Hohenberg-Kohn-Sham ground-state theory. Since the exact xc-functional is not known, practical calculations involve approximations. Most TDDFT applications use the so-called adiabatic approximation which supposes that the xc-potential responds instantaneously and without memory to any change in the self-consistent field [13]. The adiabatic approximation limits TDDFT to one hole-one particle (1h1p) excitations (i.e., single excitations), albeit dressed to include electron correlation effects [149]. Overcoming this limitation is desirable for applications of TDDFT to systems in which 2h2p excitations (i.e., double excitations) are required, including the excited states of polyenes, open-shell molecules, and many common photochemical reactions [29,258,276]. Burke and coworkers [43,44] proposed the dressed TDDFT (D-TDDFT) model, an extension to adiabatic TDDFT (A-TDDFT) which explicitly includes 2h2p states. The D-TDDFT kernel adds frequency-dependent terms from many-body theory to the adiabatic xc-kernel. While initial results on polyenic systems appear encouraging [44,150,277], no systematic assessment has been made for a large set of molecules. The present article reports the first systematic study of D-TDDFT for a large test set namely, the low-lying excited states of 28 organic molecules for which benchmark results exist [257,278]. This study has been carried out with several variations of D-TDDFT implemented in a development version of the density-functional theory (DFT) code DEMON2K [205].

The formal foundations of TDDFT were laid out by Runge and Gross (RG) [13] which put on rigorous grounds the earlier TDDFT calculations of Zangwill and Soven [279]. The original RG theorems showed some subtle problems [280], which have been since re-examined, criticized, and improved [77,281,282] providing a remarkably well-founded theory (for a recent review see [283].) A key feature of this formal theory is a time-dependent Kohn-Sham equation containing a time-dependent xc-potential describing the propagation of the density after a time-dependent perturbation is applied to the system. Casida used linear response (LR) theory to derive an equation for calculating excitation energies and oscillator strengths from TDDFT [17]. The resultant TDDFT response equations [17] are

$$\begin{bmatrix} \mathbf{A}(\omega) & \mathbf{B}(\omega) \\ -\mathbf{B}^*(\omega) & -\mathbf{A}^*(\omega) \end{bmatrix} \begin{bmatrix} \mathbf{X} \\ \mathbf{Y} \end{bmatrix} = \omega \begin{bmatrix} \mathbf{X} \\ \mathbf{Y} \end{bmatrix}. \quad (6.1)$$

However $\mathbf{A}(\omega)$ and $\mathbf{B}(\omega)$ explicitly include the Hartree (H) and xc kernels,

$$\begin{aligned} A_{ai\sigma,bj\tau} &= (\epsilon_a^\sigma - \epsilon_i^\sigma) \delta_{ij} \delta_{ab} \delta_{\sigma\tau} + (ia | f_{Hxc}^{\sigma,\tau}(\omega) | bj) \\ B_{ai\sigma,bj\tau} &= (ia | f_{Hxc}^{\sigma,\tau}(\omega) | jb), \end{aligned} \quad (6.2)$$

where ϵ_p^σ is the KS orbital energy for spin σ , and

$$\begin{aligned} (pq | f(\omega) | rs) &= \\ & \int d^3r \int d^3r' \phi_p^*(\mathbf{r}) \phi_q(\mathbf{r}) f(\mathbf{r}, \mathbf{r}'; \omega) \phi_r^*(\mathbf{r}') \phi_s(\mathbf{r}'). \end{aligned} \quad (6.3)$$

Here and throughout this paper we use the following indexes notation: i, j, \dots are occupied orbitals, a, b, \dots are virtual orbitals, and p, q, \dots are orbitals of unspecified nature.

In chemical applications of TDDFT, the Tamm-Dancoff approximation (TDA) [109],

$$\mathbf{A}(\omega)\mathbf{X} = \omega\mathbf{X}, \quad (6.4)$$

improves excited state potential energy surfaces [30, 185], though sacrificing the Thomas-Reine-Kuhn sum rule. Although the standard random-phase approximation (RPA) equations [16] provide only 1h1p states, the exact LR-TDDFT equations include also 2h2p states (and higher-order $n\text{h}n\text{p}$ states) through the ω -dependence of the xc part of the kernel $f_{xc}^{\sigma,\tau}(\omega)$. However, the matrices $\mathbf{A}(\omega)$ and $\mathbf{B}(\omega)$ are supposed ω -independent in the adiabatic approximation to the xc-kernel, thereby losing the non-linearity of the LR-TDDFT equations and the associated 2h2p (and higher) states.

Double excitations are essential ingredients for a proper description of several physical and chemical processes. Though they do not appear directly in photo-absorption spectra, (i.e., they are dark states), signatures of 2h2p states appear indirectly through mixing with 1h1p states, thereby leading to the fracturing of main peaks into satellites. [147, 148] In open-shell molecules such mixing is often required in order to maintain spin symmetry [149, 164, 284]. Perhaps more importantly dark states often play an essential important role in photochemistry and explicit inclusion of 2h2p states is often considered necessary for a minimally correct description of conical intersections [29]. A closely-related historical, but still much studied, problem is the location of 2h2p states in polyenes [56, 258, 285–291], partly because of the importance of the polyene retinal in the photochemistry of vision [292–294].

It is thus manifest that some form of explicit inclusion of 2h2p states is required within TDDFT when attacking certain types of problems [295]. This has led to various attempts to include 2h2p states in TDDFT. One partial solution was given by spin-flip TDDFT [193, 296] which describes some states which are 2h2p with respect to the ground state by beginning with the lowest triplet state and including spin-flip excitations [39, 42, 159, 197]. However, spin-flip TDDFT does not provide a general way to include double excitations. Strengths and limitations of this theory have been discussed in recent work [158].

The present article focuses on D-TDDFT, which offers a general model for including explicitly 2h2p states in TDDFT. D-TDDFT was initially proposed by Maitra, Zhang, Cave and Burke as an *ad hoc* many-body theory correction to TDDFT [43]. They subsequently tested it on butadiene and hexatriene with encouraging results [44]. The method was then reimplemented and tested on longer polyenes and substituted polyenes by Mazur *et al.* [150, 277].

In the present work, we consider several variants of D-TDDFT, implement and test them on the set of molecules proposed by Schreiber *et al.* [257, 278] The set consists of 28 organic molecules whose excitation energies are well characterized both experimentally or through high-quality *ab initio* wavefunction calculations.

This paper is organized as follows. Section 6.2.2 describes D-TDDFT in some detail and the variations that we have implemented. Section 6.2.3 describes technical aspects of how the formal equations were implemented in DEMON2K, as well as additional features which were implemented specifically for this study. Section 6.2.4 describes computational details such as basis sets and choice of geometries. Section 6.2.5 presents and discusses results. Finally, section 6.2.6 concludes.

6.2.2 Formal Equations

D-TDDFT may be understood as an approximation to exact equations for the xc-kernel [140]. This section reviews D-TDDFT and the variations which have been implemented and tested in the present work.

An *ab initio* expression for the xc-kernel may be derived from many-body theory, either from the Bethe-Salpeter equation or from the polarization propagator (PP) formalism [46, 149]. Both equations give the same xc-kernel,

$$f_{xc}(\mathbf{x}, \mathbf{x}'; \omega) = \int d^3x_1 \int d^3x_2 \int d^3x_3 \int d^3x_4 \Lambda_s(\mathbf{x}; \mathbf{x}_1, \mathbf{x}_2; \omega) K(\mathbf{x}_1, \mathbf{x}_2; \mathbf{x}_3, \mathbf{x}_4; \omega) \Lambda^\dagger(\mathbf{x}_3, \mathbf{x}_4; \mathbf{x}'; \omega) \quad (6.5)$$

where $x_p = (\mathbf{r}_p, \sigma_p)$, K is defined as

$$K(\mathbf{x}_1, \mathbf{x}_2; \mathbf{x}_3, \mathbf{x}_4; \omega) = \Pi_s^{-1}(\mathbf{x}_1, \mathbf{x}_2; \mathbf{x}_3, \mathbf{x}_4; \omega) - \Pi^{-1}(\mathbf{x}_1, \mathbf{x}_2; \mathbf{x}_3, \mathbf{x}_4; \omega) \quad (6.6)$$

and Π and Π_s are respectively the interacting and non-interacting polarization propagators, which contribute to the pole structure of the xc-kernel. The interacting and non-interacting localizers, Λ and Λ_s respectively, convert the 4-point polarization propagators into the 2-point TDDFT quantities (4-point and 2-point refer to the space coordinates of each kernel.) The localization process introduces an extra ω -dependence into the xc-kernel. Interestingly, Gonze and Scheffler [142] noticed that, when we substitute the interacting by the non-interacting localizer in Eq. (6.5), the localization effects can be neglected for key matrix elements of the xc-kernel at certain frequencies, meaning that the ω -dependence exactly cancels the spatial localization. More importantly, removing the localizers simply means replacing TDDFT with many-body theory terms. To the extent that both methods represent the same level of approximation, excitation energies and oscillator strengths are unaffected, though the components of the transition density will change in a finite basis representation. In Ref. [149], Casida proposed a PP form of D-TDDFT without the localizer. In Ref. [140], Huix-Rotllant and Casida gave explicit expressions for an *ab initio* ω -dependent xc-kernel derived from a Kohn-Sham-based second-order polarization propagator (SOPPA) formula. Equivalent expressions were derived by Zhang and Burke in Ref. [297], in which they calculated the excitation energy by truncating to second-order the Görling-Levy perturbation theory.

The calculation of the xc-kernel in SOPPA can be cast in RPA-like form. In the TDA approximation, we obtain

$$\left[\mathbf{A}_{11} + \mathbf{A}_{12} (\omega \mathbf{1}_{22} - \mathbf{A}_{22})^{-1} \mathbf{A}_{21} \right] \mathbf{X} = \omega \mathbf{X}, \quad (6.7)$$

which provides a matrix representation of the second-order approximation of the many-body theory kernel $K(\mathbf{x}_1, \mathbf{x}_2; \mathbf{x}_3, \mathbf{x}_4; \omega)$. The blocks \mathbf{A}_{11} , \mathbf{A}_{21} and \mathbf{A}_{22} couple respectively single excitations among themselves, single excitations with double excitations and double excitations among themselves. In Appendix 6.2.8 we give explicit equations for these blocks in the case of a SOPPA calculation based on the KS Fock operator. We recall that in the SOPPA kernel, the

\mathbf{A}_{11} is frequency independent, though it contains some correlation effects due to the 2h2p states. All ω -dependence is in the second term and it originates from the \mathbf{A}_{22} coupled to the \mathbf{A}_{11} block.

The D-TDDFT kernel is a mixture of the many-body theory kernel and the A-TDDFT kernel. This mixture was first defined by Maitra *et al.* [43]. They recognized that the single-single block was already well represented by A-TDDFT, therefore substituting the expression of \mathbf{A}_{11} in Eq. (6.7) for the adiabatic \mathbf{A} block of Casida's equation [Eq.(6.2).] This many-body theory and TDDFT mixture is not uniquely defined. As we will show, different combinations of \mathbf{A}_{11} and \mathbf{A}_{22} give rise to completely different kernels, and not all combinations include correlation effects consistently. In the present work, we wish to test several definitions of the D-TDDFT kernel by varying the \mathbf{A}_{11} and \mathbf{A}_{22} blocks. For each D-TDDFT kernel, we will compare the excitation energies against high-quality *ab initio* benchmark results. This will allow us to make a more accurate definition of the D-TDDFT approach.

We will use two possible adiabatic xc-kernels in the \mathbf{A}_{11} matrix: the pure LDA xc-kernel and a hybrid xc-kernel. Usually, hybrid TDDFT calculations are based on a hybrid KS wavefunction. Our implementations are done in DEMON2K, a DFT code which is limited to pure xc-potentials in the ground-state calculation. Therefore, we have devised a hybrid calculation that does not require a hybrid DFT wavefunction. Specifically, the RPA blocks used in Casida's equations are modified as

$$\begin{aligned} A_{ai\sigma,bj\tau} &= \left[\epsilon_a^\sigma \delta_{ab} + c_0 \cdot (a|\hat{M}_{xc}|b) \right] \delta_{ij} \delta_{\sigma\tau} - \left[\epsilon_i^\sigma \delta_{ij} + c_0 \cdot (i|\hat{M}_{xc}|j) \right] \delta_{ab} \delta_{\sigma\tau} \\ &\quad + (ai|(1-c_0) \cdot f_x^{\sigma\tau} + c_0 \cdot \hat{\Sigma}_x^{HF} + f_{Hc}^{\sigma\tau}|jb) \\ B_{ai\sigma,bj\tau} &= (ai|(1-c_0) \cdot f_x^{\sigma\tau} + c_0 \cdot \hat{\Sigma}_x^{HF} + f_{Hc}^{\sigma\tau}|bj), \end{aligned} \quad (6.8)$$

where $\hat{\Sigma}_x^{HF}$ is the HF exchange operator and $\hat{M}_{xc} = \hat{\Sigma}_x^{HF} - v_{xc}$ provides a first-order conversion of KS into HF orbital energies. We note that the first-order conversion is exact when the space of occupied KS orbitals coincides with the space of occupied HF orbitals. Also, the conversion from KS to HF orbital energies introduces an effective particle number discontinuity.

Along with the two definitions of the \mathbf{A}_{11} block, we will also test different possible definitions for the \mathbf{A}_{22} block. First, we will test an independent particle approximation (IPA) estimate of \mathbf{A}_{22} , consisting of diagonal KS orbital energy differences. It was shown in Ref. [140] that such a block also appears in a second-order *ab initio* xc-kernel. We will call that combination D-TDDFT. Second, we will use a first-order correction to the IPA estimate of \mathbf{A}_{22} . This might give an improved description for the placement of double excitations [298]. We call that combination extended D-TDDFT (x-D-TDDFT). We note that this is the approach of Maitra *et al.* [43].

In Table 6.1 we summarize the different variants of D-TDDFT and D-CIS, according to \mathbf{A}_{11} and \mathbf{A}_{22} blocks. All the methods share the same \mathbf{A}_{12} block unless the \mathbf{A}_{22} block is 0, in which case the \mathbf{A}_{12} is also 0. We recall that only the standard CISD has a coupling block \mathbf{A}_{01} and \mathbf{A}_{02} with the ground state, but none of the methods used in this paper has.

Table 6.1 Summary of the methods used in this work. CIS, CISD and A-TDDFT are the standard methods, whereas the (x-)D-CIS and (x-)D-TDDFT are the variations we use. The kernel f_{Hxc} represents the Hartree kernel plus the exchange-correlation kernel of DFT in the adiabatic approximation, Σ_x^{HF} is the HF exchange and $\Delta\epsilon$ is a zeroth-order estimate for a double excitation.

Method	\mathbf{A}_{02}	\mathbf{A}_{11}	\mathbf{A}_{22}
CIS	No	$f_H + \Sigma_x^{HF}$	0
A-TDDFT	No	f_{Hxc}	0
CISD	Yes	$f_H + \Sigma_x^{HF}$	$\Delta\epsilon^{HF} + \text{first-order}$
D-CIS	No	$f_H + \Sigma_x^{HF}$	$\Delta\epsilon^{KS}$
x-D-CIS	No	$f_H + \Sigma_x^{HF}$	$\Delta\epsilon^{KS} + \text{first-order}$
D-TDDFT	No	f_{Hxc}	$\Delta\epsilon^{KS}$
x-D-TDDFT	No	f_{Hxc}	$\Delta\epsilon^{KS} + \text{first-order}$

6.2.3 Implementation

We have implemented the equations described in Sec. 6.2.2 in a development version of DEMON2K. The standard code now has a LR-TDDFT module [207]. In this section, we briefly detail the necessary modifications to implement D-TDDFT.

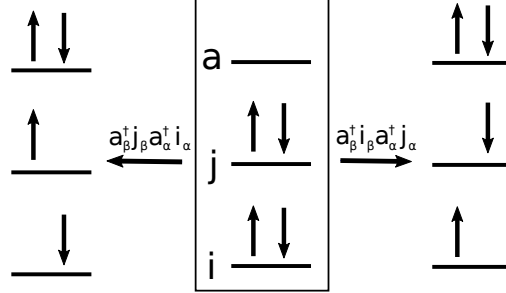
DEMON2K is a Gaussian-type orbital DFT program which uses an auxiliary basis set to expand the charge density, thereby eliminating the need to calculate 4-center integrals. The implementation of TDDFT in DEMON2K is described in Ref. [207]. Note that newer versions of the code have abandoned the charge conservation constraint for TDDFT calculations. For the moment, only the adiabatic LDA (ALDA) can be used as TDDFT xc-kernel.

Asymptotically-corrected (AC) xc-potentials are needed to correctly describe excitations above the ionization threshold, which is placed at minus the highest-occupied molecular orbital energy [25]. Such corrections are not yet present in the master version of DEMON2K. Since such a correction was deemed necessary for the present study, we have implemented Hirata *et al.*'s improved version [299] of Casida and Salahub's AC potential [300] in our development version of DEMON2K.

Implementation of D-TDDFT requires several modifications of the standard AA implementation of Casida's equation. First an algorithm to decide which 2h2p excitations have to be included is needed. At the present time, the user specifies the number of such excitations. These are then automatically selected as the N lowest-energy 2h2p IPA states. Since we are using a truncated 2h2p space, the algorithm makes sure that all the spin partners are present, in order to have pure spin states. The basic idea is illustrated in Fig. 6.1. Both 2h2p excitations are needed in order to construct the usual singlet and triplet combinations. A similar algorithm should be implemented for including all space double excitations which involve degenerate irreducible representations, but this is not implemented in the present version of the code.

These IPA 2h2p excitations are then added to the initial guess for the Davidson diagonalizer. We recognize that a perturbative pre-screening of the 2h2p space would be a more effective way

Figure 6.1 Necessary double excitations that need to be included in the truncated 2h2p space to maintain pure spin symmetry.



for selecting the excitations, but this more elaborate implementation is beyond the scope of the present study.

We need new integrals to implement the HF exchange terms appearing in the many-body theory blocks. The construction of these blocks require extra hole-hole and particle-particle three-center integrals apart from the usual hole-particle integrals already needed in TDDFT. We then construct the additional matrix elements using the resolution-of-the-identity (RI) formula

$$(pq|f_H|rs) = \sum_{IJKL} (pq|g_I)S_{IJ}^{-1}(g_J|f_H|g_K)S_{KL}^{-1}(g_L|rs), \quad (6.9)$$

where g_I are the usual DEMON2K notation for the density fitting functions and S_{IJ} is the auxiliary function overlap matrix defined by $S_{IJ} = (g_I|f_H|g_J)$, in which the Coulomb repulsion operator is used as metric.

Solving Eq.(6.7) means solving a non-linear set of equations. This is less efficient than solving linear equations. In Ref. [140] it was shown that Eq. (6.7) comes from applying the Löwdin-Feshbach partitioning technique to

$$\begin{bmatrix} \mathbf{A}_{11} & \mathbf{A}_{12} \\ \mathbf{A}_{21} & \mathbf{A}_{22} \end{bmatrix} \begin{bmatrix} \mathbf{X}_1 \\ \mathbf{X}_2 \end{bmatrix} = \omega \begin{bmatrix} \mathbf{X}_1 \\ \mathbf{X}_2 \end{bmatrix}, \quad (6.10)$$

where \mathbf{X}_1 and \mathbf{X}_2 are now the single and double excitation components of the vectors. The solution of this equation is easier and does not require a self-consistent approach, albeit at the cost of requiring more physical memory, since then the Krylov space vectors have the dimension of the single and the double excitation space.

Calculation of oscillator strengths has also to be modified when D-TDDFT is implemented. In a mixed many-body theory and TDDFT calculation, there is an extra first-order term in the ground-state KS wavefunction [140]

$$|0\rangle = \left(1 + \sum_{ia} \frac{(i|\hat{M}_{xc}|a)}{\epsilon_i - \epsilon_a} \hat{a}_a^\dagger \hat{a}_i \right) |KS\rangle \quad (6.11)$$

where $|KS\rangle$ is the reference KS wavefunction. This correction constitutes a ‘‘Brillouin correction’’ to the Kohn-Sham Hamiltonian which is absent when using a Hartree-Fock reference. The evaluation of transition dipole moments in DEMON2K was modified to include the contributions from 2h2p poles,

$$\langle \mathbf{r} | \hat{a}_a^\dagger \hat{a}_i \hat{a}_b^\dagger \hat{a}_j \rangle = X_{ajib} \left(\frac{\langle i | \hat{M}_{xc} | a \rangle}{\epsilon_i - \epsilon_a} \langle j | \mathbf{r} | b \rangle + \frac{\langle j | \hat{M}_{xc} | b \rangle}{\epsilon_j - \epsilon_b} \langle i | \mathbf{r} | a \rangle - \frac{\langle i | \hat{M}_{xc} | b \rangle}{\epsilon_i - \epsilon_b} \langle j | \mathbf{r} | a \rangle - \frac{\langle j | \hat{M}_{xc} | a \rangle}{\epsilon_j - \epsilon_a} \langle i | \mathbf{r} | b \rangle \right), \quad (6.12)$$

where X_{ajib} is an element of the eigenvector \mathbf{X}_2 , the double excitation part of the eigenvector of Eq. (6.10).

6.2.4 Computational Details

Geometries for the set of 28 organic chromophores were taken from Ref. [257]. These were optimized at the MP2/6-31G* level, forcing the highest point group symmetry in each case. The orbital basis set is Ahlrich’s TZVP basis [301]. As pointed out in Ref. [257], this basis set has not enough diffuse functions to converge all Rydberg states. We keep the same basis set for the sake of comparison with the benchmark results. Basis-set errors are expected for states with a strong valence-Rydberg character or states above 7 eV, which are in general of Rydberg nature.

Comparison of the D-TDDFT is performed against the best estimates proposed in Ref. [257]. These best estimates are taken as highly correlated *ab initio* calculations using large basis sets, if available in the literature. Otherwise, they are taken as the coupled cluster CC3/TZVP calculation if the weight of the 1h1p space is more of than 95%, and CASPT2/TZVP in the other cases.

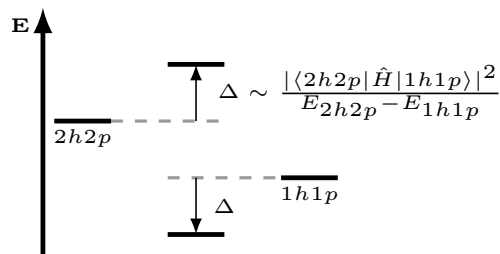
All calculations were performed with a development version of DEMON2K (unless otherwise stated) [205]. Calculations were carried out with the fixed fine option for the grid and the GEN-A3* density fitting auxiliary basis. The convergence criteria for the SCF was set to 10^{-8} .

To set up the notation used in the rest of the article, excited state calculations are denoted by TD/SCF, where SCF is the functional used for the SCF calculation and TD is the choice of post-SCF excited-state method. Additionally, the D-TD/SCF(n) and x-D-TD/SCF(n) will refer to the dressed and extended dressed TD/SCF method using n 2h2p states. Thus TDA D-ALDA/AC-LDA(10) denotes a asymptotically-corrected LDA for the DFT calculation followed by a LR-TDDFT calculation with the dressed xc-kernel kernel and the Tamm-Dancoff approximation. The D-TDDFT kernel has the adiabatic LDA xc-kernel for the \mathbf{A}_{11} block and the \mathbf{A}_{22} block is approximated as KS orbital energy differences.

In this work, all calculations are done in using the TDA and a AC-LDA wavefunction. For the sake of readability, we omit writing them when our main focus is on the discussion of the different variants of the post-SCF part.

Calculations on our test-set show few differences between ALDA/LDA and ALDA/AC-LDA. The singlet and triplet excitation energies and the oscillator strengths are shown in Table I in the supplementary material. The average absolute error is 0.16 eV with a standard deviation of

Figure 6.2 Schematic representation of the interaction between the 1h1p and the 2h2p spaces. The relaxation energy Δ is proportional to the size of the coupling and inversely proportional to the energy difference between the two spaces.



0.19 eV. The maximum difference is 0.91 eV. The states with larger differences justify the use of asymptotic correction. However, the absolute error and the standard deviation are small. We attribute this to the restricted nature of the basis set used in the present study.

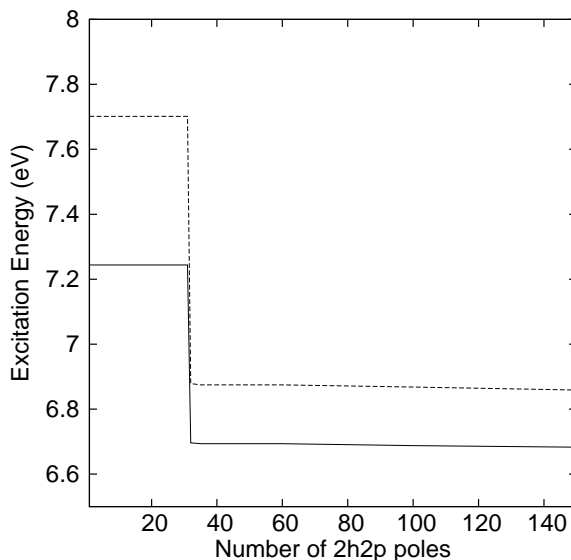
6.2.5 Results

In this section we discuss the results obtained with the different variants of D-TDDFT. In particular, we compare the quality of D-TDDFT singlet excitation energies against benchmark results for 28 organic chromophores. These chromophores can be classified in four groups according to the chemical nature of their bond: (i) unsaturated aliphatic hydrocarbons, containing only carbon-carbon double bonds; (ii) aromatic hydrocarbons and heterocycles, including molecules with conjugated aromatic double bonds; (iii) aldehydes, ketones and amides with the characteristic oxygen-carbon double bonds; (iv) nucleobases which have a mixture of the bonds found in the three previous groups.

These molecules have two types of low-lying excited states: Rydberg (i.e., diffuse states) and valence states. The latter states are traditionally described using the familiar Hückel model. The low-lying valence transitions involve mainly π orbitals, i.e. the molecular orbitals (MO) formed as combinations of p_z atomic orbitals. The π orbitals are delocalized over the whole structure. Electrons in these orbitals are easily promoted to an excited state, since they are not involved in the skeletal σ -bonding. The most characteristic transitions in these systems are represented by 1h1p $\pi \rightarrow \pi^*$ excitations. Molecules containing atoms with lone-pair electrons can also have $n \rightarrow \pi^*$ transitions, in which n indicates the MO with a localized pair of electrons on a heteroatom. In a few cases, we can also have $\sigma \rightarrow \pi^*$ single excitations, although these are exotic in the low-lying valence region.

The role of 2h2p (in general $nhnp$) poles is to add correlation effects to the single excitation picture. For the sake of discussion, it is important to classify (loosely) the correlation included by 2h2p states as static and dynamic. Static correlation is introduced by those double excitations

Figure 6.3 Dependence of the 1h1p triplet (solid line) and singlet (dashed line) excitation energies of one excitation of ethene with increasing number of double excitations. Calculations are done with D-ALDA/AC-LDA. Excitation energies are in eV.



having a contribution similar to the single excitations for a given state. This requires that the 1h1p excitations and the 2h2p excitations are energetically near and have a strong coupling between the two (Fig. 6.2.) We will refer to such states as multireference states. Dynamical correlation is a subtler effect. Its description requires a much larger number of double excitations, in order to represent the cooperative movement of electrons in the excited state.

For the low-lying multireference states found in the molecules of our set, a few double excitations are required for an adequate first approximation. Organic chromophores of the group (i) and (ii) have a characteristic low-lying multireference valence state (commonly called the L_b state in the literature) of the same symmetry as the ground-state. The L_b state is well known for having important contributions from double excitations of the type $(\pi_\alpha, \pi_\beta) \rightarrow (\pi_\alpha^*, \pi_\beta^*)$, thereby allowing mixing with the ground state. Some contributions of double excitations from σ orbitals might also be important to describe relaxation effects of the orbitals in the excited state that cannot be accounted by the self-consistent field orbitals [56].

The different effects of the 2h2p excitations that include dynamic and static correlation are clearly seen in the changes of the 1h1p adiabatic energies when we increase the number of double excitations. As an example, we take two states of ethene, one triplet and singlet 1h1p excitations, for which we systematically include a larger number of 2h2p states. The results for the D-ALDA/AC-LDA approach are shown in Fig. 6.3. We plot the adiabatic 1h1p states for which we include one 2h2p excitation at a time until 35, after which the steps are taken adding

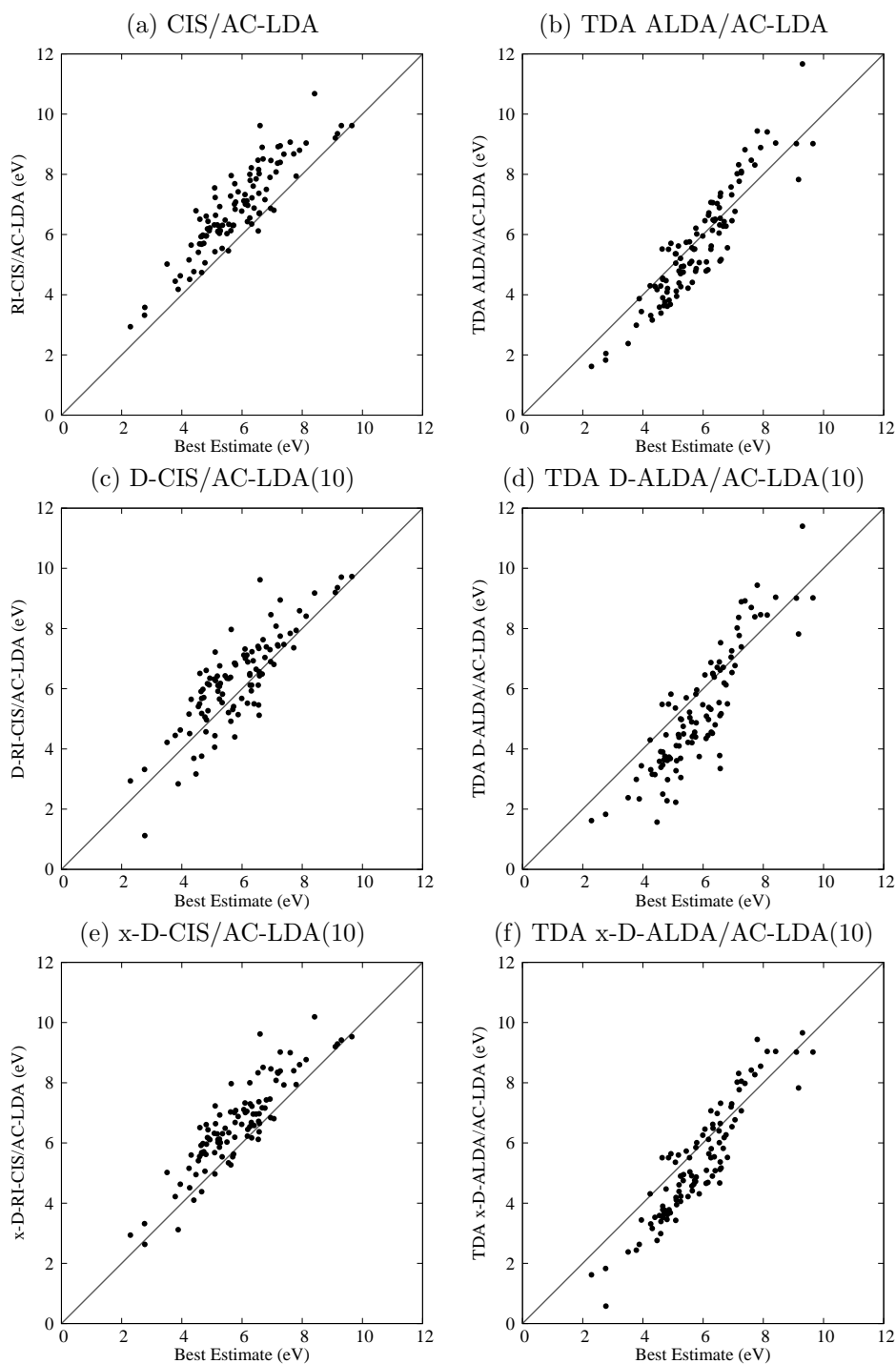
ten 2h2p states at a time. When a few 2h2p states are added, we observe that the excitation energy remains constant. This is due to the high symmetry of the molecule, which 2h2p states are not mixed with 1h1p states by symmetry selection rules. It is only when we add 32 double excitations when we see a sudden change of the excitation energy of both triplet and singlet states. This indicates that we have included in our space the necessary 2h2p poles to describe the static correlation of that particular state. Static correlation has a major effect in decreasing the excitation energy with only few number of 2h2p excitations. In this specific case, the triplet excitation energy decreases by 0.54 eV while the singlet excitation energy decreases by 0.82 eV. In this case, all static 2h2p poles are added, and a larger number of these poles does not lead to further sudden changes. The excitations are almost a flat line, with a slowly varying slope. This is the effect of the dynamic correlation, which includes extra correlation effects but which does not suddenly vary the excitation energy.

A-TDDFT includes some correlation effects in the 1h1p states, both of static and dynamic origin. However, it misses completely the states of main 2h2p character. These states are explicitly included by the D-TDDFT kernel. Additionally, D-TDDFT includes extra correlation effects into the A-TDDFT 1h1p states through the coupling of 1h1p states with the 2h2p states. This can lead to double counting of correlation, i.e., the correlation already included by A-TDDFT can be reintroduced by the coupling with the 2h2p states, leading to an underestimation of the excited state. In order to avoid double counting of correlation, it is of paramount importance to have a deep understanding of which correlation effects are included in each of the blocks that are used to construct the D-TDDFT xc-kernel. Therefore, we have compared the different D-TDDFT kernels with a reference method of the same level of theory, but from which the results are well understood. This is provided by some variations of the *ab initio* method CISD, since the mathematical form of the equations is equivalent to the TDA approximation of D-TDDFT. Standard CISD has coupling with the ground state, which we have not included in D-TDDFT. Therefore, we have made some variations on the standard CISD (Sec. 6.2.2.) We call these variations D-CIS and x-D-CIS, according to the definition of the \mathbf{A}_{22} block. In both methods, the 1h1p block \mathbf{A}_{11} is given by the CIS expressions, which does not include any correlation effect (recall that in response theory, correlation also appears in the singles-singles coupling block.) The correlation effects in D-CIS and x-D-CIS are included only through the coupling between 1h1p and 2h2p states. This will provide us with a good reference for rationalizing the results of A-TDDFT versus D-TDDFT.

Our implementation of CIS and (x-)D-CIS is done in DEMON2K. Therefore, all CI calculations actually refer to RI-CI and are based on a DFT wavefunction. We have calculated the absolute error between HF-based CIS excitation energies (performed with GAUSSIAN [206]) and CIS/AC-LDA excitation energies for the molecules in the test set. We have found little differences, giving an average absolute error is 0.18 eV with a standard deviation of 0.13 eV and a maximum absolute difference of 0.54 eV. It is interesting to note that almost all CIS/AC-LDA excitations are slightly below the corresponding HF-based CIS results.

We now discuss the results for singlet excitation energies of A-TDDFT and D-TDDFT. Since the number of states is large, we will discuss only general trends in terms of correlation graphs for each of the methods used with respect to the benchmark values provided in Refs. [257,278]. Our discussion will mainly focus on singlet excitation energies. For the numerical values of triplets, singlets, and oscillator strengths for each specific molecule, the reader is referred to Table I of the supplementary material.

Figure 6.4 Correlation graphs of singlet excitation energies for different flavors of D-CIS and D-TDDFT with respect to best estimates. Excitation energies are given in eV.



We first discuss the results of the adiabatic theories (i.e., ω -independent) CIS/AC-LDA and TDA ALDA/AC-LDA, shown in graphs (a) and (b) of Fig. 6.4 respectively. None of these theories includes 2h2p states, although ALDA includes some correlation effects in the 1h1p states through the xc-kernel. We see that CIS overestimates all excitation energies with respect to the best estimates. This is consistent with the fact that CIS does not include any correlation effects. The mean absolute error is 1.04 eV with a standard deviation of 0.63 eV. The maximum error is 3.02 eV. A better performance of the ALDA is observed. We see that ALDA underestimates most of the excitation energies, especially in the low-energy region. A similar conclusion was drawn by Silva-Junior *et al.* [278], who applied the pure BP86 xc-kernel to the molecules of the same test set. Nonetheless, the overall performance of the ALDA is clearly superior over CIS, giving an average absolute error of 0.67 eV with a standard deviation of 0.44 eV. The maximum absolute error of is 2.37 eV.

When we add explicit double excitations to CIS and A-TDDFT, we add correlation effects to the 1h1p picture and the excitation energies decrease. We have truncated the number of 2h2p states to 10 double excitations, in order to avoid the double counting of correlation in the D-TDDFT methods and in order to keep the calculations tractable. However, we realize that with our primitive implementation, the use of only 10 2h2p states may not include all static correlation necessary to correct all the states, especially for higher-energy 1h1p states.

As we have shown in Sec. 6.2.2, there is more than one way to include the 2h2p effects. We first consider the D-CIS/AC-LDA(10) and TDA D-ALDA/AC-LDA(10) variants, shown in graphs (c) and (d) of Fig. 6.4, in which we approximate the double-double block by a diagonal zeroth-order KS orbital energy difference. In both cases, we observe that the results get worse with respect to those of CIS or ALDA. This degradation is especially important for D-ALDA(10) and might be interpreted as due to double counting of correlation. Already, ALDA underestimates the excitation energies of most states. With the introduction of double excitations, we introduce extra correlation effects, which underestimates even more the excitations. In some cases, like *o*-benzoquinone, some excitation energies falls below the reference ground-state, possibly indicating the appearance of an instability. The average absolute error of the D-ALDA(10) is 1.03 eV with a standard deviation of 0.73 eV and a maximum error of 3.51 eV, decreasing the description of 1h1p states with respect to ALDA or CIS. As to D-CIS(10), the results are slightly better. The average absolute error is 0.78 eV with a standard deviation of 0.54 eV and a maximum error of 3.02 eV, improving over the CIS results. However, some singlet excitation energies are smaller than the corresponding triplet excitation energies and some state energies are now largely underestimated. This also indicates an overestimation of correlation effects, though it might be partially due to the missing \mathbf{A}_{02} block.

A better estimate of the 2h2p correlation effects is given when the \mathbf{A}_{22} block is modified to include the first-order correction to the HF orbital energy differences. This type of calculation is what we call x-D-CIS/AC-ALDA(10) and x-D-TDDFT/AC-ALDA(10), the results of which are shown respectively in graphs (e) and (f) of Fig. 6.4. In both cases we observe an improvement of the excitation energies. The x-D-CIS provides a more consistent and systematic estimation of correlation effects, and most of the excitations are still an upper limit to the best estimate result. However, the mean absolute error is still high, with an average absolute error of 0.84 eV and a standard deviation of 0.58 eV and a maximum error of 3.02 eV. The x-D-TDDFT results slightly improve over x-D-CIS, giving a mean absolute error of 0.83 eV with a standard deviation of 0.46 eV and a maximum error of 2.19 eV. The superiority of x-D-TDDFT is explained by the

fact that TDDFT includes some correlation effects in the 1h1p block. However, x-D-TDDFT still gives in overall larger errors than A-TDDFT. This might be again a problem of double-counting of correlation. Since A-TDDFT with the ALDA xc-kernel underestimates most excitation energies, the application of x-D-TDDFT leads to a further underestimation. In any case, D-TDDFT works better when 2h2p states are given by the first-order correction to the HF orbital energy difference.

From the schematic representation of the interaction between 1h1p states and 2h2p states (Fig. 6.2), we can rationalize why we observe overestimation of correlation when the \mathbf{A}_{22} block is approximated as an LDA orbital energy difference. The 2h2p states as given by the LDA fall too close together and too close to the 1h1p states (i.e., a too large value of Δ). The results show large correlation effects in the 1h1p states, indicating an overestimation of static correlation effects. The first-order correction to the KS orbital energy difference gives a better estimate of correlation effects. The reverse effect was observed in the context of HF-based response theory. In SOPPA calculations, the 2h2p states are approximated as simple HF orbital energy differences, which are placed far too high, therefore underestimating correlation. In HF-based response, it was also seen that the results are improved when adding the first-order correction to the HF orbital energy differences.

Up to this point, we have seen that D-TDDFT works best when 2h2p states are given by the first-order correction to the HF orbital energy differences. However, we have also seen that the LDA xc-kernel underestimates the 1h1p states, so that we degrade the quality of the A-TDDFT states when we apply any of the D-TDDFT schemes. A better estimate for the 1h1p states is given by an adiabatic hybrid calculation. In Fig. 6.5 (a) we show the calculation of our implementation of the hybrid xc-kernel based upon a LDA wavefunction. In this hybrid we use 20% HF exchange. This percentage is the usual amount used in most popular functionals, both for ground- and for excited state calculations [90, 91, 95, 302, 303]. The results show an improvement over all our previous calculations. The average absolute error of 0.43 eV with respect to the best estimates and a standard deviation of 0.34 eV. The maximum error is 1.44 eV. Figure 6.5 (b) shows the x-D-HYBRID(10) calculation. The mean error and the standard deviation are very similar to what the adiabatic hybrid calculation gives. The average absolute error with respect to the best estimate is 0.45 eV, and the standard deviation is 0.33 eV with a maximum error of 1.44 eV. This is a very important result, since we have been able to include the missing 2h2p states without decreasing the quality of 1h1p states.

In Table 6.2 we summarize the mean absolute errors, standard deviations and maximum errors for all the methods. The best results are given by the hybrid A-TDDFT calculation, closely followed by the x-D-TDDFT based also on the hybrid. We can therefore state that the best D-TDDFT kernel can be constructed from a hybrid xc-kernel in the \mathbf{A}_{11} block and the first-order correction to the HF orbital energy differences for \mathbf{A}_{22} .

The results given by the different D-TDDFT kernels show a close relation between the \mathbf{A}_{11} and \mathbf{A}_{22} blocks. Our results show that the singles-singles block is better given by a hybrid xc-kernel and the doubles-doubles block is better approximated by the first-order correction to the HF orbital energy difference. By simple perturbative arguments, we have rationalized that the \mathbf{A}_{22} block as given by the first-order approximation accounts better for static correlation effects. Less clear explanations can be given to understand why a hybrid xc-kernel gives the best approximation for the \mathbf{A}_{11} block, although it seems necessary for the construction of a consistent kernel.

Figure 6.5 A-TDDFT and x-D-TDDFT correlation graphs for singlet excitation energies using the hybrid xc-kernel of Eq. (6.8), in which $c_0 = 0.2$.

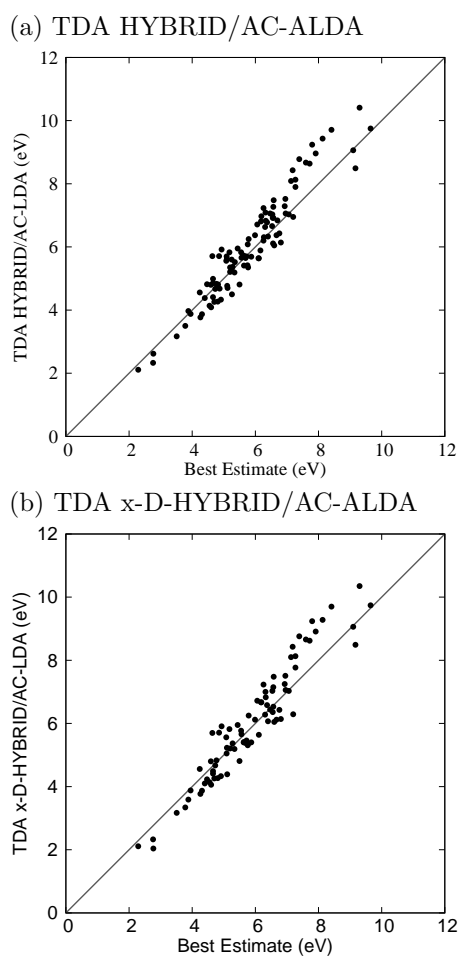


Table 6.2 Summary of the mean absolute errors, standard deviation and maximum error of each method. All quantities are in eV.

Method	Mean error	Std. dev.	Max. error
ALDA	0.67	0.44	2.37
D-ALDA(10)	1.03	0.73	3.51
x-D-ALDA(10)	0.83	0.46	2.19
CIS	1.04	0.63	3.02
D-CIS(10)	0.78	0.54	3.02
x-D-CIS(10)	0.84	0.58	3.02
HYBRID	0.43	0.34	1.44
x-D-HYBRID(10)	0.45	0.33	1.44

Table 6.3 Singlet 1h1p excitation energies and mean absolute errors (with respect to the CASPT2, in parenthesis) for the excited states with more than 10% contribution of 2h2p state. For a graphical representation, see Fig. 6.6. The extended dressed calculations are done including 10 double excitations. All energies and absolute errors are in eV.

Molecule	State	CASPT2	ALDA	HYBRID	BHLYP	RI-CIS	x-D-ALDA	x-D-HYBRID	x-D-CIS
Butadiene	2^1A_g	6.27	6.32 (0.05)	6.92 (0.65)	7.61 (1.34)	8.52 (2.25)	4.67 (1.6)	6.36 (0.09)	6.72 (0.45)
Hexatriene	2^1A_g	5.20	5.05 (0.15)	5.70 (0.50)	6.66 (1.46)	7.84 (2.64)	3.43 (1.87)	5.05 (0.15)	5.68 (0.48)
Octatetraene	2^1A_g	4.38	4.17 (0.21)	4.82 (0.44)	5.83 (1.45)	7.07 (2.69)	2.76 (1.62)	4.23 (0.15)	4.95 (0.57)
Cyclopentadiene	2^1A_1	6.31	6.14 (0.17)	6.63 (0.32)	7.23 (0.92)	8.51 (2.2)	4.90 (1.41)	6.28 (0.03)	6.68 (0.37)
Naphthalene 1	3^1A_g	6.04	6.28 (0.12)	6.37 (0.33)	7.70 (1.66)	8.90 (2.86)	5.82 (0.22)	6.12 (0.08)	7.17 (1.13)
Naphthalene 2	3^1B_{3u}	7.18	7.71 (0.53)	8.67 (1.49)	9.84 (2.66)	12.21 (5.03)	7.14 (0.04)	8.63 ¹ (1.45)	9.52 (2.34)
s-tetrazine 1	3^1B_{1g}	6.20	6.38 (0.18)	7.04 (0.84)	9.20 (3.00)	11.96 (5.76)	6.38 (0.18)	7.04 ² (0.84)	11.48 (5.28)
s-tetrazine 2	2^1B_{3g}	8.12	8.10 (0.02)	8.58 (0.46)	9.96 (1.84)	10.53 (2.33)	8.10 (0.02)	8.58 ³ (0.46)	10.77 (2.65)

The main interest of using a D-TDDFT kernel is to obtain the pure 2h2p states, which are not present in A-TDDFT and to better describe the 1h1p states of strong multireference character. We now take a closer look at the latter states in our test set. In particular, we will compare against the benchmarks those 1h1p states that have a 2h2p contribution larger than 10% (this percentage is determined by the CCSD calculation of Ref. [257].) The molecules containing such states are the four polyenes of the set, together with cyclopentadiene, naphthalene and *s*-triazine. From this sub-set, the polyenes are undoubtedly the ones which have been the most extensively discussed. Some debate persists as to whether A-TDDFT is able to represent a low-lying localized valence state which have a strong 2h2p contribution of the transition promoting two electrons from the highest- to the lowest-occupied molecular orbital. It was first shown by Hsu *et al.* that A-TDDFT with pure functionals gives the best answer for such states [261], catching both the correct energetics and the localized nature of the state. Starcke *et al.* recognize this to be a fortuitous cancellation of errors [258].

In Fig. 6.6 we show the results for the different adiabatic and dressed theories used in this work. For the numerical values of the excitation energies and the absolute errors for each state, see Table 6.3. In the top graph of Fig. 6.6 we show the behavior of CIS (100% HF exchange) and A-TDDFT with different hybrids: ALDA with 0% HF exchange, ALDA with 20% HF exchange and B3LYP which has 50% HF exchange. In this comparison, we take the CASPT2 results (stars) as the benchmark result, since the best estimates were not provided for all the studied states [257]. As seen in the graph, CIS (filled circles) seriously overestimate the excitation energies, consistent with the fact that it does not include any correlation effect. A-TDDFT with pure functionals give the best answer for doubly-excited states, very close to the CASPT2 result. This confirms the observation of Hsu *et al.* [261] Hybrid functionals, though giving the best overall answer, do not perform as well for these states. Additionally, the more HF exchange is mixed into the xc-kernel, the worse the result is. A different situation appears when we include explicitly 2h2p states. In Fig. 6.6 (b), we show the results of x-D-CIS and x-D-TDDFT. Now, the x-D-ALDA(10) underestimates the multireference excitation energies, due to overcounting of correlation effects. The best answer is now given by x-D-HYBRID(10) with 20% HF exchange. The x-D-CIS stays always higher. One can notice that the three last excitations (naphthalene 2 and *s*-triazine 1 and 2) are best described by the x-D-ALDA(10). The lack of correction might be due to the lack of inclusion of the appropriate double excitation. To check this we added 50 doubles to naphthalene and 75 doubles to *s*-tetrazine. The error of the x-D-TDDFT result was 0.18 eV for naphthalene 2, 0.07 eV for *s*-tetrazine 1 and 0.02 eV for *s*-tetrazine 2. This is consistent with our hypothesis. In future versions of the code, a pre-screened selection of double excitations will be implemented, which is required to avoid to some extent this problem.

6.2.6 Conclusion

D-TDDFT was introduced by Maitra *et al.* to explicitly include 2h2p states in TDDFT. The original work was *ad hoc*, leaving much room for variations on the original concept. A limited number of applications by Burke and coworkers [43, 44] as well as by Mazur *et al.* [150, 277] showed promising results for D-TDDFT, but could hardly be considered definitive because (i) of the limited number of molecules and excitations treated and (ii) because the importance of

the details of the specific implementations of D-TDDFT were not adequately explored. The present article has gone far towards remedying these problems, and providing further support for D-TDDFT.

We have implemented several variations of D-TDDFT and RI-CI in DEMON2K, with the aim of characterizing the minimum necessary ingredients for an effective implementation of D-TDDFT. We have seen that DFT-based CIS gives very similar answers to HF-based CIS, showing that the effects of exact (HF) exchange can indeed be added in a post-SCF calculation. We have also found that although the ALDA works better than CIS, it underestimates most of the excitation energies. Therefore, when we explicitly include 2h2p states through the D-TDLDA, it leads to worse results, due to the double counting of correlation. The x-D-ALDA give the least scatter of the results and hence a better answer. Nevertheless, the lower errors are still given by the ALDA.

With the results of the ALDA, we have shown that it is important to have a correct relative position of the 1h1p and the 2h2p manifolds in order to have a consistent account of correlation. We have introduced a hybrid TDDFT as a post-LDA calculation, and we have shown that the results are superior to those of ALDA. We have determined that the method giving the best answer for MR states is the combination of a hybrid xc-kernel with 2h2p (double) excitations approximated by first-order corrections to the HF orbital energy differences.

Our work has gone much farther than previous work in testing D-TDDFT and in detailing the necessary ingredients to make it work well, We find a hybrid approach to be essential. We recognize that our work could be improved by a perturbative pre-selection procedure and consider this work to be ample justification for a more elaborate implementation of D-TDDFT. This work also constitutes a key step towards a full implementation of the polarization propagator model of the exact $f_{xc}(\omega)$.

6.2.7 Acknowledgments

We would like to thank Bhaarathi Natarajan for helpful discussion. M. H. would like to acknowledge a scholarship from the French Ministry of Education. Those of us at the *Université Joseph Fourier* would like to thank Denis Charapoff, Régis Gras, Sébastien Morin, and Marie-Louise Dheu-Andries for technical support at the (DCM) and for technical support in the context of the *Centre d'Expérimentation du Calcul Intensif en Chimie (CECIC)* computers used for some of the calculations reported here. This work has been carried out in the context of the French Rhône-Alpes *Réseau thématique de recherche avancée (RTRA): Nanosciences aux limites de la nanoélectronique* and the Rhône-Alpes Associated Node of the European Theoretical Spectroscopy Facility (ETSF). A. R. acknowledges funding by the Spanish MEC (FIS2007-65702-C02-01), ACI-promociona project (ACI2009-1036), "Grupos Consolidados UPV/EHU del Gobierno Vasco" (IT-319-07), the European Research Council through the advance grant DY-Namo (267374), the MICINN project (FIS2010-21282-C02-01), and the European Community through projects e-I3 ETSF (Contract No. 211956) and THEMA (228539).

6.2.8 Appendix A: Kohn-Sham-based Second-Order Propagator

In this appendix, we summarize the main expressions for the construction of the matrix elements of Eqs. (6.6) and (6.10). For a detailed derivation, the reader is referred to Ref. [140], in which this equations were derived for the construction of an exact *ab initio* xc-kernel consistent to second-order in perturbation theory.

The explicit expression for the single-single block is given by

$$\begin{aligned}
[A_{11}]_{ai,bj} = & \quad (6.13) \\
& \left[\epsilon_a \delta_{ab} + (a|\hat{M}_{xc}|b) - \sum_l \frac{(a|\hat{M}_{xc}|l)(l|\hat{M}_{xc}|b)}{\epsilon_l - \epsilon_a} - \frac{1}{2} \sum_{mld} \frac{(ld||mb)(dl||ma)}{\epsilon_m + \epsilon_l - \epsilon_d - \epsilon_a} \right] \delta_{ij} \\
& - \left[\epsilon_i \delta_{ij} + (i|\hat{M}_{xc}|j) - \sum_d \frac{(i|\hat{M}_{xc}|d)(d|\hat{M}_{xc}|j)}{\epsilon_i - \epsilon_d} - \frac{1}{2} \sum_{lke} \frac{(le||jd)(dl||ei)}{\epsilon_i + \epsilon_l - \epsilon_d - \epsilon_e} \right] \delta_{ab},
\end{aligned}$$

the single-double block is given by

$$\begin{aligned}
[A_{12}]_{ck,aibj} = & \delta_{kj}(bc||ai) - \delta_{ki}(bc||aj) \\
& + \delta_{ac}(bi||kj) - \delta_{bc}(ai||kj), \quad (6.14)
\end{aligned}$$

and the double-double block is given by

$$[A_{22}]_{aibj,ckdl} = (\epsilon_b + \epsilon_a - \epsilon_i - \epsilon_j) \delta_{ac} \delta_{ik} \delta_{bd} \delta_{jl}. \quad (6.15)$$

there $(pq||rs) = (pq|rs) - (qs|rq)$, where

$$(pq|rs) = \int d^3r d^3r' \psi_p^*(\mathbf{r}) \psi_q(\mathbf{r}) \frac{1}{|\mathbf{r} - \mathbf{r}'|} \psi_r^*(\mathbf{r}') \psi_s^*(\mathbf{r}'). \quad (6.16)$$

The first-order double-double block is given by

$$\begin{aligned}
[A_{22}]_{aibj,ckdl} = & \quad (6.17) \\
& \left[(\epsilon_b \delta_{bd} + (b|\hat{M}_{xc}|d)) \delta_{ac} + (\epsilon_a \delta_{ac} + (a|\hat{M}_{xc}|c)) \delta_{bd} \right] \delta_{ik} \delta_{jl} \\
& - \left[(\epsilon_i \delta_{ik} + (i|\hat{M}_{xc}|k)) \delta_{jl} - (\epsilon_j \delta_{jl} + (d|\hat{M}_{xc}|l)) \delta_{ik} \right] \delta_{ac} \delta_{bd} \\
& - \delta_{ac} h(bd) - \delta_{bd} h(ac) + \delta_{ad} h(bc) + \delta_{bc} h(ad) - \delta_{ac} \delta_{bd} (kj||li) - \delta_{jl} \delta_{ki} (ad||bc),
\end{aligned}$$

with

$$h(pq) = \delta_{ik}(lj||pq) + \delta_{jl}(ki||pq) - \delta_{kj}(li||pq) - \delta_{il}(kj||pq). \quad (6.18)$$

Integrals with double bar are defined as in Eq. (6.3), in which the kernel f_H is changed with the kernel $f(\mathbf{r}_1, \mathbf{r}_2) = (1 - \hat{P}_{12})/|\mathbf{r}_1 - \mathbf{r}_2|$, where \hat{P}_{12} is the permutation operator that permutes the coordinates of two electrons.

6.3 Conclusions and Perspective

In this chapter, we have evaluated the validity of a hybrid TDDFT kernel that generally includes double excitations. The hybrid kernel consists of an adiabatic functional with the many-body terms that couple single and double excitations [see Chap. 5.] This kernel generalizes the dressed kernel of Maitra *et al.* [43, 44], and it is efficient enough to be applied to medium and large size systems.

There are several definitions of the dressed kernel, depending on the choice of adiabatic functional and the choice of the frequency-dependent terms. We tested several combinations by comparing the quality of singlet excitation energies of 28 organic chromophores against high quality *ab initio* results. The results with lower errors were obtained when the dressed kernel consisted of an hybrid adiabatic functional containing a portion of about 25% HF exchange, and the first-order corrected double excitations in the frequency-dependent terms.

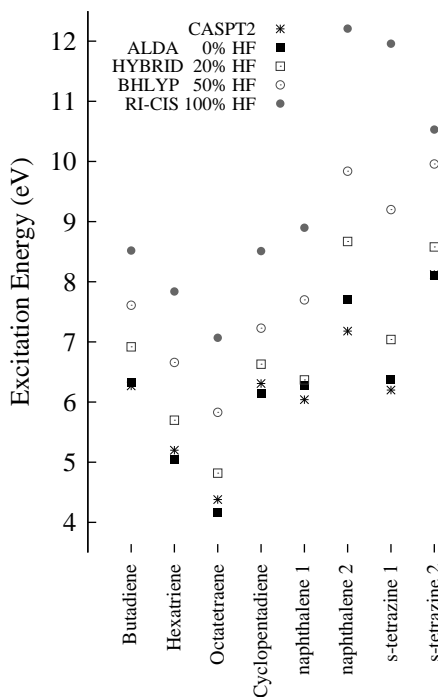
The main problem of the hybrid kernel is the double counting of correlation. This is due to the fact that the adiabatic functional includes correlation (specially of self-energy type diagrams) that is also included in the frequency-dependent terms. In the calculation, we simply avoided this problem by adding a restricted number of double excitations. A better strategy would be to include a pre-screening of double excitation and including only the ones that strongly couples with single excitations. Like the hybrid DFT kernels, some parameterization would be necessary to determine the correct number of double excitations in general. One way is to apply an “importance factor”

$$\eta^D = \sum_S \frac{|\langle S | \hat{H}^e | D \rangle|^2}{E_D - E_S}, \quad (6.19)$$

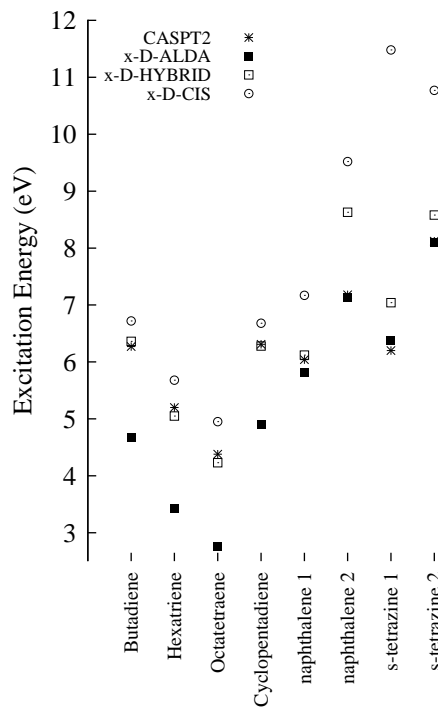
where $S(D)$ is a single(double) wave function, and $E_{S(D)}$ is the state energy. Only the double excitations with an importance factor bigger than a threshold value N , $\eta^d > N$, will be included in the calculation. The threshold value N is to be determined in general by testing the quality of the excitation energies with different threshold values for a large set of molecules. Tests to determine the N value are going on.

Figure 6.6 Effect on excited states with more than 10% of 2h2p character of mixing HF exchange in TDDFT. CASPT2 results from Ref. [257] are taken as the benchmark. BHLYP results are taken from Ref. [278].

(a) Single excitations with CIS and A-TDDFT



(b) Single excitations with D-CIS and D-TDDFT



Part III

Future Prospects and Conclusions

Chapter 7

Coupling between the Reference and the Excitations

7.1 Introduction

The dressed kernel of Chap. 6 showed promising results, although it is not yet apt for its application to problems of photochemical interest. Purposely, we furnished the terms coupling single and double excitations. However, no coupling between the excitations and the reference was taken into account. Specifically, the diagrams in Figs. 5.20, 5.21 and 5.22 were not included in our initial formulation of the kernel. These diagrams are fundamental for describing avoided crossings and conical intersections which involve the ground state (which is normally the case.) In this chapter, we explore the possibility of including an extra term to the dressed TDDFT kernel that accounts for these effects.

The coupling terms between double excitations and the reference are not directly taken from the polarization propagator, since these involve Møller-Plesset formulae, which are computationally very costly. Instead, we take advantage of the fact that the TDA approximation to the polarization propagator is equivalent to CISD to include these couplings from the latter [see Eq. (2.40).] To test the ability of such a mixed kernel, we calculate the S_1/S_2 conical intersection of the ethylene twisting. This conical intersection appears thanks to an avoided crossing between S_0 and S_2 . To our knowledge, this is the first time that such interaction is taken into account in TDDFT.

7.2 S_1/S_2 Conical Intersection of Ethylene (in preparation)

Assessment of spin-flip and dressed time-dependent density-functional theory to describe the S_1/S_2 conical intersection of ethylene along the twisting coordinate

Miquel Huix-Rotllant^{1,†}, Mark E. Casida^{1,*}

¹ *Laboratoire de Chimie Théorique,
Département de Chimie Moléculaire (DCM, UMR CNRS/UJF 5250),
Institut de Chimie Moléculaire de Grenoble (ICMG, FR2607),
Université Joseph Fourier (Grenoble I),
301 rue de la Chimie, BP 53,
F-38041 Grenoble Cedex 9, France*

Time-dependent density-functional theory (TDDFT) is widely recognized as an efficient route towards the excited states. TDDFT is formally exact, though in practice approximations of the exchange correlation functional are required. Most TDDFT functionals use the adiabatic approximation, which misses important features such as the 2-hole/2-particle (2h2p) excitations. This prevents the application of TDDFT to photochemical problems. Recently, improved TDDFT methods have been developed that could potentially be applied to photochemistry, such as the spin-flip (SF) method. SF-TDDFT couples excitations that change the spin multiplicity by ± 1 . Starting from a triplet reference, the ground-state and one 2h2p state are accessed through excitation. However, SF-TDDFT can only include one 2h2p state at a time. A more general method is the dressed TDDFT (D-TDDFT) kernel of linear response TDDFT, which mixes adiabatic functionals with many-body derived terms that introduce the missing 2h2p states. When this mixture of kernels is properly done, the dressed kernel accounts correctly both for 1h1p and 2h2p excitations, while still keeping much of the efficiency of TDDFT. In this article, we make a step forward towards the application of TDDFT to photochemistry by applying SF-TDDFT and D-TDDFT to describe the intersection point between the first two singlet excited states of ethylene along the CH₂ twisting coordinate. The two surfaces are degenerate when one of the CH₂ group is twisted 90° with respect to the other. This cannot be represented by any adiabatic TDDFT functional, since the S₂ surface, of main 2h2p character, is missing. We show that D-TDDFT describes the S₂ curve, but the S₁/S₂ degeneracy is not well represented since the excitation energy of 2h2p states is largely underestimated. This is remedied by including an extra coupling term in the dressed kernel that accounts for the interaction of 2h2p excitations with the reference state. The SF-TDDFT describes best the intersection, but the S₂ surface is unevenly represented all along the coordinate.

† Corresponding author: Miquel.Huix@gmail.com

* Corresponding author: Mark.Casida@UJF-Grenoble.Fr

7.2.1 Introduction

Time-dependent density-functional theory (TDDFT) offers an efficient route to calculate excited states. TDDFT was made formally exact by Runge and Gross [13]. In practice, one is obliged to apply approximations to the unknown exchange-correlation (xc) functional. Most calculations apply the so-called adiabatic approximation, in which the xc effects are calculated supposing that the density reacts instantaneously and without memory to temporal deformations. In this approximation, some important physical effects are not well described, which limits the applicability of TDDFT. In particular, the correlation in the excited states is crudely calculated due to the lack of double excitation poles in the TDDFT response function. This forbids the application of TDDFT to problems like photochemistry.

In quantum chemistry, the TDDFT equations are solved in the linear response (LR) regime. A suitable form of LR-TDDFT is the formulation of Casida [17], in which the equations are cast in a random phase approximation (RPA) form,

$$\begin{bmatrix} \mathbf{A}(\omega) & \mathbf{B}(\omega) \\ -\mathbf{B}(\omega) & -\mathbf{A}(\omega) \end{bmatrix} \begin{bmatrix} \mathbf{X}(\omega) \\ \mathbf{Y}(\omega) \end{bmatrix} = \omega \begin{bmatrix} \mathbf{X}(\omega) \\ \mathbf{Y}(\omega) \end{bmatrix}, \quad (7.1)$$

where the matrix elements of the $\mathbf{A}(\omega)$ and $\mathbf{B}(\omega)$ matrices are defined as

$$\begin{aligned} [A(\omega)]_{ai,bj} &= (\epsilon_a - \epsilon_i)\delta_{ij}\delta_{ab} + (ia|f_{Hxc}(\omega)|bj) \\ [B(\omega)]_{ai,bj} &= (ia|f_{Hxc}(\omega)|jb), \end{aligned} \quad (7.2)$$

in which the ϵ_p are the Kohn-Sham (KS) eigenvalues, and $f_{Hxc}(\omega)$ is the exact Hartree-exchange-correlation kernel. Throughout, the indexes i, j, \dots correspond to occupied spin orbitals, a, b, \dots to unoccupied spin orbitals and p, q, \dots can be either occupied or unoccupied. One extracts all the excitation energies of the system from Eq. (7.1). The Tamm-Dancoff approximation (TDA) of TDDFT has been shown to give better potential energy surfaces (PES), at the expense of having only approximate energy-weighted sum rules. The TDA consists in setting the $\mathbf{B}(\omega) = \mathbf{0}$, that is, decoupling excitations and de-excitations. The LR-TDDFT equations are then simply

$$\mathbf{A}(\omega)\mathbf{X}(\omega) = \omega\mathbf{X}(\omega). \quad (7.3)$$

Both Eqs. (7.1) and (7.3) have the same number of solutions when the exact kernel is used in Eq. (7.2). In practice, most calculations use the adiabatic approximation of the exchange-correlation kernel, which is given by

$$f_{xc}^{AA}(\mathbf{r}, \mathbf{r}') = \frac{\delta E_{xc}[\rho_t]}{\delta \rho_t(\mathbf{r})\delta \rho_t(\mathbf{r}')}, \quad (7.4)$$

where ρ_t represents the instantaneous density at time t . This kernel is frequency independent. This makes the matrices \mathbf{A} and \mathbf{B} frequency independent, and the number of solutions equals the number of single excitations, therefore losing 2-hole/2-particle (2h2p) and higher excitations.

There exist several methods in the literature that go beyond the adiabatic approximation. Two promising candidates that could be applied to photochemical problems are spin-flip TDDFT method [42, 193] and dressed TDDFT [43, 44]. Presently, spin-flip TDDFT can only add a few double excitations, whereas dressed TDDFT can include any number of double excitations [140]. In this article, we assess the ability of both methods to describes the S_1/S_2 conical intersection that occurs in the twisting of ethene.

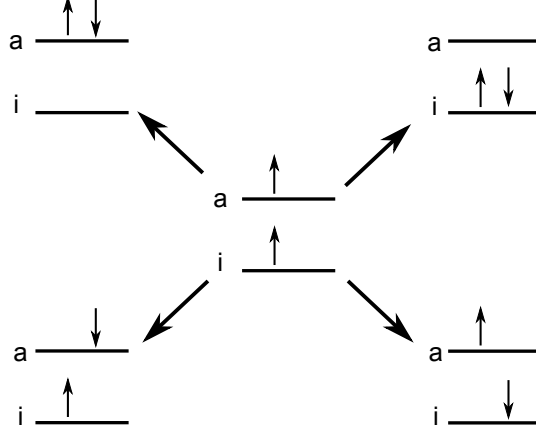
This article is organized as follow. Sec. 7.2.2 describes the spin-flip and dressed TDDFT methods, Sec. 7.2.3 specify the computational details, Sec. 7.2.4 contains the results. Sec. 7.2.5 concludes.

7.2.2 Theoretical Method

In this section, we briefly describe the two methods used in this article, namely, spin-flip TDDFT and dressed TDDFT.

7.2.2.1 Spin-flip TDDFT

Spin-flip TDDFT (SF-TDDFT) was introduced by Krylov *et al.* as a method to treat diradicals within the TDDFT framework [39]. However, in this section we will follow the formulation of Ziegler and Wang, which is the one we use in the calculations presented here [42, 193]. Ziegler and Wang proposed a SF-TDDFT method by generalizing the local spin-density functional $E_{xc}[\rho_+; \rho_-]$, to use non-collinear densities,

Figure 7.1 Pure spin spin-flip excitations from a triplet reference state.

$$\rho_+ = \frac{1}{2}(\rho + s)$$

$$\rho_- = \frac{1}{2}(\rho - s),$$

where the total noncollinear density is defined as

$$\rho = \rho_{\alpha,\alpha} + \rho_{\beta,\beta}, \quad (7.5)$$

and the noncollinear spin density is defined as

$$s = \sqrt{(\rho_{\alpha,\alpha} - \rho_{\beta,\beta})^2 + 2(\rho_{\alpha,\beta}^2 - \rho_{\beta,\alpha}^2)}. \quad (7.6)$$

On the collinear limit, $\rho_{\alpha,\beta} = \rho_{\beta,\alpha}$, one obtains the usual quantities. Taking the second functional derivative of $E_{xc}[\rho_+; \rho_-]$ with respect to the density and taking the collinear limit gives

$$\begin{bmatrix} f_{xc}^{\alpha,\alpha;\alpha,\alpha} & f_{xc}^{\alpha,\alpha;\beta,\beta} & f_{xc}^{\alpha,\alpha;\alpha,\beta} & f_{xc}^{\alpha,\alpha;\beta,\alpha} \\ f_{xc}^{\beta,\beta;\alpha,\alpha} & f_{xc}^{\beta,\beta;\beta,\beta} & f_{xc}^{\beta,\beta;\alpha,\beta} & f_{xc}^{\beta,\beta;\beta,\alpha} \\ f_{xc}^{\alpha,\beta;\alpha,\alpha} & f_{xc}^{\alpha,\beta;\beta,\beta} & f_{xc}^{\alpha,\beta;\alpha,\beta} & f_{xc}^{\alpha,\beta;\beta,\alpha} \\ f_{xc}^{\beta,\alpha;\alpha,\alpha} & f_{xc}^{\beta,\alpha;\beta,\beta} & f_{xc}^{\beta,\alpha;\alpha,\beta} & f_{xc}^{\beta,\alpha;\beta,\alpha} \end{bmatrix} = \begin{bmatrix} f_{xc}^{\alpha;\alpha} & f_{xc}^{\alpha;\beta} & 0 & 0 \\ f_{xc}^{\beta;\alpha} & f_{xc}^{\beta;\beta} & 0 & 0 \\ 0 & 0 & \frac{v_{xc}^{\alpha} - v_{xc}^{\beta}}{\rho_{\alpha} - \rho_{\beta}} & 0 \\ 0 & 0 & 0 & \frac{v_{xc}^{\alpha} - v_{xc}^{\beta}}{\rho_{\alpha} - \rho_{\beta}} \end{bmatrix} \quad (7.7)$$

The first block of four xc-kernels corresponds to the regular TDDFT, and the last two couples $\alpha \rightarrow \beta$ and $\beta \rightarrow \alpha$ excitations. The fact that the off-diagonal kernels are 0 makes most excitations spin contaminated. In Fig. 7.1, the only spin-pure SF excitations are shown, taking a triplet state as a reference.

7.2.2.2 Dressed TDDFT

Maitra, Burke and coworkers proposed an *ad hoc* correction to the adiabatic kernel to make it frequency dependent [43,44]. The initial kernel could couple one 2-hole/2-particle (2h2p) excitation to the 1h1p states at a time. One of us showed that the dressed kernel of Maitra *et. al.* was in fact an approximation of a more general kernel derived using many-body perturbation theory techniques [149]. The matrix elements of the general kernel were then derived in Ref. [140], in which the dressed kernel was clearly shown to be a special case. Following Ref. [140], the dressed kernel can be written as

$$f_{xc}^D(\mathbf{r}, \mathbf{r}'; \omega) = f_{xc}^{AA}(\mathbf{r}, \mathbf{r}'; \omega) + K^\omega(\mathbf{r}, \mathbf{r}; \mathbf{r}', \mathbf{r}'; \omega), \quad (7.8)$$

where the $K^\omega(\mathbf{r}, \mathbf{r}; \mathbf{r}', \mathbf{r}'; \omega)$ is the ω -dependent part of the kernel derived from the second-order polarization propagator of Oddershede and Jørgensen [45], where the zero-order Hamiltonian was the KS hamiltonian instead of the Hartree-Fock (HF) one.

The dressed kernel has several possible definitions, according to the exchange-correlation functional used for the f_{xc}^{AA} and the many-body kernel K^ω . In Ref. [260], we tested several possible combinations, arriving at the conclusion that only one combination could correctly describe both 1h1p and 2h2p excitations with enough accuracy. This consists of using a hybrid functional with 20%-25% HF exchange. The hybrid can be used exclusively in the TDDFT calculation, by changing the matrix elements of Eq. (7.2) to be,

$$\begin{aligned} A_{ai\sigma,bj\tau} &= \left[\epsilon_a^\sigma \delta_{ab} + c_0 \cdot (a|\hat{M}_{xc}|b) \right] \delta_{ij} \delta_{\sigma\tau} - \left[\epsilon_i^\sigma \delta_{ij} + c_0 \cdot (i|\hat{M}_{xc}|j) \right] \delta_{ab} \delta_{\sigma\tau} \\ &\quad + (ai|(1-c_0) \cdot f_x^{\sigma\tau} + c_0 \cdot \hat{\Sigma}_x^{HF} + f_{Hc}^{\sigma\tau}|jb) \\ B_{ai\sigma,bj\tau} &= (ai|(1-c_0) \cdot f_x^{\sigma\tau} + c_0 \cdot \hat{\Sigma}_x^{HF} + f_{Hc}^{\sigma\tau}|bj), \end{aligned} \quad (7.9)$$

where $\hat{\Sigma}_x^{HF}$ is the HF exchange operator and,

$$\hat{M}_{xc} = \hat{\Sigma}_x^{HF} - v_{xc}, \quad (7.10)$$

provides a first-order conversion of KS into HF orbital energies. The matrix elements of the K^ω kernel are given by

$$(ia|K^\omega(\omega)|bj) = \sum_{ckld}^{N_2} \frac{[H]_{ai,ckld}[H]_{ckld,jb}}{\omega \mathbf{1}_{22} - \omega_{cdkl}}, \quad (7.11)$$

where $\mathbf{1}_{22}$ is a unit matrix of the dimension of the 2h2p space, ω_{cdkl} is defined as

$$\omega_{cdkl} = \epsilon_c + \epsilon_d - \epsilon_k - \epsilon_l \langle \Psi_0^{KS} | \hat{a}_l^\dagger \hat{a}_d \hat{a}_k^\dagger \hat{a}_c \hat{H} \hat{a}_c^\dagger \hat{a}_k \hat{a}_d^\dagger \hat{a}_l | \Psi_0^{KS} \rangle,$$

and

$$[H]_{ia,ckld} = \langle \Psi_0^{KS} | \hat{a}_i^\dagger \hat{a}_a \hat{H} \hat{a}_c^\dagger \hat{a}_k \hat{a}_d^\dagger \hat{a}_l | \Psi_0^{KS} \rangle, \quad (7.12)$$

in which $|\Psi_0^{KS}\rangle$ is the KS wave-function and \hat{H} is the real Hamiltonian of the system. For explicit expressions for these blocks in the TDA approximation, the reader is referred to Appendix A of Ref. [260].

The solution of Eq. (7.3) with the dressed kernel Eq. (7.8) is numerically difficult, because of the non-linearity of the equations. In Ref. [260], we showed that this can be cast in a simpler linear form by expanding Eq. (7.3) in blocks, so that

$$\begin{bmatrix} \mathbf{A}_{11} & \mathbf{A}_{12} \\ \mathbf{A}_{21} & \mathbf{A}_{22} \end{bmatrix} \begin{bmatrix} \mathbf{X}_1 \\ \mathbf{X}_2 \end{bmatrix} = \omega \begin{bmatrix} \mathbf{X}_1 \\ \mathbf{X}_2 \end{bmatrix}, \quad (7.13)$$

where the blocks are,

$$\begin{aligned} [A_{11}]_{ai,jb} &= (\epsilon_a - \epsilon_i)\delta_{ij}\delta_{ab} + (ia|f_{Hxc}^{AA}|bj) \\ [A_{12}]_{ai,ckld} &= [H]_{ia,ckld} \\ [A_{22}]_{aibj,ckld} &= \delta_{ac}\delta_{ik}\delta_{bd}\delta_{jl}\omega_{ckld}. \end{aligned}$$

The subindexes 1 and 2 indicate the dimension is that of the 1h1p and the 2h2p spaces respectively.

The D-TDDFT kernel, in the form of Eq. (7.13), includes the coupling of 1h1p and 2h2p excitations. The 2h2p excitations are not coupled to the reference state, and the excitation energies can be largely underestimated or can even cause instabilities in the solution of Eq. (7.13) when calculating PESs. A simple solution is to introduce an extra coupling term in the kernel that explicitly couple the 2h2p excitations with the reference,

$$\begin{bmatrix} 0 & \mathbf{A}_{01} & \mathbf{A}_{02} \\ \mathbf{A}_{10} & \mathbf{A}_{11} & \mathbf{A}_{12} \\ \mathbf{A}_{20} & \mathbf{A}_{21} & \mathbf{A}_{22} \end{bmatrix} \begin{bmatrix} X_0 \\ \mathbf{X}_1 \\ \mathbf{X}_2 \end{bmatrix} = \omega \begin{bmatrix} X_0 \\ \mathbf{X}_1 \\ \mathbf{X}_2 \end{bmatrix}, \quad (7.14)$$

where the extra coupling blocks are

$$\begin{aligned} [A_{01}]_{jb} &= \langle \Psi_0^{KS} | \hat{H} \hat{a}_b^\dagger \hat{a}_j | \Psi_0^{KS} \rangle = (j | \hat{M}_{xc} | b) \\ [A_{02}]_{ckld} &= \langle \Psi_0^{KS} | \hat{H} \hat{a}_c^\dagger \hat{a}_k \hat{a}_d^\dagger \hat{a}_l | \Psi_0^{KS} \rangle = \\ &= 2 \cdot [(kc|f_H|ld) - (kd|f_H|lc)]. \end{aligned} \quad (7.15)$$

The Eq. (7.14) has a close resemblance with the configuration interaction singles and doubles (CISD) equation, where the only difference lies in the definition of the \mathbf{A}_{11} block. It is important to note that Brillouin theorem, i.e., the fact that $\mathbf{A}_{01} = \mathbf{0}$, only applies when the reference is the HF wave-function. This method will be dubbed henceforth b-D-TDDFT (b- stands for Brillouin) to differentiate it from the original D-TDDFT definition.

7.2.3 Computational Details

All wave-function-based calculations were performed with the GAMESS-US package [304], and all the TDDFT calculations with a development version of DEMON2K [205].

The initial ethylene geometry was optimized at the MP2 level with a convergence criterion of 10^{-6} . The geometry was never relaxed along the twisting coordinate.

The benchmark results have been calculated at the configuration active space self-consistent field (CASSCF) level with a perturbative treatment of dynamic correlation. The multireference calculations were performed with the GAMESS-US package [304]. The active space consisted of two electrons in an active space consisting of the π and π^* orbitals. The CASSCF(2,2) wavefunctions have been converged by state averaging the three singlet states with equal weights. The convergence threshold of the SCF was set to 10^{-6} . No symmetry was used in any calculation. The multi-reference perturbative treatment was done using the multi-configuration quasi-degenerate perturbation theory (MCQDPT) method [305,306].

The TDDFT calculations were performed using the local density approximation was used for the DFT calculations. The convergence criterion was set to 10^{-6} . The GEN-A3* auxiliary basis set was used. The grid was specified by the options FIXED and FINE. The implementation of D-TDDFT in DEMON2K is described in Ref. [260], and the implementation of SF-TDDFT in the same code in Ref. [158]. The D-TDDFT calculations were performed with the LDA kernel including 20% of Hartree-Fock exchange [260]. The 2h2p excitation energies were corrected to first order.

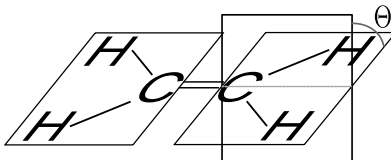
All the calculations were performed using a 6-311++G** basis set [209].

7.2.4 Results and Discussion

Ethylene is the simplest polyene, and an excellent prototype for understanding the photochemistry of polyenes. The molecule at the minimum energy geometry has a simple electronic structure. The ground-state (S_0) is represented mainly by the electronic configuration $(\pi)^2(\pi^*)^0$, the first singlet excited state (S_1) is represented by the configuration $(\pi)^1(\pi^*)^1$ and the second singlet excited state (S_2) is represented by $(\pi)^0(\pi^*)^2$. Upon absorption of a photon of the appropriate wavelength, the molecule is transferred from S_0 to S_1 , where it relaxes non-radiatively to the ground-state through a conical intersection between the two surfaces. The branching space of this conical intersection is represented by a twisting of one of the CH_2 groups (see Fig. 7.2) and a pyramidalization of the opposite CH_2 group. This conical intersection is difficult to be represented in TDDFT, since non-interacting v -representability (NVR) problems occur at the DFT level due to the degeneracies in the ground state KS system, which would require using an ensemble of densities. This is beyond the scope of the present work. Instead, we focus on the conical intersection occurring between the S_1 and S_2 along the twisting coordinate. Although NVR occurs around 90° too (the S_0 becomes degenerate with the first triplet state,) the need of a coupling between the reference determinant and the 2h2p states will be made apparent.

In Fig. 7.3, the potential energy surfaces (PES) of S_0 , S_1 and S_2 are shown at different levels of theory. Since only the relative energies are of interest here, we have shifted all the S_0 curves to 0 eV at 0° .

The CAS(2,2) result with a post-perturbative treatment [Fig. 7.3,(a)] will be taken as our benchmark. The conical intersection between S_1 and S_2 occurs at 90° . This intersection occurs due to the avoided crossing between S_0 and S_2 . In fact, around this geometry, the S_0 and S_2 strongly mix, whereas the S_1 remains well represented by the configuration $(\pi)^1(\pi^*)^1$. The gap between the S_0 and the S_1/S_2 intersection is 2.31 eV.

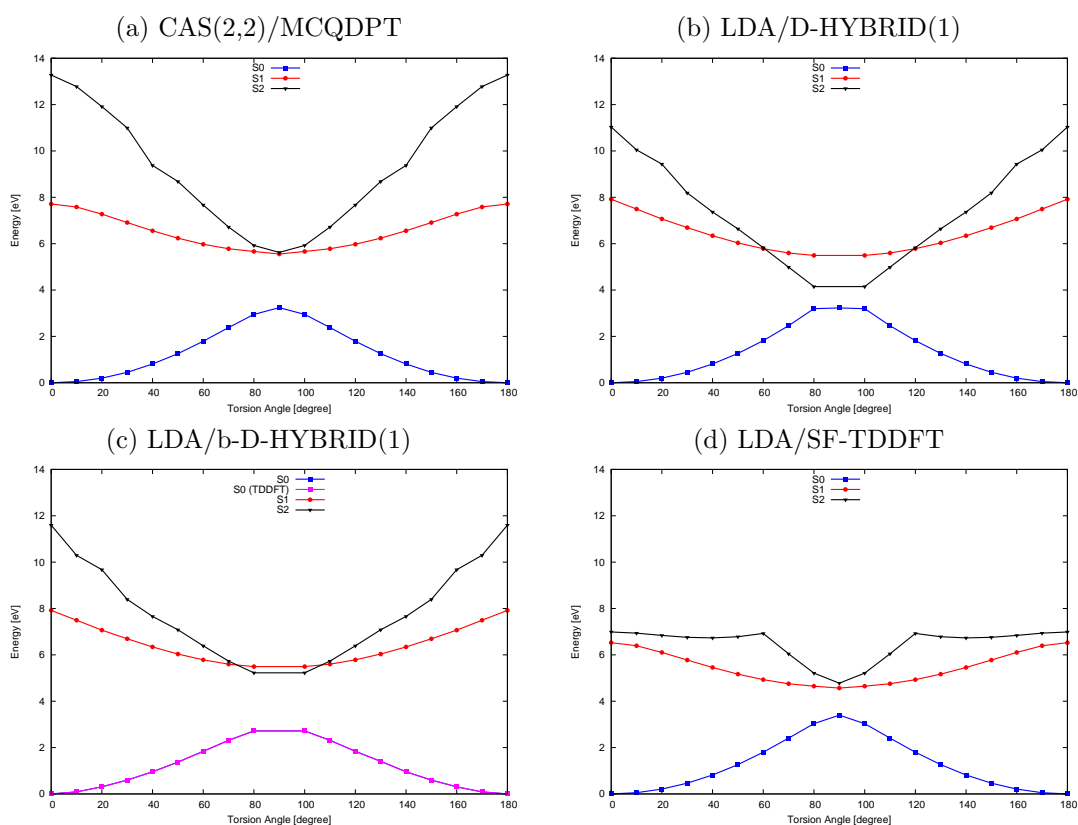
Figure 7.2 Graphical depiction of ethene torsion coordinate (Θ).

Any adiabatic approximation will not be able to reproduce the intersection, since the S_2 state is represented by a 2h2p excitation. The D-TDDFT approach is a prominent candidate for the application to this coordinate. The results of D-TDDFT are shown in Fig. 7.3 (b). In overall, S_0 and S_1 are very well represented, but the S_2 is underestimated by about 2 eV at all geometries. At 60° , the S_1 and S_2 curves cross. The point at 90° cannot be calculated, since the NVR problem occur, but it would indicate that on S_0/S_2 a recrossing would occur. This is clearly wrong when compared to the benchmark curves. This problem occurs due to the fact that the 2h2p excitations are not interacting with the reference. As a consequence, S_2 is purely represented by the configuration $(\pi)^0(\pi^*)^2$.

The introduction of an interaction term that couples the 2h2p excitations with the ground-state largely remedies this problem. The results of the b-D-TDDFT kernel are shown in Fig. 7.3 (c). We observe that the S_2 state is shifted up with respect to D-TDDFT, in better accordance with the benchmark results. At around 90° , the S_2 is correctly represented as a mixture of the $(\pi)^2(\pi^*)^0$ and $(\pi)^0(\pi^*)^2$ states. This mixture is possible thanks to the extra term included in the original formulation of D-TDDFT. Interestingly, the correction to the S_0 curve due to the interaction of S_2 is very small and appears almost superimposed to the original DFT S_0 . This is important, since the S_0 was already properly described at the DFT level. Though a general improvement is observed, the intersection S_1/S_2 is still not perfectly described.

Finally, the results of spin-flip TDDFT (SF-TDDFT) are shown in Fig. 7.3 (d). In this case, the reference DFT calculation is taken as the triplet state, therefore avoiding the NVR problem. The three singlet states S_0 , S_1 and S_2 are accessed through excitations. The results of SF-TDDFT show a good representation of both S_0 and S_1 curves with respect to the benchmark, but the S_2 curve is unevenly represented. The S_2 excited state shows a change of configuration at around 60° . Before this angle, the curve belongs to a different singlet state with a small portion of 2h2p configuration and only after 60° the desired S_2 appears. In fact, SF-TDDFT only can calculate a reduced number of double excitations, and selecting the correct one is not straightforward (see another example in Ref. [158].) In the case of SF-TDDFT, the S_1/S_2 intersection at 90° is almost perfectly described. The gap between S_0 and S_1/S_2 is 1.7 eV, which is 0.6 eV lower than the benchmark. In global, both S_1 and S_2 after 60° are underestimated by about 1 eV with respect to the benchmark. This is probably due to the fact that the LDA functional is used to construct the SF-TDDFT kernel and probably a hybrid version of SF-TDDFT would improve the energetics.

Figure 7.3 Potential energy surfaces of the first three excited states of ethene along the twisting coordinate at various levels of theory. All the curves have been shifted so that the ground-state curve at 0° corresponds to 0 eV.



7.2.5 Conclusion and Perspectives

Recent developments in TDDFT open the venue to an efficient way of performing photochemical simulations. In this article, we have applied two candidates, namely SF-TDDFT and D-TDDFT, to describe the S_1/S_2 conical intersection of ethylene along the twisting coordinate. The two states are degenerate when one of the CH_2 groups form an angle of 90° with respect to the other.

We have shown that the original formulation of D-TDDFT largely underestimates the S_2 , which rather intersects with the S_0 state rather than the S_1 . In fact, the S_2 is represented by a pure 2h2p excitation, whereas the multireference calculations predict an avoided crossing between S_0 and S_2 . This effect could not be represented due to the lack of coupling between the reference and the 2h2p excitations. Taking into account the similarities between CISD and D-TDDFT in the TDA approximation, we have added an extra term in the D-TDDFT kernel that introduces this coupling. The results show that the S_2 state is still slightly underestimated, but the improvement is remarkable. The correction does not affect much S_0 , which was already well described at the DFT level. The D-TDDFT could not be applied in the present form to the 90° due to the NVR problem. This problem will be addressed in the future.

The SF-TDDFT method is more successful in representing the S_1/S_2 conical intersection. The fact that the reference is the first triplet instead of the first singlet, avoids the NVR problem, and the calculation of 90° is without problem. One of the drawbacks of the method is that the excited states are underestimated by about 1 eV. Additionally, the S_2 surface is unevenly represented along the twisting coordinate. The 2h2p configuration $(\pi)^0(\pi^*)^2$ seems only predominant after 60° . At smaller angles, some other singlet surface is obtained which does not correspond to the expected predominant configuration. The fact that other excitations are highly spin contaminated, makes it difficult to assign the correct excitation.

7.2.6 Acknowledgments

M. H. would like to acknowledge a scholarship from the French Ministry of Education. We would like to thank Denis Charapoff and Sébastien Morin for technical support at the (DCM) and for technical support in the context of the *Centre d'Expérimentation du Calcul Intensif en Chimie* (CECIC) computers used for some of the calculations reported here. This work has been carried out in the context of the French Rhône-Alpes *Réseau thématique de recherche avancée (RTRA): Nanosciences aux limites de la nanoélectronique* and the Rhône-Alpes Associated Node of the European Theoretical Spectroscopy Facility (ETSF).

7.3 Conclusions and Perspective

In this chapter, we have explored the possibility of including a coupling term between the double excitations and the reference configuration, which is necessary to represent correctly

funnels between excited states and the ground-state. The correction has been added to the general dressed TDDFT kernel derived in Chap. 6. Due to the resemblance of the TDDFT/TDA equations to CI, we have added the correction from CISD.

The application of such kernel to the S_1/S_2 conical intersection along the ethylene twisting coordinate shows promising results. Without the correction, the dressed kernel predicts an S_2 long below the S_1 , due to the fact that the avoided crossing between S_0 and S_2 is largely underestimated. With the additional term in the dressed kernel, the representation of the avoided crossing is largely improved, although the intersection point is still underestimated.

Although the approach presented here shows an improvement, more tests should be done to validate this correction. In case of failure, we will add the extra diagrams from the polarization propagator, which we did not include to the dressed kernel. This, in fact, would correspond to use a double hybrid functional in DFT and TDDFT. In such case, the validity of the TDA approximation should be studied, since a large part of the interaction between the excited states and the reference is taken into account in the in the \mathbf{B}_{11} matrix. The expressions of these terms were given in Eqs. (5.138) and (5.138), which makes it apparent that this would be a bottleneck in the calculation of the kernel.

Chapter 8

Real-time Dressed TDDFT

In this chapter, I briefly describe an on-going project on a formulation of real-time dressed time-dependent density-functional theory (RT-D-TDDFT). The objective of this formulation is to understand how potential with memory behaves during the real-time propagation in cases where double excitations are important. This is a project started with Ángel Rubio and Mark E. Casida.

As seen in Chap. 3 Sec. 3.3.2.2, the propagation of the KS wave function in real time is written in terms of a propagator

$$|\Phi(t)\rangle = \mathcal{T} \left[e^{-i \int_{t_0}^t \hat{H}_s(t) dt} \right] |\Phi(t_0)\rangle. \quad (8.1)$$

This formula is valid for both strong and weak fields, but in this chapter we will restrict to fields in which linear response is valid. In linear response, the time-dependent KS Hamiltonian can be written as

$$\hat{H}_s(t) = \hat{H}_s + \delta v_s(t) = \hat{H}_s + \delta v_{Hxc}(t) + \delta v_{appl}(t), \quad (8.2)$$

where the only unknown ingredient is the xc-potential. Normally, the adiabatic approximation of the potential is used [see Eq. (3.116),] giving essentially the same results as linear response with adiabatic kernels.

In linear response, we took advantage of the relation of the Dyson-like equation for kernel in terms of the response functions to construct the frequency-dependence from the polarization propagator. The xc-potential possess a similar Dyson-like equation with the self-energy. However, the construction of the self-energy in real time requires the application of non-equilibrium perturbation theory techniques, which are not straightforward. In the limit in which the linear response is valid, we can use a simpler alternative, by taking the xc-kernel to construct the xc-potential. From the definition of the xc-kernel [see Eq. (3.63)], we can write it as

$$\delta v_{xc}(\mathbf{r}, t) = \int_{t_0}^t dt \int d^3r' f_{xc}(\mathbf{r}, \mathbf{r}'; t - t') \delta \rho(\mathbf{r}', t'). \quad (8.3)$$

Inserting the adiabatic kernel [see Eq. (3.117)] in Eq. (8.3) straightforwardly gives the adiabatic potential [Eq. (3.116).] Memory can be introduced by using a kernel beyond the adiabatic approximation.

In this thesis, we derived a general form of the dressed TDDFT kernel, that could be used to construct a memory potential. The assumption here is that the hybrid kernel corresponds to a self-energy, but this seems a reasonable assumption. The dressed kernel can be written in two parts as

$$f_{xc}^D(\mathbf{r}, \mathbf{r}'; \omega) = f_{xc}^{AA}(\mathbf{r}, \mathbf{r}') + K^\omega(\mathbf{r}, \mathbf{r}; \mathbf{r}', \mathbf{r}'; \omega), \quad (8.4)$$

where K^ω is the frequency-dependent part of the second-order polarization propagator kernel. Inserting this kernel in Eq. (8.3), we have

$$\delta v_{xc}^D(\mathbf{r}, t) = v^{AA}(\mathbf{r}, t) + \int_{t_0}^t dt' \int d^3r' K^\omega(\mathbf{r}, \mathbf{r}; \mathbf{r}', \mathbf{r}'; t - t') \delta \rho(\mathbf{r}', t'), \quad (8.5)$$

where the inverse Fourier transformed kernel $K^\omega(t - t')$ is defined as

$$K^\omega(\mathbf{r}, \mathbf{r}; \mathbf{r}', \mathbf{r}'; t - t') = \int \frac{d\omega}{2\pi} e^{i\omega(t-t')} K^{\omega}(\mathbf{r}, \mathbf{r}; \mathbf{r}', \mathbf{r}'; \omega). \quad (8.6)$$

When we defined the dressed kernel, only one part was used to extract the excitation energies, since the poles are just repeated in the other part. In this case, however, we have to use the full retarded kernel in order to preserve time-reversal symmetry, that is,

$$[K^\omega(\omega)]_{ai,bj} = \sum_{ckld} \frac{(ai|\check{V}|ckld)(ckld|\check{V}|bj)}{\omega - \omega_{ckld}} - \frac{(bj|\check{V}|ckld)(ckld|\check{V}|ai)}{\omega + \omega_{ckld}}, \quad (8.7)$$

where the definitions are the usual used in previous sections. Note that the convergence factors were omitted for simplicity. The inverse Fourier transform of such kernel gives

$$[K^\omega(t - t')]_{ai,bj} = -\sqrt{(2\pi)} \sum_{ckld} (ai|\check{V}|ckld)(ckld|\check{V}|bj) \sin[\omega_{ckld}(t - t')], \quad (8.8)$$

in which we assumed that the orbitals are real and all $\omega_{ckld} > 0$. The time-dependent kernel

$$K^\omega(\mathbf{r}, \mathbf{r}, \mathbf{r}', \mathbf{r}'; t - t') = \sum_{iajb} [K^\omega(t - t')]_{ai,bj} \phi_i^*(\mathbf{r}) \phi_a(\mathbf{r}) \phi_b^*(\mathbf{r}') \phi_j(\mathbf{r}'), \quad (8.9)$$

can be inserted in Eq. (8.5) to obtain

$$\delta v_{xc}^D(\mathbf{r}, t) = v^{AA}(\mathbf{r}, t) + \delta v_{xc}^\omega(\mathbf{r}, t), \quad (8.10)$$

where I used the definition

$$\delta v_{xc}^\omega(\mathbf{r}, t) = -\sqrt{2\pi} \sum_{aibj} \phi_i^*(\mathbf{r}) \phi_a(\mathbf{r}) \sum_{ckld} (ai|\check{V}|ckld)(ckld|\check{V}|bj) \int_{t_0}^t dt' \sin[\omega_{ckld}(t - t')] (\delta \rho(t')|jb). \quad (8.11)$$

There are obvious negative features from this definition of the potential. First, the double excitations that are not coupled to any single excitation are zero. For example, the S_2 state of H_2 , which appears in linear response with the dressed kernel, would not be present. Second, the virtual orbitals are required, which is not the case when one uses an adiabatic xc-potential. The virtual orbitals are usually difficult to converge in a grid-based code..

This potential has been implemented in OCTOPUS [307, 308]. The implementation of the time integration in OCTOPUS was done numerically. The integral is done (which is not necessarily the same as the real-time propagation step) using the composite trapezoidal formula

$$\int_{t_0}^t dt' f(t') \approx \Delta t \cdot \frac{f(t_0) + f(t)}{2} + \sum_{k=1}^{n-1} f(t_0 + k \cdot \Delta t), \quad (8.12)$$

where $n = t - t_0 / \Delta t$. Due to the convolution appearing in Eq. (8.11), the integration cannot be updated, and each time has to be recalculated. For example, for a fixed value of indexes j and b at $t_1 = t_0 + \Delta t$, the integration gives

$$\int_{t_0}^{t_1} dt' \sin(t - t') (\delta\rho(t') |bj) = \Delta t' \cdot \frac{\sin(\Delta t) (\delta\rho(t_0) |bj)}{2}. \quad (8.13)$$

The next step, at time $t_2 = t_0 + 2 \cdot \Delta t$, the integration gives

$$\int_{t_0}^{t_2} dt' \sin(t - t') (\delta\rho(t') |bj) = \Delta t' \cdot \frac{\sin(2 \cdot \Delta t) (\delta\rho(t_0) |bj)}{2} + \sin(\Delta t) (\delta\rho(t_0 + \Delta t) |bj), \quad (8.14)$$

which is obviously not equal to the integration at step t_1 plus extra terms. This just means that all densities have to be saved, from time t_0 to time t , during the whole time propagation. This is not practical, since the number of time steps is usually large in order to converge the absorption spectrum. Only a certain number of densities around t are selected, and all others are dismissed.

The implementation in OCTOPUS was tested for butadiene. The dressed part was restricted to contain only to contain the $\alpha\beta$ double excitations (HOMO,HOMO-1) \rightarrow (LUMO+1,LUMO) and the other spin partners. These excitations mix with the HOMO \rightarrow LUMO single excitation, with the effect that the position of the main peak in the dipole spectrum experiences a red-shift. However, the results were not successful, and the same spectrum as adiabatic TDDFT is obtained. One reason could be that the $(\delta\rho(t) |jb)$ is almost zero at all times, therefore giving results similar to adiabatic TDDFT. Another source of the problem could be the truncation of the time integration appearing in Eq. (8.11), which is not justified. In fact, it is known that the potential is highly non-local in time, and it can strongly depend on densities far from the present time. This could be improved by using non-uniform grids in time. More tests are going on to determine the source of the problem. Once this is resolved, 3D plots of both the memory and the adiabatic xc-potentials will be done in order to understand the effects that are introduced by memory over time.

Chapter 9

Final Conclusions ¹

Time-dependent density-functional theory is a promising candidate for an efficient description of dynamics in the excited state. However, present approximate functionals limit the applicability of TDDFT. Most common functionals use the so-called adiabatic approximation, in which the adiabatic limit of the exact TDDFT functional is taken for all times. Adiabatic functionals describe correlation inaccurately, and are inadequate for representing the key mechanistic steps of relaxation in photochemistry. In this thesis, we have extensively studied the description of correlation in TDDFT, and we have proposed several solutions with the aim to apply TDDFT to photochemical problems.

At the moment of the publication of this thesis, only two methods partially improved the description of correlation beyond adiabatic TDDFT: spin-flip TDDFT and dressed TDDFT. Spin-flip is especially suitable for describing photochemical problems. This method was initially conceived for calculating multiconfiguration ground-states from a single-reference model, working around the noninteracting v -representability problem. SF-TDDFT can only include a reduced number of double excitations, which might be insufficient for some applications. In fact, the application to the photochemical ring-opening of oxirane confirms this suspicion. On the one hand, the avoided crossing in the symmetric C_{2v} ring opening showed a cusp in the S_0 surface, and the S_2 surface could not be correctly interpreted along the reaction coordinate. On the other hand, the geometry of the conical intersection point between S_0 and S_1 PESs in the asymmetric ring opening is shifted with respect to multireference benchmark results. Although SF-TDDFT improves the description of correlation over any adiabatic functional, the restricted number of pure spin states and the reduced number of double excitations included are two major drawback of the method.

A main result of this thesis is the derivation of an exact second-order correlation kernel derived from *ab initio* techniques. To our knowledge, this is the first kernel that can include all double excitations. The kernel is calculated in two steps: the first consists of a polarization propagator kernel [45], in which we applied the perturbation theory starting from a general Fock operator, and the second consists of a localization function, which converts the many-body kernel into a local TDDFT kernel. The first-order approximation to the polarization propagator kernel produces the time-dependent exact-exchange kernel. The second-order approximation gives an order-consistent approximation to the correlation kernel. The consistency is important to avoid unphysical effects in the kernel [46, 48].

The exact correlation kernel allowed us to identify the origin of the problems of the adiabatic approximation. Adiabatic functionals are static, with no dependence on the frequency (time.) In the time-dependent exact exchange kernel, the frequency dependence comes exclusively from the localizer. This frequency dependence is not enough to include double excitation. In the correlation part, the polarization propagator kernel introduces an additional frequency dependence, which is fundamental for including double excitation poles in the response functions. The dia-

1. Pour les conclusions en français voir le chapitre Introduction et Conclusions (en français) à la fin de la thèse

grammatic expansion of the kernel allowed us to identify specifically the second-order correlation diagrams which are missing in the adiabatic approximation. These diagrams are of self-energy type and particle-hole type and introduce the coupling between single and double excitations through the frequency-dependent terms.

We explored the possibility of including the missing diagrams directly to the adiabatic functionals, without taking into account the localization. These many-body corrections to adiabatic TDDFT functionals can be viewed as a hybrid memory functional, that generalizes the idea of dressed TDDFT. Such kernel is more efficient than the exact *ab initio* correlation kernel and therefore more suitable for applications to systems of medium and large size. Several definitions of the hybrid memory kernel are possible, depending on the choice of adiabatic functional and many-body terms. We showed that not all combinations are successful by comparing the singlet excitation energies of 28 organic chromophores with the different hybrid memory kernels against high-quality benchmark results. We concluded that the kernel works best when a hybrid functional with 20-25% HF exchange is used in the adiabatic part and the double excitations are corrected to first order in perturbation theory. This result is important, as it demonstrates that hybrid functionals are successful not only in DFT but also in TDDFT. Still, a main drawback of the dressed kernel is the problem of double counting of correlation, that is, the dynamic correlation effects are included twice in the single excitation block when a large number of double excitations are included. This could be avoided by implementing a pre-screening of double excitations.

The hybrid memory kernel could potentially be applied to photochemical problems, as it includes pure-spin double excitations in general. However, in the present form it cannot describe correctly dissociation and funnels which involve the ground state. This is due to the missing coupling term between the reference and the double excitation poles. We have added this terms to the dressed kernel from CISD. There are two reasons for taking the terms from CISD. On the one hand, this block is less expensive than the equivalent terms from the polarization propagator. On the other hand, the dressed TDDFT kernel in the TDA approximation has a similar structure to the CISD equations, which allows to compare the two theories and transfer missing information from one to the other. The preliminary tests on the ethylene twisting show that this choice is sensible. We used the hybrid kernel with the CISD terms to describe the conical intersection between the S_1 and S_2 surfaces. This cannot be described by any adiabatic functional, as the S_2 state is of double excitation nature and therefore missing in adiabatic TDDFT. The hybrid kernel largely underestimates the S_2 state, whereas when we include the CISD correction the S_1/S_2 conical intersection is more accurately described, although it is still slightly underestimated compared to *ab initio* results.

With the results of this thesis, new problems might be tackled with TDDFT, both of formal and applied nature. One of the problems we would like to explore in the future is the representation of excited states in open-shell systems. These excited states are highly spin contaminated in adiabatic TDDFT, due to the fact that double excitations are missing. This could be resolved by combining a restricted open-shell DFT calculation and our kernel with double excitations. Another problem that we would like to explore is the formulation of a real-time dressed TDDFT. We propose to use the dressed kernel and integrate the second derivative to obtain a potential with memory. For photochemical applications, a problem that should be tackled is the non-interacting v -representability. The solution is probably to use fractional

occupation numbers. Then, the *ab initio* kernel should be rederived with a metric that accepts non-integer occupations.

In conclusion, the work in this thesis has clarified the problem of double excitations and has provided two solutions, one rigorous and one practical, of possible functionals in linear response that could be potentially applied to photochemical problems. The results of this thesis open new perspectives to construct TDDFT functionals, and offer an important step towards the application of TDDFT to photochemistry.

Bibliography

- [1] A. Albini and M. Fagnoni. Green chemistry and photochemistry were born at the same time. *Green Chem.*, 6:1–6, 2004.
- [2] A. Ben Haj Yedder, C. Le Bris, O. Atabek, S. Cheikowski, and A. D. Bandrauk. Optimal control of attosecond pulse synthesis from high-order harmonic generation. *Phys. Rev. A*, 69:041802(R), 2004.
- [3] G. S. Engel, T. R. Calhoun, E. L. Read, T. Ahn, T. Mančal, Y. Cheng, R. E. Blankenship, and G. R. Fleming. Evidence for wavelike energy transfer through quantum coherence in photosynthetic systems. *Nature*, 446:782–786, 2007.
- [4] A. Ishizaki and G. R. Fleming. Theoretical examination of quantum coherence in photosynthetic system at physiological temperature. *Proc. Nat. Ac. Sci.*, 41:17255–17260, 2009.
- [5] R. J. Ellingson, M. C. Beard, J. C. Johnson, P. Yu, O. I. Micic, A. J. Nozik, A. Shabaev, and A. L. Efros. Highly efficient multiple exciton generation in colloidal PbSe and PbS quantum dots. *Nano Lett.*, 5:865–871, 2005.
- [6] M. B. Smith and J. Michl. Singlet fission. *Chem. Rev.*, 110:6891–6936, 2010.
- [7] A. Luque, A. Martí, and A. J. Nozik. Solar cells based on quantum dots: Multiple exciton generation and intermediate bands. *Mat. Res. Soc. Bull.*, 32:236, 2007.
- [8] P. M. Zimmerman, Z. Zhang, and C. B. Musgrave. Singlet fission in pentacene through multi-exciton quantum states. *Nature Chemistry*, 2:648–652, 2010.
- [9] A. Zewail. Femtochemistry: Atomic-scale dynamics of the chemical bond using ultrafast lasers. In I. Grenthe, editor, *Nobel Lectures, Chemistry 1996–2000*, pages 274–367. World Scientific Publishing Co., Singapore, 2003.
- [10] D. Polli, P. Altoè, O. Weingart, K. M. Spillane, C. Manzoni, D. Brida, G. Tomasello, G. Orlandi, P. Kukura, R. A. Mathis, M. Garavelli, and G. Cerullo. Conical intersection dynamics of the primary photoisomerization event in vision. *Nature*, 467:440–443, 2010.
- [11] E. Tapavicza, I. Tavernelli, and U. Rothlisberger. Trajectory surface hopping within linear response time-dependent density-functional theory. *Phys. Rev. Lett.*, 98:023001, 2007.
- [12] H. Hirai and O. Sugino. A time-dependent density-functional approach to nonadiabatic electron-nucleus dynamics: formulation and photochemical application. *Phys. Chem. Chem. Phys.*, 11:4570–4578, 2009.
- [13] E. Runge and E. K. U. Gross. Density-functional theory for time-dependent systems. *Phys. Rev. Lett.*, 52:997–1000, 1984.
- [14] P. Hohenberg and W. Kohn. Inhomogeneous electron gas. *Phys. Rev. B*, 136:B864, 1964.
- [15] W. Kohn and L. J. Sham. Self-consistent equations including exchange and correlation effects. *Phys. Rev.*, 140:A1133–A1138, 1965.
- [16] A. L. Fetter and J. D. Walecka. *Quantum Theory of Many-Particle Systems*. McGraw-Hill, New York, 1971.

- [17] M. E. Casida. Time-dependent density-functional response theory for molecules. In D. P. Chong, editor, *Recent Advances in Density Functional Methods, Part I*, page 155. World Scientific, Singapore, 1995.
- [18] P. Jørgensen. Molecular and atomic applications of time-dependent Hartree-Fock theory. *Ann. Rev. Phys. Chem.*, 26:359–380, 1975.
- [19] F. Furche and R. Ahlrichs. Absolute configuration of D_2 -symmetric fullerene C_{84} . *J. Am. Chem. Soc.*, 124:3804–3805, 2002.
- [20] O. T. Ehrler, J. M. Weber, F. Furche, and M. M. Kappes. Photoelectron spectroscopy of C_{84} dianions. *Phys. Rev. Lett.*, 91:113006, 2003.
- [21] O. T. Ehrler, J. P. Yang, C. Hättig, H. Unterreiner, A-N. an Hippler, and M. M. Kappes. Femtosecond pump/probe photoelectron spectroscopy of isolated C_{60} negative ions. *J. Chem. Phys.*, 125:074312, 2006.
- [22] M. A. L. Marques, X. López, D. Varsano, A. Castro, and A. Rubio. Time-dependent density-functional approach for biological chromophores: The case of the green fluorescent protein. *Phys. Rev. Lett.*, 90:258101, 2003.
- [23] D. M. Rogers, N. A. Besley, P. O’Shea, and J. D. Hirst. Modeling the absorption spectrum of tryptophan in proteins. *J. Phys. Chem. B*, 109:23061–23069, 2005.
- [24] J. Neugebauer, C. R. Jacob, T. A. Wesolowski, and E. J. Baerends. An explicit quantum chemical method for modeling large solvation shells applied to aminocoumarin C151. *J. Phys. Chem. A*, 109:7805–7814, 2005.
- [25] M. E. Casida, C. Jamorski, K. C. Casida, and D. R. Salahub. Molecular excitation energies to high-lying bound states from time-dependent density-functional response theory: Characterization and correction of the time-dependent local density approximation ionization threshold. *J. Chem. Phys.*, 108:4439, 1998.
- [26] A. Dreuw, J. L. Weisman, and M. Head-Gordon. Long-range charge-transfer excited states in time-dependent density functional theory require non-local exchange. *J. Chem. Phys.*, 119:6–9, 2003.
- [27] A. Heßelmann, A. Ipatov, and A. Görling. Charge-transfer excitation energies with a time-dependent density-functional method suitable for orbital-dependent exchange-correlation kernels. *Phys. Rev. A*, 80:012507, 2009.
- [28] M. J. G. Peach, P. Benfield, T. Helgaker, and D. J. Tozer. Excitation energies in density functional theory: An evaluation and a diagnostic test. *J. Chem. Phys.*, 128:044118, 2008.
- [29] B. G. Levine, C. Ko, J. Quenneville, and T. J. Martinez. Conical intersections and double excitations in time-dependent density functional theory. *Mol. Phys.*, 104:1039, 2006.
- [30] F. Cordova, L. Joubert Doriol, A. Ipatov, M. E. Casida, C. Filippi, and A. Vela. Troubleshooting time-dependent density-functional theory for photochemical applications: oxirane. *J. Chem. Phys.*, 127:164111, 2007.
- [31] E. Tapavicza, I. Tavernelli, U. Rothlisberger, C. Filippi, and M. E. Casida. Mixed time-dependent density-functional theory/classical surface hopping study of oxirane photochemistry. *J. Chem. Phys.*, 129:124108, 2008.
- [32] A. Görling. Exact exchange-correlation kernel for dynamic response properties and excitation energies in density-functional theory. *Phys. Rev. A*, 57:3433–3436, 1998.

- [33] M. Hellgren and U. von Barth. Linear density response function within the time-dependent exact-exchange approximation. *Phys. Rev. B*, 78:115107, 2008.
- [34] M. Hellgren and U. von Barth. Exact-exchange kernel of time-dependent density functional theory: Frequency dependence and photoabsorption spectra of atoms. *J. Chem. Phys.*, 131:044110, 2009.
- [35] J. F. Dobson. Harmonic-potential theorem: Implications for approximate many-body theories. *Phys. Rev. Lett.*, 73:2244–2247, 1994.
- [36] G. Vignale. Current density functional theory. In M. A. L. Marques, C. A. Ullrich, F. Nogueira, A. Rubio, K. Burke, and E. K. U. Gross, editors, *Lecture Notes in Physics*, chapter 5, pages 75–91. 2006.
- [37] L. O. Wagner and K. Burke. The role of exact conditions in TDDFT. In E. K. U. Gross, M. A. L. Marques, F. Nogueira, and A. Rubio, editors, *Fundamentals of Time-Dependent Density-Functional Theory*, Lecture Notes in Physics. Springer, 2012. (in press).
- [38] L. V. Slipchenko and A. I. Krylov. Electronic structure of the trimethylenemethane diradical in its ground and electronically excited states: Bonding, equilibrium geometries, and vibrational frequencies. *J. Chem. Phys.*, 118:6874, 2003.
- [39] Y. Shao, M. Head-Gordon, and A. I. Krylov. The spin-flip approach within time-dependent density functional theory: Theory and applications to diradicals. *J. Chem. Phys.*, 118:4807, 2003.
- [40] A. Krylov. Spin-flip equation-of-motion coupled-cluster electronic structure method for a description of excited states, bond breaking, diradicals, and triradicals. *Acc. Chem. Res.*, 39:83, 2006.
- [41] F. Wang and T. Ziegler. The performance of time-dependent density functional theory based on a noncollinear exchange-correlation potential in the calculation of excitation energies. *J. Chem. Phys.*, 122:074109, 2005.
- [42] F. Wang and T. Ziegler. Use of noncollinear exchange-correlation potentials in multiplet resolutions by time-dependent density functional theory. *Int. J. Quant. Chem.*, 106:2545, 2006.
- [43] N. T. Maitra, F. Zhang, R. J. Cave, and K. Burke. Double excitations within time-dependent density functional theory linear response. *J. Chem. Phys.*, 120:5932, 2004.
- [44] R. J. Cave, F. Zhang, N. T. Maitra, and K. Burke. A dressed TDDFT treatment of the 2^1A_g states of butadiene and hexatriene. *Chem. Phys. Lett.*, 389:39, 2004.
- [45] J. Oddershede and P. Jørgensen. An order analysis of the particle-hole propagator. *J. Chem. Phys.*, 66:1541, 1977.
- [46] P. Romaniello, D. Sangalli, J. A. Berger, F. Sottile, L. G. Molinari, L. Reining, and G. Onida. Double excitations in finite systems. *J. Chem. Phys.*, 130:044108–11, 2009.
- [47] D. Sangalli. *Challenges for first-principles methods in theoretical and computational physics: multiple excitations in many-electrons systems and the Aharonov-Bohm effect in carbon nanotubes*. PhD thesis, Università degli studi di Milano / Università degli studi di Roma Tre, 2010.
- [48] D. Sangalli, P. Romaniello, G. Onida, and A. Marini. Double excitations in correlated systems: A many-body approach. *J. Chem. Phys.*, 134:034124, 2011.

- [49] M. E. Casida, B. Natarajan, and T. Deutsch. Non-Born-Oppenheimer dynamics and conical intersections. In E. K. U. Gross, M. A. L. Marques, F. Nogueira, and A. Rubio, editors, *Fundamentals of Time-Dependent Density-Functional Theory*, Lecture Notes in Physics. Springer, 2012. (in press).
- [50] M. Born and R. Oppenheimer. Zur Quantentheorie der Molekeln. *Ann. Phys.*, 87:457–484, 1927.
- [51] M. Born and K. Huang. *The Dynamical Theory of Crystal Lattices*. Oxford Univ. Press, 1954.
- [52] G. A. Worth and L. S. Cederbaum. Beyond Born-Oppenheimer: Molecular dynamics through a conical intersection. *Annu. Rev. Phys. Chem.*, 55:127–158, 2004.
- [53] W. Domcke, D. R. Yarkony, and H. Koeppel, editors. *Modern Methods and Algorithms of Quantum Chemistry*, volume 15 of *Advanced Series in Physical Chemistry*. World Scientific, 2004.
- [54] M. Baer. *Beyond Born-Oppenheimer: Electronic Nonadiabatic Coupling Terms and Conical Intersections*. Wiley, 2006.
- [55] C. Angeli. On the nature of the $\pi \rightarrow \pi^*$ ionic excited state: The V state of ethene as a prototype. *J. Comput. Chem.*, 30:1319–1333, 2009.
- [56] C. Angeli. An analysis of the dynamic σ polarization in the V state of ethene. *Int. J. Quant. Chem.*, 110:2436–2447, 2010.
- [57] A. Szabo and N. S. Ostland. *Modern Quantum Chemistry: Introduction to Advanced Electronic Structure Theory*. MacMillan Publishing Co., New York, 1982.
- [58] W. Heitler and F. London. Wechselwirkung neutraler Atome and homöopolare Bindung nach der Quantenmechanik. *Zeitschrift für Physik*, 44:455–472, 1927.
- [59] D. M. Leitner, B. Levine, J. Quenneville, T. J. Martinez, and P. G. Wolynes. Quantum energy flow and trans-stilbene photoisomerization: an example of a non-rrkm reaction. *J. Chem. Phys.*, 107:10706, 2003.
- [60] R. McWeeny. *Methods of Molecular Quantum Mechanics*. Academic Press, 2001.
- [61] T. Koopmans. Über die Zuordnung von Wellenfunktionen und Eigenwerten zu den Einzelnen Elektronen Eines Atoms. *Physica*, 1:104–113, 1934.
- [62] E. A. Hylleras and B. Undheim. Numerische Berechnung der 2 S-Terme von Ortho- an Par-Helium. *Z. Physik*, 65:759–772, 1930.
- [63] J. K. L. MacDonald. Successive approximations by the Rayleigh-Ritz variation method. *Phys. Rev.*, 43:830–833, 1933.
- [64] E. Dalggaard. Expansion and completeness theorems for operators manifolds. *Int. J. Quant. Chem.*, 15:169–180, 1979.
- [65] H. Shull and P. O. Löwdin. Variation theorem for excited states. *Phys. Rev.*, 110:1466–1467, 1958.
- [66] J. Schirmer. Beyond the random phase approximation: A new approximation scheme for the polarization propagator. *Phys. Rev. A*, 26:2395, 1982.
- [67] E. Schrödinger. An ondulatory theory of the mechanics of atoms and molecules. *Phys. Rev.*, 28:1049–1070, 1926.

- [68] L. H. Thomas. The calculation of atomic fields. *Proc. Cambridge Phil. Soc.*, 23:542–548, 1927.
- [69] E. Fermi. Un metodo statistico per la determinazione di alcune proprietà dell'atomo. *Rend. Accad. Naz. Lincei*, 6:602–607, 1927.
- [70] E. Teller. On the stability of molecules in the Thomas-Fermi theory. *Rev. Mod. Phys.*, 34:627–631, 1962.
- [71] M. Levy. Universal variational functionals of electron densities, first-order density matrices, and natural spin-orbitals and solution of the v -representability problem. *Proc. Natl. Acad. Sci.*, 76:6062, 1979.
- [72] R. O. Jones and O. Gunnarsson. The density functional formalism, its applications and prospects. *Rev. Mod. Phys.*, 61:689–746, 1989.
- [73] T. Ziegler, A. Rauk, and E. J. Baerends. On the calculation of multiplet energies by the Hartree-Fock-Slater method. *Theor. Chem. Acc.*, 43:261–271, 1977.
- [74] Q. Wu and T. van Voorhis. Direct optimization method to study constrained systems within density-functional theory. *Phys. Rev. A*, 72:024502, 2005.
- [75] A. Castro and M. A. L. Marques. Propagators for the time-dependent Kohn-Sham equation. In M. A. L. Marques, C. A. Ullrich, F. Nogueira, A. Rubio, K. Burke, and E. K. U. Gross, editors, *Lecture Notes in Physics*. 2006.
- [76] R. van Leeuwen. Causality and symmetry in time-dependent density-functional theory. *Phys. Rev. Lett.*, 80:1280–1283, 1998.
- [77] G. Vignale. Real-time resolution of the causality paradox of time-dependent density-functional theory. *Phys. Rev. A*, 77:0625119, 2008.
- [78] R. van Leeuwen. Mapping from densities to potentials in time-dependent density-functional theory. *Phys. Rev. Lett.*, 82:3863–3866, 1999.
- [79] N. T. Maitra, T. N. Todorov, C. Woodward, and K. Burke. Density-potential mapping in time-dependent density-functional theory. *Phys. Rev. A*, 81:1–7, 2010.
- [80] I. V. Tokatly. A unified approach to the density-potential mapping in a family of time-dependent density functional theories. *Chem. Phys.*, 2011. (accepted).
- [81] R. G. Parr and W. Yang. *Density-Functional Theory of Atoms and Molecules*. Oxford University Press, 1989.
- [82] W. Kohn. v -representability and density functional theory. *Phys. Rev. Lett.*, 51:1596–1598, 1983.
- [83] M. Levy. Electron densities in search of Hamiltonians. *Phys. Rev. A*, 26:1200–1208, 1982.
- [84] E. H. Lieb. Density functionals for Coulomb systems. *Int. J. Quant. Chem.*, 24:243–277, 1983.
- [85] H. Englisch and R. Englisch. Hohenberg-Kohn theorem and non- v -representable densities. *Physica*, 121A:253–268, 1983.
- [86] T. L. Gilbert. Hohenberg-Kohn theorem for nonlocal external potentials. *Phys. Rev. B*, 12:2111–2120, 1975.

- [87] J. P. Perdew and K. Schmidt. Jacob's ladder of density functional approximations for the exchange-correlation energy. volume 577. AIP Conf. Proc., 2001. Density functional theory and its application to materials.
- [88] D. M. Ceperley and B. J. Alder. Ground state of the electron gas by a stochastic method. *Phys. Rev. Lett.*, 45:566–569, 1980.
- [89] S. H. Vosko, L. Wilk, and M. Nusair. Accurate spin-dependent electron liquid correlation energies for local spin density calculations: a critical analysis. *Can. J. Phys.*, 58:1200–1211, 1980.
- [90] J. P. Perdew, K. Burke, and M. Ernzerhof. Generalized gradient approximation made simple. *Phys. Rev. Lett.*, 77:3965–3968, 1996.
- [91] J. Perdew, K. Burke, and M. Ernzerhof. Errata: Generalized gradient approximation made simple. *Phys. Rev. Lett.*, 78:1396, 1997.
- [92] Y. Zhao, N. E. Schultz, and D. G. Truhlar. Exchange-correlation functional with broad accuracy for metallic and nonmetallic compounds, kinetics, and noncovalent interactions. *J. Chem. Phys.*, 123:161103, 2005.
- [93] Becke3LYP Method References and General Citation Guidelines. *Gaussian NEWS*, 5:2, 1994.
- [94] T. Yanai, D. Tew, and N. Handy. A new hybrid exchange-correlation functional using the Coulomb-attenuating method (CAM-B3LYP). *Chem. Phys. Lett.*, 393:51–57, 2004.
- [95] C. Adamo and V. Barone. Toward reliable density functional methods without adjustable parameters: The PBE0 model. *J. Chem. Phys.*, 110:6158, 1999.
- [96] S. Grimme. Semiempirical hybrid density functional with perturbative second-order correlation. *J. Chem. Phys.*, 124:034108, 2006.
- [97] J. D. Talman and Phys. Rev. A W. F. Shadwick. Optimized effective atomic central potential. 14:36, 1976.
- [98] J. B. Krieger, Y. Li, and G. J. Iafrate. Construction and application of an accurate local spin-polarized Kohn-Sham potential with integer discontinuity: Exchange-only theory. *Phys. Rev. A*, 45:101, 1992.
- [99] J. B. Krieger, Y. Li, and G. J. Iafrate. Self-consistent calculations of atomic properties using self-interaction-free exchange-only Kohn-Sham potentials. *Phys. Rev. A*, 47:165, 1993.
- [100] R. van Leeuwen. The Sham-Schlüter equation in time-dependent density-functional theory. *Phys. Rev. Lett.*, 76:3610, 1996.
- [101] M. Fuchs and X. Gonze. Accurate density functionals: Approches using the adiabatic-connection fluctuation dissipation theorem. *Phys. Rev. B*, 65:235109, 2002.
- [102] A. K. Rajagopal and J. Callaway. Inhomogeneous electron gas. *Phys. Rev. B*, 7:1912–1919, 1973.
- [103] V. Peuckert. A new approximation method for electron systems. *J. Phys. C*, 11:4945, 1978.
- [104] L. J. Bartolotti. Time-dependent extension of the Hohenberg-Kohn-Levy energy-density functional. *Phys. Rev. A*, 24:1661–1667, 1981.

- [105] B. M. Deb and S. K. Ghosh. Schrödinger fluid dynamics of many-electron systems in a time-dependent density-functional framework. *J. Chem. Phys.*, 77:342–348, 1982.
- [106] E. K. U. Gross and W. Kohn. Time-dependent density-functional theory. In P. O. Löwdin, J. R. Sabin, and M. C. Zerner, editors, *Adv. Quant. Chem.*, volume 21, pages 255–291. Academic Press, Inc., 1990.
- [107] D. Mearns and W. Kohn. Frequency-dependent v -representability in density-functional theory. *Phys. Rev. A*, 35:4796, 1987.
- [108] M. Petersilka, U. J. Gossmann, and E. K. U. Gross. Excitation energies from time-dependent density-functional theory. *Phys. Rev. Lett.*, 76:1212, 1996.
- [109] S. Hirata and M. Head-Gordon. Time-dependent density functional theory within the Tamm-Dancoff approximation. *Chem. Phys. Lett.*, 314:291–299, 1999.
- [110] A. Ipatov, A. Fouqueau, C. Pérez del Valle, F. Cordova, M. E. Casida, A. M. Köster, A. Vela, and C. J. Jamorski. Excitation energies from an auxiliary-function formulation of time-dependent density-functional response theory with charge conservation constraint. *J. Molec. Struct.: THEOCHEM*, 762:179–191, 2006.
- [111] C. Jamorski, M. E. Casida, and D. R. Salahub. Dynamic polarizabilities and excitation spectra from a molecular implementation of time-dependent density-functional response theory: N₂ as a case study. *J. Chem. Phys.*, 104:5134, 1996.
- [112] S. Goedecker and A. Hoisie. *Performance Optimization of Numerically Intensive Codes*. SIAM, 2001.
- [113] R. L. Vander Wal, J. L. Scott, F. F. Crim, K. Weide, and R. Schinke. An experimental and theoretical study of the bond selected photodissociation of iodine. *J. Chem. Phys.*, 94:3548–3555, 1991.
- [114] M. E. Casida and M. Huix-Rotllant. Progress in time-dependent density-functional theory. *Ann. Rev. Phys. Chem.*, 2012. (in press).
- [115] K. Burke. Exact conditions. In E. K. U. Gross, M. A. L. Marques, F. Nogueira, and A. Rubio, editors, *Fundamentals of Time-Dependent Density-Functional Theory*, volume 706 of *Lecture Notes in Physics*, pages 181–197. Springer, 2005.
- [116] K. J. H. Giesbertz and E. J. Baerends. Failure of time-dependent density functional theory for excited state surfaces in case of homolytic bond dissociation. *Chem. Phys. Lett.*, 461:338–342, 2008.
- [117] M. van Fassen, P. L. de Boeij, R. van Leeuwen, J. A. Berger, and J. G. Snijders. Ultranon-locality in time-dependent current-density-functional theory: Application to conjugated polymers. *Phys. Rev. Lett.*, 88:186401, 2002.
- [118] D. Varsano, A. Marini, and A. Rubio. Optical saturation driven by exciton confinement in molecular chains: a time-dependent density-functional theory approach. *Phys. Rev. Lett.*, 101:133002, 2008.
- [119] G. Onida, L. Reining, and A. Rubio. Electronic excitations: density-functional versus many-body Green’s-function approaches. *Rev. Mod. Phys.*, 74:601, 2002.
- [120] L. Reining, V. Olevano, A. Rubio, and G. Onida. Excitonic effects in solids described by time-dependent density-functional theory. *Phys. Rev. Lett.*, 88:066404, 2002.

- [121] R. Del Sole, G. Adragna, V. Olevano, and L. Reining. Long-range behavior and frequency dependence of exchange-correlation kernels in solids. *Phys. Rev. B*, 67:045207, 2003.
- [122] Y. Kurzweil and R. Baer. Time-dependent exchange-correlation current density functionals with memory. *J. Chem. Phys.*, 121:8731, 2004.
- [123] E. K. U. Gross and W. Kohn. Local density-functional theory of frequency-dependent linear response. *Phys. Rev. Lett.*, 55:2850–2852, 1985. E. K. U. Gross and W. Kohn. Errata. *Phys. Rev. Lett.*, 57:923, 1986.
- [124] J. F. Dobson, M. J. Bünner, and E. K. U. Gross. Time-dependent density functional theory beyond linear response: An exchange-correlation potential with memory. *Phys. Rev. Lett.*, 79:1905–1908, 1997.
- [125] Y. Kurzweil and R. Baer. Adapting approximate-memory potentials for time-dependent density functional theory. *Phys. Rev. B*, 77:1–8, 2008.
- [126] G. Vignale and W. Kohn. Current-dependent exchange-correlation potential for dynamical linear response theory. *Phys. Rev. Lett.*, 77:2037, 1996.
- [127] G. Vignale, C. A. Ullrich, and S. Conti. Time-dependent density functional theory beyond the adiabatic local density approximation. *Phys. Rev. Lett.*, 79:4878, 1997.
- [128] C. A. Ullrich and G. Vignale. Time-dependent current-density-functional theory for the linear response of weakly disordered systems. *Phys. Rev. B*, 65:245102, 2002.
- [129] I. V. Tokatly and O. Pankratov. Local exchange-correlation vector potential with memory in time-dependent density functional theory: The generalized hydrodynamics approach. *Phys. Rev. B*, 67:201103(R), 2003.
- [130] I. V. Tokatly. Quantum many-body dynamics in a Lagrangian frame: I. Equations of motion and conservation laws. *Phys. Rev. B*, 71:165104, 2005.
- [131] I. V. Tokatly. Quantum many-body dynamics in a Lagrangian frame: II. Geometric formulation of time-dependent density functional theory. *Phys. Rev. B*, 71:165105, 2005.
- [132] C. A. Ullrich and I. V. Tokatly. Nonadiabatic electron dynamics in time-dependent density-functional theory. *Phys. Rev. B*, 73:235102, 2006.
- [133] R. D’Agosta and G. Vignale. Relaxation in time-dependent current-density-functional theory. *Phys. Rev. Lett.*, 96:016405, 2006.
- [134] P. L. de Boeij, F. Kootstra, J. A. Berger, R. van Leeuwen, and J. G. Snijders. Current density functional theory for optical spectra: A polarization functional. *J. Chem. Phys.*, 115:1995, 2001.
- [135] V. U. Nazarov, G. Vignale, and Y.-C. Chang. Communications: On the relation between the scalar and tensor exchange-correlation kernels of the time-dependent density-functional theory. *J. Chem. Phys.*, 133:021101, 2010.
- [136] C. A. Ullrich, U. J. Grossman, and E. K. U. Gross. Time-dependent optimized effective potential. *Phys. Rev. Lett.*, 74:872–875, 1995.
- [137] S. Hirata, S. Ivanov, I. Grabowski, and R. J. Bartlett. Time-dependent density functional theory employing optimized effective potentials. *J. Chem. Phys.*, 116:6468, 2002.
- [138] U. von Barth, N. Dahlen, R. van Leeuwen, and G. Stefanucci. Conserving approximations in time-dependent density functional theory. *Phys. Rev. B*, 72:1–10, 2005.

- [139] F. Bruneval, F. Sottile, V. Olevano, R. Del Sole, and L. Reining. Many-body perturbation theory using the density-functional concept : Beyond the GW approximation. *Phys. Rev. Lett.*, 186402:12–15, 2005.
- [140] M. Huix-Rotllant and M. E. Casida. Condensed Matter arXiv <http://arxiv.org/abs/1008.1478>. Formal Foundations of Dressed Time-Dependent Density-Functional Theory for Many-Electron Excitations.
- [141] U. von Barth, N. E. Dahlen, R. van Leeuwen, and G. Stefanucci. Conserving approximations in time-dependent density functional theory. *Phys. Rev. B*, 72:235109, 2005.
- [142] X. Gonze and M. Scheffler. Exchange and correlation kernels at the resonance frequency: Implications for excitation energies in density-functional theory. *Phys. Rev. Lett.*, 82:4416–4419, 1999.
- [143] M. Gatti, V. Olevano, L. Reining, and I. V. Tokatly. Transforming nonlocality into a frequency dependence : A shortcut to spectroscopy. *Phys. Rev. Lett.*, 057401:1–4, 2007.
- [144] A. Heßelmann and A. Görling. Efficient exact-exchange time-dependent density-functional theory methods and their relation to time-dependent Hartree-Fock. *J. Chem. Phys.*, 134:034120, 2011.
- [145] Open problems and new solutions in time dependent density functional theory. a special volume of Chem. Phys. guest edited by Roi Baer, Leor Kronik and Stephan Kummel, 2011 (in press).
- [146] H. O. Wijewardane and C. A. Ullrich. Real-time electron dynamics with exact-exchange time-dependent density-functional theory. *Phys. Rev. Lett.*, 100:056404, 2008.
- [147] N. Helbig, J. I. Fuks, I. V. Tokatly, H. Appel, E. K. U. Gross, and A. Rubio. Time-dependent density-functional and reduced density-matrix methods for few electrons: Exact versus adiabatic approximations. *Chem. Phys.*, 2011. (in press).
- [148] P. Elliott, S. Goldson, C. Canahui, and N. T. Maitra. Perspectives on double-excitations in tddft. *Chem. Phys.*, 2011. (in press).
- [149] M. E. Casida. Propagator corrections to adiabatic time-dependent density-functional theory linear response theory. *J. Chem. Phys.*, 122:054111, 2005.
- [150] G. Mazur and R. Włodarczyk. Application of the dressed time-dependent density functional theory for the excited states of linear polyenes. *J. Comput. Chem.*, 30:811, 2009.
- [151] G. Mazur, M. Makowski, R. Włodarczyk, and Y. Aoki. Dressed TDDFT study of low-lying electronic excited states in selected linear polyenes and diphenylopolynes. *Int. J. Quant. Chem.*, 111:819–825, 2011.
- [152] K. Pernal, K. Giesbertz, O. Gritsenko, and E. J. Baerends. Adiabatic approximation of time-dependent density matrix functional response theory. *J. Chem. Phys.*, 127:214101, 2007.
- [153] K. J. H. Giesbertz, E. J. Baerends, and O. V. Gritsenko. Charge transfer, double and bond-breaking excitations with time-dependent density matrix functional theory. *Phys. Rev. Lett.*, 101:033004, 2008.
- [154] K. J. H. Giesbertz, K. Pernal, O. V. Gritsenko, and E. J. Baerends. Excitation energies with time-dependent density matrix functional theory: Single two-electrons systems. *J. Chem. Phys.*, 130:114104, 2009.

- [155] K. J. H. Giesbertz, O. V. Gritsenko, and E. J. Baerends. Response calculations with an independent particle system with an exact one-particle density matrix. *Phys. Rev. Lett.*, 105:013002, 2010.
- [156] K. J. H. Giesbertz, O. V. Gritsenko, and E. J. Baerends. The adiabatic approximation in time-dependent density matrix functional theory: Response properties from dynamics of phase-including natural orbitals. *J. Chem. Phys.*, 133:174119, 2010.
- [157] K. J. H. Giesbertz and E. J. Baerends. Aufbau derived from a unified treatment of occupation numbers in Hartree-Fock, Kohn-Sham, and natural orbital theories with the Karush-Kuhn-Tucker conditions for the inequality constraints $n_i \leq 1$ and $n_i \geq 0$. *J. Chem. Phys.*, 132:194108, 2010.
- [158] M. Huix-Rotllant, B. Natarajan, A. Ipatov, M. C. Wawire, T. Deutsch, and M. E. Casida. Assessment of noncollinear spin-flip Tamm-Dancoff approximation time-dependent density-functional theory for the photochemical ring-opening of oxirane. *Phys. Chem. Chem. Phys.*, 12:12811–12825, 2010.
- [159] Z. Rinkevicius, O. Vahtras, and H. Ågren. Spin-flip time dependent density functional theory applied to excited states with single, double or mixed electron excitation character. *J. Chem. Phys.*, 133:114104, 2010.
- [160] Z. Rinkevicius and H. Ågren. Spin-flip time dependent density functional theory for singlet-triplet splittings in σ - σ -biradicals. *Chem. Phys. Lett.*, 491:132–135, 2010.
- [161] N. Minezawa and M. S. Gordon. Photoisomerization of stilbene: A spin-flip density functional theory approach. *J. Phys. Chem. A*, 115:7901, 2011.
- [162] O. Vahtras and Z. Rinkevicius. General excitations in time-dependent density functional theory. *J. Chem. Phys.*, 126:114101, 2007.
- [163] M. Filatov and S. Shaik. Spin-restricted density functional approach to the open-shell problem. *Chem. Phys. Lett.*, 288:689–697, 1998.
- [164] Z. Li and W. Liu. Spin-adapted open-shell random phase approximation and time-dependent density functional theory. I. Theory. *J. Chem. Phys.*, 133:064106, 2010.
- [165] Z. Li, W. Liu, Y. Zhang, and B. Suo. Spin-adapted open-shell time-dependent density functional theory. II. Theory and pilot application. *J. Chem. Phys.*, 134:134101, 2011.
- [166] E. W. G. Diau, C. Kötting, and A. H. Zewail. Femtochemistry of Norrish type-1 reactions: I. Experimental and theoretical studies of acetone and related ketones on the S_1 surface. *ChemPhysChem*, 2:273, 2001.
- [167] E. W. G. Diau, C. Kötting, and A. H. Zewail. Femtochemistry of Norrish type-1 reactions: II. The anomalous predissociation dynamics of cyclobutanone on the S_1 surface. *ChemPhysChem*, 2:294, 2001.
- [168] E. W.-G. Diau, C. Kötting, T. I. Sølling, and A. H. Zewail. Femtochemistry of Norrish type-I reactions: III. Highly excited ketones – theoretical. *ChemPhysChem*, 3:57, 2002.
- [169] T. I. Sølling, E. W.-G. Diau, C. Kötting, S. De Feyter, and A. H. Zewail. Femtochemistry of Norrish type-I reactions: IV. Highly excited ketones–experimental. *ChemPhysChem*, 3:79, 2002.
- [170] J. C. Tully. Molecular dynamics with electronic transitions. *J. Chem. Phys.*, 93:1061, 1990.

- [171] J. C. Tully. Nonadiabatic dynamics. In D. L. Thompson, editor, *Modern Methods for Multidimensional Dynamics Computations in Chemistry*, page 34, Singapore, 1998. World Scientific.
- [172] N. L. Doltsinis and D. Marx. First principles molecular dynamics involving excited states and nonadiabatic transitions. *J. Theo. Comput. Chem.*, 1:319, 2002.
- [173] C. F. Craig, W. R. Duncan, and O. V. Prezhdo. Trajectory surface hopping in the time-dependent Kohn-Sham approach for electron-nuclear dynamics. *Phys. Rev. Lett.*, 95:163001, 2005.
- [174] U. Werner, R. Mitrić, T. Suzuki, and V. Bonačić-Koutecký. Nonadiabatic dynamics within the time dependent density functional theory: Ultrafast photodynamics in pyrazine. *Chem. Phys.*, 349:319–324, 2008.
- [175] R. Mirić, U. Werner, and V. Bonačić-Koutecký. Nonadiabatic dynamics and simulation of time resolved photoelectron spectra within time-dependent density functional theory: Ultrafast photoswitching in benzylideneaniline. *J. Chem. Phys.*, 129:164118, 2008.
- [176] U. Werner, R. Mitrić, T. Suzuki, and V. Bonačić-Koutecký. Nonadiabatic dynamics and simulation of time resolved photoelectron spectra within time-dependent density functional theory: Ultrafast photoswitching in benzylideneaniline. *J. Chem. Phys.*, 129:164118, 2008.
- [177] A. D. Becke. Density-functional exchange-energy approximation with correct asymptotic behavior. *Phys. Rev. A*, 38:3098, 1988.
- [178] C. Lee, W. Yang, and R. G. Parr. Development of the Colle-Salvetti correlation-energy formula into a functional of the electron density. *Phys. Rev. B*, 37:785, 1988.
- [179] J. Schirmer and A. Dreuw. Critique of the foundations of time-dependent density-functional theory. *Phys. Rev. A*, 75:022513, 2007.
- [180] N. T. Maitra, K. Burke, and R. van Leeuwen. Critique of the foundations of time-dependent density functional theory. *Phys. Rev. A*, 75:022513, 2007.
- [181] J. Schirmer and A. Dreuw. Reply to “Comment on ‘Critique of the foundations of time-dependent density functional theory’ ”. *Phys. Rev. A*, 78:056502, 2008.
- [182] M. E. Casida. Jacob’s ladder for time-dependent density-functional theory: Some rungs on the way to photochemical heaven. In M. R. H. Hoffmann and K. G. Dyall, editors, *Accurate Description of Low-Lying Molecular States and Potential Energy Surfaces*, page 199. ACS Press, Washington, D.C., 2002.
- [183] M. E. Casida. Review: Time-dependent density-functional theory for molecules and molecular solids. *J. Mol. Struct. (Theochem)*, 914:3, 2009.
- [184] O. V. Gritsenko and E. J. Baerends. Double excitation effect in non-adiabatic time-dependent density functional theory with an analytic construction of the exchange-correlation kernel in the common energy denominator approximation. *Phys. Chem. Chem. Phys.*, 11:4640, 2009.
- [185] M. E. Casida, F. Gutierrez, J. Guan, F. Gadea, D. Salahub, and J. Daudey. Charge-transfer correction for improved time-dependent local density approximation excited-state potential energy curves: Analysis within the two-level model with illustration for H₂ and LiH. *J. Chem. Phys.*, 113:7062, 2000.

- [186] M. E. Casida, A. Ipatov, and F. Cordova. Linear-response time-dependent density-functional theory for open-shell molecules. In M.A.L. Marques, C. Ulrich, F. Nogueira, A. Rubio, and E.K.U. Gross, editors, *Time-Dependent Density Functional Theory*. Springer, Berlin, 2006.
- [187] S. Hirata and M. Head-Gordon. Time-dependent density functional theory within the Tamm-Dancoff approximation. *Chem. Phys. Lett.*, 314:291, 1999.
- [188] M. A. L. Marques, C. A. Ullrich, F. Nogueira, A. Rubio, K. Burke, and E. K. U. Gross, editors. *Time-dependent Density Functional Theory*. Lecture Notes of Physics. Springer, Berlin, 2006.
- [189] M. A. L. Marques and A. Rubio. Time-dependent density-functional theory. Special Issue: Phys. Chem. Chem. Phys. **11**, issue 22, pp. 4421-4688 (2009).
- [190] M. E. Casida, H. Chermette, and D. Jacquemin. Time-dependent density-functional theory for molecules and molecular solids. Special Issue: J. Mol. Struct. (Theochem), **914** (2009).
- [191] E. Gomer and Jr. W. A. Noyes. Photochemical studies. XLII. Ethylene oxide. *J. Am. Chem. Soc.*, 72:101, 1950.
- [192] E. Hasegawa and M. Kamata. Photoinduced electron transfer reactions of oxiranes and epoxyketones. In W. Horspool and F. Lenci, editors, *CRC Handbook of Organic Photoreactions and Photobiology, Second Edition*, page 53. CRC Press, New York, 2004.
- [193] F. Wang and T. Ziegler. Time-dependent density functional theory based on a noncollinear formulation of the exchange-correlation potential. *J. Chem. Phys.*, 121:12191, 2004.
- [194] R. Kishi, M. Nakano, S. Ohta, A. Takebe, M. Nate, H. Takahashi, T. Kubo, K. Kamada, K. Ohta, B. Champagne, and E. Botek. Finite-field spin-flip configuration interaction calculation of the second hyperpolarizabilities of singlet diradical systems. *J. Chem. Theor. Comput.*, 3:1699, 2007.
- [195] A. Thomas, K. Srinivas, C. Prabhakara, K. Bhanuprakash, and V. J. Rao. Estimation of the first excitation energy in diradicaloid croconate dyes having absorption in the near infra red (NIR): A DFT and SF-TDDFT study. *Chem. Phys. Lett.*, 454:36, 2008.
- [196] A. De La Lande, H. Gérard, and O. Parisel. How to optimize a CH cleavage with a mononuclear copper-dioxygen adduct? *Int. J. Quant. Chem.*, 108:1898, 2008.
- [197] N. Minezawa and M. S. Gordon. Optimizing conical intersections by spin-flip density functional theory: Application to ethylene. *Phys. Chem. A Lett.*, 113:12749, 2009.
- [198] J. Gao, W. Zou, W. Liu, Y. Xiao, D. Peng, B. Song, and C. Liu. Time-dependent four-component relativistic density functional theory for excitation energies: II. The exchange-correlation kernel. *J. Chem. Phys.*, 123:054102, 2005.
- [199] H. Eshrig and V. D. P. Servidio. Relativistic density functional approach to open shells. *J. Comput. Chem.*, 20:23, 1999.
- [200] C. van Wüllen. Spin densities in two-component relativistic density functional calculations: Noncollinear versus collinear approach. *J. Comput. Chem.*, 23:779, 2002.
- [201] M. Seth and T. Ziegler. Calculation of excitation energies of open-shell molecules with spatially degenerate ground states. I. Transformed reference via an intermediate configuration Kohn-Sham density-functional theory and applications to d^1 and d^2 systems with octahedral and tetrahedral symmetries. *J. Chem. Phys.*, 123:144105, 2005.

- [202] J. Guan, F. Wang, T. Ziegler, and H. Cox. Time-dependent density functional study of the electronic potential energy curves and excitation spectrum of the oxygen molecule. 125:044314, 2006.
- [203] L. M. Lawson Daku, J. Linares, and M.-L. Boillot. Ab initio static and molecular dynamics study of the absorption spectra of the 4-styrylpyridine photoswitch in its cis and trans forms. *Phys. Chem. Chem. Phys.*, 12:6107–6123, 2010.
- [204] A. V. Luzanov and O. A. Zhikol. Electron invariants and excited state structural analysis for electronic transitions within CIS, RPA, and TDDFT models. *Int. J. Quant. Chem.*, 110:902, 2010.
- [205] DEMON2K@GRENOBLE, the Grenoble development version of DEMON2K, Andreas M. Köster, Patrizia Calaminici, Mark E. Casida, Roberto Flores-Morino, Gerald Geudtner, Annick Goursot, Thomas Heine, Andrei Ipatov, Florian Janetzko, Sergei Patchkovskii, J. Ullis Reveles, Dennis R. Salahub, and Alberto Vela, *The International deMon Developers Community* (Cinvestav-IPN, Mexico, 2006).
- [206] M. J. Frisch, G. W. Trucks, H. B. Schlegel, G. E. Scuseria, M. A. Robb, J. R. Cheeseman, J. A. Montgomery, Jr., T. Vreven, K. N. Kudin, J. C. Burant, J. M. Millam, S. S. Iyengar, J. Tomasi, V. Barone, B. Mennucci, M. Cossi, G. Scalmani, N. Rega, G. A. Petersson, H. Nakatsuji, M. Hada, M. Ehara, K. Toyota, R. Fukuda, J. Hasegawa, M. Ishida, T. Nakajima, Y. Honda, O. Kitao, H. Nakai, M. Klene, X. Li, J. E. Knox, H. P. Hratchian, J. B. Cross, C. Adamo, J. Jaramillo, R. Gomperts, R. E. Stratmann, O. Yazyev, A. J. Austin, R. Cammi, C. Pomelli, J. W. Ochterski, P. Y. Ayala, K. Morokuma, G. A. Voth, P. Salvador, J. J. Dannenberg, V. G. Zakrzewski, S. Dapprich, A. D. Daniels, M. C. Strain, O. Farkas, D. K. Malick, A. D. Rabuck, K. Raghavachari, J. B. Foresman, J. V. Ortiz, Q. Cui, A. G. Baboul, S. Clifford, J. Cioslowski, B. B. Stefanov, G. Liu, A. Liashenko, P. Piskorz, I. Komaromi, R. L. Martin, D. J. Fox, T. Keith, M. A. Al-Laham, C. Y. Peng, A. Nanayakkara, M. Challacombe, P. M. W. Gill, B. Johnson, W. Chen, M. W. Wong, C. Gonzalez, and J. A. Pople, GAUSSIAN 03, Revision B.05, Gaussian, Inc., Pittsburgh PA, 2003.
- [207] A. Ipatov, A. Fouqueau, C. Perez del Valle, F. Cordova, M. E. Casida, A. M. Köster, A. Vela, and C. Jödicke Jamorski. Excitation energies from an auxiliary-function formulation of time-dependent density-functional response theory with charge conservation constraint. *J. Mol. Struct. (Theochem)*, 762:179, 2006.
- [208] G. te Velde, F. M. Bickelhaupt, E. J. Baerends, C. Fonseca, C. Guerra, S. J. A. van Gisbergen, J. G. Snijders, and T. Ziegler. Chemistry with ADF. *J. Comput. Chem.*, 22:931, 2001.
- [209] R. Krishnan, J. S. Binkley, R. Seeger, and J. A. Pople. Self-consistent molecular orbital methods. XX. A basis set for correlated wave functions. *J. Chem. Phys.*, 72:650, 1980.
- [210] T. Clark, J. Chandrasekhar, and P. v. R. Schleyer. Efficient diffuse function-augmented basis sets for anion calculations. III. the 3-21+G basis set for first-row elements, Li-F. *J. Comp. Chem.*, 4:294–301, 1983.
- [211] Enrico Tapavicza. Personal Communication.
- [212] V. Chernyak and S. Mukamel. Density-matrix representation of nonadiabatic couplings in time-dependent density functional (TDDFT) theories. *J. Chem. Phys.*, 112:3572, 2000.

- [213] R. Baer. Non-adiabatic couplings by time-dependent density functional theory. *Chem. Phys. Lett.*, 364:75, 2002.
- [214] C. Hu, H. Hirai, and O. Sugino. Nonadiabatic couplings from time-dependent density functional theory: Formulation in the Casida formalism and practical scheme within modified linear response. *J. Chem. Phys.*, 127:064103, 2007.
- [215] C. Hu, H. Hirai, and O. Sugino. Nonadiabatic couplings from time-dependent density functional theory. II. Successes and challenges of the pseudopotential approximation. *J. Chem. Phys.*, 128:154111, 2008.
- [216] I. Tavernelli, E. Tapavicza, and U. Rothlisberger. Nonadiabatic coupling vectors within linear response time-dependent density functional theory. *J. Chem. Phys.*, 130:124107, 2009.
- [217] I. Tavernelli, E. Tapavicza, and U. Rothlisberger. Non-adiabatic dynamics using time-dependent density functional theory: Assessing the coupling strengths. *J. Molec. Struct. (Theochem)*, 914:22, 2009.
- [218] R. van Leeuwen. The Sham-Schlüter Equation in Time-Dependent Density-Functional Theory. *Phys. Rev. Lett.*, 76:3610–3613, 1996.
- [219] E. S. Nielsen, P. Jørgensen, and J. Oddershede. Transition moments and dynamic polarizabilities in a second order polarization propagator approach. *J. Chem. Phys.*, 73:6238, 1980.
- [220] E. S. Nielsen, P. Jørgensen, and J. Oddershede. Erratum *J. Chem. Phys.*, **73**, 6238 (1980). *J. Chem. Phys.*, 75:499, 1981.
- [221] P. Jørgensen and J. Simons. *Second Quantization-Based Methods in Quantum Chemistry*. Academic Press, New York, 1981.
- [222] A. B. Trofimov, G. Stelter, and J. Schirmer. A consistent third-order propagator method for electronic excitation. *J. Chem. Phys.*, 111:9982, 1999.
- [223] M. E. Casida. Time-dependent density functional response theory of molecular systems: Theory, computational methods, and functionals. In J. Seminario, editor, *Recent Developments and Applications of Modern Density Functional Theory*, page 391. Elsevier, Amsterdam, 1996.
- [224] P.-O. Löwdin. Studies in perturbation theory. part VI. contraction of secular equations. *J. Mol. Spectr.*, 14:112, 1964.
- [225] D. Bokhan, I. G. Schweigert, and R. J. Bartlett. Interconnection between functional derivative and effective operator approaches in *ab initio* density functional theory. *Mol. Phys.*, 103:2299, 2005.
- [226] D. Bokhan and R. J. Bartlett. Adiabatic *ab initio* time-dependent density-functional theory employing optimized-effective-potential many-body perturbation theory potentials. *Phys. Rev. A*, 73:022502, 2006.
- [227] J. D. Talman. A program to compute variationally optimized effective atomic potentials. *Comp. Phys. Commun.*, 54:85, 1989.
- [228] A. Görling. New KS method for molecules based on an exchange charge density generating the exact local KS exchange potential. *Phys. Rev. Lett.*, 83:5459, 1999.

- [229] S. Ivanov, S. Hirata, and R. J. Bartlett. Exact exchange treatment for molecules in finite-basis-set Kohn-Sham theory. *Phys. Rev. Lett.*, 83:5455, 1999.
- [230] M. E. Casida. Generalization of the optimized effective potential model to include electron correlation: A variational derivation of the Sham–Schlüter equation for the exact exchange-correlation potential. *Phys. Rev. A*, 51:2505, 1995.
- [231] M. E. Casida. Correlated optimized effective potential treatment of the derivative discontinuity and of the highest occupied Kohn-Sham eigenvalue: A Janak-type theorem for the optimized effective potential method. *Phys. Rev. B*, 59:4694, 1999.
- [232] D. Bokhan and R. J. Barlett. Exact-exchange density functional theory for hyperpolarizabilities. *J. Chem. Phys.*, 127:174102, 2007.
- [233] F. Sottile, V. Olevano, and L. Reining. Parameter-free calculation of response functions in time-dependent density-functional theory. *Phys. Rev. Lett.*, 91:056402, 2003.
- [234] A. Marini, R. Del Sole, and A. Rubio. Bound excitons in time-dependent density-functional theory: Optical and energy-loss spectra. *Phys. Rev. Lett.*, 91:256402, 2003.
- [235] R. Stubner, I. V. Tokatly, and O. Pankratov. Excitonic effects in time-dependent density-functional theory: An analytically solvable model. *Phys. Rev. B*, 70:245119, 2004.
- [236] I. V. Tokatly and O. Pankratov. Many-body diagrammatic expansion in a Kohn-Sham basis: Implications for time-dependent density functional theory of excited states. *Phys. Rev. Lett.*, 86:2078, 2001.
- [237] I. V. Tokatly, R. Stubner, and O. Pankratov. Many-body diagrammatic expansion of the exchange-correlation kernel in time-dependent density-functional theory. *Phys. Rev. B*, 65:113107, 2002.
- [238] D. Sangalli, P. Romaniello, G. Colò, A. Marini, and G. Onida. unpublished. preprint: “Double excitation in correlated systems: A many-body approach”.
- [239] J. Paldus and J. Čížek. Green’s function approach to the direct perturbation calculation of the excitation energy of closed shell fermion systems. *J. Chem. Phys.*, 60:149, 1974.
- [240] J. Paldus and J. Čížek. Time-independent diagrammatic approach to perturbation theory of fermion systems. In Per-Olov Löwdin, editor, *Advances in Quantum Chemistry*, volume 9, page 105. Academic Press, 1975.
- [241] E. E. Salpeter and H. A. Bethe. A relativistic equation for bound-state problems. *Phys. Rev.*, 84:1232, 1951.
- [242] L. Hedin. New method for calculating the one-particle Green’s function with application to the electron-gas problem. *Phys. Rev.*, 139:A796, 1965.
- [243] M. Gatti, V. Olevano, L. Reining, and I. V. Tokatly. Transforming nonlocality into a frequency dependence: A shortcut to spectroscopy. *Phys. Rev. Lett.*, 99:057401, 2007.
- [244] S. Hamel, M. E. Casida, and D. R. Salahub. Exchange-only optimized effective potential for molecules from resolution-of-the-identity techniques: Comparison with the local density approximation, with and without asymptotic correction. *J. Chem. Phys.*, 116:8276, 2002.
- [245] See supplementary material at Sec. 5.3 for an explicit list of Hugenholtz diagrams that have been resummed to obtain the expressions reported in this article.

- [246] T. Shibuya, J. Rose, and V. McKoy. Equations-of-motion method including renormalization and double-excitation mixing. *J. Chem. Phys.*, 1973.
- [247] P. Jørgensen, J. Oddershede, and M. A. Ratner. Two-particle, two-hole corrections to a self-consistent time-dependent Hartree-Fock scheme. *Chem. Phys. Lett.*, 32:111, 1975.
- [248] J. Oddershede and J. R. Sabin. The use of modified virtual orbitals in perturbative polarization propagator calculations. *J. Chem. Phys.*, 1983.
- [249] J. Oddershede, P. Jørgensen, and D. L. Yeager. Polarization propagator methods in atomic and molecular calculations. *Comp. Phys. Rep.*, 2:33–92, 1984.
- [250] S. Hirata, S. Ivanov, R. J. Bartlett, and I. Grabowski. Exact-exchange time-dependent density-functional theory for static and dynamic polarizabilities. *Phys. Rev. A*, 71:032507, 2005.
- [251] C. Filippi, C. J. Umrigar, and X. Gonze. Excitation energies from density functional perturbation theory. *J. Chem. Phys.*, 107:9994–10002, 1997.
- [252] A. Görling. Density-functional theory for excited states. *Phys. Rev. A*, 54:3912–3915, 1996.
- [253] D. H. Kobe. Linked cluster theorem and the Green’s function equations of motion for a many-fermion system. *J. Math. Phys.*, 7:1806–1820, 1966.
- [254] J. Oddershede, P. Jørgensen, and N. H. F. Beebe. Analysis of excitation energies and transition moments. *J. Phys. B: Atom. Molec. Phys.*, 11:1, 1978.
- [255] A. B. Trofimov and J. Schirmer. An efficient polarization propagator approach to valence electron excitation spectra. *J. Phys. B: At. Mol. Opt. Phys.*, 28:2299, 1995.
- [256] M. H. Palmer and I. C. Walker. The electronic states of buta-1,3-diene studied by *ab initio* configuration interaction and DFT methods, and electron energy loss spectroscopy. *Chem. Phys.*, 373:159–169, 2010.
- [257] M. Schreiber, M. R. Silva-Junior, S. P. A. Sauer, and W. Thiel. Benchmarks for electronically excited states: CASPT2, CC2, CCSD, and CC3. *J. Chem. Phys.*, 128:134110, 2008.
- [258] J. H. Starcke, M. Wormit, J. Schirmer, and A. Dreuw. How much double excitation character do the lowest excited states of linear polyenes have? *Chem. Phys.*, 329:39–49, 2006.
- [259] L. Serrano-Andrés, , R. Lindh, B. O. Roos, and M. Merchán. Theoretical study of the electronic spectrum of *all-trans*-1,3,5,7-octatetraene. *J. Phys. Chem.*, 97:9360, 1993.
- [260] M. Huix-Rotllant, A. Ipatov, A. Rubio, and M. E. Casida. Assessment of dressed time-dependent density-functional theory for the low-lying valence states of 28 organic chromophores. *Chem. Phys.*, 391:120–129, 2011.
- [261] C. P. Hsu, S. Hirata, and M. Head-Gordon. Excitation energies from time-dependent density functional theory for linear polyene oligomers: Butadiene to decapentaene. *J. Phys. Chem. A*, 105:451, 2001.
- [262] DALTON, a molecular electronic structure program, Release 2.0 (2005), see <http://www.kjemi.uio.no/software/dalton/dalton.html>.
- [263] R. T. Sharp and G. K. Horton. A variational approach to the unipotential many-electron problem. *Phys. Rev.*, 90:317, 1953.

- [264] J. E. Harriman. Geometry of density-matrices. 4. The relationship between density-matrices and densities. *Phys. Rev. A*, 27:632, 1983.
- [265] J. E. Harriman. Densities, operators, and basis sets. *Phys. Rev. A*, 34:29, 1986.
- [266] V. N. Staroverov, G. E. Scuseria, and E. R. Davidson. Optimized effective potentials yielding Hartree-Fock energies and densities. *J. Chem. Phys.*, 124:141103, 2006.
- [267] V. N. Staroverov, G. E. Scuseria, and E. R. Davidson. Effective local potentials for orbital-dependent density functionals. *J. Chem. Phys.*, 125:081104, 2006.
- [268] A. F. Izmaylov, V. N. Staroverov, G. E. Scuseria, E. R. Davidson, G. Stoltz, and E. Cancès. The effective local potential method: Implementation for molecules and relation to approximate optimized effective potential techniques. *J. Chem. Phys.*, 126:084107, 2007.
- [269] A. Heßelmann, A. W. Götz, F. Della Salla, and A. Görling. Numerically stable optimized effective potential method with balanced Gaussian basis sets. *J. Chem. Phys.*, 127:054102, 2007.
- [270] O. V. Gritsenko and E. J. Baerends. Orbital structure of the Kohn-Sham exchange potential and exchange kernel and the field-counteracting potential for molecules in an electric field. *Phys. Rev. A*, 64:042506, 2001.
- [271] F. Della Sala and A. Görling. Efficient localized Hartree-Fock methods as effective exact-exchange Kohn-Sham methods for molecules. *J. Chem. Phys.*, 115:5718, 2001.
- [272] A. Unsöld. Quantentheorie des Wasserstoffmolekülions und der Born-Landéschen Abstoßungskräfte. *Z. Physik*, 43:563, 1927.
- [273] M. G. Sylvain and I. G. Csizmadia. Average polarizabilities from the Unsöld approximation and *ab initio* data. *Chem. Phys. Lett.*, 136:575, 1987.
- [274] J. C. Slater. A simplification of the Hartree-Fock method. *Phys. Rev.*, 81:385, 1951.
- [275] S. Wilson. *Electron correlation in Molecules*. Clarendon Press, 1984.
- [276] B. O. Roos. Theoretical studies of electronically excited states of molecular systems using multiconfigurational perturbation theory. *Acc. Chem. Res.*, 32:137–144, 1999.
- [277] G. Mazur, M. Makowski, R. Włodarczyk, and Y. Aoki. Dressed TDDFT study of low-lying electronic excited states in selected linear polyenes and diphenylpolyenes. *Int. J. Quant. Chem.*, 111:819–825, 2010.
- [278] M. R. Silva-Junior, M. Schreiber, S. P. A. Sauer, and W. Thiel. Benchmarks for electronically excited states: Time-dependent density functional theory and density functional theory based multireference configuration interaction. *J. Chem. Phys.*, 129:104103, 2008.
- [279] A. Zangwill and P. Soven. Density-functional approach to local-field effects in finite systems: Photoabsorption in the rare gases. *Phys. Rev. A*, 21:1561–1572, 1980.
- [280] R. van Leeuwen. Causality and symmetry in time-dependent density-functional theory. *Phys. Rev. Lett.*, 80:1280–1283, 1998.
- [281] A. K. Rajagopal. Time-dependent variational principle and the effective action in density-functional theory and Berrys phase. *Phys. Rev. A*, 54:3916–3922, 1996.
- [282] S. Mukamel. Generalized time-dependent density-functional-theory response functions for spontaneous density fluctuations and nonlinear response: Resolving the causality paradox in real time. *Phys. Rev. A*, 71:1–4, 2005.

- [283] T. A. Niehaus and N. H. March. Brief review related to the foundations of time-dependent density functional theory. *Theor. Chem. Acc.*, 125:427–432, 2009.
- [284] M. E. Casida, A. Ipatov, and F. Cordova. Linear-response time-dependent density-functional theory for open-shell molecules. In Miguel A. L. Marques, C. A. Ullrich, F. Nogueira, and A. Rubio, editors, *Lecture Notes in Physics*. Springer, Berlin, 2006.
- [285] M. Wanko, M. Hoffmann, P. Strodel, A. Koslowski, W. Thiel, F. Neese, T. Frauenheim, and M. Elstner. Calculating absorption shifts for retinal proteins: computational challenges. *J. Phys. Chem. B*, 109:3606–15, 2005.
- [286] R. J. Cave and E. R. Davidson. Theoretical investigation of several low-lying states of trans,trans-1,3,5-hexatriene. *J. Phys. Chem.*, 92:614–620, 1988.
- [287] L. Serrano-Andrés, J. Sánchez-Marin, and I. Nebot-Gil. Theoretical study of the lowlying states of trans-1,3-butadiene. *J. Chem. Phys.*, 97:7499, 1992. Erratum, **98**, 7663 (1993).
- [288] J. Lappe and R. J. Cave. On the vertical and adiabatic excitation energies of the 2^1A_g state of trans-1,3-butadiene. *J. Phys. Chem. A*, 104:2294–2300, 2000.
- [289] M. Boggio-Pasqua, M. J. Bearpark, M. Klene, and M. A. Robb. A computational strategy for geometry optimization of ionic and covalent excited states, applied to butadiene and hexatriene. *J. Chem. Phys.*, 120:7849–60, 2004.
- [290] J. Catalán and J. L. G. de Paz. On the photophysics of all-trans polyenes: Hexatriene versus octatetraene. *J. Chem. Phys.*, 124:034306, 2006.
- [291] I. A. Mikhailov, S. Tafur, and A. E. Masunov. Double excitations and state-to-state transition dipoles in $\pi - \pi^*$ excited singlet states of linear polyenes: Time-dependent density-functional theory versus multiconfigurational methods. *Phys. Rev. A*, 77:012510, 2008.
- [292] G. Wald. The molecular basis of visual excitation. In *Nobel Lectures, Physiology or Medicine 1963-1970*, pages 293–315. Elsevier Publishing Company, Amsterdam, 1972.
- [293] R. Granit. The development of retinal neurophysiology. In *Nobel Lectures, Physiology or Medicine 1963-1970*, pages 255–265. Elsevier Publishing Company, Amsterdam, 1972.
- [294] H. K. Hartline. Visual receptors and retinal interaction. In *Nobel Lectures, Physiology or Medicine 1963-1970*, pages 269–288. Elsevier Publishing Company, Amsterdam, 1972.
- [295] N. T. Maitra. Initial-state dependence and memory. In Miguel A. L. Marques, C. A. Ullrich, F. Nogueira, and Angel Rubio, editors, *Lecture Notes in Physics*. Springer, Berlin, 2 edition, 2011.
- [296] A. I. Krylov. Spin-flip configuration interaction: an electronic structure model that is both variational and size-consistent. *Chem. Phys. Lett.*, 350:522–530, 2001.
- [297] F. Zhang and K. Burke. Adiabatic connection for near degenerate excited states. *Phys. Rev. A*, 69:052510, 2004.
- [298] A. B. Trofimov and J. Schirmer. An efficient polarization propagator approach to valence electron excitation spectra. *J. Phys. B: At. Mol. Opt. Phys.*, 28:2299–2324, 1995.
- [299] S. Hirata, C. Zhan, E. Aprà, T. L. Windus, and D. A. Dixon. A new, self-contained asymptotic correction scheme to exchange-correlation potentials for time-dependent density functional theory. *J. Phys. Chem. A*, 107:10154–10158, 2003.

- [300] M. E. Casida and D. R. Salahub. Asymptotic correction approach to improving approximate exchange-correlation potentials: Time-dependent density-functional theory calculations of molecular excitation spectra. *J. Chem. Phys.*, 113:8918, 2000.
- [301] A. Schäfer, H. Horn, and R. Ahlrichs. Fully optimized contracted Gaussian basis sets for atoms Li to Kr. *J. Chem. Phys.*, 97:2571, 1992.
- [302] A. D. Becke. Density-functional thermochemistry. III. The role of exact exchange. *J. Chem. Phys.*, 98:5648–5652, 1993.
- [303] C. Adamo and V. Barone. Accurate excitation energies from time-dependent density functional theory: assessing the PBE0 model for organic free radicals. *Chem. Phys. Lett.*, 314:152–157, 1999.
- [304] M.W. Schmidt, K.K. Baldridge, J.A. Boatz, S.T. Elbert, M.S. Gordon, J.H. Jensen, S. Koseki, N. Matsunaga, K.A. Nguyen, S.J. Su, T.L. Windus, M. Dupuis, and J.A. Montgomery. General atomic and molecular electronic structure system. *J. Comput. Chem.*, 14:1347–1363, 1993. Version 12 Jan 2009 (R1).
- [305] H. Nakano. Quasidegenerate perturbation theory with multiconfigurational self-consistent-field reference functions. *J. Chem. Phys.*, 99:7983–7992, 1993.
- [306] H. Nakano. MCSCF reference quasidegenerate perturbation theory with Epstein-Nesbet partitioning. *Chem. Phys. Lett.*, 207:372–378, 1993.
- [307] A. Castro, H. Appel, M. Oliveira, C. A. Rozzi, X. Andrade, F. Lorenzen, M. A. L. Marques, E. K. U. Gross, and A. Rubio. octopus: a tool for the application of time-dependent density-functional theory. *Phys. Stat. Sol. B*, 243:2465–2488, 2006.
- [308] M. A. L. Marques, A. Castro, G. F. Bertsch, and A. Rubio. octopus: a first-principles tool for excited electron-ion dynamics. *Comput. Phys. Commun.*, 151:60–78, 2003.

List of Figures

1.1	Schematic plot of a potential energy surface	11
1.2	Photoisomerization of stilbene	14
1.3	Schematic mechanism of stilbene photoisomerization	15
1.4	A dark states shows up in the spectrum due to the coupling with a bright state	17
3.1	Jacob's ladder of static density functionals	42
3.2	Schematic plot of the response function	53
4.1	Gomer-Noyes mechanism	75
4.2	Two-orbital model of excitations (triplet reference)	76
4.3	Dissociation of H ₂ with spin-flip TDDFT	77
4.4	Two-orbital model of excitations (singlet reference)	80
4.5	Diagram of frontier orbitals for symmetric ring opening	84
4.6	Potential energy surfaces for symmetric ring opening	86
4.7	Comparison of spin-flip with other methods for the symmetric ring opening	87
4.8	Illustration of orbital relaxation effects in SF versus SP TDDFT	88
4.9	Potential energy surfaces for asymmetric ring opening	90
4.10	Walsh diagram during asymmetric ring opening in regular TDDFT	91
4.11	Conical intersection beteen S_0 and S_1 with different methods	92
4.12	Excitation energy surface between at the intersection point of S_0 and S_1	92
4.13	Walsh diagram during the asymmetric ring opening in spin-flip TDDFT	93
5.1	Two-level model used by Maitra <i>et al.</i> in the derivation of dressed TDDFT.	105
5.2	Graphical representation of the localization of the Bethe-Salpeter equation	118
5.3	Diagrammatic representation of the polarization propagator kernel	122
5.4	First-order time-unordered diagrams of the Bethe-Salpeter equation	123
5.5	Frontier molecular orbitals of butadiene	130
5.6	Dominant contributions to the low-lying excited states in <i>trans</i> -butadiene.	131
5.7	Basic time-ordered finite basis set representation PP diagram.	141
5.8	Basic frequency and finite basis set representation PP diagram.	142
5.9	Basic frequency and real space representation PP diagram.	142
5.10	Time-unordered representation PP diagram.	142
5.11	Zero-order PP diagrams.	143
5.12	Electron repulsion integral diagrams.	144
5.13	Diagrammatic contributions due to Eq.(5.195)	146
5.14	Diagrammatic contributions due to Eq.(5.196)	147
5.15	Diagrammatic contributions due to Eq.(5.197)	148
5.16	Diagrammatic contributions due to Eq.(5.198)	149
5.17	Diagrammatic contributions due to Eq.(5.199)	150
5.18	Diagrammatic contributions due to Eq.(5.200)	151

5.19	Diagrammatic contributions due to Eq.(5.201)	152
5.20	Diagrammatic contributions due to Eq.(5.202)	153
5.21	Diagrammatic contributions due to Eq.(5.203)	154
5.22	Diagrammatic contributions due to Eq.(5.204)	155
6.1	Spin contamination in truncated 2h2p spaces	164
6.2	Schematic representation of the interaction between 1h1p and 2h2p states	166
6.3	Dependence of the 1h1p states of ethene on the number of 2h2p states	167
6.4	Correlation graphs of singlet excitations with different dressed methods	169
6.5	Correlation graphs for singlet excitations using a hybrid kernel	172
6.6	Effect of dressed TDDFT on states with high 2h2p contribution	180
7.1	Pure spin spin-flip excitations from a triplet reference state.	186
7.2	Graphical depiction of ethene torsion coordinate (Θ)	190
7.3	First three excited states of ethene along the twisting coordinate	191

List of Tables

5.1	Butadiene vertical excitation energies (eV).	132
6.1	Summary of method abbreviations	163
6.2	Mean absolute errors and standard deviations of different methods	173
6.3	Singlet 1h1p excitations for excited states with high 2h2p contribution	175

Introduction et Conclusions (en français)

Introduction

La photochimie est l'étude de la réactivité chimique qui a lieu dans les états excités. Dans la plupart des molécules, les états excités se trouvent dans une gamme d'énergie entre l'infrarouge lointain (700-1200 nm) et l'ultraviolet proche (200-400 nm). Cette énergie est transférée au système par une réaction chimique, par transfert d'énergie intermoléculaire ou par absorption de radiation. Ensuite, le système excité se relâche jusqu'à atteindre l'état stationnaire le plus bas en énergie, libérant ainsi l'excès d'énergie par une combinaison de mécanismes de relaxation radiatifs et non-radiatifs.

La photochimie a été utilisée traditionnellement comme voie de synthèse alternative aux réactions thermales. Les cycloadditions sont un exemple bien connu de réaction photochimique. Par exemple, la cycloaddition Diels-Alder produit des anneaux de carbone à partir d'un diène, d'un diénophile et d'un photon. La réactivité photochimique reprend de l'importance dans le domaine de la chimie verte, qui essaie de développer des voies de synthèse utilisant des réactifs non dangereux et respectueux de l'environnement [1].

Durant la dernière décennie, le développement de lasers d'impulsion ultracourte a doté la photochimie d'une nouvelle dimension. Ces lasers permettent le développement du contrôle quantique, où des impulsions ultracourtes sont utilisées pour produire des interférences à des états quantiques cohérents pour diriger la dynamique de paquets d'onde [2]. Ainsi, la réactivité dans l'état excité peut être contrôlée, ouvrant une gamme de nouvelles applications.

Un exemple important, qui illustre le potentiel de contrôle de la photochimie, est la photosynthèse des plantes vertes. La photosynthèse capture, transfère et accumule l'énergie solaire à partir d'une série de réactions en chaîne à travers plusieurs protéines. La dynamique exacte de l'efficace transfert des électrons est toujours inconnue. Des expériences menées récemment au complexe Fenna-Mathews-Olson sur la bactérie verte fluorescente (une protéine plus simple avec un rôle similaire à celui des photosystèmes I-II des plantes vertes) montre que l'efficace transfert d'énergie peut être du à un état cohérent de longue vie entre les antennes d'absorption et le site d'accumulation [3]. Cet état est modulé par l'environnement, permettant de sélectionner, sur chaque absorption d'un photon, les molécules antenne qui accomplissent le transfert d'énergie plus efficacement [4].

Comprendre la dynamique des électrons en systèmes biologiques aurait de gros impacts sur l'amélioration de l'efficacité des cellules photovoltaïques. Pour le moment, des stratégies plus simples sont explorées, comme par exemple l'utilisation de matériaux qui génèrent multiples couples d'électron-trous (excitons) à partir de l'absorption d'un seul photon [5,6]. Si ces excitons pouvaient être diffusés et dissociés aux parois conductrices de la cellule photovoltaïque, cela augmenterait énormément le nombre de transporteurs de charge [7]. Les possibilités de trouver ces matériaux sont faibles mais des matériaux aux propriétés intéressantes sont actuellement découverts dans ce domaine [8].

Les possibilités qu’offre la photochimie commencent à être comprises et exploitées grâce à l’utilisation de lasers d’impulsion ultracourte en chimie – que l’on appelle femtochimie – eux-mêmes utilisés pour la première fois par le prix Nobel A. Zewail [9]. Avant cela, les mécanismes dans les états excités n’étaient pas accessibles expérimentalement, car les photoproduits ayant un temps de vie de quelque femtoseconde et ne pouvant pas être détectés par les techniques spectroscopiques traditionnelles. Les prédictions théoriques ont été comparées avec les temps de vie radiatives ou les distributions de produits à la fin de la réaction. Actuellement, les lasers femtoseconde permettent une observation directe d’événements ultracourts dans les états excités. Une contribution importante est la publication récente de la première observation expérimentale d’un entonnoir moléculaire dans la réaction d’isomérisation cis-trans de la molécule 11-trans-retinal, qui se trouve au centre actif de la protéine rhodopsine responsable de la vision [10]. Les entonnoirs moléculaires (intersections coniques et croisements évités) sont un mécanisme très courant en photochimie, qui permet un saut ultrarapide des paquets d’onde entre deux états excités. Les entonnoirs moléculaires ont été prédis en 1950, mais ils n’ont jamais été observés expérimentalement avant 2010.

Les nouvelles techniques expérimentales résolues dans le temps requièrent de nouvelles méthodes théoriques. La spectroscopie femtoseconde doit être comparée avec des simulations de dynamique moléculaire en temps réel. Les dynamiques sont numériquement lourdes car elles peuvent inclure des degrés de liberté nucléaires et de l’environnement au même temps que des degrés électroniques. On a besoin de méthodes théoriques pouvant décrire la dynamique électron-nucléaire efficacement. Un bon candidat pour une telle méthode est la théorie de la fonctionnelle de la densité dépendante du temps (TDDFT) [11, 12]. Malheureusement, les approximations normalement appliquées à la TDDFT limitent l’application à des problèmes de photochimie. La TDDFT est une théorie exacte, formulée par les théorèmes de Runge et Gross en 1984 [13], qui permet l’application de la théorie de la fonctionnelle de la densité (DFT) [14, 15] sur des Hamiltoniens non-stationnaires. En pratique, on doit faire des approximations de la fonctionnelle d’échange-corrélation, qui reste inconnue. L’approximation adiabatique de la fonctionnelle est la plus utilisée et consiste en prenant la limite adiabatique de la fonctionnelle exacte pour tous les temps. Cette approximation décrit l’énergie de corrélation de façon inexacte et par conséquent, elle ne peut pas décrire correctement la photochimie. En particulier, les entonnoirs moléculaires ne sont pas bien décrits en raison de certains types de corrélation qui manquent à l’approximation adiabatique. L’objectif global de la thèse est d’améliorer les fonctionnelles de la TDDFT pour décrire de façon adéquate la corrélation afin qu’elle puisse être appliquée à des problèmes de photochimie.

La corrélation est un effet quantique qui englobe les mouvements coopératifs des électrons, qui normalement réduit l’énergie de répulsion électronique classique. Par convenance, la corrélation sera décrite en seconde quantification [16]. En seconde quantification, les contributions de la corrélation sont illustrées en diagrammes de Feynman, montrant avec précision les interactions électroniques, permettant une classification des effets de corrélation. Pour les objectifs de cette thèse, il est suffisant de restreindre la discussion de la corrélation à l’ordre le plus bas et donc à des diagrammes avec des interactions d’excitations au maximum doubles. La généralisation à un ordre plus haut est triviale.

Les objectifs spécifiques de cette thèse sont de (i) évaluer les méthodes existantes qui peuvent inclure un nombre réduit d’excitations doubles, (ii) fournir d’une nouvelle méthode qui peut inclure les excitations doubles en général, (iii) identifier quels diagrammes manquent à

l'approximation adiabatique de la fonctionnelle de la TDDFT, et (iv) ajouter des diagrammes aux fonctionnelles adiabatiques et tester le potentiel de ces corrections de théorie de perturbation à plusieurs corps pour décrire plus efficacement les excitations doubles de systèmes de moyenne et grosse taille.

Dans notre travail vers la résolution du problème des excitations doubles, nous avons adopté la perspective de la chimie quantique. La TDDFT entrerait dans la boîte à outils de la chimie quantique grâce à la formulation de Casida de la réponse linéaire de la TDDFT (LR-TDDFT) [17]. Casida formulait LR-TDDFT dans une forme matricielle similaire à Hartree-Fock dépendant du temps (TDHF) [18]. Ainsi, LR-TDDFT pouvait être facilement programmé en utilisant les algorithmes de la TDHF. Peu après le travail de Casida, LR-TDDFT fut disponible pour une grande communauté d'utilisateurs dans les logiciels de chimie quantique les plus utilisés. LR-TDDFT est devenue très populaire grâce à la grande efficacité de la méthode pour calculer les états excités et les forces d'oscillation, ouvrant une voie à de nouvelles applications qui n'étaient pas accessibles avec les méthodes basées sur la fonction d'onde. Des propriétés optiques de systèmes telles que les fullerenes [19–21], les protéines [22, 23] ou les effets du solvant dans les propriétés optiques [24] sont régulièrement publiés dans les revues scientifiques. Cependant, LR-TDDFT avec les fonctionnelles courantes montrait quelques déficiences importantes, telles que la sous-estimation du continuum [25], des excitations Rydberg et du transfert de charge [26]. Ces déficiences sont partiellement améliorées en utilisant de meilleures fonctionnelles d'échange [27, 28].

L'utilité de la LR-TDDFT est largement acceptée. Néanmoins, les photochimistes théoriciens se méfient (avec raison) de la capacité de la TDDFT à représenter des surfaces d'énergie potentielles des états excités aux points-clé du mécanisme de réaction. Dans ce domaine, la TDDFT doit rivaliser avec les méthodes multi-références basées sur la fonction d'onde, qui arrivent à la limite de la capacité des ordinateurs. En 2006, Martínez *et al.* ont exposé les deux principaux problèmes de la TDDFT pour des applications en photochimie: les excitations doubles et les intersections coniques [29]. En 2007, Casida *et al.* clarifient leurs idées dans une perspective plus correcte du point de vue de la TDDFT, faisant une étude très complète sur l'ouverture photochimique de l'anneau d'oxirane et la dynamique à travers l'intersection conique [30, 31]. De ces études, on peut reformuler les deux problèmes de la TDDFT comme la nécessité de meilleures fonctionnelles de corrélation et le problème de la v -représentativité non-interactive. Dans cette thèse, nous discuterons largement le problème de la corrélation dans la TDDFT et nous mentionnerons brièvement le problème de la v -représentativité non-interactive.

Les propriétés de la fonctionnelle d'échange dans la TDDFT sont largement étudiées dans la littérature [27, 32–34]. La fonctionnelle de corrélation a attiré moins l'attention, probablement en raison des propriétés très complexes de la fonctionnelle, qui dépende non localement des densités passées. Cette dépendance fait que la fonctionnelle de corrélation en TDDFT est non-locale dans les variables d'espace et de temps [35–37]. Les fonctionnelles adiabatiques, qui sont complètement locales dans le temps, sont fréquemment une approximation rudimentaire à la fonctionnelle de corrélation. Au moment de la publication de cette thèse, il existe seulement deux méthodes qui améliorent partiellement la description de la corrélation au delà de l'approximation adiabatique : spin-flip TDDFT développée par Krylov, Ziegler et Wang [38–42] et la TDDFT habillée développée par Maitra, Burke et leurs collaborateurs [43, 44]. Nous fournirons une solution plus générale qui conduira à un noyau pour la LR-TDDFT avec corrélation en utilisant les techniques *ab initio* [45]. Nous montrerons que la fonctionnelle adiabatique de corrélation

de la TDDFT manque complètement de diagrammes de seconde ordre, qui sont responsables du couplage entre les excitations simples et doubles. Ces diagrammes peuvent être ajoutés aux fonctionnelles adiabatiques existantes pour améliorer la description de la corrélation. Une méthode similaire a été développée par Sangalli et ses collaborateurs dans le cadre de l'équation Bethe-Salpeter pour les systèmes périodiques utilisant des potentiels écrantés [46–48]. Ils arrivent à des conclusions similaires.

La thèse est organisée en trois parties. La Partie I présente le matériel de base. Dans le chapitre 1, nous décrivons la photochimie théorique ; dans le chapitre 2, la théorie de la fonction d'onde *ab initio*, en se focalisant sur la description de la corrélation dans les états excités ; dans le chapitre 3, la théorie de la structure électronique basée sur la densité électronique. La partie II de la thèse contient la recherche originale. Le chapitre 4 traite de l'évaluation de la méthode spin-flip TDDFT pour décrire la photoréaction de l'oxirane. Dans le chapitre 5, nous exposons la dérivation du noyau de corrélation à partir des techniques *ab initio*, ce noyau incluant toutes les excitations doubles. Dans le chapitre 6, quelques noyaux approximatifs sont dérivés et testés ; ils permettent de généraliser l'idée de la méthode TDDFT habillée et peuvent être appliqués à des systèmes de taille moyenne et large. Enfin, la partie III contient les résultats non publiés, les perspectives et les conclusions finales.

Résumé par chapitre

Chapitre 1: Photochimie Théorique

La photochimie est l'étude de la réactivité dans les états excités. La description théorique des mécanismes de réaction est basée sur le calcul de la surface d'énergie potentielle, qui s'obtient à partir de l'approximation Born-Oppenheimer. Ce chapitre se focalise principalement sur les effets de corrélation dans les états excités, ainsi que sur la description de la structure électronique pendant le déroulement de la réaction photochimique.

Chapitre 2: Théorie de la Structure électronique Basée sur la Fonctionne d'Onde.

La théorie de la structure électronique basée sur la fonction d'onde est la seule théorie qui peut décrire les mécanismes de réaction photochimique à présent. Dans ce chapitre, on explique les méthodes théoriques les plus courantes pour résoudre les équations de Schrödinger statiques et dynamiques, en mettant l'accent sur les méthodes qui décrivent les états excités.

Chapitre 3: Théorie de la Structure électronique Basée sur la Densité électronique

Les méthodes basées sur la densité électronique sont plus efficaces que les méthodes basées sur la fonction d'onde. Dans ce chapitre, on décrit de façon détaillée la reformulation des équations de Schrödinger statiques et dynamiques en fonction de la densité.

Chapitre 4: Théorie de la Fonctionnelle de la Densité Dépendent du Temps avec spin-flip

La formulation classique de la théorie de la fonctionnelle de la densité dépendante du temps n'est pas facilement applicable au calcul d'intersections coniques et d'excitations doubles, deux composantes indispensables pour décrire la photochimie. La méthode spin-flip est une extension de la TDDFT qui résout partiellement ce problème. Dans ce chapitre, on expose les résultats du test effectué avec spin-flip pour étudier la photoréaction d'ouverture de l'anneau d'oxirane.

Chapitre 5: Noyau *Ab Initio* d'Échange-Corrélation Exacte

Au moment de la publication de cette thèse, aucune méthode ne peut inclure les excitations doubles de façon générale. Ce chapitre expose la dérivation d'un noyau pour la réponse linéaire de la TDDFT qui inclut toutes les excitations doubles. Le noyau est calculé en deux parties: la première partie est constituée par le noyau du propagateur de la polarisation, la deuxième partie est une fonction qui localise le noyau du propagateur à un noyau local pour la TDDFT.

Chapitre 6: Réponse Linéaire de la Théorie de la Fonctionnelle de la Densité Dépendent du Temps Habillé

Les calculs sur le noyau général du Chapitre 5 sont très coûteux numériquement. Dans ce chapitre, on présente le test d'un noyau avec des excitations doubles plus efficaces. Le noyau consiste en une partie basée sur une fonctionnelle TDDFT adiabatique, qui décrit les excitations simples, habillées par une partie du noyau du propagateur sans localisation, qui décrit les excitations doubles. Le test a été fait en comparant les énergies d'excitation des états singulet du noyau habillé avec des énergies d'excitation *ab initio* de référence.

Chapitre 7: Couplage entre la référence et les excitations en la Théorie de la Fonctionnelle de la Densité

Le noyau habillé est très efficace mais il ne peut pas décrire une partie importante des intersections coniques et des croisements évités qui se produisent avec l'état fondamental. Pour cette raison, on a inclus un terme additionnel au noyau habillé qui décrit cette interaction. Le terme a été tiré de la théorie CISD, le terme équivalent dans le propagateur étant trop coûteux. On a testé ce nouveau noyau pour décrire l'intersection conique entre les états S_1 et S_2 de l'éthylène dans le chemin de torsion. On expose les résultats préliminaires.

Chapitre 8: Théorie de la Fonctionnelle de la Densité Dépendent du Temps Habillé en Temps Réel

La formulation de la réponse linéaire de la TDDFT peut inclure les excitations doubles alors que la formulation en temps réel ne les inclut pas encore facilement. Une proposition est faite pour inclure ces excitations à partir du noyau habillé de la réponse linéaire.

Conclusions

La théorie de la fonctionnelle de la densité dépendante du temps est une méthode qui peut décrire efficacement la dynamique dans les états excités. Cependant, les approximations des fonctionnelles limitent l'application de la TDDFT. La majorité des fonctionnelles utilisent l'approximation adiabatique qui utilise la limite adiabatique de la fonctionnelle exacte pour tous les temps. Les fonctionnelles adiabatiques décrivent la corrélation de façon inexacte et elles ne sont pas aptes à représenter les points-clés des mécanismes de relaxation photochimique. Dans cette thèse, nous avons largement étudié la description de la corrélation en TDDFT et nous avons proposé quelques solutions pour permettre l'application de la TDDFT aux problèmes photochimiques.

Au moment de la publication de cette thèse, il n'y avait que deux méthodes qui pouvaient améliorer partiellement la description de la corrélation au delà de l'approximation adiabatique : spin-flip TDDFT et TDDFT habillée. Spin-flip convient pour décrire les problèmes photochimiques. Cette méthode a été initialement conçue pour calculer des états fondamentaux multiconfigurationaux à partir d'un modèle d'une seule référence, évitant le problème de la v -représentativité non-interactive. SF-TDDFT peut seulement inclure un nombre réduit d'excitations doubles, ce qui peut être insuffisant pour certaines applications, comme l'application à ouverture photochimique de l'anneau d'oxirane. D'une part, les croisements évités dans l'ouverture symétrique C_{2v} montre un petit *cusp* dans la surface S_0 , et la surface S_2 ne peut pas être convenablement interprétée pendant toute la coordonnée de réaction. D'autre part, la géométrie du point d'intersection conique entre S_0 et S_1 dans l'ouverture asymétrique est déplacée par rapport aux calculs multiréférenciaux. Même si SF-TDDFT améliore la description de la corrélation par rapport aux fonctionnelles adiabatiques, le nombre réduit d'états purs de spin et le nombre réduit d'excitations doubles incluses représentent deux des problèmes les plus importants de cette méthode.

L'un des principaux résultats de cette thèse est la présentation d'un noyau exact avec corrélation jusqu'au second ordre dérivé à partir de techniques *ab initio*. À notre avis, ce noyau est le premier à pouvoir inclure toutes les excitations doubles. Ce noyau est calculé en deux étapes : la première on construit un noyau du propagateur de la polarisation, auquel nous avons appliqué la théorie de perturbation commençant par un opérateur de Fock général, et la deuxième étape consiste d'une fonction de localisation qui transforme le noyau à plusieurs corps en un noyau local TDDFT. L'approximation de premier ordre du noyau à plusieurs corps donne le noyau d'échange exact dépendant du temps. L'approximation à ordre seconde donne une

approximation au noyau de corrélation consistante. La consistance d'ordre est importante pour éviter des effets physiques artificuels.

Le noyau de corrélation exacte nous permet d'identifier l'origine des problèmes de l'approximation adiabatique. Les fonctionnelles adiabatiques prennent en compte la limite adiabatique pour tous les temps et peuvent par conséquent être considérées comme des fonctionnelles statiques sans aucune dépendance de la fréquence (ou du temps.) Dans le noyau exact d'échange dépendant du temps, la dépendance de la fréquence est exclusivement due à la fonction de localisation. Cette fréquence n'est pas suffisante pour inclure les excitations doubles. Dans la partie de corrélation, le noyau du propagateur de la polarisation introduit une dépendance additionnelle qui est fondamentale pour inclure les excitations doubles dans les fonctions de réponse. Le développement en diagrammes du noyau nous permet d'identifier spécifiquement les diagrammes de corrélation du second ordre manquant dans l'approximation adiabatique. Ces diagrammes sont de type auto-énergie et particule-trou, et ils introduisent un couplage entre les excitations simples et doubles à partir des termes dépendants de la fréquence. Nous avons exploré la possibilité d'inclure les diagrammes manquants directement aux fonctionnelles adiabatiques, sans prendre en considération les effets de localisation. Ces corrections des fonctionnelles adiabatiques de la TDDFT correspondent à une sorte de fonctionnelle hybride avec mémoire qui généralise l'idée de la TDDFT habillée. Ce noyau est plus efficace que le noyau de corrélation exact *ab initio* et donc plus adapté pour des applications de systèmes de taille moyenne et large. Plusieurs définitions du noyau hybride sont possibles, elles dépendent du choix de fonctionnelle adiabatique et de termes à plusieurs corps. Nous montrons que toutes les combinaisons ne conviennent pas pour comparer les énergies d'excitation singulet de 28 chromophores organiques données par les noyaux hybrides avec résultats de référence de haute qualité. Nous concluons que le meilleur noyau s'obtient quand la partie adiabatique est constituée par une fonctionnelle hybride avec 20-25% d'échange HF et quand les excitations doubles sont corrigées au premier ordre en théorie des perturbations. Ce résultat est important car il montre que les fonctionnelles hybrides sont possibles non seulement en DFT mais aussi en TDDFT. Néanmoins, le noyau hybride pose le problème du double calcul de la corrélation, c'est-à-dire que les effets de corrélation dynamiques sont inclus deux fois dans le bloc d'excitations simples quand un grand nombre d'excitations doubles sont inclus. Ceci pourrait être évité avec la programmation d'une préselection perturbative d'excitations doubles.

Le noyau hybride avec mémoire pourrait être appliqué à des problèmes photochimiques car il inclut généralement les excitations doubles de spin pur. Cependant, dans sa forme présente, il ne peut pas décrire correctement la dissociation ou les entonnoirs moléculaires quand l'état fondamental intervient. Cela est dû au couplage manquant entre les excitations doubles et la référence. Nous avons inclus ces termes au noyau de CISD pour deux raisons. La première est que les termes de couplage de CISD sont plus facilement calculables que les équivalents du propagateur de la polarisation. La deuxième est que le noyau TDDFT habillé dans l'approximation Tamm-Dancoff a une structure similaire à celles des équations CISD, ce qui permet de comparer les deux théories et de transférer l'information manquante de l'une à l'autre. Les tests préliminaires dans la réaction de torsion de l'éthène montrent que ce choix est correct. Nous avons utilisé le noyau hybride avec les termes CISD pour décrire l'intersection conique qui se passe entre les surfaces S_1 et S_2 . Cela ne peut être décrit par aucune fonctionnelle adiabatique car l'état S_2 étant à un fort caractère d'excitation double. Cet état manque dans la TDDFT adiabatique. Le noyau hybride sous-estime largement l'énergie de l'état S_2 et, avec les corrections

de CISD, la description de l'intersection est à améliorer, même si elle est encore sous-estimée par rapport aux calculs *ab initio*.

Avec les résultats de cette thèse, de nouveaux problèmes (formels et d'application) peuvent être abordés avec la TDDFT. L'un des problèmes qui nous intéressent pour le futur est la représentation d'états excités de systèmes à couche ouverte. Les états excités dans ces systèmes ont une forte contamination de spin avec les fonctionnelles adiabatiques car les excitations doubles manquent. Ceci pourrait être résolu en combinant un calcul DFT à couche ouverte restreint avec notre noyau à excitations doubles. Un autre problème que nous voudrions explorer est la formulation d'une TDDFT habillée en temps réel. Nous proposons d'utiliser le noyau habillé et d'intégrer la dérivée seconde pour obtenir un potentiel avec mémoire. Pour les applications de photochimie, le problème de la v -représentativité non-interactive doit être abordé. Une solution consiste probablement à utiliser de nombreuses occupations fractionnaires. Le noyau *ab initio* devrait ainsi être redérivé de nouveau pour inclure dans la métrique qui accepte nombres d'occupation non-entiers.

En conclusion, le travail de cette thèse a clarifié le problème des excitations doubles et elle a proposé deux solutions, l'une rigoureuse et l'autre pratique, de fonctionnelles possibles pour la réponse linéaire, qui peuvent être appliquée à des problèmes photochimiques. Les résultats de cette thèse ouvrent de nouvelles perspectives pour la construction de fonctionnelles pour la TDDFT et marque un pas important dans l'application de la TDDFT en photochimie.